ACTA UNIVERSITATIS SZEGEDIENSIS

ACTA PHYSICA ET CHEMICA

NOVA SERIES

TOMUS XX FASCICULUS 3

AUSHAF 20 (3) 185—366 (1974)
HU ISSN 0001—6721

SZEGED, HUNGARIA
1974

Adiuvantibus

M. BARTÓK, L. CSÁNYI, P. FEJES, F. GILDE, P. HUHN, I. KETSKEMÉTY, F. MÁRTA, L. SZALAY et F. SZÁNTÓ

redigit

KÁLMÁN KOVÁCS

Edit

Facultas Scientiarum Naturalium Universitatis Szegediensis de Attila József nominatae

Editionem curant

J. ANDOR, G. BERNÁTH et Á. SÜLI

Nota

Acta Phys. et Chem. Szeged

Szerkeszti

KOVÁCS KÁLMÁN

A szerkesztőbizottság tagjai:

BARTÓK M., CSÁNYI L., FEJES P., GILDE F., HUHN P., KETSKEMÉTY I., MÁRTA F., SZALAY L. és SZÁNTÓ F.

Kiadja

a József Attila Tudományegyetem Természettudományi Kara
(Szeged, Aradi Vértanúk tere 1.)

Szerkesztőbizottsági titkárok:

ANDOR J., BERNÁTH G. és SÜLI Á.

Kiadványunk rövidítése:
Acta Phys. et Chem. Szeged

IN MEMORIAM ÁGOSTON BUDÓ

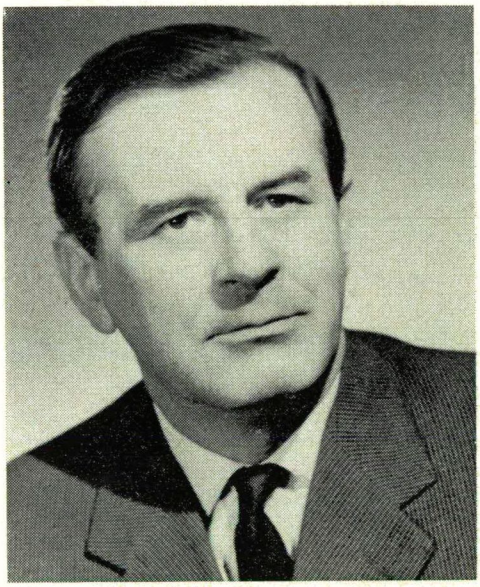

1914—1969

ÁGOSTON BUDÓ, Professor und Leiter des Instituts für Experimentelle Physik der Attila József Universität Szeged, ordentliches Mitglied der Ungarischen Akademie der Wissenschaften, der unvergessliche Forscher und Erzieher der jüngeren Physikergeneration hätte in diesem Jahre sein sechzigtes Lebensjahr vollendet. Seine ehemaligen Schüler, Mitarbeiter, Freunde und Verehrer wünschen diese Gelegenheit zu benützen, mit ihren in diesem Hefte veröffentlichten Beiträgen dem Andenken des leider zu früh Verstorbenen zu opfern.

I. Ketskeméty

ОБ ИССЛЕДОВАНИИ ОКГ НА РАСТВОРАХ ОРГАНИЧЕСКИХ КРАСИТЕЛЕЙ, ВОЗБУЖДЁННЫХ ИЗЛУЧЕНИЕМ АЗОТНОГО ЛАЗЕРА

И. КЕЧКЕМЕТИ, Б. РАЦ, Ж. БОР, Л. КОЗМА

Институт экспериментальной физики университета им. А. Йожефа, г. Сегед

(Поступило в редакцию 1 июля 1974 г.)

В работе проведено исследование ОКГ на органических красителях, возбуждённых азотным лазером. В широкополосном резонаторе, образованном стенками кюветы, получилась генерация от 3620 Å до 6600 Å на любой длине волны.

Уникальные свойства ОКГ на красителях общеизвестны. Лазерам на растворах красителей характерны высокая мощность в импульсе, высокая частота повторения и широкая область непрерывного перестраивания генерации излучения [1]. Однако потери, возникающие во время генерации, требуют большой скорости накачки, так как триплетный уровень быстро заселяется и выступающие триплет-триплетные поглощения могут конкурировать с усилением [2]. Термооптические искажения раствора также могут срывать генерацию. Ввиду этого мало число тех красителей, которые генерируют при ламповой накачке. Более эффективное возбуждение можно осуществить излучением твёрдотельных лазеров; однако, в этом случае усложняется экспериментальная работа. После создания азотного лазера открылся новый путь для накачки лазеров на красителях. Азотные ОКГ имеют простую конструкцию и без использования удвоителя частоты можно их эффективно использовать для возбуждения растворов красителей.

Для возбуждения лазеров на красителях был использован импульсный азотный ОКГ с поперечным разрядом, построенный авторами [3]. Лазерный переход на длине волны 3371 Å соответствует переходу между уровнями $C^3\pi_u$ и $B^3\pi_g$ молекулы азота. Лазер относится к лазерам на самоограниченных переходах [4, 5, 6]. Так как время жизни верхнего уровня 40 нсек, а среднего 10 мксек, инверсия населённости может образоваться только в начале возбуждающего разряда на короткое (меньше 5—10 нсек) время. Необходимая плотность тока накачивающего разряда порядка 1 ка/см^2.

Принципиальная электрическая схема питания лазерной камеры приведена на рис. 1. Источник высокого напряжения через сопротивления R_1 и R_2 заряжает полосковые линии C_1 и C_2. С помощью разрядного промежутка S быстро разряжаем C_2, вследствие которого между верхними обкладками C_1 и C_2 появлется высокое напряжение и происходит пробой в лазерной камере. Время разряда определяется временем распространения электрического сиг-

нала в C_2, а ток разряда волновым сопротивчением линии и прикладываемым к системе напряжением. Рис. 2. показывает конструкцию ОКГ на азоте. Расстояние между электродами Е в разрядной камере L 8 мм. С целью увеличения пространственной однородности разряда на поверхности электродов было создано 750 выступов. Длина камеры $a = 50$ см, а общая длина линий $b = 110$ см.

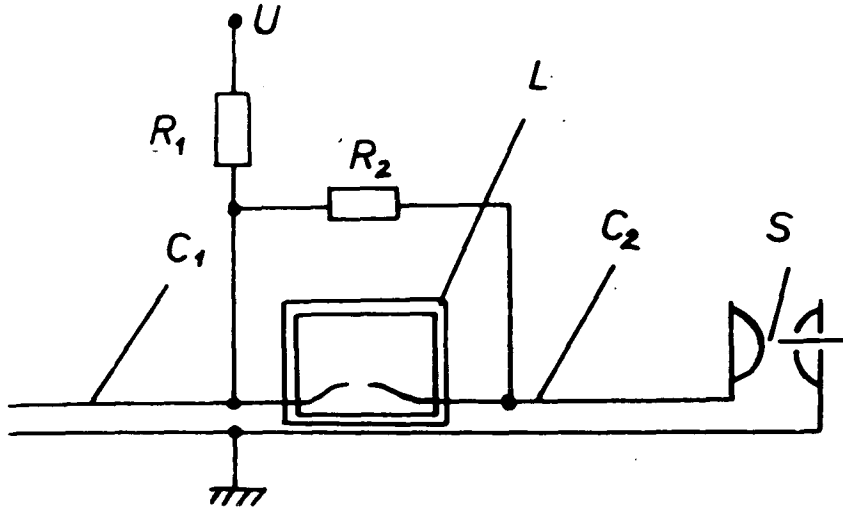

Рис. 1. Принципиальная электрическая схема лазера

Толщина диэлектрика $D = 300$ мк и волновое сопротивление полосковых линий 0,15 ом. Вывод излучения осуществляется через кварцевое окно, а с противоположной строны установлено плоское зеркало T. При необходимости продув азота через камеру осуществляется с помощью вакуумной системы через выводы V. Зависимость энергии в импульсе лазера от давления p рабочего газа приведена на рис. 3. Оказалось, что энергия максимальная, если значение $\frac{E}{p} = 165 \frac{\text{в}}{\text{см. мм. рт. ст.}}$. Мощность в импульсе приблизительно 235 квт. Частота повторения импульсов 25 гц, что ограничивается мощностью источника высокого напряжения. Азотный лазер не требует особо чистого азота.

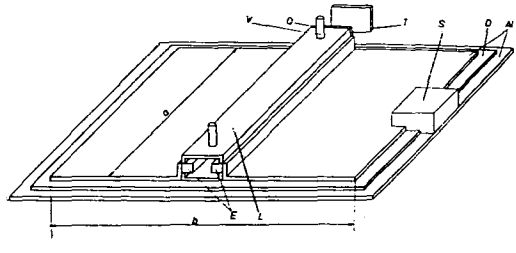

Рис. 2. Конструкция азотного лазера

Поперечный и продольный варианты накачки ОКГ на красителях приведены на рис. 4а и 4б. Короткие, мощные импульсы накачки азотного лазера позволяют получить такие высокие коэффициенты усиления, что даже четырёхпроцентное отражение на

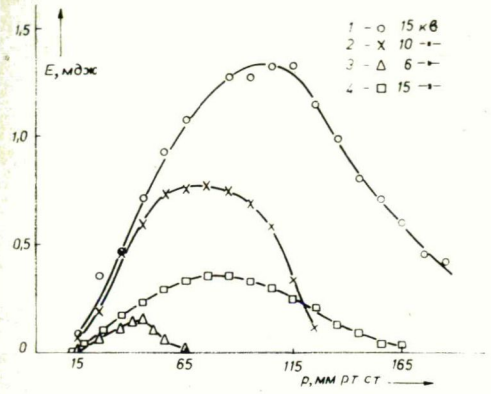

Рис. 3. Зависимость энергии генерации от давления рабочего газа при разных напряжениях; 1—3 — рабочий газ азот, 4 — воздух

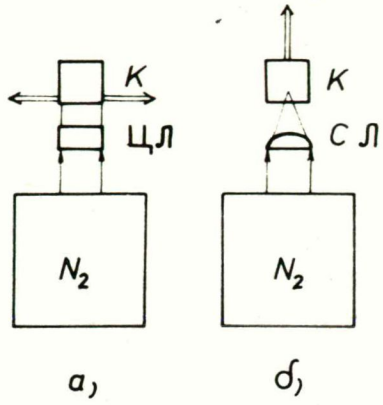

Рис. 4. Возбуждение генерации растворов красителей; *а* — поперечный, *б* — продольный вариант. *К* — кювета с раствором, *цл* — цилиндрическая линза, *сл* — сферическая линза, N_2 — азотный лазер

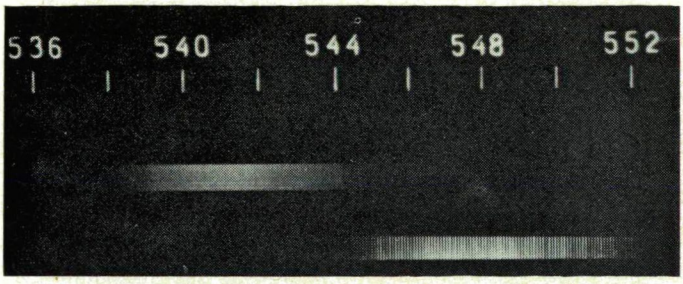

Рис. 5. Спектры сверхизлучения (вверху) и генерации (внизу) раствора флуоресцеина. Концентрация 10^{-3} моль/л, растворитель этанол

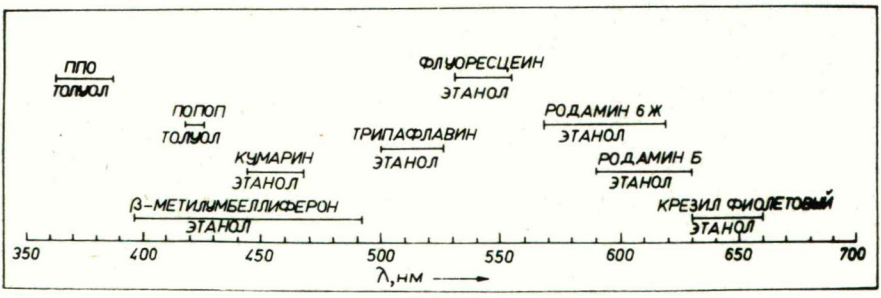

Рис. 6. Спектральная область генерации разных красителей

поверхностях кюветы достаточно для получения генерации. Далее при устранении обратной связи можно получить и сверхизлучение. Рис. 5. показывает спектры лазерного излучения и сверхизлучения раствора флуоресцеина. Значит, использование лазера даёт возможность исследовать спонтанную эмиссию, генерацию и сверхизлучение различных материалов.

Так как при накачке красителей с помощью азотного лазера не происходит интенсивное разрушение молекул красителей, триплетные состояния красителей не заселяются и во время генерации не возникают термооптические искажения в растворе, частота повторения может быть высоким и КПД даже может стать больше 50 процентов. Число веществ, на которых можно получить генерацию, весьма большое. Рис. 6 показывает области генерации растворов по схеме, приведенной на рис. 4а и 4б. Видно, что с помощью такой простой схемы мы получили генерацию в спектральной области 3620 Å — 6600 Å. Спектральная ширина генерации 100—200 Å. При использовании других материалов можно расширить область генерации.

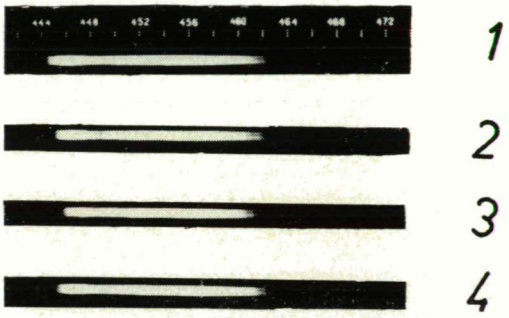

Рис. 7. Спектры генерации растворов при концентрации *а* — кумарина 1—$5\cdot10^{-4}$, 2—$2\cdot10^{-3}$, 3—$5\cdot10^{-3}$, 4—$1\cdot10^{-2}$ (моль/л),

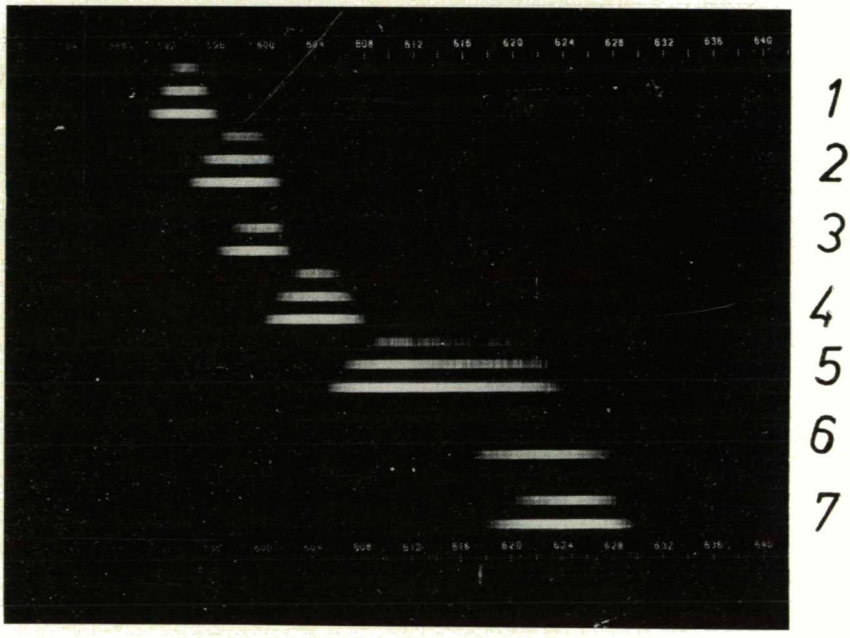

Рис. 7. б — родамина 6Ж (при разных количествах вспышек) 1—$4\cdot10^{-4}$, 2—$8\cdot10^{-4}$, 3—$1\cdot10^{-3}$, 4—$2\cdot10^{-3}$, 5—$4\cdot10^{-3}$, 6—$8\cdot10^{-3}$, 7—$1\cdot10^{-2}$ (моль/л)

Преимуществом лазеров на растворах является их перестраиваемость. Одним из методов перестройки является метод изменения концентрации активных молекул [7]. Рис. 7 показывает изменение спектра генерации при разных концентрациях красителей для родамина 6Ж и 7-диметиламино-4--метилкумарина. Как видно, область генерации раствора кумарина практически не меняется с увеличением концентрации, а родамина 6Ж наоборот, перестраивается. Для объяснения данного эффекта рассмотрим коэффициент усиления, который имеет следующий вид [8]:

$$k_{ус}(v) = n_3 \frac{v^2}{8\pi\tau_0} \frac{f_q(v)}{v^2} - \left(1 - \frac{n_3}{n}\right) k(v)\eta^*(v) \qquad (1)$$

где $f_q(v)$ — спектр люминесценции, $k(v)$ — коэффициент поглощения, τ_0 — естественное время затухания, $\eta^*(v)$ — спектр квантового выхода люминесценции, n_3 — концентрация возбуждённых молекул, v — скорость света в растворе. Так как для кумарина (спектры которого не перекрываются) величиной $k(v)\eta^*(v)$ можно пренебречь в области генерации и спектральное положение спектра усиления определяется спектром люминесценции $f_q(v)$, изменение концентрации не вызывает перестройку генерации. Спектры поглощения и люминесценции родамина 6Ж сильно перекрываются, и так частота максимума коэффициента усиления зависит от n и от значения $k(v)\eta^*(v)$ При увеличении, концентрации красителя в коротковолновой области генерации потери на поглощение сильнее увеличиваются чем в длинноволновой части, а генерация смещается в область меньших частот. Количественный анализ соотношения (1) показывает довольно хорошее соглашение с экспериментом.

Другим методом перестройки генерации является введение в резонатор какого-то спектрально-селективного элемента [9]. При добавлении в активный раствор какого-то вещества, имеющего круто меняющийся спектр поглощения в ожидаемой области генерации и поэтому селективно меняющиеся потери в резонаторе, можно получить перестройку генерации. Рис. 8 показывает спектры генерации родамина 6Ж при добавлении родамина Б в раствор. Видно, что простой метод перестройки, разработанный нами, применим и в том случае, когда генерация происходит в резонаторе, образованном только торцами кюветы.

Известно, что спектр люминесценции — и соответственно спектр генерации — β-метилумбеллиферона зависит

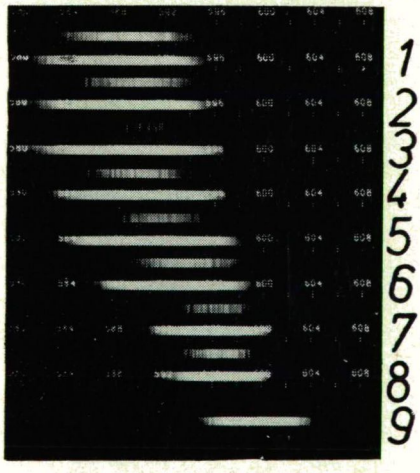

Рис. 8. Перестройка генерации раствора родамина 6Ж при добавлении в раствор родамина Б. Спектры сняты при разных количествах вспышек. Концентрация родамина 6Ж $5 \cdot 10^{-3}$ моль/л, концентрация родамина Б 1—$5 \cdot 10^{-6}$, 2—$7 \cdot 10^{-6}$, 3—$1 \cdot 10^{-5}$, 4—$2 \cdot 20^{-5}$, 5—$5 \cdot 10^{-5}$, 6—$7 \cdot 10^{-5}$, 7—$1 \cdot 10^{-4}$, 8—$2 \cdot 10^{-4}$, 9—$5 \cdot 10^{-4}$(моль/л)

от растворяющей среды. Рис. 9 показывает спектры генерации растворов β-метилумбеллиферона в нейтральной, щёлочной и кислотной средах. Спектры показывают, что растворы этого вещества дают возможность для перестройки

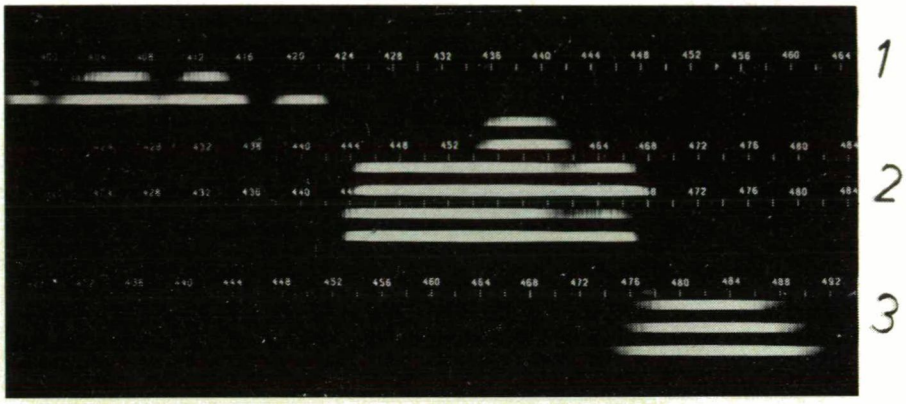

Рис. 9. Спектры генерации раствора β — метилумбеллиферона в 1 — нейтральной, 2 — кислоной, 3 — щёлочной средах, снятые при разных количествах вспышек

Рис. 10. Спектр генерации смешанного раствора родамина 6Ж и крезилфиолетового

генерации в широком спектральном диапазоне. Изменением характера растворяющей среды можно перестраивать спектр генерации.

В лабораторной практике часто употребляется одновременная двухполосная генерация. Одним из методов получения одновременной двухполосной генерации является использование в качестве активной среды лазера такого смешанного раствора, в котором для обоих компонентов условия для генерации имеют место. Рис. 10 показывает спектр двухполосной генерации смешанного раствора родамина 6Ж и крезилфиолетового. Соответствующим выбором различных компонентов генерацию можно получить на двух нужных длинах волн. Одновременную многополосную генерацию осуществили показанным на рис. 11 методом, где лазеры накачивают друг друга. Тот факт, что три жидких лазера генерируют одновременно, показывает большую эффек-

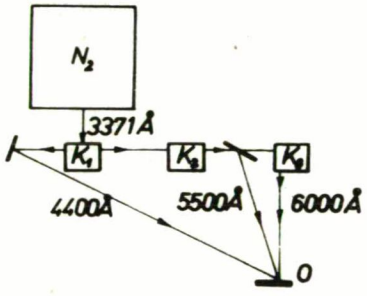

Рис. 11. Одновременная генерация трёх лазеров. N_2 — азотный лазер, K_1, K_2, K_3 — кюветы с растворами 7,4-кумарина, флуоресценина и родамина 6Ж соответственно, О — образец

тивность возбуждения короткими, мощными импульсами. Из рисунка видно, что определенный образец можно освещать тремя световыми пучками на разных длинах волны.

Целью дальнейших исследований является разработка таких смесей растворов красителей, которые позволяют получить широкую область генерации с высоким к. п. д. Лазеры на красителях дают возможность исследовать быстрые разнообразные межмолекулярные взаимодействия, вызванные светом различных длин волн.

* * *

Авторы выражают благодарность М. В. Белоконю за ценные советы при создании N_2 лазера.

Литература

[1] *Степанов, Б. И., А. Н. Рубинов:* УФН, **95,** 45 (1968).
[2] *Степанов, Б. И.:* Методы расчёта ОКГ. Препринт, Минск (1968).
[3] *Кечкемети, И., Б. Рац, Ж. Бор, Л. Козма:* Acta Tech. Hung. (в печати)
[4] *Gerry, E. T.:* Appl. Phys. Lett., **7,** 6 (1963).
[5] *Ali, A.W., A. G. Kolb and Anderson:* Appl. Opt. **6,** 2115 (1967).
[6] *Ali, A. W.:* Appl. Opt. **8,** 993 (1969).
[7] *Кечкемети, И., Л. Козма, И. Салма, Б. Рац, Э. Хун:* ЖПС, **14,** 1000 (1971).
[8] *Ketskeméty, I., L. Kozma:* Acta Phys. Acad. Sci. Hung., **35,** 63 (1974).
[9] *Кечкемети, И. ,Б. Рац, И. Салма, Э. Хун, Л. Козма:* Acta Phys. et Chem. Szeged, **17,** 9 (1971).

INVESTIGATION OF DYE LASERS PUMPED WITH NITROGEN LASER

I. Ketskeméty, B. Rácz, Zs. Bor, L. Kozma

The paper reports on the investigation of dye lasers excited by a nitrogen laser. In a broad band resonator formed by the walls of the cuvette, generation could be obtained at any wavelength between 3620 Å and 6600 Å.

DETERMINATION OF THE FLUORESCENCE EXCITATION SPECTRA OF PROTEINS

By

Z. VÁRKONYI AND L. SZALAY

Institute of Biophysics, József Attila University, Szeged

(Received July 1, 1974)

Methods for determining true fluorescence excitation spectra by applying corrections for reabsorption and secondary fluorescence are described for different conditions of observation.The results are illustrated by fluorescence excitation spectra of horse-radish peroxidase, lysozyme, Triton X-100 detergent and peroxidase solutions containing fluorescein-isothiocyanate indicator.

1. *Introduction*

The fluorescence excitation spectrum

$$f_{exc}(\lambda', \lambda) = \frac{I_{fl}(\lambda', \lambda)}{I_0(\lambda)}, \tag{1}$$

i.e. the fluorescence intensity $I_{fl}(\lambda', \lambda)$ observed at a given wavelength λ' with unit intensity of the exciting light of wavelength λ, yields information about the properties of the fluorescent systems and the processes occurring in them. Until now, the uncorrected excitation spectra were generally given, *i.e.* the directly measured fluorescence intensities were published. Several authors [1—4] have called the attention to the importance of excitation spectra given for constant intensity of exciting light. In this case the shape of the excitation spectrum of a material of "not too high" extinction, containing a single absorbing component, will coincide with the absorption spectrum [5]. The excitation spectrum of aqueous tryptophan solution of extinction 0.1 is in good accordance with the absorption spectrum, while in solutions of higher extinction marked differences occured [6]. McDONALD and SELINGER [4] pointed out that excitation spectra depend on the geometry of observation and on the extinction of the solution. It has been generally recognized that the excitation spectrum may be distorted by reabsorption of fluorescence. If the reabsorption is significant, the secondary fluorescence may also be important and has to be taken into consideration. BUDÓ *et al.* [7], gave methods of corrections for secondary fluorescence in cases of different luminescence characteristics, therefore, the correction of the excitation spectrum can be given as an extension of the results of [7].

The aim of the present paper is to summarize our present knowledge concerning the determination of true excitation spectra, to describe the methods for the necessary corrections with special respect to reabsorption and secondary luminescence.

2. *Determination of true fluorescence excitation spectra*

a) *General remarks.* In order to obtain the excitation spectrum $f_{exc}(\lambda', \lambda)$ defined in Eq. (1), (i) the true fluorescence intensity $I_{fl}(\lambda', \lambda)$ at the wavelengths λ' and λ of observation and excitation, respectively, and (ii) the intensity of excitation $I_0(\lambda)$ for different exciting wavelengths λ have to be determined.

(i) For the determination of $I_{fl}(\lambda', \lambda)$ the values $I_{meas}(\lambda', \lambda)$ measured directly with the spectrofluorimeter have to be corrected a) for the spectral sensitivity $Q(\lambda')$ of the measuring instrument, including the sensitivity of the photomultiplier used, the band width, and changes in transmittivity of the monochromator [2, 8]; (b) for the factor $\varphi(\lambda', \lambda)$ taking into account reabsorption, and (c) for the factor containing $\varkappa$, which takes into account secondary luminescence according to [7] and [8],

$$I_{fl}(\lambda', \lambda) = \text{const} \cdot I_{meas}(\lambda', \lambda) \cdot Q(\lambda) \cdot \varphi(\lambda', \lambda) \cdot [1 - \varkappa(\lambda', \lambda)]. \tag{2}$$

(ii) The true fluorescence intensity obtained in this way has to be referred to unit exciting intensity, therefore the spectral energy distribution of the light source should be known. Replacing the fluorescent sample by a thermopile, the thermocurrents $I_T(\lambda)$ will be proportional to the incident energy of light, and independent of the wavelength; $I_T(\lambda) = \text{const} \cdot I_0(\lambda)$. Thus $I_{fl}(\lambda)/I_T(\lambda)$ is proportional to the exciting spectrum. It is more expedient to calibrate the multiplier of the apparatus for energy measurements. By reflecting the exciting light into the photomultiplier and measuring the photocurrent $I_{Ph}(\lambda)$, $E(\lambda) = I_T(\lambda)/I_{Ph}(\lambda)$ will give the energy value pertaining to the unit deflection of the galvanometer in the circuit of the photocell, *i.e.* I_T is obtained in the form $I_T(\lambda) = E(\lambda) \cdot I_{Ph}(\lambda)$. Thus the excitation spectrum is

$$f_{exc}(\lambda', \lambda) = \text{const} \frac{1}{I_{Ph}(\lambda) \cdot E(\lambda)} \cdot I_{meas}(\lambda', \lambda) \cdot Q(\lambda') \cdot \varphi(\lambda', \lambda) \cdot [1 - \varkappa(\lambda', \lambda)]. \tag{3}$$

The constant in the equation is determined by the geometry of the apparatus, but independent of the wavelength (λ) of exciting light. $Q(\lambda)$ has to be calculated with the method described for the determination of the emission spectrum (see *e.g.* [3]).

b) *Correction for reabsorption and secondary luminescence. Determination of* $\varphi(\lambda', \lambda)$ *and* $\varkappa(\lambda', \lambda)$.

The correction for reabsorption. $\varphi(\lambda', \lambda)$ depends on the wavelengths of the exciting and emitted light, and on the geometry of excitation and observation. As the fluorescence intensity has to be determined for the excitation spectrum, the value of φ will be the same as that used in determining the true fluorescence spectrum. According to FÖRSTER [8], the values of φ are as follows:

for front-surface observation (excitation and observation parallel)

$$\varphi = \frac{1}{\alpha} \cdot \frac{\alpha + \beta}{1 - e^{-(\alpha+\beta)}} \tag{4}$$

for in-line observation

$$\varphi = \frac{1}{\alpha \cdot e^{\alpha}} \cdot \frac{\beta - \alpha}{1 - e^{-(\beta-\alpha)}} \tag{5}$$

for right-angle observation

$$\varphi = \frac{1}{\alpha} \cdot \frac{\beta}{1 - e^{-\beta}} \tag{6}$$

where $\alpha = k(\lambda) \cdot l$ and $\beta = k(\lambda') \cdot l$; $k(\lambda)$ and $k(\lambda')$ are absorption coefficients and l is the layer thickness. It has been shown [9] that under certain conditions a simpler formula can be used.

The correction for secondary fluorescence is completed by giving the ratio of the intensities of secondary fluorescence S to the primary fluorescence P, *i.e.* the quotient $\varkappa = \frac{S}{P}$, $\varkappa$ is a constant depending on the properties of the solution, on the geometry of observation and that of the sample, as well as on the absorption and emission spectra. The calculation of $\varkappa$ is rather complicated [7], but several values are tabulated or can be determined with computer methods [10]. Therefore it is advantageous to choose experimental conditions for which the secondary fluorescence can be neglected. When α and β are less than 0.5, the error caused by neglecting the correction will be less than 1 %.

c) *The choice of adequate geometry* is very important. The excitation spectra are subject to changes not only by reabsorption, but also by absorption of the exciting light, which are not taken into consideration in the formulae (4)—(6).

The following limiting cases are possible.

In the case of strong absorption the exiting light will be absorbed in a thin layer, causing fluorescence only in this layer (surface fluorescence). In this case the intensity of the fluorescence for right-angle observation will be strongly reduced with increasing distance from the excited surface. If the reabsorption of fluorescence light is weak, the same fluorescence intensities will be obtained for front-surface and in-line observation. If the reabsorption is strong, higher intensities will be found for front-surface observation, because the path of light in the medium will be shorter. In this case front-surface observation or layer thicknesses corresponding to $k(\lambda)_{max} \cdot l < 0{,}1$ should be used for determining the excitation spectrum. In the case of right-angle observation the intensity of fluorescence will depend both on wavelength and on the observed part of the lateral face. Further, it is difficult to determine the path-length of fluorescence in Eq. (6). The errors resulting from these circumstances cannot be considered by calculation, therefore they have to be avoided by choosing proper experimental methods.

If the absorption of exciting light is weak, the reabsorption of fluorescence can be calculated with Eqs. (4)—(6), depending on the geometry of observation. In this case, right-angle observation will be the most favourable, while in the case of strong reabsorption front-surface observation should be used.

3. *Connection between excitation and absorption spectra*

The excitation spectrum is proportional to the intensity $I_{abs}(\lambda)$ of the absorbed light and the fluorescence yield $\eta(\lambda', \lambda)$. The intensity of fluorescence is

$$I_{fl}(\lambda', \lambda) = \text{const} \cdot I_{abs}(\lambda) \cdot \eta(\lambda', \lambda),$$

where

$$I_{abs}(\lambda) = I_0(\lambda) \cdot [1 - e^{-k(\lambda) \cdot l}].$$

Thus the excitation spectrum is as follows:

$$f_{exc}(\lambda', \lambda) = \frac{I_{fl}(\lambda', \lambda)}{I_0(\lambda)} = \text{const} \cdot [1 - e^{-k(\lambda) \cdot l}] \cdot \eta(\lambda', \lambda). \tag{7}$$

For the two limiting cases, this equation leads to the following consequences.

In the case of great layer thickness and solutions of high concentration $e^{-k(\lambda) \cdot l} \approx 0$; the excitation spectrum does not depend on the absorption, but on the other hand, the spectrum obtained will be false, therefore such conditions must be avoided.

For low concentrations and small layer thicknesses $k(\lambda) \cdot l \ll 1$ and $1 - e^{-k(\lambda) \cdot l} \sim k(\lambda) \cdot l$, *i.e.* the excitation spectrum is proportional to the active absorption spectrum $k(\lambda) \cdot \eta(\lambda', \lambda)$; the absorption spectrum and the excitation spectrum of solutions with a single fluorescent component have the same shape.

4. *Experimental results*

The excitation spectra of phosphate buffered neutral solutions of horse-radish peroxidase (HRP) and lysozyme with the detergent Triton X-100 and the protein indicator dye fluorescein isothiocyanate (FITC) were measured with a Perkin—Elmer—Hitachi Type PMF-3 spectrofluorimeter.

Fig. 1 shows the relative excitation spectrum of a $2 \cdot 10^{-3}$ M Triton X-100 solution at 305 nm with right-angle and with front-surface observation under an

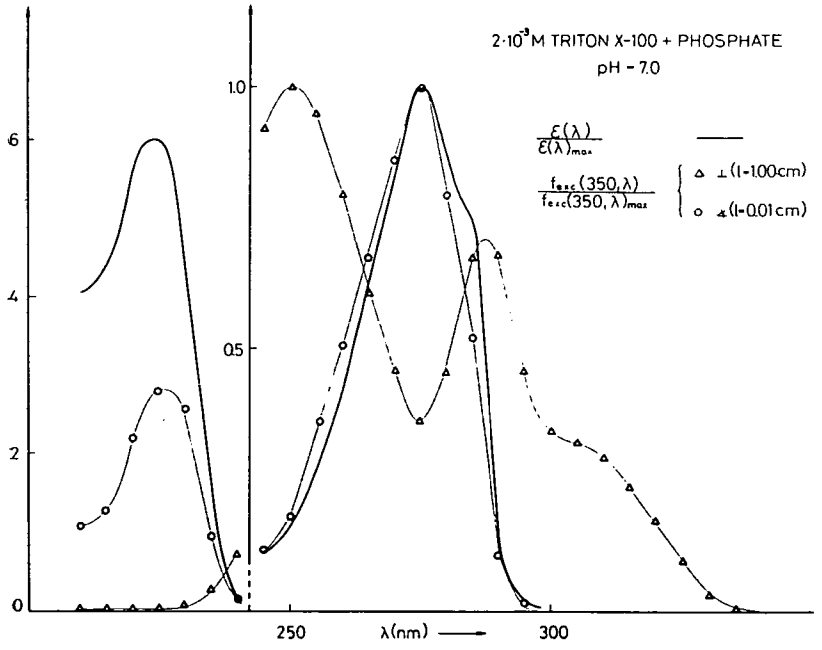

Fig. 1

angle of $\sim 7°$ ($l = 0.01$ cm), together with the relative absorption spectrum. In the case of right-angle observation, an excitation minimum is obtained where the absorption spectrum has a maximum, and reversely. The excitation spectrum obtained in the 250—300 nm band with front-surface observation shows good coincidence with the absorption spectrum, because the 305 nm fluorescence band of Triton X-100 is due to the 275 nm absorption band. The short wavelength bands of excitation and absorption do not coincide, because its participation in the fluorescence is less.

A similar picture is shown by a $5 \cdot 10^{-5}$ M lysozyme solution. Consequently the right-angle observation cannot be used for determining the excitation spectra of proteins, even at concentrations as low as $5 \cdot 10^{-5}$ M (Fig. 2).

Fig. 3 shows the relative absorption spectrum, the directly measured excitation spectrum, the relative excitation spectra corrected for unit exciting intensity and for reabsorption, respectively. The coincidence with the absorption spectrum is the best in the case of the curve corrected for reabsorption.

In Fig. 4 the relative absorption spectrum of the protein—dye complex HRP+FITC, the relative excitation spectra measured with two geometries of observation and corrected for reabsorption, as well as the absorption spectrum of the dye solution in the wavelength range 420—520 nm are presented. The participation of the dye in the fluorescence observed at the emission maximum of the FITC ($\lambda' = 525$ nm)

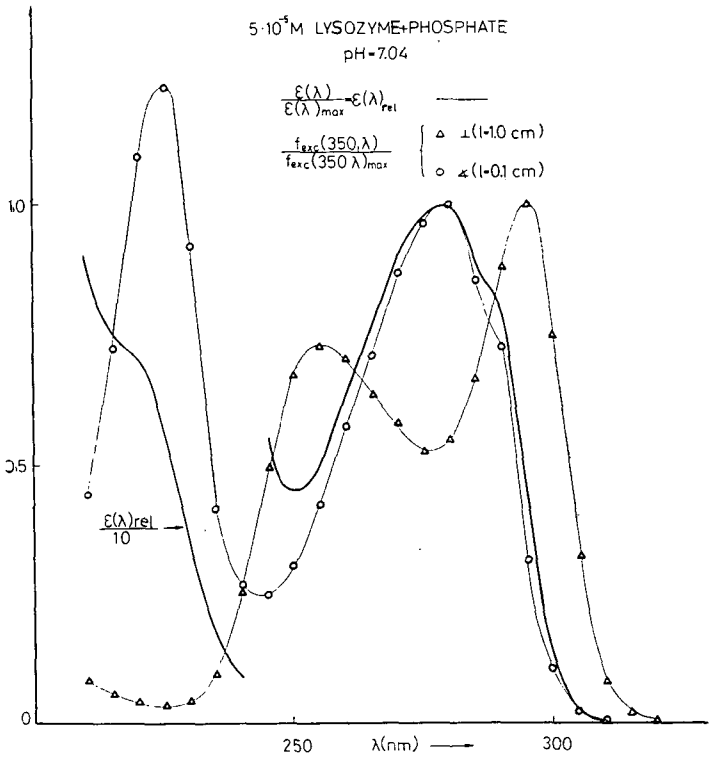

Fig. 2

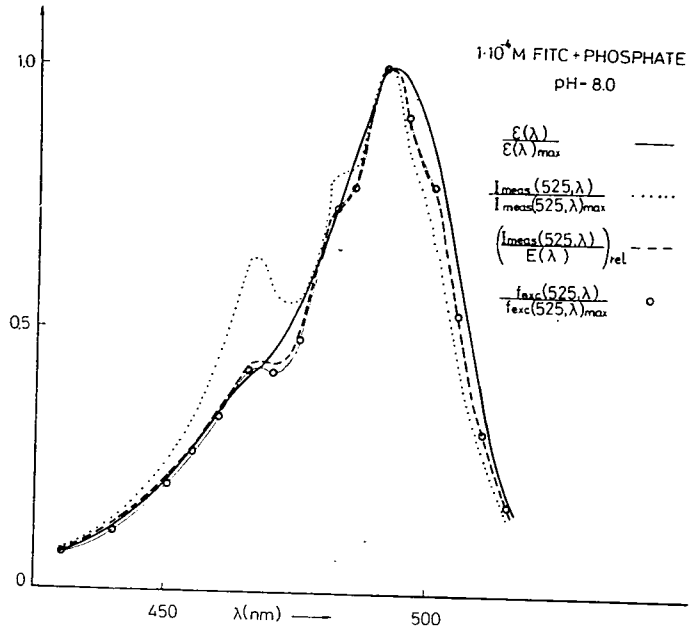
1·10⁻⁴M FITC + PHOSPHATE
pH - 8.0
ε(λ)/ε(λ)max
Imeas(525,λ)/Imeas(525,λ)max
(Imeas(525,λ)/E(λ))rel
fexc(525,λ)/fexc(525,λ)max
1.0
0.5
0
450
λ(nm)
500

Fig. 3

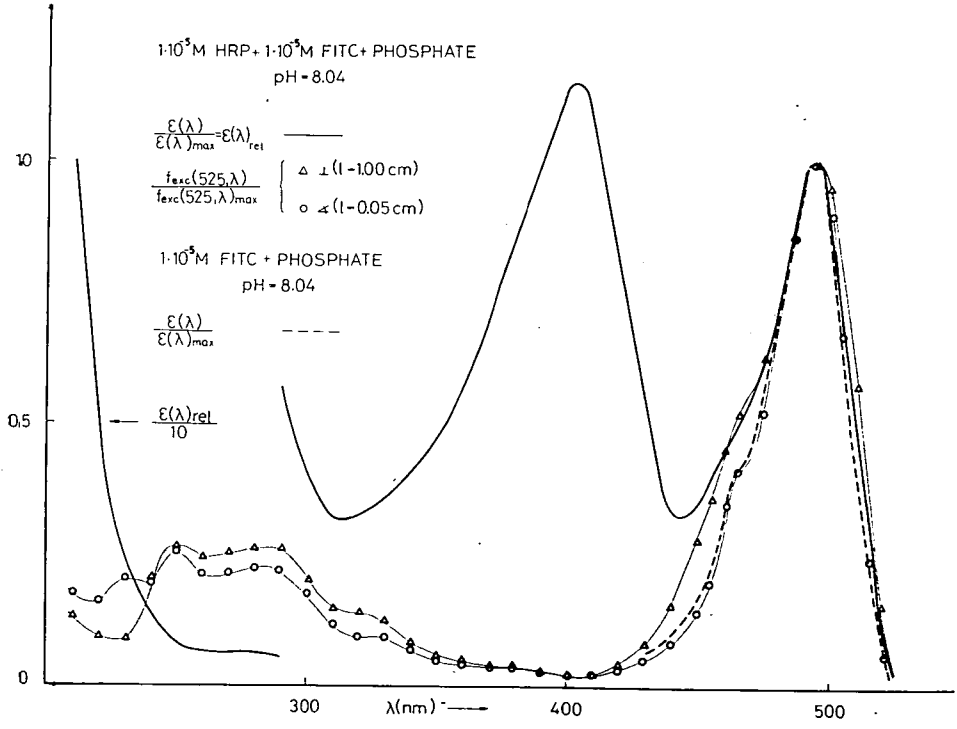
1·10⁻⁵M HRP + 1·10⁻⁵M FITC + PHOSPHATE
pH - 8.04
ε(λ)/ε(λ)max = ε(λ)rel
fexc(525,λ)/fexc(525,λ)max
△ ⊥ (l - 1.00 cm)
○ ∠ (l - 0.05 cm)
1·10⁻⁵M FITC + PHOSPHATE
pH - 8.04
ε(λ)/ε(λ)max
ε(λ)rel/10
1.0
0.5
0
300
λ(nm)
400
500

Fig. 4

is high, that of the HRP—protein is low and the contribution of the haem is insignificant despite its high absorption band at 405 nm. This means that, in accordance with our earlier results [11], the haem does not take part in the transfer of the exciting energy.

The excitation spectra measured with different geometries of observation and corrected for reabsorption show marked deviations in the wavelength ranges 260—300 nm and 450—500 nm. These deviations are due to the high absorption of the

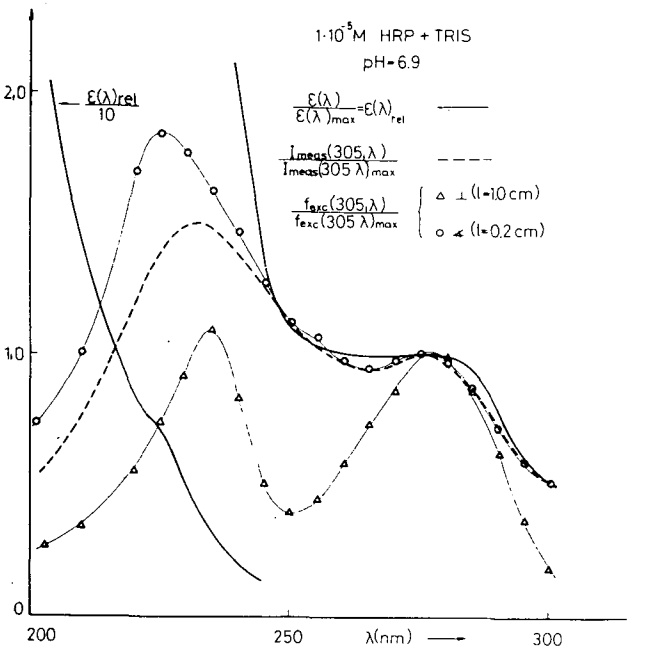

Fig. 5

protein-dye complex in this wavelength range. This explanation is confirmed by the fact that in the wavelength range 420—500 nm the excitation spectrum obtained with front-surface observation and corrected for reabsorption coincides with the relative absorption spectrum of the dye.

An interesting observation is shown in Fig. 5. The corrected excitation spectrum of the HRP fluorescence obtained at $\lambda' = 305$ nm by front-surface observation in the 250—300 nm range coincides with the absorption spectrum. This means that the 305 nm fluorescence is due to the 276 nm absorption maximum of tyrosine (see [11]). A contribution to this fluorescence originates from the component causing a shoulder in the absorption spectrum at 225 nm. This component can be found in the excitation spectrum only by front-surface observation and performing the corrections; otherwise the maximum of the curve shifts towards longer wavelengths and its ratio relative to the protein maximum becomes less.

Our remarks in connection with Figs. 4 and 5 point to the important role of the corrections and of the adequate geometry used for the measurements.

References

[1] *Teale, F. W. J., G. Weber:* Biochem. J. **65**, 476 (1957).
[2] *Parker, C. A., W. T. Rees:* Analyst. **85**, 587 (1960).
[3] *Parker, C. A., W. T. Rees:* Analyst. **87**, 83 (1962).
[4] *McDonald, R. J., B. K. Selinger:* Photochem. and Photobiol. **14**, 753 (1971).
[5] *Parker, C. A.:* Photoluminescence of Solutions pp. 19—22 Elsevier, Amsterdam, (1968).
[6] *Pluchennichak, A., G. M. Barenboim:* Biofizika **16**, 773 (1971).
[7] *Budó Á.:* Magyar Fizikai Folyóirat **9**, 269 (1961).
[8] *Förster, Th.:* Fluoreszenz Organischer Verbindungen Vandenhoeck und Ruprecht, Göttingen, (1951).
[9] *Ketskeméty, I., J. Dombi, R. Horvai, J. Hevesi, L. Kozma:* Acta Phys. et Chem. Szeged **7**, 17 (1961).
[10] *Török, M.:* Lumineszkáló anyagok valódi spektrális kvantumhatásfokára vonatkozó újabb vizsgálatok. (Recent Investigations on the True Spectral Yield of Fluorescent Materials; D. Ph. Thesis, in Hungarian.) Szeged, (1967).
[11] *Várkonyi, Z., L. Szalay:* Acta Biochem. Biophys. **9** (3), 255 (1974).
[12] *Vigny, P., M. Duquesne:* Photochem. Photobiol. **20**, 15 (1974).*

* The paper under [12] has been published after the submission of the manuscript, therefore, the results of [12] could not be considered.

ОПРЕДЕЛЕНИЕ ДЕЙСТВИТЕЛЬНЫХ СПЕКТРОВ ФЛУОРЕСЦЕНЦИИ ВОЗБУЖДЕННЫХ БЕЛКОВ

З. Варкони, Л. Салаи

Описаны способы определения действительных спектров возбуждения, получаемые с применением коррекций на реабсорбцию и вторичную флуоресценцию, для разных методов возбуждения и наблюдения. Результаты иллюстрируются спектрами флуоресценции растворов пероксидазы (HRP) лизоцима, детергента тритона X—100 и пероксидазы содержащего в качестве индикатора флуоресцеин-изотиоцианат (FITC).

ВЛИЯНИЕ СТРУКТУРНЫХ ЭЛЕМЕНТОВ РОДАМИНОВЫХ КРАСИТЕЛЕЙ НА ЭФФЕКТИВНОСТЬ ГЕНЕРАЦИИ ИХ РАСТВОРОВ

Б. И. СТЕПАНОВ, А. Н. РУБИНОВ, В. А. МОСТОВНИКОВ
Институт физики АН БССР

(Поступило в редакцию 1 июля 1974 г.)

Исследовано влияние структуры родаминовых красителей на генерационные и флуоресцентные свойства их растворов. При разных условиях ламповой накачки определено влияние отдельных заместителей и мест замещения на параметры генерации.

Требования к спектрально-люминесцентным характеристикам эффективно генерирующих красителей в настоящее время хорошо известны. Однако целенаправленный поиск таких красителей невозможен без установления связи спектрально-люминесцентных и генерационных характеристик со строением молекул [1, 2, 3.]

Для исследования генерационных свойств использовался лазер с ламповой накачкой. Электрическая схема питания импульсных ламп лазера обеспечивала их работу в следующих режимах: *а)* максимальная энергия импульса накачки $E_{нак} = 500$ дж, длительност импульса накачки $t_{нак} = 120$ мксек, время нарастания переднего фронта импульса накачки $\tau_{нак} = 15$ мксек; *б)* $E_{нак} = 500$ дж, $t_{нак} = 30$ мксек, $\tau_{нак} = 2{,}5$ мксек; *в)* $E_{нак} = 300$ дж, $t_{нак} = 1$ мксек, $\tau_{нак} = 0{,}6$ мксек. Названия исследованных красителей, а также спектрально-люминесцентные характеристики их растворов приведены в табл. I—III, где η — квантовый выход люминесценции; $\lambda_{погл.}^{max}$ и $\lambda_{люм}^{max}$ — длины волн, соответствующие максимумам спектров поглощения и люминесценции; $(\lambda_1 - \lambda_2)_{ген}$-спектральный интервал генерации; $K_{\lambda\ ген}^{погл.}$-коэффициент поглощения в области спектра генерации; $K_{погл.}^{max}$-коэффициент поглощения в максимуме полосы; $E_{ген}$-энергия генерируемого излучения; $\tau_{ген}$-длительность импульса генерации; $d_{сум}$-суммарная вероятность безызлучательной дезактивации уровня S_1; P_{S_1-T}-вероятность интеркомбинационного перехода; $U_{пор}$-пороговая энергия накачки. Структурные формулы молекул приведены на рис. 1 и 2.

Перейдем теперь к анализу полученных результатов. В табл. 1 приведены спектральные и генерационные характеристики незамещенного родамина, *N, N′*-диэтилродамина и родамина В (1, 2, 5). Эти красители отличаются степенью замещения водорода при атомах азота этильной группой C_2H_5. Из таблицы видно, что с увеличением степени замещения спектры поглощения, люминесценции и генерации смещаются в красную область. Наиболее высокой люминесцентной способностью характеризуется *N, N′*-диэтилродамин, а наи-

Таблица 1

Режим накачки б, $K_{погл}^{max} = 25\ см^{-1}$

№№ ПП	Краситель	η %	$\lambda_{погл}^{max}$ нм	$\lambda_{люм}^{max}$ нм	$K_{\lambda\ ген}^{погл}$ $см^{-1}$	$U_{пор}$ дж	$E_{ген}$ дж	$\tau_{ген}$ мксек	$(\lambda_1 - \lambda_2)_{ген}$ нм	Номер структурных формул на рис. 1 и 2
1	2	3	4	5	6	7	8	9	10	11
1	Незамещенный родамин	85	505	529	0,033	45	0,13	9	556—567	1
2	*N, N′*-диэтилродамин	93	519	547	0,035	46	0,46	19	579—587	2
3	Родамин 6Ж-Д	99	530	558	0,035		0,9		583—593	3
4	Родамин 6Ж	84	530	551	0,033		0,6		591—604	4
5	Родамин В	62	543	574	0,016		0,3		611—624	5
6	Родамин 3В	61	555	578	0,018		0,37		622—632	6

более низкой — родамин В. Наименьший КПД генерации характерен для незамещенного родамина, имеющего достаточно высокий квантовый выход люминесценции (85%). Таким образом, генерационная способность в данном случае не коррелирует с люминесцентной. Характерно, что пороговая плотность накачки для рассматриваемых красителей в случае режима *б* практически одинакова, но энергия и длительность генерации существенно отличаются. Это свидетельствует о различной скорости нарастания стимулированных потерь, обусловленных, по-видимому, в основном, накоплением молекул в триплетном состоянии.

Спектральные и генерационные характеристики растворов родаминов в сильной степени зависят от этерифицирования карбоксильной группы молекулы. Из табл. I видно, что при этерифицировании карбоксильной группы (переход от *N, N′*-диэтилродамина к родамину 6Ж, а также от родамина В к родамину 3В) квантовый выход люминесценции падает. При этом наблюдается смещение спектров поглощения, люминесценции и генерации в длинноволновую область. Интересно отметить, что падение квантового выхода люминесценции при этерифицировании карбоксильной группы у данных соединений сопровождается значительным ростом генерационной эффективности. Так, например, переход от *N, N′*-диэтилродамина к родамину 6Ж приводит к увеличению КПД генерации в 1,3 раза.

Весьма благоприятное влияние на люминесцентную и генерационную способность родаминов оказывает введение в положения 3 и 7 метильных групп CH_3 [3]. Замещение атомов водорода в положениях 3 и 7 метильными группами вызывает смещение максимума спектра люминесценции на 7 нм в длинноволновую область (ср. №№ 3, 4). Положение максимума полосы

Таблица II

Режим накачки б, $K^{max}_{погл} = 10\ см^{-1}$

№№ ПП	Краситель	η_1 %	$\lambda^{max}_{погл}$ нм	$\lambda^{max}_{люм}$ нм	$K^{погл}_{\lambda\ ген}$ $см^{-1}$	$E_{ген}$ дж	$\tau_{ген}$ мксек	$U_{пор}$ дж	$(\lambda_1-\lambda_2)_{ген}$ нм	$d_{сум}\,10^{-7}$ $сек^{-1}$	$P_{S_1-T}\cdot 10^{-6}$ $сек^{-1}$	Номер структурных формул на рис. 1 и 2
1	2	3	4	5	6	7	8	9	10	11	12	13
7	Незамещенный родамин	85	505	529	0,033	0,0027 0,07*	1,0	3	556—567	4	1,9	7
8	N_1N'-диэтилродамин	93	520	547	0,035	5,008 0,3	1,3	1,92	579—587	1,7	1,2	8
9	N_1N'-дибензилродамин	84	510	540	0,03	0,0033 0,05	1,1	3	576—589	4,2	1,9	9
10	N_1N'—*Ди*—*β*-фенилэтилродамин	84	520	549	0,028	0,0035 0,02	0,8	3,60	588—600	4,4	2,2	10
11	N_1N'—*Ди*—*β*-фенилизопропилродамин	86	530	550	0,016	0,005 0,03	1	3,3	589—604	3,8	2,1	11

* Значения взятые в рамку соответствуют режиму б при $K^{max}_{погл} = 23\ см^{-1}$.

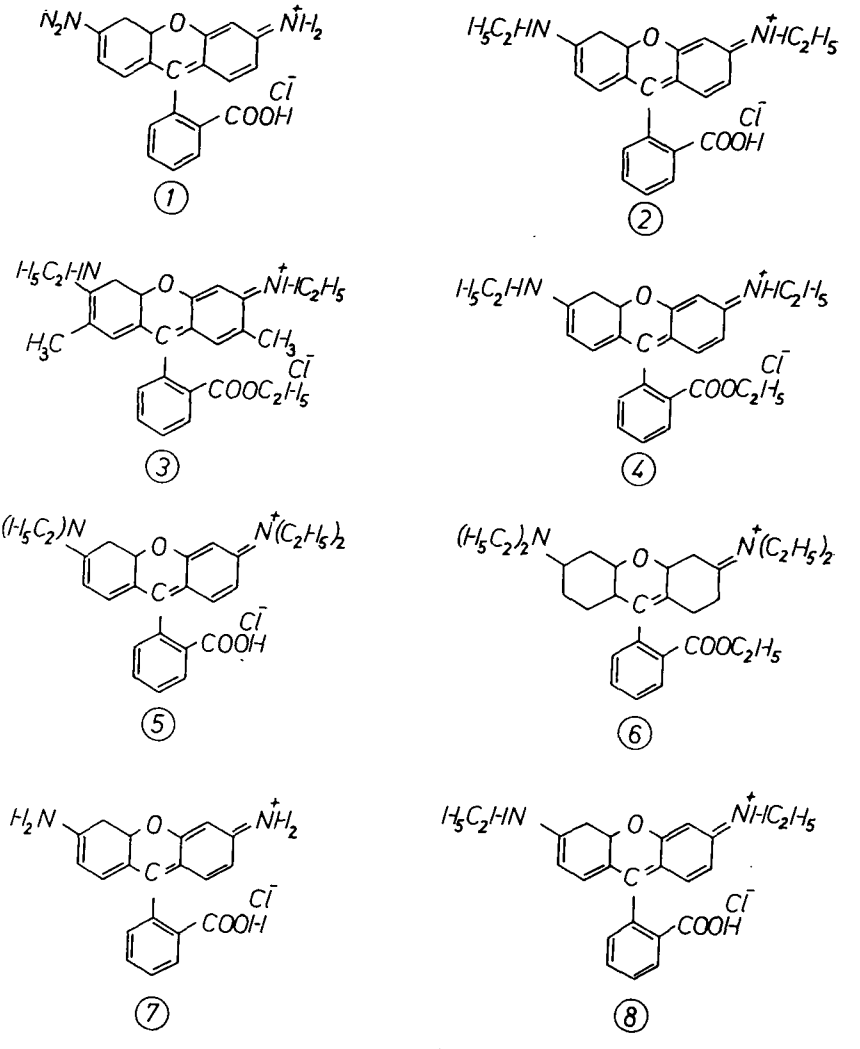

Рис. 1. Структурные формулы молекул

Таблица III

Режим накачки б, $K_{погл}^{нак} = 23\ см^{-1}$

№№ ПП	Краситель	η_1 %	$\lambda_{погл}^{max}$ нм	$\lambda_{люм}^{max}$ нм	$\lambda_{ген}$ нм	$E_{ген}$ дж	Номер структурных формул на рис. 1 и 2
12	Родамин 3В	61	555	578	627	0,022	12
13	Сульфа-родамин	60	550	574	624	0,015	13
14	Родамин *S* (экстра)	47	545	562	626	0,004	14
15	Родамин 3GO	26	535	564	623	0,001	15

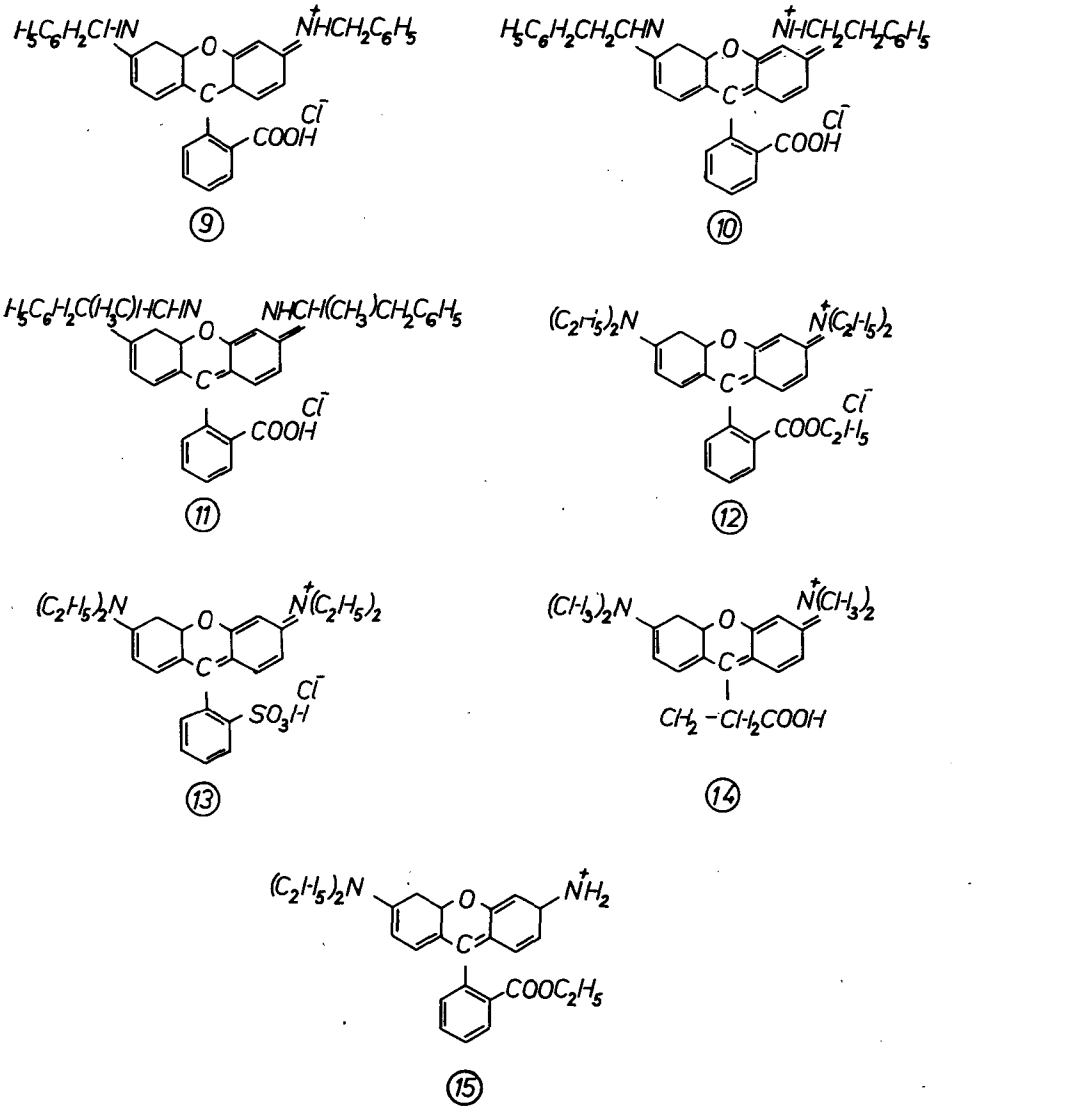

Рис. 2. Структурные формулы молекул

поглощения при этом не изменяется. Квантовый выход люминесценции такого родамина практически равен единице, а КПД генерации возрастает в 1,5 раза по сравнению с родамином 6Ж.

Установлено влияние степени сложности заместителей при атомах азота на эффективность генерации родаминовых красителей (табл. II). Как видно из таблицы, при возбуждении в режиме *в* ($t_{нак} = 1$ мксек) изменение энергии генерации коррелирует с изменением квантового выхода люминесценции. Харак-

терно, что при переходе к более длинным накачкам различие в генерационной эффективности проявляется более четко. Так, например, в случае режима *б* ($t_{нак} = 30$ мксек) энергия генерации *N, N′*-диэтилродамина в 15 раз больше, чем у худшего из представленных красителей, в то время как в режиме *в* эти энергии различались только вдвое. При дальнейшем увеличении длительности (режим *а*) из всех приведенных в таблице красителей генерирует только *N, N′*-диэтилродамин.

Расчет показывает, что изменение вероятности дезактивации триплетного уровня не может объяснить наблюдаемое изменение эффективности генерации. Остается предположить, что оно обусловлено различием вероятностей P_{S_1-T}. Расчетная зависимость порога генерации родамина 6Ж от P_{S_1-T}, полученная для рассматриваемого случая с учетом условий возбуждения, приведена на рис. 3. При помощи этой кривой можно по измеренным значениям порога генерации найти величину P_{S_1-T} для каждого красителя (см. табл. II). Для *N, N′*-диэтил-родамина эта величина оказалась почти вдвое меньше, чем для других красителей.

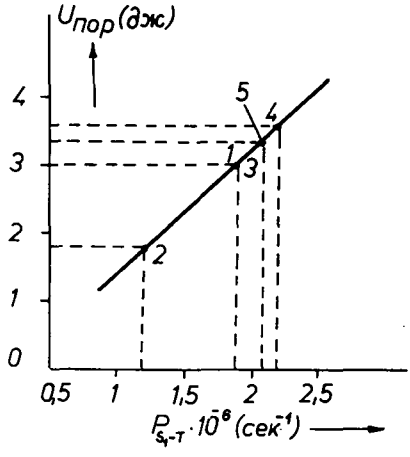

Рис. 3. Расчетная зависимость порога генерации родамина 6Ж от вероятности P_{S_1-T}.

Этот вывод подтверждается тем, что родамины с большим P_{S_1-T} совсем перестают генерировать при уменьшении крутизны переднего фронта импульса накачки (например, режим *а*). Во всех случаях оказалось, что вероятность P_{S_1-T} значительно меньше суммарной вероятности безызлучательной дезактивации $d_{сум}$ синглетного уровня S_1.

В табл. III приведен ряд отличающихся по структуре и симметрии дважды замещенных родаминовых красителей. Так, например, для сульфородамина характерно наличие группы SO_3 в нижнем бензольном кольце скелета молекулы. Это приводит к уменьшению его генерационной эффективности по сравнению с родамином 3В, хотя квантовый выход люминесценции при этом остается практически неизменным. Нарушение симметрии в замещении атомов водорода (родамин 3GO) вызывает сильное падение квантового выхода люминесценции и генерационной эффективности.

Таким образом, даже небольшие структурные изменения родаминовых красителей, не приводящие к существенному изменению спектрально-люминесцентных свойств, оказывают сильное влияние на эффективность генерации. Это можно объяснить следующим образом. Высокая эффективность генерации родаминовых красителей обусловлена прежде всего тем, что в них процесс безызлучательной дезактивации происходит, главным образом, минуя Т-состояние. Вероятность перехода в триплет почти на порядок меньше вероятности безызлучательных переходов посредством внутренней конверсии $d_{S_1-S_0}$. Увеличение этой вероятности в 2 раза, как было показано выше, приводит к уменьшению энергии генерации за счет накопления молекул в триплетном состоя-

нии более чем на порядок. В то же время поскольку вероятность P_{S_1-T} вносит незначительный вклад в тушение люминесценции, то люминесцентная способность остается практически неизменной.

В некоторых случаях ухудшение генерационной эффективности сопровождается значительным возрастанием квантового выхода люминесценции (например, незамещенный родамин и родамин В, *N*, *N'*-диэтилродамин и родамин 6Ж). В этом случае происходит уменьшение суммарной вероятности безызлучательных переходов $d_{S_1-S_0}+P_{S_1-T}$ при абсолютном увеличении вероятности интерконверсии P_{S_1-T}. Расшифровка механизма влияния строения молекул на вероятность P_{S_1-T} в настоящее время затруднительна. Насомненно, что существенную роль в формировании скорости интерконверсии играет находящийся в растворе молекулярный кислород. Это обнаружено нами при исследовании влияния кислорода на эффективность генерации родаминовых красителей.

В заключение, исходя из результатов проведенных исследований, можно предложить ряд симметричных родаминовых красителей (всего 20 соединений), позводляющих получать эффективную генерацию при ламповой накачке в спектральном диапазоне 540—640 нм.

Обобщенная структруная формула соединений этого ряда имеет следующий вид (рис. 4).

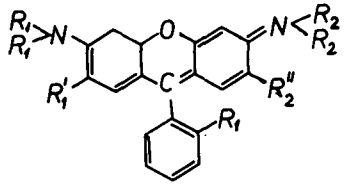

Рис. 4,

где

$R_1 = R_2 = H$; CH_3; C_2H_5;
$R_1' = COOH$; $COOC_2H_5$
$R_1'' = R_2'' = H$; CH_3

Литература

[1] *Мостовников В. А., А. Н. Рубинов, В. И. Авдеева* и др. «Исследование влияния структурных изменений в молекулах полиметиновых красителей на генерационные и спектроскопические характеристики их растворов». Препринт ин-та физики АН БССР. Минск, 1971.
[2] *Drexhage, H. H.:* Laser Focus, March, **35** (1973).
[3] *Pavlopulos, T. G.:* IEEE. J. Quant. Electron. **9**, and **5**, 510 (1973).

INFLUENCE OF STRUCTURAL ELEMENTS OF RHODAMINE DYES ON LASER EFFICIENCY OF THEIR SOLUTIONS

B. I. Stepanov, A. N. Rubinov, V. I. Mostovnikov

The structure of rhodamine dyes has an influence on luminescence and laser properties of their solutions. The influence of several substituents and the position of substituents on the parameters of flash-lamp pumped dye lasers were investigated.

A CONCISE FORMULATION OF FRESNEL'S FORMULAE

By

L. JÁNOSSY

Central Research Institute for Physics, Budapest

(Received June 1, 1974)

It is shown that the well known formulae of Fresnel can be obtained in a rather straightforward way using consequent vector formalism. The aim of the article is to clarify some general questions connected with Maxwell's theory and, in particular, to improve from the didactical point of view the method of derivation of the formulae.

Fresnel's formulae give the relations between polarization and intensities of the beams which appear if a primary beam is reflected on the plane boundary of two homogeneous media. The considerations of Fresnel are well-known and can be regarded as a well established result of classical electrodynamics. From the didactical point of view it is, however, disturbing that the formulae are obtained as a result of tiresome calculations; we shall give presently a rather symmetric treatment of the problem—at the same time we make a few remarks about the physical contents of the theory. We hope that our consideration may facilitate the teaching of this phenomenon.

Maxwell's equations of the electromagnetic field can be written in the form of the wave equations

$$\begin{aligned} \nabla^2 \mathbf{A} - \frac{1}{c^2} \ddot{\mathbf{A}} &= -4\pi \mathbf{i}, \\ \nabla^2 \Phi - \frac{1}{c^2} \ddot{\Phi} &= -4\pi \varrho, \\ \operatorname{div} \mathbf{A} + \frac{1}{c} \dot{\Phi} &= 0. \end{aligned} \tag{1}$$

The charge and current densities arise partly or wholly as charges and currents inside the atoms of the material in which the field spreads. If we consider $\mathbf{P}$ the electric and $\mathbf{I}$ the magnetic polarization of the material, then we can write

$$\begin{aligned} \varrho &= -\operatorname{div} \mathbf{P}, \\ \mathbf{i} &= \frac{1}{c} \dot{\mathbf{P}} + \operatorname{rot} \mathbf{I}, \end{aligned} \tag{2}$$

provided no outer current and charges appear.

One usually supposes

$$\mathbf{P} = \varkappa \mathbf{E}, \quad \mathbf{I} = \chi' \mathbf{B}, \tag{3}$$

where

$$\left.\begin{aligned} 1 + 4\pi\varkappa = \varepsilon, \quad 1 + 4\pi\chi = \mu, \\ \chi' = \chi/\mu, \end{aligned}\right\} \tag{4}$$

ε and μ are the dielectric constant and the magnetic permeability; usually such cases are considered when (3) is valid and ε, χ' and therefore ε, μ are given functions of the coordinate vector $\mathbf{r}$.

We note that for rapidly changing fields (3) cannot be taken to be valid — since the polarizations come about by the displacements and changes of velocities of the atomic electrons. Because of the inertia of the electrons the polarizations follow the field only with some delay. One might *e.g.* suppose in place of the first equation (3) the following dynamical equation

$$\frac{1}{\omega_0^2} \ddot{\mathbf{P}} + \mathbf{P} = \varkappa \mathbf{E}, \tag{3a}$$

where ω_0 is one of the characteristic frequencies of the atom. Introducing the inertia of the electrons by (3*a*) or some more elaborate expressions, one is led to a theory which accounts for the dispersion phenomena of light. We cannot deal with this problem—we note here only that, considering waves of a given frequency ν, we can suppose (3) to be valid in a good approximation only; $\varkappa$ and χ' have to be taken as the dynamical polarization depending on the frequency ν.

We make this remark because it is often incorrectly stated that Maxwell's theory is incomplete as it does not give an account of the phenomena of dispersion. The fact seems, however, that the theory does give the correct description of dispersion phenomena—provided the correct relation between polarization and field strength are made use of. The question of the correct relation between polarization and field is rather a question of describing the structure of matter than one of the theory of the electromagnetic field.* The electromagnetic field strength can be derived from the potentials as

$$\begin{aligned} \mathbf{E} &= -\operatorname{grad} \Phi - \frac{1}{c} \dot{\mathbf{A}}, \\ \mathbf{B} &= \operatorname{rot} \mathbf{A}. \end{aligned} \tag{5}$$

Thus making use of (2) and (3) we find

$$\begin{aligned} \varrho &= -\operatorname{div} \varkappa \mathbf{E} = -\varkappa \operatorname{div} \mathbf{E} - \mathbf{E} \operatorname{grad} \varkappa, \\ \mathbf{i} &= \frac{1}{c} \varkappa \dot{\mathbf{E}} + \chi' \operatorname{rot} \mathbf{B} + \operatorname{grad} \chi' \times \mathbf{B}. \end{aligned} \tag{6}$$

* See *e.g. L. Jánossy:* Theory of relativity based on physical reality, Publishing House of the Hungarian Academy of Sciences, Budapest, 1971. p. 197.

With the help of (5) and (6) the current and charge densities can be expressed in terms of the potentials. If we insert the latter expression into the wave equations (1), we find

$$\nabla^2 \mathbf{A} - \frac{1}{c^2}\ddot{\mathbf{A}} = \frac{4\pi\varkappa}{c}\operatorname{grad}\dot{\Phi} + \frac{4\pi\varkappa}{c^2}\dot{\mathbf{A}} - 4\pi\chi' \operatorname{rot}\operatorname{rot}\mathbf{A} - 4\pi \operatorname{grad}\chi' \times \mathbf{B},$$

$$\nabla^2 \Phi - \frac{1}{c^2}\ddot{\Phi} = -4\pi\varkappa\left(\nabla^2\Phi + \frac{1}{c}\operatorname{div}\dot{\mathbf{A}}\right) + 4\pi\mathbf{E}\operatorname{grad}\varkappa,$$

since

$$\frac{1}{c}\operatorname{div}\dot{\mathbf{A}} = -\frac{1}{c^2}\ddot{\Phi}.$$

The equation can also be written

$$\nabla^2 \mathbf{A} - \frac{1}{V^2}\ddot{\mathbf{A}} + (\varepsilon\mu - 1)\operatorname{grad}\operatorname{div}\mathbf{A} = -4\pi\mu(\operatorname{grad}\chi' \times \mathbf{B}),$$

$$\nabla^2\Phi - \frac{1}{c^2}\ddot{\Phi} = \frac{4\pi}{\varepsilon}\mathbf{E}\operatorname{grad}\varkappa, \tag{7a}$$

$$V = \frac{c}{\sqrt{\varepsilon\mu}}.$$

Thus in homogeneous regions where

$$\operatorname{grad}\chi' = \operatorname{grad}\varkappa = 0,$$

we find

$$\nabla^2 \mathbf{A} - \frac{1}{V^2}\ddot{\mathbf{A}} = 0, \tag{7}$$

$$\operatorname{div}\mathbf{A} = 0, \quad V = \frac{c}{\sqrt{\varepsilon\mu}},$$

when supposing $\Phi = 0$. The latter supposition is permissible, as it can be shown by a more detailed analysis. Particular solutions of (7) can be written as

$$\mathbf{A} = \mathbf{A}_0 \cos(\mathbf{kr} - \omega t + \varphi),$$
$$\mathbf{kA}_0 = 0, \quad k = \omega/V. \tag{8}$$

Thus

$$\mathbf{E} = -\frac{1}{c}\dot{\mathbf{A}} = -\frac{\omega}{c}\mathbf{A}_0 \sin(\mathbf{kr} - \omega t + \varphi),$$
$$\mathbf{B} = \operatorname{rot}\mathbf{A} = -\mathbf{k} \times \mathbf{A}_0 \sin(\mathbf{kr} - \omega t + \varphi), \tag{8a}$$

thus

$$\mathbf{B} = n\frac{\mathbf{k}}{k} \times \mathbf{E}.$$

The general solutions of (7) can be obtained as a superposition of solutions of the form (8). Because of the inertia of the electrons, $V = c/n$ is a function of ω and n is thus the refractive index for the circular frequency ω.

Boundary conditions

Consider two homogeneous regions I and II with velocities $\mathbf{V}^{\mathrm{I}}$ and $\mathbf{V}^{\mathrm{II}}$ and a boundary surface S separating them. The waves propagating in I or in II can be obtained as superpositions of plane waves of the form (8). In the region in the immediate vicinity of S, instead of the homogeneous wave equation (7) the inhomogeneous equations (*7a*) are valid. We can take that in this region χ' and $\varkappa$ change rapidly from the values χ_1' and $\varkappa_1$ which they take up in the one region into values χ_2' and $\varkappa_2$ which they take up in the second region. Owing to those rapid change some of the components of $\mathbf{A}$ and Φ suffer also rapid changes, which can be taken in the limit as discrete jumps of those quantities across S.

The detailed analysis shows that on the boundary S a surface charge density

$$\sigma = 4\pi(P_N^{\mathrm{II}} - P_N^{\mathrm{I}}); \tag{9a}$$

$\mathbf{P}^{\mathrm{I}}$, $\mathbf{P}^{\mathrm{II}}$ and P_N^{I}, P_N^{II} their components perpendicular to S, are the polarization vectors on both sides of S.

Similarly a surface current density $\mathbf{i}$ appears

$$\mathbf{i} = 4\pi(\mathbf{I}_p^{\mathrm{II}} - \mathbf{I}_p^{\mathrm{I}}) \tag{9b}$$

where $\mathbf{I}_p^{\mathrm{II}}$ and $\mathbf{I}_p^{\mathrm{I}}$ are the components of the magnetic polarizations $\mathbf{I}^{\mathrm{II}}$ and $\mathbf{I}^{\mathrm{I}}$ parallel to the surface.

The discontinuity and thus the boundary conditions can be expressed more conveniently in terms of the field strength than of the potentials.*

Denoting by $\mathbf{K}$ the unit vector perpendicular to S, the boundary conditions expressing the presence of the surface charges and currents (*9a*) and (*9b*) can be written as

$$\mathbf{K}(\mathbf{E}^{\mathrm{II}} - \mathbf{E}^{\mathrm{I}}) = -4\pi\mathbf{K}(\mathbf{P}^{\mathrm{II}} - \mathbf{P}^{\mathrm{I}}), \tag{10a}$$

$$\mathbf{K}\times(\mathbf{B}^{\mathrm{II}} - \mathbf{B}^{\mathrm{I}}) = 4\pi\mathbf{K}\times(\mathbf{I}^{(\mathrm{II})} - \mathbf{I}^{(\mathrm{I})}). \tag{10b}$$

The tangential component of $\mathbf{E}$ and the normal components of $\mathbf{B}$ must be continuous* — this can be expressed as

$$\mathbf{K}\times(\mathbf{E}^{(\mathrm{II})} - \mathbf{E}^{(\mathrm{I})}) = 0, \tag{11a}$$

$$\mathbf{K}(\mathbf{B}^{(\mathrm{II})} - \mathbf{B}^{(\mathrm{I})}) = 0. \tag{11b}$$

* This is so because although the waves can be expressed in both regions supposing $\Phi=0$, nevertheless from the Lorentz condition it follows that a discontinuity of $\mathbf{A}$ at the boundary corresponds to a change of Φ; therefore if we want to describe the waves on both sides of S in a form $\Phi=0$ then we have to construct the field in II matching it to that in I and then we have to submit the latter solution to a transformation of gauge to make $\Phi^{\mathrm{II}}=0$.

* The relations

$$\mathrm{rot}\,\mathbf{E} = -\frac{1}{c}\dot{\mathbf{B}} \quad \text{and} \quad \mathrm{div}\,\mathbf{B} = 0$$

are valid in the region of the boundary. From the latter relations follows that the tangential component of $\mathbf{E}$ must be continuous — a discontinuity of this component would leed to infinitely large values of $\dot{\mathbf{B}}$ thus the field would change rapidly until the break in the tangential component of $\mathbf{E}$ vanishes. From $\mathrm{div}\,\mathbf{B}=0$ it follows that the normal component of $\mathbf{B}$ must be continuous in any state of the field.

With the help of (3) and (4), (10*a*, *b*) can be written

$$\mathbf{K}(\varepsilon_{\mathrm{II}}\mathbf{E}^{\mathrm{II}} - \varepsilon_{\mathrm{I}}\mathbf{E}^{\mathrm{I}}) = 0 \tag{11c}$$

$$\mathbf{K}\times\left(\frac{\mathbf{B}^{\mathrm{II}}}{\mu_{\mathrm{II}}} - \frac{\mathbf{B}^{\mathrm{I}}}{\mu_{\mathrm{I}}}\right) = 0. \tag{11d}$$

Thus (11*a*—*d*) give the boundary conditions on the surface S.

The equation of the surface S can be written in a parameter representation

$$\mathbf{r} = \mathbf{K}\times\mathbf{s} \quad \text{if } \mathbf{r} \text{ a point of } S, \tag{12}$$

where $\mathbf{s}$ is arbitrary. If we want the field on both sides of S to satisfy any kind of boundary condition identically in t then it is necessary that the arguments of the wave functions appearing in the fields on both sides of S should be identical. Thus two waves may satisfy a boundary condition if

$$\mathbf{k}(\mathbf{K}\times\mathbf{s}) - \omega t + \varphi = \mathbf{k}'(\mathbf{K}\times\mathbf{s}) - \omega' t + \varphi' \tag{13}$$

where we have made use of (12); $\mathbf{k}$, ω, t and, $\mathbf{k}'$, ω', φ' respectively, are the parameters of the wave to be matched at the surface. From (13) it follows that.

$$\omega = \omega' \quad \varphi = \varphi' \tag{14}$$

and therefore

$$\mathbf{k}(\mathbf{K}\times\mathbf{s}) = \mathbf{k}'(\mathbf{K}\times\mathbf{s}) \tag{15}$$

for all values of $\mathbf{s}$. Since

$$\mathbf{k}(\mathbf{K}\times\mathbf{s}) = \mathbf{s}(\mathbf{k}\times\mathbf{K})$$

(15) is fulfilled then and only then if

$$\mathbf{k}\times\mathbf{K} = \mathbf{k}'\times\mathbf{K}. \tag{16}$$

From (16) it follows that $\mathbf{k}$, $\mathbf{k}'$ and $\mathbf{K}$ lie in one plane. Thus the plane defined by the propagation vectors $\mathbf{k}$ and $\mathbf{k}'$ of two matched waves is perpendicular to the plane S.

Furthermore it follows from (16) that

$$k \sin \vartheta = k' \sin \vartheta' \tag{17}$$

where ϑ and ϑ' are the angles between the vectors $\mathbf{k}$, $\mathbf{k}'$ and $\mathbf{K}$; thus in accordance with

$$\frac{\sin \vartheta}{\sin \vartheta'} = \frac{V}{V'}.$$

If $V = V_{\mathrm{I}}$, $V' = V_{\mathrm{II}}$, then (10) gives the Snellius law; considering, however, two waves on the same side of S, then we have $V = V'$, and $\vartheta \neq \vartheta'$ can only be satisfied if

$$\vartheta' = \pi - \vartheta;$$

thus we obtain the law of reflection. We obtained thus the connection between the wave vectors of waves which match on the surface S.

To match the fields on both sides of S the amplitudes of the fields have also to be matched.

Considering one wave in each of the regions we obtain an overdetermined set of equations—therefore the matching is only possible if at least three waves are considered. This corresponds to the fact that one wave approaching the surface *e.g.* coming through I, this wave produces a reflected wave returning into I and a refracted wave autcoming into II. The amplitude of the vector potentials can be denoted, using the suffies 0, 1, 2, thus

$\mathbf{A}_0$, $\mathbf{k}_0$ describe the incident wave,

$\mathbf{A}_1$, $\mathbf{k}_1$ describe the reflected wave,

$\mathbf{A}_2$, $\mathbf{k}_2$ describe the refracted wave.

As the vector potentials are perpendicular to the directions of propagation, we can express them in terms of components in the directions $\mathbf{M}$ and $\mathbf{k}_m \times \mathbf{M}$, thus

$$\mathbf{A}_m = a_m \mathbf{M} + b_m(\mathbf{k}_m \times \mathbf{M}).$$

The boundary condition contains the electric field strength its amplitudes can be written, since $\omega/c = k_m/n_m$ as

$$\mathbf{E}_m = \frac{k_m}{n_m}\left(a_m \mathbf{M} + b_m(\mathbf{k}_m \times \mathbf{M})\right). \tag{18}$$

The amplitudes of the magnetic field strength are

$$\mathbf{B}_m = \mathbf{k}_m \times \mathbf{A}_m.$$

We find thus easily

$$\mathbf{B}_m = -n_m k_m b_m \mathbf{M} + a_m(\mathbf{k}_m \times \mathbf{M}). \tag{19}$$

The boundary condition for components of the field strength; in accord with (11*a*—*d*) can be written

$$\begin{aligned}
\mathbf{K}(\varepsilon_2 \mathbf{E}_2 - \varepsilon_1 \mathbf{E}_1) &= \mathbf{K}\varepsilon_0 \mathbf{E}_0, \\
\mathbf{K}(\mathbf{B}_2 - \mathbf{B}_1) &= \mathbf{K}\mathbf{B}_0, \\
\mathbf{K} \times (\mathbf{E}_2 - \mathbf{E}_1) &= \mathbf{K} \times \mathbf{E}_0, \\
\mathbf{K} \times \left(\frac{\mathbf{B}_2}{\mu_2} - \frac{\mathbf{B}_1}{\mu_1}\right) &= \mathbf{K} \times \frac{\mathbf{B}_0}{\mu_0}.
\end{aligned} \tag{20}$$

Giving the values of a_0, b_0 *i.e.* intensity and polarization of the incident beam, (20) gives six equations for the four coefficients a_m, b_m, $m = 1, 2$. The system is, however, not overdetermined as we find that among the six equations obtained, two pairs are identical; indeed, introducing (18) and (19) into (20) there are only four different ones. The result of a short calculation shows that (20) reduces to

$$\begin{aligned}
\varepsilon_2 b_2 - \varepsilon_1 b_1 &= \varepsilon_0 b_0 \\
(\mathbf{k}_2 \mathbf{K}) b_2 - (\mathbf{k}_1 \mathbf{K}) b_1 &= (\mathbf{k}_0 \mathbf{K}) b_0
\end{aligned} \tag{21}$$

and

$$a_2 - a_1 = a_0$$
$$\frac{\mathbf{k}_2\mathbf{K}}{\mu_2} a_2 - \frac{\mathbf{k}_1\mathbf{K}}{\mu_1} a_1 = \frac{\mathbf{k}_0\mathbf{K}}{\mu_0} a_0. \tag{22}$$

We see thus that the equations separate automatically into two sets, one containing the amplitudes of the components polarized in the direction of **M**, thus components polarized parallel to *S*. The other set of equations gives the components polarized perpendicular to **M**. We see thus that the consequent calculation leads automatically to the separation of the two states of polarization.

The explicite solutions of (21) and (22) can be written as follows,

$$b_1 = -\frac{(\varepsilon_2\mathbf{k}_0 - \varepsilon_0\mathbf{k}_2)\mathbf{K}}{(\varepsilon_2\mathbf{k}_1 - \varepsilon_1\mathbf{k}_2)\mathbf{K}} \cdot b_0$$

$$b_2 = -\frac{(\varepsilon_1\mathbf{k}_0 - \varepsilon_0\mathbf{k}_1)\mathbf{K}}{(\varepsilon_2\mathbf{k}_1 - \varepsilon_1\mathbf{k}_2)\mathbf{K}} \cdot b_0 \tag{23}$$

$$a_1 = -\frac{\left(\frac{\mathbf{k}_0}{\mu_0} - \frac{\mathbf{k}_2}{\mu_2}\right)\mathbf{K}}{\left(\frac{\mathbf{k}_1}{\mu_1} - \frac{\mathbf{k}_2}{\mu_2}\right)\mathbf{K}} \cdot a_0$$

$$a_2 = -\frac{\left(\frac{\mathbf{k}_0}{\mu_0} - \frac{\mathbf{k}_1}{\mu_1}\right)\mathbf{K}}{\left(\frac{\mathbf{k}_1}{\mu_1} - \frac{\mathbf{k}_2}{\mu_2}\right)\mathbf{K}} \cdot a_0.$$

The expressions (23) are equivalent with the well-known expressions of Fresnel. We note, that one should insert into (22)

$$\varepsilon_0 = \varepsilon_1 = \varepsilon_{\mathrm{I}} \quad \varepsilon_2 = \varepsilon_{\mathrm{II}}$$
$$\mu_0 = \mu_1 = \mu_{\mathrm{I}} \quad \mu_2 = \mu_{\mathrm{II}}$$

where ε_{I}, $\varepsilon_{\mathrm{II}}$, μ_{I} and μ_{II} are the dielectric constants and permeabilities in the regions I and II.

ЧЁТКАЯ ФОРМУЛИРОВКА ФОРМУЛ ФРЕНЕЛЯ

Л. Яноши

Показано, что хорошо известные формулы Френеля можно получить простым путём при последовательном использовании векторного формализма. Главная цель работы — осветить некоторые общие вопросы, связанные с теорией Максвелла, и, в частности, улучшить с дидактической точки зрения метод получения формул.

EFFECTS PRODUCED BY EXCITATION TRANSFER BETWEEN LUMINESCENT MOLECULES IN FLUORESCENT SOLUTIONS

By

A. JABŁOŃSKI

Institute of Physics, Nicholas Copernicus University, Toruń

(Received June 1, 1974)

The method of treating the problem of effects produced by excitation transfer between luminescent molecules in fluorescent solutions, put forward by the author, is further developed and extended to the case of solutions containing different kinds of dissolved luminescent molecules.

The considerations described below are devoted to the problem of effects produced by excitation transfer between luminescent molecules (*LM*s) in (rigid) solutions. Several methods of treating this problem were already proposed (for references see *e.g.* [4]; a critical review of theories published before 1968 is given in a paper by KNOX [5]). One of these was put forward by the present writer [4]. It was applied so far to solutions of identical *LM* only. Our aim is to develop further the theory and to extend its application to solutions containing two (or more) kinds of dissolved *LM*. In our treatment the notion of a luminescent centre (*LC*) plays an essential role.

A *LC* is assumed to consist of a donor molecule (*D*) situated in the centre of its "active sphere" in which also a few acceptor molecules (*A*s) may be present. By we denote a *LM* excited directly by the exciting light, and by *A* a *LM* unexcited at the moment of the excitation of *D*. The radius of the active sphere may be chosen somewhat arbitrarily, but most be in any case large enough to allow direct excitation transfer from *D* to *A*s situated outside the active sphere to be neglected, but otherwise rather small for convenience of calculation. In the following the intensity of the exciting light is assumed to be low enough practically not to affect the numerical density of unexcited *LM*s in the solution and to make possible for more than one *D* to appear in a practically negligeable *LC* (this would be not the case if *e.g.* intensive laser light were used for excitation).

In an excited solution, various *LC*s containing various numbers of *A*s will appear with different probabilities. The derivation of expressions for the probability distribution of *LC* given below is based on SMOLUCHOWSKI's theory of fluctuations [6]. Smoluchowski derived among others an expression for the probability $W(n)$ of n molecules appearing in an volume element of a perfect gas [6]. Later on he has shown that the same expression is valid in the case of colloidal solutions. The fact that the colloidal particles can be observed directly by means of a microscope per-

mitted to TH. SVEDBERG the experimental verification of Smoluchowski's theory. The results obtained agree very well with the theoretical predictions [7]. In the simplest case of solutions containing only one kind of dissolved *LM*, Smoluchowski's expression for $W(n)$ can be even directly applied without any modification to the probability distribution of various *LC*s (as was already done in [4]), in cases when the influence of intermolecular forces on this distribution can be neglected.

A *LC* is created at the moment in which a *LM* becomes excited, *i.e.*, it becomes a *D*. The probability $P(k)$ that the created *LC* contains, apart from *D*, $(k-1)$ *A*s (k denoting the total number of *LM*s in the centre) is given, as mentioned above, by Smoluchowski's distribution (=Poisson distribution) which reads in our notations

$$P(k) = e^{-\chi}\frac{\chi^{k-1}}{(k-1)!}, \quad k = 1, 2, 3, \ldots \tag{1}$$

fulfilling the condition

$$\sum_{k=1}^{\infty} P(k) = 1. \tag{2}$$

Here $\chi = \frac{4}{3}\pi R_a^3 N = vN$, where v cm^3 is the volume of the active sphere (of radius R_a) and N cm^{-3} the numerical density of unexcited *LM*s in the solution.

In each particular centre, the following processes will occur after the moment of excitation: excitation transfers and back transfers between pairs of *LM* with a rate μ depending on the mutual distances and orientations of *LM*s, and decay of the excited *LM*s due to emission of fluorescence and to radiationless transitions. Due to transfers of excitation from *D* to *A*s, the *A*s become excited and can emit fluorescence, thus causing a partial depolarization of fluorescence of the solution.

This results from the fact that the emission anisotropy (*EA*) of fluorescence of *A*s is always very low [3]. In rigid or very viscous solutions considered here, the *EA* of *D* fluorescence is usually rather high. Thus the *EA* of fluorescence may be neglected in a fair approximation.

Our principal aim is to give an expression for the mean value of $EA\langle r\rangle$ of steadily excited fluorescence as a function of concentration of the solution. The probabilities of emission by *D* and by *A*s in each particular centre appear in this expression. First of all these probabilities must be determined for a particular configuration of *LM*s in the *LC* and then averaged (by means of a computer) over all possible configurations in this centre.

Let us illustrate the procedure on a simple example of a *LC* containing one *A*. Let γ denote the probability for unit time of transition with emission of fluorescence, q that of radiationless transition, μ the rate of excitation transfer between *D* and *A* for a particular configuration (mutual distances and orientations of *D* and *A*), p_D and p_A the probabilities of *D* and *A*, respectively, being excited. We have to solve the following set of two coupled differential equations:

$$\frac{dp_D}{dt} = -(\gamma+q+\mu)p_D + \mu p_A \tag{3}$$

and

$$\frac{dp_A}{dt} = -(\gamma+q+\mu)p_A + \mu p_D. \tag{4}$$

The solution with the initial conditions $p_D=1$ and $p_A=0$ for the moment of excitation $t=0$ reads:

$$p_D(t) = \frac{1}{2}(e^{-(\gamma+q)t} + e^{-(\gamma+q+2\mu)t}), \tag{5}$$

$$p_A(t) = \frac{1}{2}(e^{-(\gamma+q)t} - e^{-(\gamma+q+2\mu)t}). \tag{6}$$

The probability of emission by D is

$$F_D = \gamma \int_0^\infty p_D\,dt = \eta\frac{1+\mu\eta\tau_0}{1+2\mu\eta\tau_0} \tag{7}$$

and that by A

$$F_A = \gamma \int_0^\infty p_A\,dt = \eta\frac{\mu\eta\tau_0}{1+2\mu\eta\tau_0}. \tag{8}$$

The probability of the conversion of excitation energy into heat by D is

$$Q_D = q \int_0^\infty p_D\,dt = (1-\eta)\frac{1+\mu\eta\tau_0}{1+2\mu\eta\tau_0} \tag{9}$$

and that by A

$$Q_A = (1-\eta)\frac{\mu\eta\tau_0}{1+2\mu\eta\tau_0}. \tag{10}$$

The following substitutions were made in Eqs. (7)—(10):

$$\tau_0 = \frac{1}{\gamma} \quad \text{and} \quad \eta = \frac{\gamma}{\gamma+q} \quad (\eta \text{ is the yield of fluorescence}).$$

Clearly $F_D+F_A=\eta$ and $Q_D+Q_A=1-\eta$. Eqs. (7) and (8) were already obtained by FÖRSTER [1] and later (without knowledge of Förster's paper) in a different way and differently normalized by myself [2, 3], where an error is corrected.

Since μ depends on mutual distances and orientations of LM the values of F_D, F_A, Q_D and Q_A given by Eqs. (7)—(10) depend on values of μ. By averaging these expressions over all distances and orientations of LM (over all μ occurring in the centre) one obtains the mean values $\langle F_{D2}\rangle$, $\langle F_{A2}\rangle$, $\langle Q_{D2}\rangle$ and $\langle Q_{A2}\rangle$, being the respective probabilities of emission by D and by A and those of the conversion of the excitation energy into heat by D and by A. Such calculation was already performed for $\mu = \frac{F^2}{\tau_0}\left(\frac{R_0}{R}\right)^6$, where F^2 is the orientational factor and R the mutual distance of LMs [3].

In the general case of a LC containing k LMs, a set of k coupled differential equations must be solved and the obtained expressions for F_{Dk}, F_{Ak}, Q_{Dk} and Q_{Ak} averaged over all configurations. The mean values of these quantities $\langle F_{Dk}\rangle$, $\langle F_{Ak}\rangle$, $\langle Q_{Dk}\rangle$ and $\langle Q_{Ak}\rangle$ thus obtained are the probabilities of emission and conversion into heat by D and As, respectively.

If the probability distribution $P(k)$ of LC (Eq. (1)) is taken into account, the corresponding probabilities $\overline{F_D}$, $\overline{F_A}$, $\overline{Q_F}$ and $\overline{Q_A}$ for the whole solution can be obtained:

$$\overline{F_D} = \sum_{k=1}^{\infty} P(k)\langle F_{Dk}\rangle = e^{-\chi} \sum_{k=1}^{\infty} \frac{\chi^{k-1}}{(k-1)!}\langle F_{Dk}\rangle, \tag{11}$$

$$\overline{F_A} = e^{-\chi} \sum_{k=1}^{\infty} (k-1)\frac{\chi^{k-1}}{(k-1)!}\langle F_{Ak}\rangle = e^{-\chi}\chi \sum_{k=2}^{\infty} \frac{\chi^{k-2}}{(k-2)!}\langle F_{Ak}\rangle, \tag{12}$$

$$\overline{Q_D} = e^{-\chi} \sum_{k=1}^{\infty} \frac{\chi^{k-1}}{(k-1)!}\langle Q_{Dk}\rangle, \tag{13}$$

and

$$\overline{Q_A} = e^{-\chi}\chi \sum_{k=2}^{\infty} \frac{\chi^{k-2}}{(k-2)!}\langle Q_{Ak}\rangle. \tag{14}$$

The quantum yield $\bar{\eta}$ of the solution (the meaning $\bar{\eta}$ being not the same as that of η in Eqs. (7)—(10)) is

$$\bar{\eta} = \frac{\overline{F_D} + \overline{F_A}}{\overline{F_D} + \overline{F_A} + \overline{Q_D} + \overline{Q_A}}. \tag{15}$$

The emission anisotropy (EA) of fluorescence of the solution, if the EA of fluorescence of As is neglected, reads

$$r = r_0 \frac{\overline{F_D}}{\overline{F_D} + \overline{F_A}}, \tag{16}$$

where r_0 denotes the EA of fluorescence emitted by D.

Let us now consider the case of mixed solutions containing two kinds of dissolved LM, m and m'. If the solution is excited by monochromatic light absorbed by both m and m', two groups of LX with different donors D and D' are created: D-centres and D'-centres.

The relative numbers of these centres depend on the ratio of the numerical densities $\frac{N}{N'}$ of m and m' and their molar absorption coefficients $\frac{\alpha}{\alpha'}$ for the absorbed light.

These relative numbers may be written as

$$W_D = \frac{N\alpha}{N\alpha + N'\alpha'} = \frac{\chi\alpha}{\chi\alpha + \chi'\alpha'} \quad \text{for } D\text{-centres} \tag{17}$$

and

$$W_{D'} = \frac{N'\alpha'}{N\alpha + N'\alpha'} = \frac{\chi'\alpha'}{\chi\alpha + \chi'\alpha'} \quad \text{for } D'\text{-centres} \tag{18}$$

where $\chi = vN$ and $\chi' = vN'$, v being the volume of the active sphere.

The probability that a LC is a D-centre containing k m-molecules $(1D+(k-1)As)$ and l m'-molecules (l A's) is the product of the corresponding probabilities multiplied with W_D:

$$P_{kl} = \frac{\alpha\chi}{\alpha\chi+\alpha'\chi'} e^{-(\chi+\chi')} \frac{\chi^{k-l}}{(k-l)!} \frac{\chi'^{l}}{(l!)}, \tag{19}$$

$$k = 1, 2, 3, \ldots \quad \text{and} \quad l = 0, 1, 2, 3, \ldots .$$

The corresponding expression for D'-centres is

$$P'_{lk} = \frac{\alpha'\chi'}{\alpha\chi+\alpha'\chi'} e^{-(\chi+\chi')} \frac{\chi'^{l-1}}{(l-1)!} \frac{\chi^{k}}{k!}, \tag{20}$$

$$l = 1, 2, 3, \ldots \quad \text{and} \quad k = 0, 1, 2, 3, \ldots$$

Eqs. (19) and (20) are so normalized that

$$\sum_{k=1}^{\infty} \sum_{l=0}^{\infty} P_{kl} + \sum_{l=1}^{\infty} \sum_{k=0}^{\infty} P'_{lk} = 1.$$

In a way similar to that used in Eqs. (4)—(10), various quantities for each particular LC have to be calculated. Let the probabilities of emission by D, by an A and by an A', respectively, averaged over all configurations in a Dkl centre be denoted by $\langle F_{Dkl}\rangle$, $\langle F_{Akl}\rangle$ and $\langle F_{A'kl}\rangle$ for and those of the conversion into heat due to radiationless transitions in D, A and A', by $\langle Q_{Dkl}\rangle$, $\langle Q_{Akl}\rangle$ and $\langle Q_{A'kl}\rangle$, respectively. The corresponding values for the total solution (for all D-centres) are

$$\overline{F_D} = \sum_{k=1}^{\infty} \sum_{l=0}^{\infty} P_{kl} \langle F_{Dkl}\rangle, \tag{21}$$

$$\overline{F_A} = \sum_{k=1}^{\infty} \sum_{l=0}^{\infty} P_{kl}(k-1) \langle F_{Akl}\rangle, \tag{22}$$

$$\overline{F_{A'}} = \sum_{k=1}^{\infty} \sum_{l=0}^{\infty} P_{kl}\, l \langle F_{A'kl}\rangle \tag{23}$$

$$\overline{Q_D} = \sum_{k=1}^{\infty} \sum_{l=0}^{\infty} P_{kl} \langle Q_{Dkl}\rangle, \tag{24}$$

$$\overline{Q_A} = \sum_{k=1}^{\infty} \sum_{l=0}^{\infty} P_{kl}(k-1) \langle Q_{Akl}\rangle, \tag{25}$$

$$\overline{Q_{A'}} = \sum_{k=1}^{\infty} \sum_{l=0}^{\infty} P_{kl}\, l \langle Q_{A'kl}\rangle. \tag{26}$$

Similar expressions for the D'-centres ($\overline{F'_{D'}}$, $\overline{F'_{A'}}$, $\overline{F'_A}$, $\overline{Q'_{D'}}$, $\overline{Q'_{A'}}$, $\overline{Q'_A}$) result if P'_{lk} and D' are used instead of P_{kl}, and k and l are interchanged. The obtained values of $\overline{F_D}$ etc. and those of $\overline{F'_{D'}}$ etc. depend on the assumptions made, and in particular on those concerning the transfer and the back transfer of excitation between LMs

of the same and different type. The pertinent calculations were started by H. CHEREK of this Institute (private communication). Let us give some expressions which may be useful in certain applications. The ratio of the intensities of fluorescence bands emitted by m and m' is

$$\frac{J}{J'} = \frac{\overline{F_D} + \overline{F_A} + \overline{F'_A}}{\overline{F'_{D'}} + \overline{F'_{A'}} + \overline{F_{A'}}}. \tag{27}$$

The emission anisotropy of fluorescence emitted by m-molecules is given by

$$r = r_0 \frac{\overline{F_D}}{\overline{F_D} + \overline{F_A} + \overline{F'_A}}, \tag{28}$$

where r_0 is the emission anisotropy of fluorescence of D.

The corresponding expression for fluorescence of m' reads

$$r' = r'_0 \frac{\overline{F'_{D'}}}{\overline{F'_{D'}} + \overline{F'_{A'}} + \overline{F_{A'}}}. \tag{29}$$

By means of Eqs. (21)—(26) one obtains for the fraction ΔE of the total energy E absorbed by D-centres transferred in these centres to A's

$$\Delta E = E \frac{\overline{F_{A'}} + \overline{Q_{A'}}}{\overline{F_D} + \overline{F_A} + \overline{F_{A'}} + \overline{Q_D} + \overline{Q_A} + \overline{Q_{A'}}}. \tag{30}$$

The quantum yield of the total fluorescence emitted by D-centres (emitted both by m and m') reads

$$\bar{\eta} = \frac{\overline{F_D} + \overline{F_A} + \overline{F_{A'}}}{\overline{F_D} + \overline{F_A} + \overline{F_{A'}} + \overline{Q_D} + \overline{Q_A} + \overline{Q_{A'}}}. \tag{31}$$

Expressions similar to those given by Eqs. (30) and (31) may be easily written for D'-centres.

In the case when $\alpha' = 0$, all $P'(lk) = 0$, and only one group of centres is created (see Eq. (22)). Eq. (20) becomes simply

$$P_{kl} = e^{-(\chi+\chi')} \frac{\chi^{k-1}}{(k-1)!} \frac{\chi'^{l}}{l!}. \tag{20a}$$

Let us remark that Eq. (19) for $\chi' = 0$ becomes identical with Eq. (1). The expressions given in this paper for the case of fluorescent solutions containing two kinds of dissolved LM may be very easily extended to solutions containing more than two kinds of LM.

The number of terms which must be taken into account in expressions given here in the form of infinite series depends on the concentration of the solution and must be determined for each particular case separately.

References

[1] *Förster, T.:* Ann. Phys. **2**, 55 (1948).
[2] *Jabłoński, A.:* Acta Phys. Polon. **14**, 295 (1955).
[3] *Jabłoński, A.:* Acta Phys. Polon. **A38**, 453 (1970).
[4] *Jabłoński, A.:* Acta Phys. Polon. **A41**, 85 (1972).
[5] *Knox, R. S.:* Physica **39**, 361 (1968).
[6] *Smoluchowski, M.:* Boltzmann-Festschrift p. 626 (1904); Phys. ZS, **13**, 1906 (1912).
[7] *Smoluchowski, M.:* Sitzungsberichte der Akademie der Wissenschaften in Wien, mathem.-naturw. Klasse, 123, Abt IIa, 2381 (1914), see also: Oeuvres de M. Smoluchowski Vol. I (1924) and Vol. II (1927), publiés sous les auspices de l'Académie Polonaise des Sciences et de Lettres (Cracovie).

ЭФФЕКТЫ, ВЫЗВАННЫЕ ПЕРЕНОСОМ ВОЗБУЖДЕНИЯ МЕЖДУ ЛЮМИНЕСЦИРУЮЩИМИ МОЛЕКУЛАМИ, В ФЛУОРЕСЦИРУЮЩИХ РАСТВОРАХ

А. Яблонски

Метод трактовки проблемы эффектов, вызванных переносом возбуждения между молекулами в флуоресцирующих растворах, выдвинутый автором, распространяется на случай растворов, содержащих различные сорта растворенных люминесцентных молекул.

MIGRATION OF EXCITATION ENERGY IN DYE—DETERGENT SYSTEMS*

By

J. HEVESI and ZS. RÓZSA

Institute of Biophysics, József Attila University, Szeged

(Received June 1, 1974)

In dye-detergent solutions of methylene blue and thionine the migration of electron excitation energy from thionine (donor) to methylene blue (acceptor) can be observed. This process was studied by the examination of the fluorescence spectra of $2 \cdot 10^{-6}$ to $1 \cdot 10^{-4}$ equimolar solutions with sodium lauryl sulphate detergent. For each dye concentration there is an "optimal" detergent concentration at which the energy transfer is most efficient. This transfer is observed at the critical micelle concentration ($3.5 \cdot 10^{-3}$ M detergent concentration) in $2 \cdot 10^{-6}$ M solution and shifts to higher concentration with increasing dye concentration. This result proves that the effectivity of the energy transfer in dye-detergent systems depends on the dye concentration.

Introduction

It is well known that micelle systems are suitable models for studying the processes—first of all the migration of electron excitation energy—taking place in photosynthesizing *in vivo* systems [1]. Micelles were applied as model for studying the energy transfer by TEALE [2]. SINGHAL *et al.* [3] studied the migration of electron excitation energy from thionine (Th) to methylene blue (MB) in micelles. The most efficient energy transfer was observed at the critical micelle concentration (c.m.c.) of the detergent and at equivalent concentrations of the dyes applied.

The influence of temperature on the structure of dye-detergent systems and on the migration of electron excitation energy has been investigated by HEVESI *et al.* [4]. The results showed that the efficiency of the energy transfer from Th to MB was the highest at c.m.c. and at 25 °C temperature. This conclusion was drawn from the experimental results that, in the case of Th and MB ions adsorbed into the micelles, the quenching of Th luminescence was mainly due to intermolecular energy transfer from Th to MB. The influence of temperature on the energy migration was also studied in [5] and the results reported in [4] were corroborated. It was shown further in [5] that the effectivity of the energy migration is very closely connected with the number of the micelles present in the system and with the structure of the dye-detergent solution.

* Delivered at the International Conference on the Excited States of Biological Molecules, Lisbon, 1974.

The aim of the present work was to investigate the influence of changes in dye concentration on the effectivity of the excitation energy transfer. Since this process can be tracked by the changes in luminescence intensities of the donor and those of the acceptor, the luminescence properties of the dye-detergent solutions had to be studied.

Experimental results and discussion

The systems examined were aqueous solutions of sodium lauryl sulphate (SLS) containing thionine (Th) and methylene blue (MB) in equal concentrations. The concentrations of the dyes were varied from $2 \cdot 10^{-6}$ to $1 \cdot 10^{-4}$ M, that of the detergent between 2 and $8 \cdot 10^{-3}$ M. The experimental methods and conditions used are described in [1] and [5].

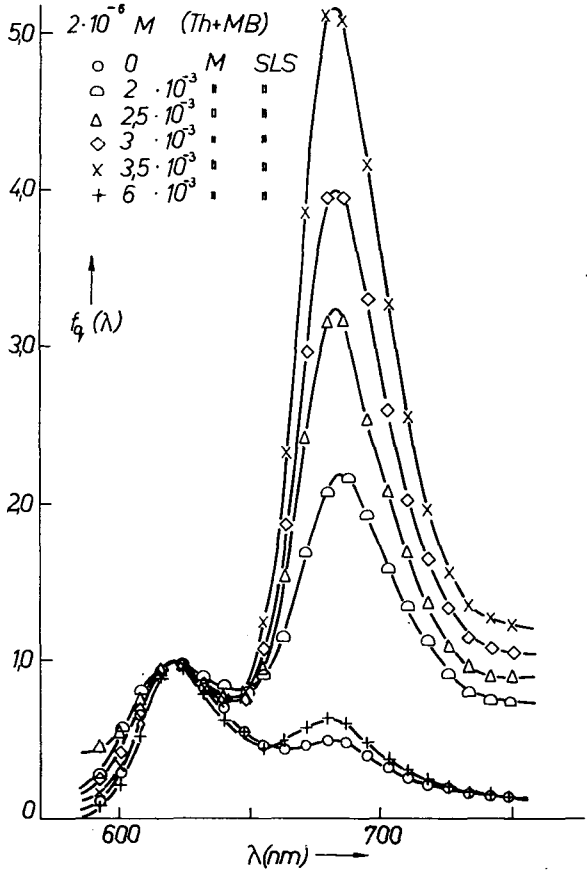

Fig. 1. Fluorescence spectra of mixed solutions of Th+MB of $2 \cdot 10^{-6}$ mol/l dye concentration at different SLS concentrations

Figs. 1, 2 and 3 show the fluorescence spectra at different SLS concentrations for $2 \cdot 10^{-6}$, $1 \cdot 10^{-5}$ and $5 \cdot 10^{-5}$ M dye concentrations excited at 546 nm, in the region of Th absorption. They show that in the aqueous solutions the fluorescence intensity of Th is about double compared to that of MB for each dye concentration. Adding, however, detergent to the solutions, the relative fluorescence intensity of MB increases with increasing detergent concentration up to a maximum which depends on the dye concentration. For $2 \cdot 10^{-6}$ M concentrations of the dyes the

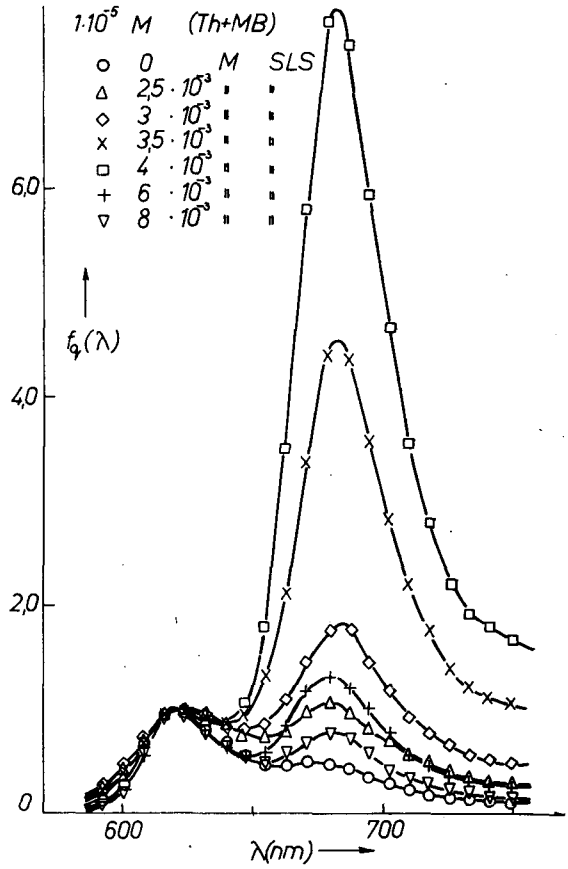

Fig. 2. Fluorescence spectra of mixed solutions of Th+MB of $1 \cdot 10^{-5}$ mol/l dye concentration at different SLS concentrations

maximum is at $3.5 \cdot 10^{-6}$ M SLS concentration, and the fluorescence intensity of MB is about five times higher than that of Th (Fig. 1). The increase in detergent concentration causes a decrease in the relative intensity of MB fluorescence. The relative fluorescence intensity of MB in solutions of $1 \cdot 10^{-5}$ M dye concentration

has a maximum at $4 \cdot 10^{-3}$ M SLS concentration and its value is almost eight times higher (Fig. 2). At higher SLS concentration, a decrease in the fluorescence intensity of MB can be observed again. In solutions of $5 \cdot 10^{-5}$ M dye concentration the fluorescence intensity of MB has a maximum at $6 \cdot 10^{-3}$ M SLS concentration and it is more than eight times higher than that of Th (Fig. 3). The observation of the high increase in the fluorescence intensity of MB at a given SLS concentration is explained by the transfer of electron excitation energy of Th to MB. The effectivity of this transfer depends on the concentration of SLS. For each dye concentration there is an "optimal" SLS concentration at which the transferred energy is most

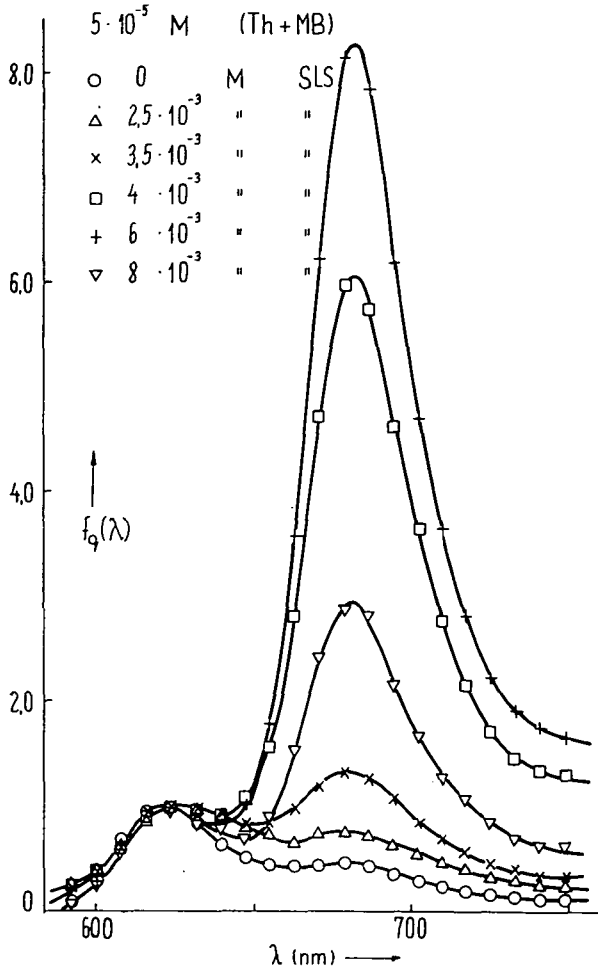

Fig. 3. Fluorescence spectra of mixed solutions of Th+MB of $5 \cdot 10^{-5}$ mol/l dye concentration at different SLS concentrations

efficiently used for the sensitization of the fluorescence of MB. Below c.m.c. there are no micelles and the dye molecules are randomly distributed with an avarage distance leading to a given transfer frequency. Above c.m.c. micelles are present in the solution, their number is increasing with the increase of the concentration of SLS. The dye molecules are concentrated within the micelles, therefore the mean distance of the molecules is less and the transfer frequency is higher. With the increase of concentration of SLS the number of micelles is increasing and the number of dye molecules within a micelle is smaller, their distribution is more random, therefore their mean distance is greater again. This leads to a smaller transfer frequency.

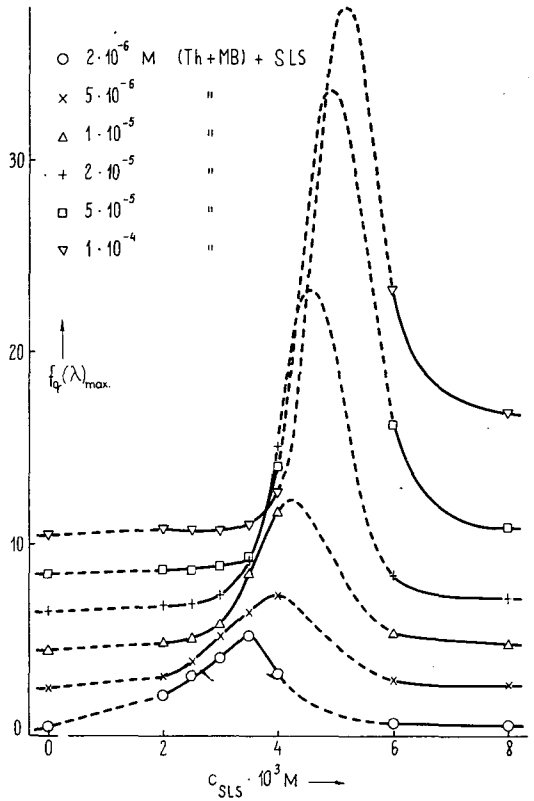

Fig. 4. Ratios of the fluorescence intensities of MB and Th as a function of SLS concentration at different dye concentrations

The picture is more complex due to the presence of aggregates, but the concentration-dependent aggregation leading to a quenching of fluorescence runs parallel with the change of the mean distances of molecules, therefore both transfer and quenching contribute to the changes of fluorescence intensity in the same sense.

Fig. 4 shows the relative fluorescence intensities of MB *vs.* SLS concentration for different dye concentrations. (The zero points of the curves are shifted by two units for better discernment.) It can be seen from the figure that at increasing dye concentrations, the optimal detergent concentration becomes higher and higher. For a given dye concentration the optimal distance depends on the number of micelles present in the solution, *i.e.* on the detergent concentration. At higher dye concentration more micelles are necessary for ensuring this optimal distance between the dye molecules. Consequently, the effectivity of the excitation energy transfer is influenced by the change of the dye concentration, too.

Table I.

$c_{SLS} \cdot 10^{-3}$ (M)	c_{Th} (M)					
	c_{Th+MB} (M)					
	$2 \cdot 10^{-6}$	$5 \cdot 10^{-6}$	$1 \cdot 10^{-5}$	$2 \cdot 10^{-5}$	$5 \cdot 10^{-5}$	$1 \cdot 10^{-4}$
2	9.7	6.7	3.2	2.0	1.2	0.9
	2.7	1.3	0.6	0.4	0.4	0.5
2.5	22.6	11.1	4.8	3.3	1,2	0.9
	4.0	1.4	0.7	0.5	0.4	0.5
3	41.9	15.6	7.9	5.2	1.4	1.0
	7.3	2.3	0.8	0.7	0.5	0.5
3.5	77.4	28.9	12.7	7.2	2.1	1.1
	15.0	4.1	1.3	0.8	0.7	0.5
4	96.8	80.0	49.2	24.8	7.8	3.3
	39.8	13.8	3.7	1.7	0.9	0.6
6	132.3	148.9	134.9	143.1	79.2	55.0
	152.9	105.7	80.9	48.9	9.0	4.1
8	151,6	148.9	141.3	166.7	118.4	122.2
	162.0	121.4	120.0	102.5	43.8	13.3

The maxima of fluorescence intensities for Th measured in solutions of Th+SLS (above the dotted line) and that of Th+ +MB+SLS (under the dotted line) are listed in Table I. The intensities measured in aqueous solutions of Th and those of Th+MB are arbitrarily considered to be 100%. For Th+SLS systems the fluorescence intensity at the optimal detergent concentration is between 25 and 81% (depending on the dye concentration.) For mixed solutions of Th and MB the intensity of Th fluorescence is between 2 and 15%. This means that in mixed solutions the Th fluorenscence is almost totally quenched at the optimal detergent concentration, due to the migration of the excitation energy from Th to MB.

References

[1] *Hevesi, J., E. Lehoczki, E. Bálint:* Zh. Prikl. Spektr. **13**, 458 (1970).
[2] *Teale, F. W. J.:* Nature **181**, 416 (1958).
[3] *Singhal, G. S., E. Rabinowitch, J. Hevesi, V. Srinivasan:* Photochem. Photobiol. **11**, 531 (1970).
[4] *Hevesi, J., E. Bálint, E. Lehoczki:* Acta Phys. Polon. **A38**, 829 (1970).
[5] *Lehoczki, E., E. Bálint, J. Hevesi:* Zh. Prikl. Spektr. **16**, 97 (1972).

МИГРАЦИЯ ЭНЕРГИИ ВОЗБУЖДЕНИЯ В СИСТЕМЕ КРАСИТЕЛЬ—ДЕТЕРГЕНТ

Я. Хевеши, Ж. Рожа

В растворах метиленового голубого и тионина типа краситель-детергент наблюдается миграция энергии возбуждения от тионина (донор) к метиленовому голубому. Этот процесс был изучен путём исследования спектра флуоресценции ($2 \cdot 10^{-6} - 1 \cdot 10^{-4}$) эквимолярных растворов с детергентом натрий-лаурилсульфатом. Для каждой концентрации красителя существует оптимальная концентрация детергента, при которой перенос энергии происходит наиболее эффективно. Этот перенос наблюдается при критической концентрации мицеллообразования (концентрация детергента $3{,}5 \cdot 10^{-3}$) в растворе $2 \cdot 10^{-6}$ моль$\cdot$л$^{-1}$ и смещается к более высоким концентрациям красителя. Результаты свидетельствуют о том, что эффективность переноса энергии в системе краситель—детергентзависит от концентрации красителя.

ÜBERTRAGUNG VON ANREGUNGSENERGIE IN DREIKOMPONENTENLÖSUNGEN

Von

I. KETSKEMÉTY und J. KUŚBA*

Institut für Experimentalphysik der Attila József Universität, Szeged

(Eingegangen am 1. Juni 1974)

Es wurde eine allgemeine Abhängigkeit zwischen direkt gemessenen Fluoreszenzspektren von Dreikomponentenlösungen und den Spektren der einzelnen Komponenten angegeben. In den Erwägungen wurden strahlungsverbundene und strahlungslose Energieübertragungsprozesse in Betracht gezogen, wobei auch Energiemigration sowie die Möglichkeit inaktiver Übertragung beachtet wurden. Die erhaltene Abhängigkeit wurde am Beispiel zweier Lösungssysteme überprüft und in beiden Fällen eine gute Übereinstimmung zwischen theoretischen und experimentellen Ergebnissen festgestellt.

1. *Einleitung*

In Zusammenhang mit der Entwicklung von Farbstofflasern hat die Anregungsenergieübetragung in Mehrkomponentenlösungen zunehmend an Bedeutung gewonnen. In vielen Fällen wird durch die Anwendung solcher Systeme als Aktivstoff eine bedeutende Verstärkung der Akzeptorgeneration erreicht [1—5]. In Lösungen mit zureichend hoher Zähigkeit, bei denen der Einfluß der Diffusionsübertragung vernachlässigt werden kann, sind zweierlei Prozesse für die Anregungsenergieübertragung in Betracht zu nehmen: strahlungsverbundene und strahlungslose Prozesse.

Fig. 1 zeigt das Schema der grundlegenden Strahlungsprozesse in Dreikomponentensystemen. Die einfachen Pfeile entsprechen der Emission und der Absorption zweiter Ordnung, die doppelten Pfeile der Sekundäremission und der Absorption dritter Ordnung. Allgemein sind auch noch analoge Prozesse höherer Ordnung möglich, die aber aus Gründen der Übersichtlichkeit auf der Zeichnung nicht dargestellt sind.

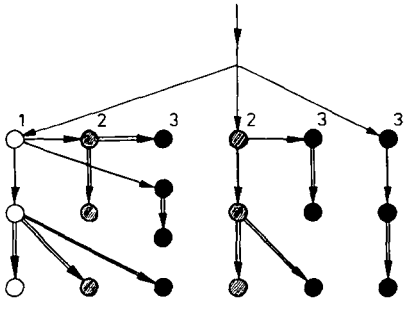

Fig. 1. Schema der elementaren Strahlungsprozesse in Dreikomponentenlösungen

Es ist hervorzuheben, daß mit jedem Emissionsakt beliebiger Zentren auch innere Löschung und strahlungslose Anregungsenergieübertragung zu anderen Molekülen verbunden sind. Mögliche Prozesse dieser Art

* Institut für Physik, Technische Universität, Gdańsk, Polen.

für ein Dreikomponentensystem sind in Fig. 2 dargestellt. Die Größen k_{Fi} kennzeichnen hier die Häufigkeiten spontaner Emissionen, k_{qi} die Häufigkeiten der inneren Löschung und k_{ik} diejenigen für strahlungslose Übertragungen vom der i-ten zur k-ten Komponente, wobei im Falle von Dipol—Dipol-Wechselwirkung nach Förster [6] gilt:

$$k_{ik} = (k_{Fi} + k_{qi}) \left(\frac{R_{0ik}}{r}\right)^6; \tag{1}$$

r und R_{0ik} sind der Abstand bzw. der kritische Abstand für die Energieübertragung zwischen den einzelnen Komponenten.

In Wirklichkeit können die Strahlungsprozesse bzw. die strahlungslosen Prozesse in beliebiger Reihenfolge ablaufen, so daß allgemein die wirkliche Darstellung der Anregungswege nur durch entsprechende Kombination der Fig. 1 und 2 gefunden werden kann.

Unter der Voraussetzung, daß: 1. die Fluoreszenz der Lösung durch ein monochromatisches, senkrecht zu der Vorderfläche der Küvette von Schichtdicke l einfallendes paralleles Lichtbündel von kreisformigem Querschnitt $R^2\pi$ erregt wird und ein durch die Mitte der Vorderfläche austretendes, zu den Einstrahlungsrichtung paralleles aber entgegengesetzt gerichtetes Bündel des Fluoreszenzlichtes zur Messung gelangt, 2. die Strahlungsprozesse höherer als zweiter Ordnung zu vernachlässigen sind, 3. die Emissionsspektren der Akzeptoren sich mit den Absorptionsspektren der Donoren nicht überlappen und daß 4. keine chemische Reaktion zwischen den Komponenten auftritt, erhielten KETSKEMÉTY und SCHIBISTYJ folgende Abhängigkeit zwischen dem direkt gemessenen Fluoreszenzspektrum $B(\lambda')$ der Dreikomponentenlösung und dem wahren, auf 1 genormten Quantenfluoreszenzspektren $f_1(\lambda')$, $f_2(\lambda')$ und $f_3(\lambda')$ der einzelnen Komponenten [7, 8]:

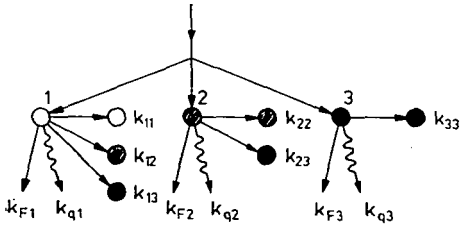

Fig. 2. Schema der elementaren strahlungslosen Prozesse in Dreikomponentenlösungen

$$B(\lambda') = C(\lambda, \lambda')\{(1+\varkappa_{11})\eta_1'(\lambda)f_1(\lambda') + [(1+\varkappa_{22})\eta_2'(\lambda) + \varkappa_{12}\eta_1'(\lambda)]f_2(\lambda') + \\ + [(1+\varkappa_{33})\eta_3'(\lambda) + \varkappa_{13}\eta_1'(\lambda) + \varkappa_{23}\eta_2'(\lambda)]f_3(\lambda')\}, \tag{2}$$

worin

$$C(\lambda, \lambda') = \frac{\varrho}{4\pi n^2} E_{\lambda 0} \frac{\alpha}{\alpha+\beta}(1 - e^{-(\alpha+\beta)}); \tag{3}$$

λ und λ' bezeichnen die Wellenlänge des Anregungslichtes und der beobachteten Lumineszenz, $\alpha = k(\lambda)l$ und $\beta = k(\lambda')l$, wobei $k(\lambda)$ und $k(\lambda')$ die Absorptionskoeffizienten der Lösung sind, ϱ ist der Reflexionskoeffizient, n der Brechungsindex und $E_{\lambda 0}$ die Intensität des Erregungslichtes.

Die Parameter $\varkappa_{ik}$ beschreiben die mit Strahlung verbundene Energieübertragung, wobei nach [9]

$$\varkappa_{ik} = \int_0^\infty \eta_k'(\lambda'') f_i(\lambda'') M(\lambda'') d\lambda''. \tag{4}$$

Die Größen $\eta_i'(\lambda)$ bezeichnen hier die sogenannten effektiven Quantenausbeuten der einzelnen Komponenten

$$\eta_i'(\lambda) = \frac{N_{iem}}{N_{abs}}, \tag{5}$$

d. h. das Verhältnis der Anzahl der durch den i-ten Komponenten im Volumen dV ausgestrahlten Quanten zur Anzahl der durch die Lösung in demselben Volumen absorbierten Quanten.

Die Funktion $M(\lambda'')$ ist durch folgende Gleichung angegeben:

$$M(\lambda'') = \frac{(\alpha+\beta)(1+e^{-\alpha})(1+e^{-\beta})}{2\alpha\beta[1-e^{-(\alpha+\beta)}]}[\gamma Ei(-m\gamma) - \gamma Ei(-\gamma)] +$$

$$+ \frac{1}{2[1-e^{-(\alpha+\beta)}]} \cdot [\chi(\alpha,\gamma) + \chi(\beta,\gamma) + e^{-\beta}\psi(\alpha,\gamma) + e^{-\alpha}\psi(\beta,\gamma)],$$

wo $\gamma = k(\lambda'')l$, $m = \frac{R}{l}$, und

$$Ei(x) = 0{,}5772 \ldots + \ln|x| + x + \frac{x^2}{2\cdot 2!} + \frac{x^3}{3\cdot 3!} + \ldots,$$

$$\psi(x,\gamma) = \frac{\gamma e^{-x}}{x}[G(-\gamma) - G(-\gamma + x)].$$

und $G(x) = Ei(x) - \ln|x|$, sowie

$$\chi(x,\gamma) = \frac{\gamma}{x}[G(-\gamma) - G(-\gamma - x)].$$

Wenn man die Wahrscheinlichkeit des Überganges in den angeregten Elektronenzustand der Moleküle des i-ten Komponenten beim Absorptionsvorgang mit $\eta_i^*(\lambda)$ bezeichnet, erhält man aus [5]:

$$\eta_1'(\lambda) = \frac{k_1(\lambda)}{k(\lambda)}\eta_1^*(\lambda)K_1$$

$$\eta_2'(\lambda) = \frac{k_2(\lambda)}{k(\lambda)}\eta_2^*(\lambda)K_2 + \frac{k_1(\lambda)}{k(\lambda)}\eta_1^*(\lambda)K_{12}K_2 \tag{6}$$

$$\eta_3'(\lambda) = \frac{k_3(\lambda)}{k(\lambda)}\eta_3^*(\lambda)K_3 + \frac{k_1(\lambda)}{k(\lambda)}\eta_1^*(\lambda)K_{13}K_3 +$$

$$+ \frac{k_2(\lambda)}{k(\lambda)}\eta_2^*(\lambda)K_{23}K_3 + \frac{k_1(\lambda)}{k(\lambda)}\eta_1^*(\lambda)K_{12}K_{23}K_3,$$

wobei die Konstante K_i die Quantenausbeuten der einzelnen Komponenten und K_{ik} die Übertragungsausbeuten von der i-ten zur k-ten Komponente bezeichnen (in beiden Fällen werden nur die strahlungslosen Vorgänge betrachtet). Es folgt aus (4) und (6):

$$\begin{aligned}
\varkappa_{11} &= K_1 R_{11}, \\
\varkappa_{12} &= K_2 R_{12} + K_{12} K_2 R_{11}, \\
\varkappa_{13} &= K_3 R_{13} + K_{13} K_3 R_{11} + K_{12} K_{23} K_3 R_{11} + K_{23} K_3 R_{12}, \\
\varkappa_{22} &= K_2 R_{22}, \\
\varkappa_{23} &= K_3 R_{23} + K_{23} K_3 R_{22}, \\
\varkappa_{33} &= K_3 R_{33},
\end{aligned} \tag{7}$$

wobei

$$R_{ik} = \int_0^\infty \frac{k_k(\lambda'')}{k(\lambda'')} \eta_k^*(\lambda'') f_i(\lambda'') M(\lambda'') d\lambda''. \tag{8}$$

Die Bestimmung der Parameter K_{ik} und K_i bildete das Ziel und bedeutet gleichzeitig die Hauptschwierigkeit der Arbeiten [7] und [8]. Es zeigt sich nun, daß, ähnlich wie bei den von BOJARSKI und DOMSTA durchgeführten Überlegungen für ein- und zweikomponentenlösungen [10, 11], im Falle der Dreikomponentenlösung, für die sich die Akzeptoremissionsspektren und Donorabsorptionsspektren nicht überlappen, folgende Gleichungen gültig sind:

$$K_i = \eta_{0i} \frac{1 - f(\Gamma_i)}{1 - \alpha_{0ii} \frac{\gamma_{ii}}{\Gamma_i} f(\Gamma_i)} \tag{9}$$

$$K_{ik} = \frac{\alpha_{0ik} \frac{\gamma_{ik}}{\Gamma_i} f(\Gamma_i)}{1 - \alpha_{0ii} \frac{\gamma_{ii}}{\Gamma_i} f(\Gamma_i)} \tag{10}$$

wo

$$\Gamma_i = \sum_{k=1}^{k=3} \gamma_{ik} \quad \text{und} \quad \gamma_{ik} = \frac{\sqrt{\pi}}{2} \cdot \frac{C_k}{C_{0ik}}$$

ist.

In den oben angeführten Gleichungen bezeichnen η_{0i} und C_i die absolute Quantenausbeute bzw. die Konzentration der i-ten Komponente, C_{0ik} dagegen die kritische Konzentration für die Energieübertragung von der i-ten zur k-ten Komponente. Es gilt nach [6]

$$C_{0ik} = 5{,}18 \cdot 10^{-10} \frac{n^2}{\sqrt{\eta_{0i}}} \left[\int_0^\infty f_i(\lambda) \varepsilon_k(\lambda) \lambda^4 d\lambda \right]^{-\frac{1}{2}} \left[\frac{\mathrm{M}}{\mathrm{l}} \right], \tag{11}$$

wobei $\varepsilon_k(\lambda)$ der dekadische molare Absorptionskoeffizient ist. Die Funktion $f(\Gamma)$ ist durch folgende Gleichung definiert:

$$f(\Gamma) = 2\Gamma \int_0^\infty e^{-x^2-2\Gamma x}\, dx.$$

Die in den Gleichungen (9) und (10) auftretenden Parameter α_{0ik} drücken die Voraussetzung aus, daß nur ein Teil der strahlungslosen Energieübertragungsakte zum angeregten Zustand der Akzeptoren führt. In Übereinstimmung mit [12] kann man die Häufigkeit dieser Prozesse folgendedurch Gleichung ausdrücken:

$$k'_{ik} = (k_{Fi} + k_{qi}) \left(\frac{R'_{0ik}}{r}\right)^6, \tag{12}$$

worin

$$R'^6_{0ik} = R^6_{0ik} \frac{\int_0^\infty f_i(\lambda)\varepsilon_k(\lambda)\eta_k^*(\lambda)\lambda^4 d\lambda}{\int_0^\infty f_i(\lambda)\varepsilon_k(\lambda)\lambda^4 d\lambda} \tag{13}$$

ist; α_{0ik} bedeutet hier, ähnlich wie in [11], die Wahrscheinlichkeit, daß bei der Energieübertragung keine Löschung auftritt, oder anders gesagt, daß die gegebene Energieübertragung aktiv ist. Es ist zu beachten, daß der übliche Mechanismus der mit dem Prozess der Energieübertragung verbundenen Löschung weniger allgemeine Bedeutung hat als [11]. Das erlaubt jedoch, den Parametern eine noch bestimmtere physikalische Interpretation zuzuschreiben und ihren Wert mit meßbaren Eigenschaften zu verbinden. Die hier angenommene Definition der Parameter α_{0ik} im Sinne der Gleichung (13) ist äquivalent mit derjenigen des von GALANIN [13] angegebenen „maximalen Wertes der Ausbeute nach dem Übertragungsakt". Die direkte Anwendung der Gleichung (2) ist wegen der Kompliziertheit der einzelnen Faktoren schwer. Deshalb wurde ein Programm für die automatische Rechnenmaschine „Minsk 22" vorbereitet, das die Berechnung der Größen K_i, K_{ik}, R_{ik}, $\varkappa_{ik}$ sowie der für die einzelnen Komponenten gemessenen Emissions- und Absorptionsspektren, der Konzentrationen und der kritischen Konzentrationen wie auch der Quantenausbeuten und der Werte α_{0ik}, ermöglicht.

2. *Versuche*

2.1. *Untersuchte Lösungen*

Um die oben angeführten theoretischen Erwägungen experimentell zu überprüfen, wurden zwei Versuchsreihen mit Lösungen von folgenden Zusammensetzungen vorbereitet: System I: 7-Dimethylamino-4-methylkumarin (DMC), 3,6-Diamino-10-methylacridinium-chlorid-hydrochlorid (DMA), Rhodamin 6G (Rh6G); und System II: DMC, Rh6G und Kresylviolett (CV). DMA und CV waren Erzeugnisse der Fluka AG Buchs, DMA wurde durch Umkristallisierung aus Äthylalkohol, und CV mit der in [14] angeführten Methode gereinigt. DMC war ein Erzeugnis der Eastman Kodak Co und Rh6G der BDH, beide ohne vorherige Reinigung.

In beiden Systemen wurde als Lösungsmittel Äthylalkohol mit zugabe von 6% Essigsäure verwendet. In Falle des Systems I war die Konzentration von DMC und Rh6G $C_1=C_3=5\cdot10^{-4}$ M/l, dagegen änderte sich die Konzentration C_2 von DMA von 10^{-5} M/l bis 10^{-2} M/l. Ähnlicherweise war im System II die Konzentration von DMC und CV konstant, $C_1=C_3=5\cdot10^{-4}$ M/l und die Konzentration C_2 von Rh6G änderte sich von 10^{-5} M/l bis $2\cdot10^{-3}$ M/l.

2.2. *Meßmethoden*

Die Absorptionsspektren wurden mit einem Spektrophotometer Optica Milano Typ CF—4, und die Emissionspektren mit dem in [15] beschriebenen Gerät gemessen. Die Lumineszenzanregung erfolgte mit einer Hochdruckquecksilberlampe durch einen Monochromator SPW—1 von Carl Zeiss Jena. Die absolute Quantenausbeute wurde in Abhängigkeit von der Wellenlänge des Erregungslichtes, mit der in [16] und [17] angegebenen Methode mit einer Standardlampe bestimmt. Für alle Messungen der Emissionseigenschaften der untersuchten Lösungen wurde eine zylindriche Quarzküvette der Schichtdicke $l=0{,}1$ cm benutzt, wobei die Rückfläche der Küvette immer mit Tusche bedeckt war.

3. *Ergebnisse und Auswertung*

In Fig. 3 sind die mit F bezeichneten Fluoreszenzspektren, die mit ε bezeichneten Absorptionsspektren, sowie die η^*-Kurven dargestellt. Diese Kurven wurden unter der Voraussetzung erhalten, daß

$$\eta_i(\lambda) = \eta_{0i}\eta_i^*(\lambda) = \frac{k_{Fi}}{k_{Fi}+k_{qi}}\eta_i^*(\lambda),$$

wobei $\eta_i(\lambda)$ das direkt gemessene Quantenausbeutespektrum und η_{0i} den Maximalwert von $\eta_i(\lambda)$ bezeichnen.*

Es ist leicht zu erkennen, daß die Bedingung der Nichtüberdeckung der Akzeptoremissionsspektren mit den Donorabsorptionsspektren für alle Fälle erfüllt ist. Für jeden Farbstoff (mit Ausnahme von DMC, für den der $\lambda>415$ nm entsprechende Teil der η^*-Kurve nur abgeschätzt werden konnte) wurde ein Abfall der η^*-Werte im Antistokesbereich erhalten. Bei R6G und CV wurden bei 430 nm und 450 nm lokale Minima der η^*-Werte gefunden. Diese Minima sind durch die Anwesenheit geringer Mengen nichtlumineszierender Verunreinigungen mit den Minima entsprechenden Absorptionsbändern zu erklären. Im Falle von Rh6G wurden solche Verunreinigungen mit Dünnschichtchromatographie wirklich festgestellt.

Mit Hilfe der obigen Daten und der Gleichungen (11) und (13) wurden die Parameter C_{0ik} und α_{0ik} berechnet. Die erhaltenen Ergebnisse sind in Tab. I zu sehen.

In Fig. 4 bezeichnen die Punkte die gemessenen Emissionsspektren des Systems I für die DMA Konzentrationen 10^{-5} M/l bzw. $2\cdot10^{-3}$ M/l bei Anregung mit der Wellenlänge 365 nm. Der Vergleich dieser Ergebnisse mit den dem Aus-

* Für die untersuchten Farbstoffe wurden folgende η_{0i}-Werte bestimmt: DMC 0,72; DMA 0,76; Rh6G 0,90; CV 0,61.

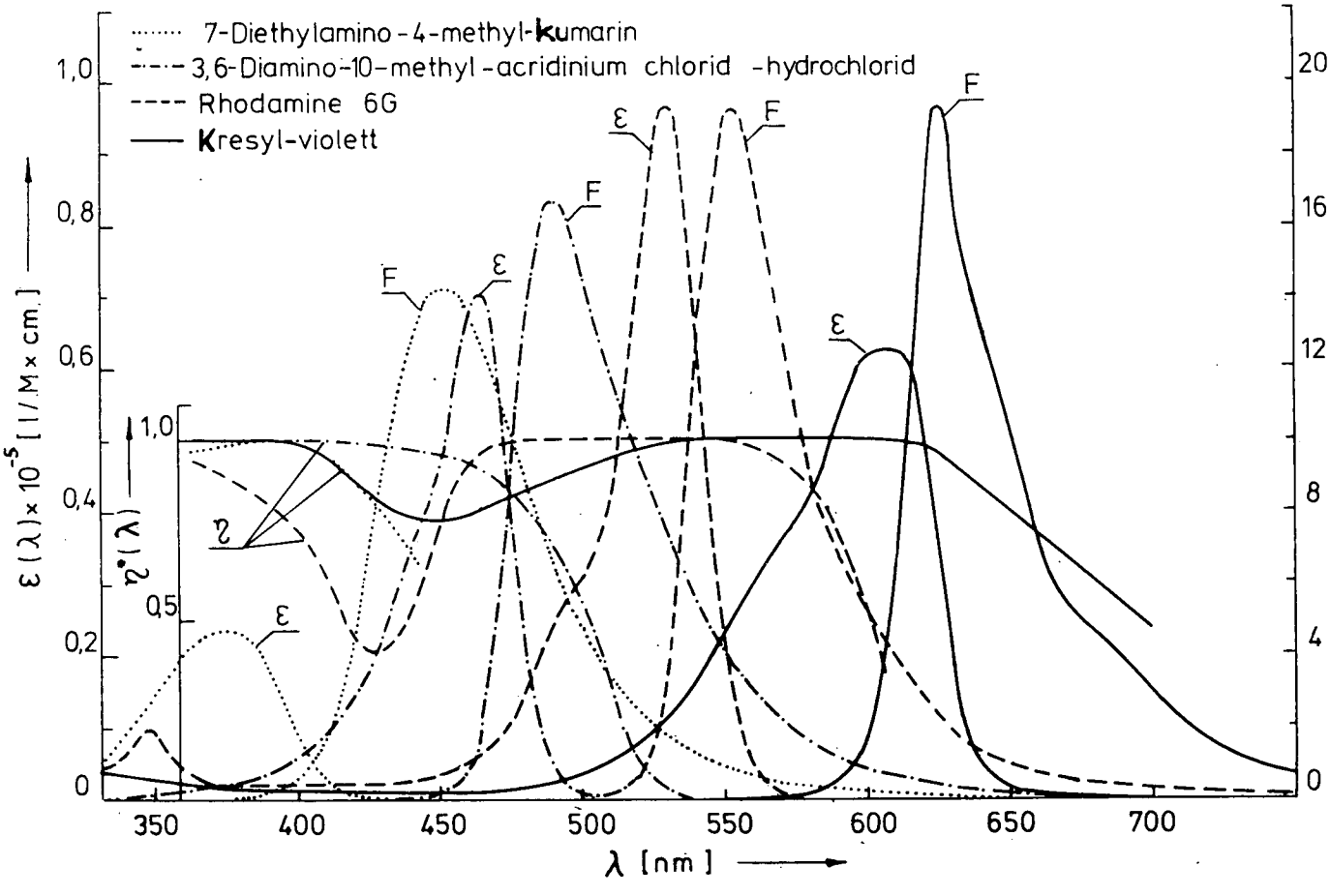

Fig. 3. Absorptionsspektren ε, Emissionsspektren F und relative Quantenausbeute $\eta^*(\lambda)$ für die einzelnen Komponenten der untersuchten Systeme

druck (2) entsprechenden theoretischen Kurven zeigt, daß es in diesem Falle nicht genügt, nur die Sekundärprozesse in Betracht zu ziehen. Unter der vereinfachenden Annahme, daß das Verhältnis der Emissionsintensität $(n+1)$-ter Ordnung zur Emissionsintensität n-ter Ordnung unabhängig von n und gleich dem Verhältnis der

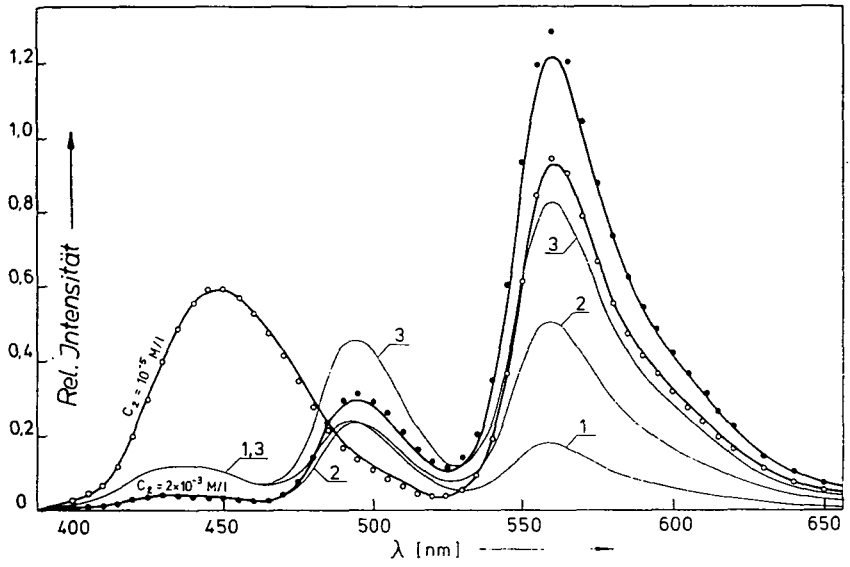

Fig. 4. Experimentell (Punkte) und theoretisch ermittelte Emissionsspektren (Kurven) für zwei Lösungen des System I mit den DMA-Konzentrationen $C_2=10^{-5}$ M/l und $C_2=2\cdot10^{-3}$ M/l

Sekundär- zur Primäremissionsintensität ist, läßt sich analog zu (2) unter Berücksichtigung der mit Strahlung verbundenen Übertragungen höherer Ordnungen folgende Gleichung erhalten [15]:

$$B(\lambda,\lambda')=C(\lambda,\lambda')\left\{\frac{1}{1-\varkappa_{11}}\eta_1'(\lambda)f_1(\lambda')+\left[\frac{1}{1-\varkappa_{22}}\eta_2'(\lambda)+\varkappa_{12}(1+\varkappa_{22})\eta_1'(\lambda)\right]f_2(\lambda')+\right.$$

$$\left.+\left[\frac{1}{1-\varkappa_{33}}\eta_3'(\lambda)+\varkappa_{23}(1+\varkappa_{22}+\varkappa_{33})\eta_2'(\lambda)+(\varkappa_{13}+\varkappa_{13}\varkappa_{33}+\varkappa_{12}\varkappa_{23}+\varkappa_{11}\varkappa_{13})\eta_1'(\lambda)\right]f_3(\lambda')\right\}. \tag{14}$$

Es ist ersichtlich, daß im Falle größerer Werte von $\varkappa_{ik}$ die Unterschiede zwischen den aus (2) und (14) erhaltenen Ergebnisse auch bedeutend sein können.*

* Im allgemeinen waren die Parameter $\varkappa_{ik}$ in geringem Maße von der Wellenlänge des beobachteten Lichtes abhängig. Für das System I waren die Maximalwerte von $\varkappa_{ik}$ wie folgt:

$$\varkappa_{11}-0{,}007,\quad \varkappa_{12}-0{,}320,\quad \varkappa_{13}-0{,}403,\quad \varkappa_{22}-0{,}088,\quad \varkappa_{23}-0{,}661,\quad \varkappa_{33}-0{,}360;$$

und für das System II:

$$\varkappa_{11}-0{,}009,\quad \varkappa_{12}-0{,}308,\quad \varkappa_{13}-0{,}184,\quad \varkappa_{22}-0{,}184,\quad \varkappa_{23}-0{,}468,\quad \varkappa_{33}-0{,}259.$$

Die in Fig. 4 dargestellten dicker ausgezogenen Kurven entsprechen den mit Hilfe der Gleichung (14) berechneten Emissionsspektren für zwei Lösungen des Systems I. Man erkennt in beiden Fällen eine befriedigende Übereinstimmung der experimentellen und theoretischen Ergebnisse. In derselben Abbildung sind, dünn ausgezogen, auch die aus der mit gewissen vereinfachenden Annahmen angewendeten Gleichung (14) gewonnenen Ergebnisse für die Konzentration $C_2 = 2 \cdot 10^{-3}$ M/l dargestellt. Und zwar entspricht die Kurve 1 dem Falle, daß in Gleichung (14) keine Form von Energieübertragung in Betracht gezogen ist, die Kurve 2 dem, daß nur Resonanzenergieübertragungen und Kurve 3, daß nur strahlungsvebundene Übertragungen stattfinden. Es ist leicht zu sehen, daß im Gegensatz zu den dick ausgezogenen Kurven keine der drei Kurven 1, 2 oder 3 dem experimentellen Ergebnissen entspricht.

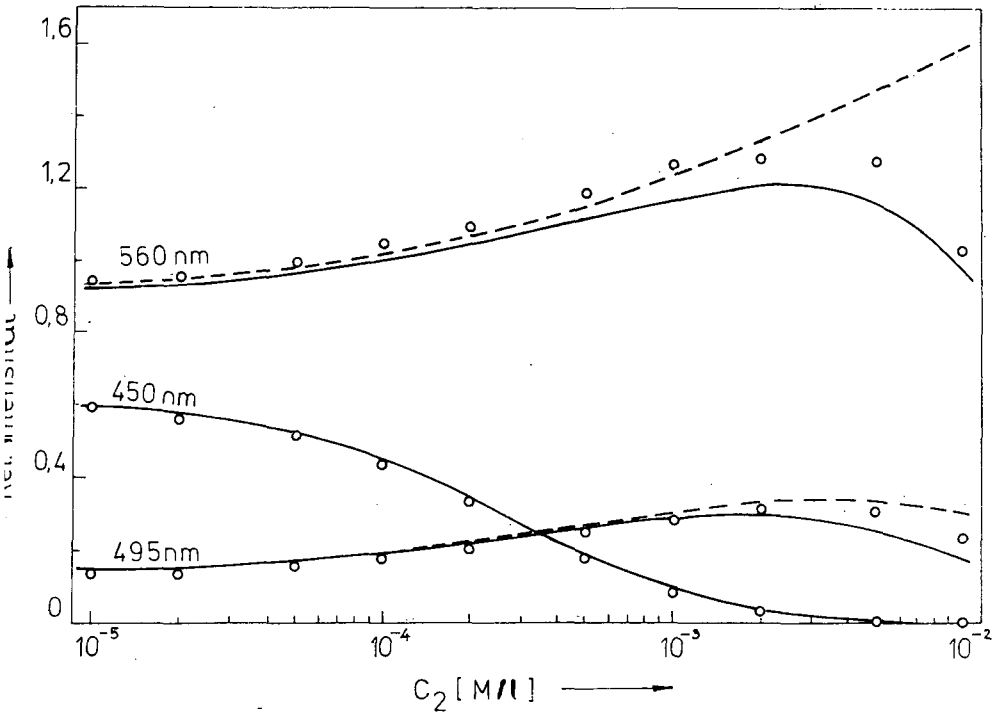

Fig. 5. Abhängigkeit von der DMA-Konzentration der für die einzelnen Emissionmaxima des Systems I experimentell und theoretisch erhaltenen Intensitäten (ausgezogene und gestrichte Kurven)

Die Punkte der Fig. 5 zeigen die Emissionsmaxima der einzelnen Komponenten des Systems I in Abhängigkeit von der DMA-Konzentration, und die ausgezogenen Linien die aus Gleichung (14) berechneten Kurvenverläufe. Die Gestrichelten Kurven wurden aus Gleichung (14) mit der Voraussetzung erhalten, daß alle α_{0ik}-Parameter gleich eins sind, d. h. daß keine Löschung bei dem Übertragungsprozess auftritt. Die Übereinstimmung der experimentellen und theoretischen Ergebnisse ist im

gesamten DMA-Konzentrationsbereich gut. Es ist zu sehen, daß bei hohen Konzentrationen die mit dem Energieübertragungsprozess verbundene Löschung eine grosse Bedeutung hat.

Analog dazu sind die Ergebnisse für das System II in Fig. 6 und 7 dargestellt. Die Übereinstimmung zwischen den theoretischen und experimentellen Ergebnissen

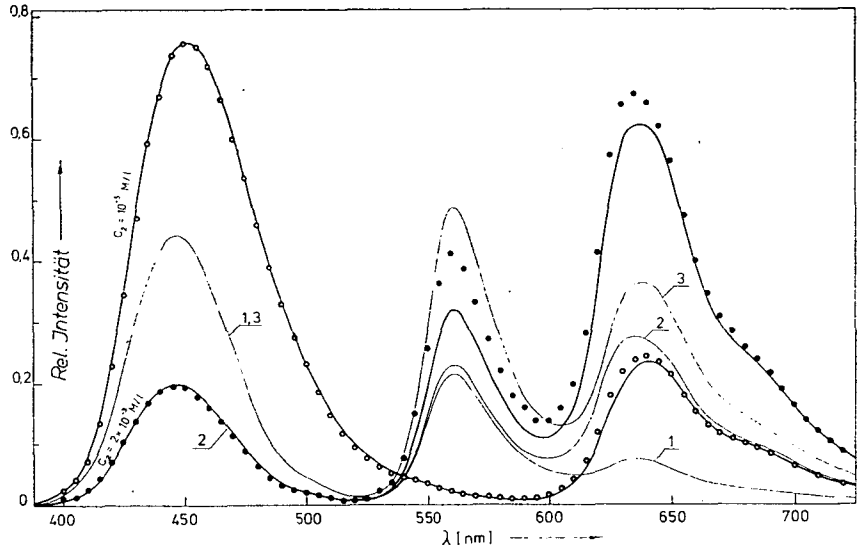

Fig. 6. Experimentell (Punkte) und theoretisch ermittelte Emissionsspektren (Kurven) für zwei Lösungen des Systems II mit den Rh6G-Konzentrationen $C_2 = 10^{-5}$ M/l und $C_2 = 2 \cdot 10^{-3}$ M/l

ist hier nicht so gut wie im Falle des Systems 1, dennoch entsprechen die mit Gleichung (14) berechneten Kurven viel besser den experimentellen Punkten als im Falle der Kurven 1, 2 oder 3 in Fig. 4. Der Einfluß der Parameter α_{0ik} war im Falle des System II vernachlässigbar klein.

4. *Schlußfolgerungen*

In den oben angegebenen Gleichungen sind gleichzeitig Energieübertragungsprozesse mit und ohne Strahlung bei der Interpretation der beobachteten Lumineszenzspektren von Dreikomponentenlösungen in Betracht genommen. Der Einfluß der einzelnen Übertragungsmechanismen wurde in Abhängigkeit von sämtlichen Parametern dargestellt, die die Geometrie des untersuchten Systems, wie auch die wahren Lumineszenzeigenschaften der einzelnen Komponenten der Lösung beschreiben. Alle diese Parameter haben eine genaue physikalische Bedeutung.

Der Vergleich der erhaltenen theoretischen Ausdrücke mit den experimentellen Ergebnissen für die untersuchten Dreikomponentensysteme führt zur Feststellung,

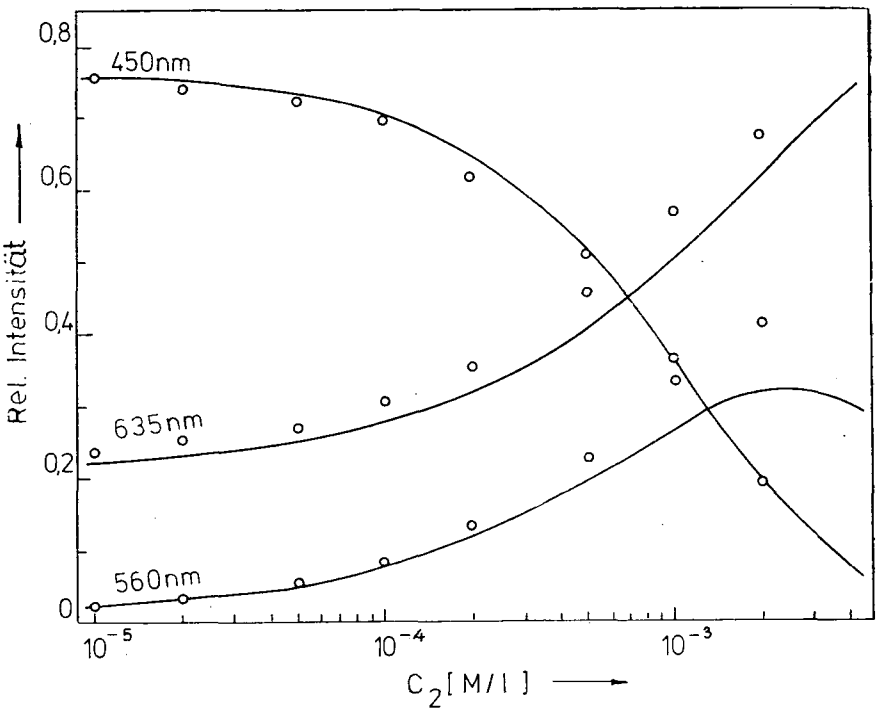

Fig. 7. Abhängigkeit von der Rh6G-Konzentration der für die einzelnen Emissionsmaxima des Systems II experimentell (Punkte) und theoretisch erhaltenen Intensitäten (Kurven)

daß die angegebenen Gleichungen die Energieübertragung in einem breiten Konzentrationsbereich und bei sehr verschiedener Dicke der Meßküvette in befriedigendem Maße beschreiben.

Die befriedigenden Resultate sind dem Umstand zu verdanken, daß bei den zu Grunde gelegten Überlegungen sowohl die Fluoreszenzen höherer Ordnung wie auch alle strahlungslosen Energieübertragungen nach [11] in Betracht gezogen wurden.

Auf Grund der erreichten Ergebnisse läßt sich sagen, daß in gewissen Fällen auch die Einbeziehung der inaktiven Resonanzenergieübertragung große Bedeutung haben kann. Es ist zu bemerken, daß die theoretisch ermittelten Spektren im Bereich größerer Wellenlängen ein wenig niedriger sind als die entsprechenden experimentell bestimmten Werte. Das kann sowohl durch Ungenauigkeiten bei der Bestimmung der Parameter aus Gleichung (14), wie auch durch die Nichtbeachtung der Diffusion der Donoren und Akzeptoren während der Zeit des Anregungszustandes bedingt sein. Auf Grund der erhaltenen Ergebnisse läßt sich jedoch feststellen, daß in den untersuchten Systemen der letzterwähnte Prozeß nur einen geringen Einfluß auf die Emissionsspektren hat.

* * *

Die Verfasser möchten an dieser Stelle Herrn Dozent. Dr. C. BOJARSKI für seine wertvollen Ratschläge ihren aufrichtigen Dank aussprechen.

Tabelle I.

Die für die untersuchten Systeme aus Gleichungen (11) und (13) berechneten Parameter C_{0ik} und α_{0ik}

	C_{011}	C_{012}	C_{013}	C_{022}	C_{023}	C_{033}
	[10^{-4} M/l]					
System I	510	30,5	39,7	56,7	22,1	40,0
System II	510	39,7	77,0	26,3	17,6	23,9
	α_{011}	α_{012}	α_{013}	α_{022}	α_{023}	α_{033}
System I	0,96	0,931	0,974	0,833	1,0	1,0
System II	0,96	0,974	0,958	0,995	0,997	0,968

Literatur

[1] *Rácz, B., I. Ketskeméty, L. Kozma:* Zh. Prikl. Spektroskopii **16**, 914 (1972).
[2] *Maller, C. E., C. M. Verber, A. A. Adelman:* Appl. Phys. Lett. **18**, 278 (1971).
[3] *Vu Thien Han:* C. R. Acad. Sci. (Paris) **274B**, 266 (1972).
[4] *Schmidt, W., W. Appt, N. Wittekindt:* Z. Naturforsch. **27a**, 37 (1972).
[5] *Ahmed, S. A., D. A. Infante, J. S. Gergely:* J. Opt. Soc. Am. **63**, 1321 (1973).
[6] *Förster, Th.:* Ann. Physik (Leipzig) **2**, 55 (1948).
[7] *Ketskeméty, I., A. N. Schibistyj:* Zh. Prikl. Spektroskopii **18**, 843 (1973).
[8] *Schibistyj, A. N., I. Ketskeméty, L. Kozma, E. Hun:* Izw. Akad. Nauk SSSR Ser. Fiz. **37**, 763 (1973).
[9] *Ketskeméty, I.:* Acta Phys. Hung. **10**, 429 (1959).
[10] *Bojarski, C., J. Domsta:* Z. Naturforsch. **25a**, 1760 (1970).
[11] *Bojarski, C., J. Domsta:* Acta Phys. Hung. **30**, 145 (1971).
[12] *Ketskeméty, I.:* Z. Naturforsch. **17a**, 666 (1962).
[13] *Galanin, M. D.:* Trudy Fiz. Inst. Ak. Nauk USSR **12**, 3 (1960).
[14] *Gacoin, P., P. Flamant:* Opt. Comm. **5**, 351 (1972).
[15] *Dombi, J.:* Acta Phys. Hung. **25**, 287 (1968).
[16] *Budó, Á., J. Dombi, L. Szöllősy:* Acta Phys. et Chem. Szeged **2**, 18 (1956).
[17] *Ketskeméty, I., J. Dombi, R. Horvai, J. Hevesi, L. Kozma:* Acta Phys. et Chem. Szeged **7**, 17 (1961).

ПЕРЕДАЧА ЭНЕРГИИ ВОЗБУЖДЕНИЯ В ТРЁХКОМПОНЕНТНЫХ РАСТВОРАХ

И. Кечкемети, Й. Кушба

Показана общая зависимость между прямо измеренными спектрами флуоресценции трёхкомпонетных растворов и спектрами отдельных компонентов. В рассуждениях принимались во внимание излучательные и безызлучательные процессы передачи энергии, причём учитывалась также миграция энергии и возможность неактивной передачи. Полученная зависимость проверялась на примере двух систем растворов и в обоих случаях было установлено хорошее совпадение теоретических и экспериментальных результатов.

ЛЮМИНЕСЦЕНЦИЯ И ВЫНУЖДЕННОЕ ИЗЛУЧЕНИЕ ПАРОВ ФЕНИЛПРОИЗВОДНЫХ ОКСАЗОЛА И БЕНЗОКСАЗОЛА

Н. А. БОРИСЕВИЧ, Л. А. БАРКОВА, В. В. ГРУЗИНСКИЙ

Институт физики АН БССР, Минск

(Поступило в редакцию 1 июля 1974 г.)

В газовой фазе изучены спектрально-люминесцентные свойства молекул с протяженной системой сопряженных связей: 2,5-дифенилоксазол; 1,4-ди[2-(5-фенилоксазолил)]бензол; 1,4-ди(бензоксазол-2′-ил)бензол. Установлена эквивалентность термического и оптического способов изменения запаса колебательной энергии и определены их колебательные теплоемкости. Сопоставлены люминесцентные и генерационные характеристики этих молекул.

К настоящему времени в газовой фазе детально изучены спектрально-люминесцентные свойства преимущественно молекул с плотной структурой колец [1]. Значительный интерес представляет исследование люминесцентных и генерационных свойств важных в сцинтилляционной и лазерной технике ароматических и гетероциклических соединений с протяженной системой сопряженных связей. Вследствие высоких температур, необходимых для испарения вещества, отсутствия стабилизирующего влияния среды и ряда других причин могут усилиться внутримолекулярные взаимодействия, фотоизомеризация и нарушение компланарности молекул, что приведет к росту безызлучательных переходов или вообще потере люминесцентной способности молекул в газовой фазе. Например, хорошо флуоресцирующие в нейтральных растворителях 1,4-дифенилбутадиен и 1,1,4,4-тетрафенилбутадиен (в *н*-гептане квантовый выход, соответственно, $\gamma = 0{,}31$ и $0{,}43$ [2]), не флуоресцируют в парах ($\gamma < 0{,}001$).

В настоящей работе рассмотрены спектральные свойства паров фенилпроизводных оксазола и бензоксазола: 2,5-дифенилоксазол (I-ППО); 1,4-ди [2-(5-фенилоксазолил)]бензол (II-ПОПОП) и 1,4-ди(бензоксазол-2′-ил)бензол (III). Эти и родственные им соединения в растворах [3, 4] и твердой фазе [5] являются эффективными активными средами ОКГ. На фенилпроизводных оксазола впервые получена генерация в газовой фазе [6, 7].

Флуоресценция возбуждалась излучением ртутной лампы ДРШ-500 и в разряде. Поглощение изучалось на установке, собранной на базе спектрофотометра *SP*-700, флуоресценция — на нестандартном светосильном спектрофлуориметре.

Упругость насыщенных паров P определена в [8] для соединения I при одной температуре T_H. Зависимость $P(I/T_H)$ получена для II и III путем из-

мерения оптической плотности D при полном или частичном испарении в кювете определенного количества вещества. Путем несложных расчетов в предположении пропорциональности изменения P и D от T_H можно получить коэффициенты a и b для изветсного соотношения: $\log p = -\frac{a}{T_H} + b$. Для соединений II и III, соответственно, a = 2770 и 4730, b = 3,9 и 7,6. Из зависимости $P(I/T_H)$ следует, что соединение III более летучее, чем II.

Изученные соединения имеют высокие значения коэффициента поглощения в максимумах электронных полос. На длинноволном крыле полосы поглощения этих N-гетероциклических соединений не обнаружено слабой $n\pi^*$-полосы [8, 9], как у паров карбонилсодержащих соединений [10]. Значения коэффициента экстинкции ε в максимуме длинноволновой полосы и рассчитанные по спектрам поглощения вероятности излучательного перехода A для II и III приведены в табл. 1, из которой следует, что в пределах точности измерений значения ε в газовой фазе и растворах близки.

Таблица 1

Соединение	ε, л. моль$^{-1}$ см$^{-1}$		A·10^{-8}, сек$^{-1}$	
	пары	раствор	пары	раствор
II	48 200	47 000*	7,15	5,5*
III	52 500	53 300**	7,7	7,1**

* — в циклогексане, ** — в хлороформе.

Свечение паров имеет малую длительность τ. Значения τ для соединения I при различных длинах волн возбуждающего излучения в пределах длинноволновой полосы поглощения приведены в табл. 2. Там же для сравнения дано значение τ раствора в толуоле. В хлороформе τ(III) = 1,25 нсек [II], в толуоле τ(II) = 0,8 нсек. Для паров II и III можно считать ориентировочно $\tau \sim$ I нсек.

Таблица 2

	Пары (T=408 °K)			Раствор
λ_b, нм	313	302	296,7	313
τ, нсек	0,9	0,44	0,44	1,6

По измеренной флуориметрической длительности τ и рассчитанной естественной длительности возбужденного состояния τ_0 для I оценен квантовый выход $\gamma \sim 0{,}24$ [8]. Число столкновений молекулы за время жизни в возбужденном состоянии при выбранных упругостях паров $\tau \cdot z \sim 10^{-2} \div 10^{-3}$, т. е. пары являются разреженными.

Спектры флуоресценции изученных соединений зависят от запаса колебательной энергии, сообщаемой молекуле оптическим (λ_b) или термическим (T) путем. Такие зависимости представлены на рис. 1. Повышение T, как и умень-

шение $\lambda_в$, вызывает размытие колебательной структуры и смещение спектра в длинноволновую сторону. Однако эти изменения спектров невелики и меньшие, чем, например, у антрацена [12]. Удлинение цепи сопряженных связей приводит к сдвигу спектров в длинноволновую область (рис. 1а и б).

При возбуждении паров ПОПОПа высокочастотным безэлектродным разрядом наблюдается интенсивная полоса свечения, совпадающая по положению с полосой флуоресценции при оптическом возбуждении. Для поджига разряда использовалась смесь ПОПОПа с гелием при небольших давлениях последнего. Спектр свечения ПОПОПа в разряде (температура печи $T = 523$ °К) более размыт, чем спектр при оптическом возбуждении ($\lambda_в = 296{,}7$ нм, $T = 773$ °К), максимумы колебательных полос совпадают. Такое размытие

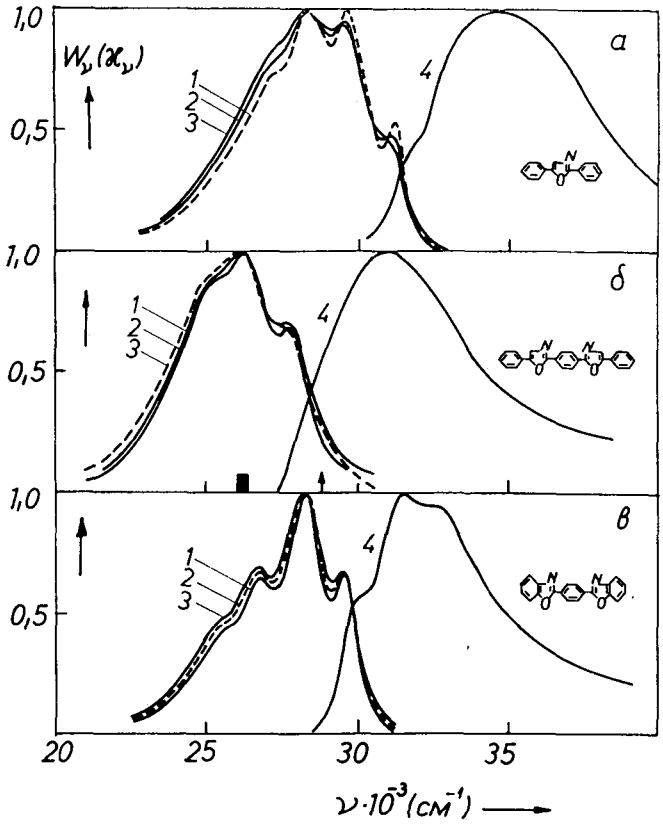

Рис. 1. Спектры флуоресценции (1—3) паров для различных $\lambda_в$ и T и спектры поглощения (4). а — 2,5-дифенилоксазол ($T=388$ °К $P=10^{-2}$ мм рт. ст.): 1 — $\lambda_в=313{,}2$ — 302,3 — 289,3 нм, 4 — $T=388$ °К; б — 1,4-ди[2-(5-фенилоксазолил)]бензол ($\lambda_в=334$ нм, $P=2\cdot10^{-2}$ мм рт. ст.) 1 — $T=458{,}2-603$, 3 — 773, 4 — 573 °К, стрелкой показана частота накачки, область полосы генерации заштрихована; в — 1,4-ди(бензоксазол-2′-ил)бензол ($T=469$ °К, $P=1{,}2\cdot10^{-3}$ мм рт. ст.) 1 — $\lambda_в=313{,}2-334$, 3 — 296,7 нм, 4 — $T=573$ °К.

спектра является следствием высоких энергий возбуждения и температуры в области разряда. Нами совместно с **В. В. Рожковым** показано, что введение в разряд дополнительно к парам исследуемого вещества эффективно стабилизирующих посторонних газов приводит к более заметной колебательной структуре в спектре флуоресценции. Аналогичные изменения происходят со спектрами II в присутствии посторонних газов и при оптическом возбуждении, если $\lambda_b < \lambda_{\text{инверсии}}$.

Спектр свечения в разряде ПОПОПа и других изученных нами соединений состоит из одной электронной полосы $S_1^* \rightarrow S_0$, что существенно для получения генерации излучения. У ряда соединений при таком способе возбуждения часто излучательным переходом является $T \rightarrow S_0$. Например, при оптическом возбуждении паров антрахинона наблюдается замедленная флуоресценция [10], а в разряде осуществляется испускание, за которое ответственны переходы $S_1^* \rightarrow S_0$ и $T \rightarrow S_0$ [13].

По сравнению с растворами в толуоле (рис. 2), максимумы спектров флуоресценции и поглощения паров сдвинуты в коротковолновую сторону, соответственно, для II на 2250 и 3450 $см^{-1}$, для III на 2200 и 3100 $см^{-1}$. Колебатель-

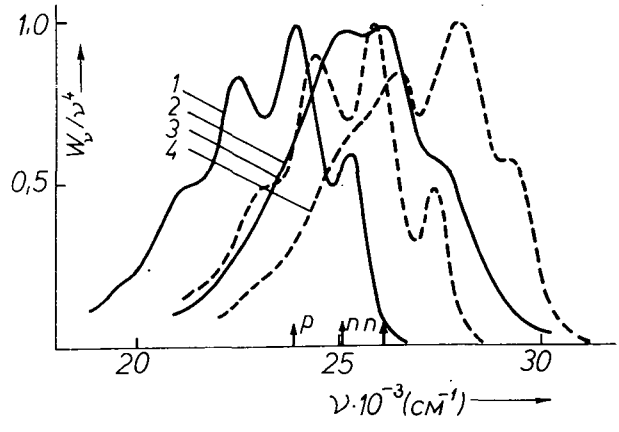

Рис. 2. Спектры флуоресценции ($\lambda_в = 334$ нм) 1,4-ди[2-(5-фенилоксазолил)]-бензола (1,2) и 1,4-ди(бензоксазол-2′-ил)-бензола (3,4) в толуольном растворе (1,3) и в парах (2 – T = = 543 °К, 4 – T = 578 °К). Стрелками указаны частоты максимумов полос генерации.

ная структура спектров паров более размыта вследствие высокой температуры, чем спектров растворов. Структура спектра паров III при близких Т более выражена, чем II. В нейтральных же растворителях их спектры мало различаются по форме.

Зависимость спектров флуоресценции разреженных паров органических молекул от $\lambda_в$ и Т позволяет определить их колебательные теплоемкости $C_{кол.}$ в предположении эквивалентности оптического и термического способов изменения запаса колебательной энергии [14]. Наиболее простой способ зак-

лючается в сопоставлении спектров флуоресценции, измеренных при различных $\lambda_в$ и Т. При их совпадении

$$C_{кол.} = \frac{\nu_{в_1} - \nu_{в_2}}{T_2 - T_1}. \quad (1)$$

Значения найденных $C_{кол.}$ приведены в табл. 3.

Таблица 3

Соединение	T, °К	$C_{кол.}$, $см^{-1}\,град^{-1}$	$C^{расч.}_{кол.}$, $см^{-1}\,град^{-1}$
I	390	18,2	19,6
II	536	38,0	44,6
III	493	34,5	35,2

Проведен также расчет теплоемкостей молекул с помощью соотношения [15], полученного на основе квантовой теории:

$$C_{p_0} = 4R + \alpha'\left(\frac{R}{2}\right) + \sum q_i E_{\nu_i} + \psi \sum q_i E_{\delta_i}, \quad (2)$$

где $\psi = (3n-6-\alpha'-\sum q_i)/\sum q_i$, n — общее число атомов в молекуле, q_i и α' — число связей и внутренних вращений в молекуле, E_{ν_i} и E_{δ_i} — функции Эйнштейна, ν и δ — частоты валентных и деформационных колебаний. Два последних члена в соотношении (2) определяют вклад колебательного движения в общую теплоемкость молекулы. Значения рассчитанных колебательных теплоемкостей также приведены в табл. 3. Различие между экспериментальными значениями $C_{кол.}$ и рассчитанными $C^{расч.}_{кол.}$ невелики и для данных молекул с протяженной системой сопряженных связей имеет место эквивалентность оптического и термического способов изменения запаса колебательной энергии.

В отличие от некоторых ароматических соединений со структурными спектрами флуоресценции (антрацен [16], перилен [17, 18]), у которых наблюдается независимость γ и τ от λ, у ППО τ падает с уменьшением $\lambda_в$ (табл. 2). Значительно уменьшается и γ с повышением T у паров ППО и ПОПОПа. На рис. 3 представлена зависимость от Т в широких пределах относительной интенсивности флуоресценции $W^{отн.}$ ПОПОПа в максимуме полосы. При

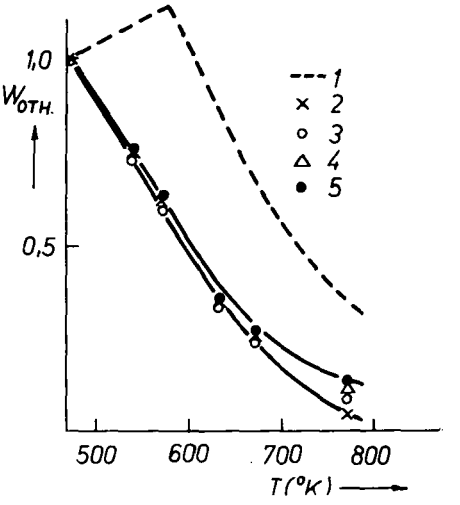

Рис. 3. Зависимость интенсивности флуоресценции 1,4-ди[2-(5-фенилоксазолил)] бензола ($P = 6 \cdot 10^{-3}$ мм рт. ст.) от температуры: 1—$\lambda_в$=365, 2—334, 3—313, 4—302, 5—296,7 нм.

антистоксовом возбуждении $W^{\text{отн.}}$ сначала медленно растет, а затем резко уменьшается. В стоксовой области возбуждения коэффициент поглощения обычно медленно убывает с ростом T [1], поэтому в первом приближении можно принять, что приведенная зависимость $W^{\text{отн.}}(T)$ соответствует зависимости $\gamma^{\text{отн.}}(T)$. Поскольку для ПОПОПа имеет место эквивалентность оптического и термического способов изменения запаса колебательной энергии, можно ожидать и значительного изменения $\gamma(\lambda_в)$. Так при возбуждении молекул паров в пределах второй полосы поглощения, несмотря на большие значения ε, флуоресценция практически отсутствует. У паров ПОПОПа с увеличением T интенсивность флуоресценции значительно уменьшается, поэтому должно сокращаться и τ, так как в отсутствие других тушащих факторов при возбуждении в пределах первой полосы поглощения обычно γ и τ изменяются пропорционально [1].

Совокупность полученных данных (высокий коэффициент поглощения, отсутствие длинноволновой $n\pi^*$-полосы поглощения, небольшая длительность люминесценции, зависимость спектров флуоресценции и τ от энергии возбуждающего кванта) свидетельствует о том, что длинноволновая полоса поглощения и полоса флуоресценции изученных и родственных соединений [8, 9] в газовой фазе обусловлены переходом $S_0 \rightleftarrows S_1^*$.

Большое значение вероятности излучательного перехода A (табл. 1) во многом определяет высокий коэффициент усиления изученных и родственных соединений. В случае структурных спектров усиления в зависимости от вида растворителя и условий накачки в спектре генерации наблюдается несколько полос, соответствующих максимумам спектра флуоресценции (предельного усиления) $\lambda_{\max}^{\text{фл.}}$, причем наиболее интенсивный максимум полосы генерации обычно совпадает с наиболее интенсивным максимумом $\lambda_{\max}^{\text{фл.}}$ (0—1). На рис. 4

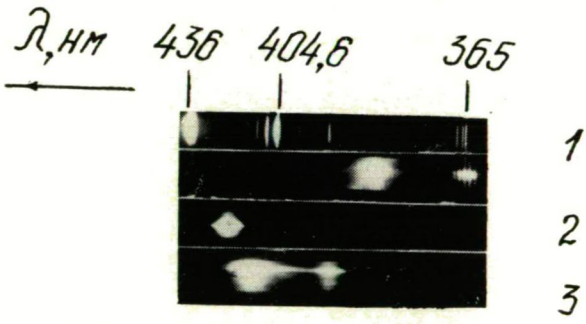

Рис. 4. Спектры излучения, генерируемого растворами: 1—2,5-дифенилоксазол в толуоле, 2—1,4-ди[2-(5-фенилоксазолил)]бензол в толуоле, 3—1,4-ди-(бензоксазол-2′-ил)бензол в диметилформамиде.

приведены спектры излучения, генерируемого рассматриваемыми соединениями в растворах [3, 4, 19]. У соединений I и III в используемых растворителях интенсивность колебательных полос (0—1) и (0—2) мало различается и генерация осуществляется на двух полосах даже в резонаторе с малой добротностью и в пороговом режиме. У ПОПОПа (рис. 2, кр. 1) вследствие значительного

перепада интенсивности полос (0—1) и (0—2) обычно наблюдается однополосная генерация (рис. 4, спектр 2).

Интересно сопоставить спектры генерируемого излучения и флуоресценции в газовой фазе для изолированных молекул и при добавлении посторонних химически неактивных газов. Как отмечалось ранее, генерация впервые была получена на парах ПОПОПа [6]. Накачка производилась на длинноволновом крыле полосы поглощения (рис. 1б), $\varepsilon_{347} = 28000$ л. моль$^{-1}$. см$^{-1}$. На рис. 5 представлены спектры генерируемого излучения парами этого соединения без постороннего газа (спектр 1) и в присутствии пентана (спектры 2—4), взятые из работы [20]. В газовой фазе на контур полосы флуоресценции (усиления) существенное влияние оказывают температура и энергия возбуждающего кванта [1]. В чистых парах для соответствующих $\lambda_в$ и T максимум полосы генерируемого излучения $\lambda_в = 383$ нм практически совпадает с наиболее интенсивным максимумом в спектре флуоресценции (0—1). По данным [20] при давлениях постороннего газа порядка атмосферы длина волны максимума полосы генерации $\lambda_г$ паров ПОПОПа практически совпадает с λ_2 чистых паров, однако мощность генерации возрастает. Посторонний газ пентан ($p = 460$ мм рт. ст.) оказывает стабилизирующее влияние при возбуждении паров ПОПОПа $\lambda_в = 334$ нм, колебательная структура спектра становится резче. Дальнейшее увеличение давления постороннего газа, согласно [22, 23] приводит к смещению спектра флуоресценции паров в длинноволновую сторону и после перехода через критическое состояние он приближается к спектру раствора (рис. 2, кр. 1). Этим объясняется сдвиг полосы генерируемого излучения ПОПОПом в длинноволновую сторону при увеличении P пентана, наблюдавшийся в [20]. В области давлений пентана 3—8 атм генерируется две полосы излучения $\lambda_в = 383$ и 403 нм (рис. 5, спектр 2). Дальнейшее увеличение давления пентана приводило к смещению спектра генерации в длинноволновую область (рис. 5, спектры 3 и 4). Наблюдавшаяся при более высоких $T = 683$—773 °К полоса генерации чистых паров ПОПОПа $\lambda_г = 400$ нм [21] соответствует колебательной полосе в спектре флуоресценции (0—2), что, вероятно, вызвано температурным изменением спектра флуоресценции (рис. 2, кр. 2). С увеличением T увеличивается поглощение на длинноволновом крыле полосы, что приводит к росту вредных потерь в области генерации. Отсутствие генерации при $T > 773$ °К связано со значительным уменьшением выхода флуоресценции с ростом T (рис. 3).

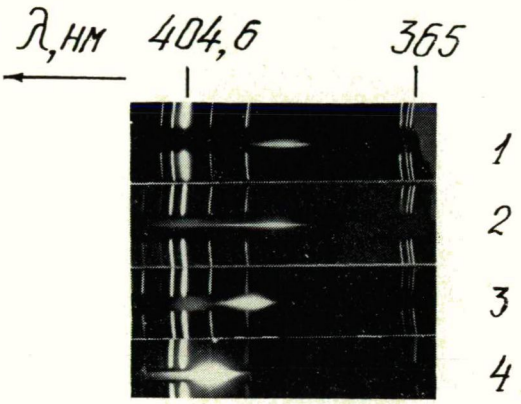

Рис. 5. Спектры генерации паров 1,4-ди[2-(5-фенилоксазолил)]бензола: 1—без постороннего газа ($T - 543$ °К). 2—4 — в присутствии пентана ($T = 513$ °К), 2—концентрация пентана $Сп = 1{,}3 \cdot 10^{20}$ см$^{-3}$, 2—$Сп = 6 \cdot 10^{20}$ см$^{-3}$, 4—$Сп = 4 \cdot 10^{21}$ см$^{-3}$

Эффективная генерация 1,4-(бензоксазол-2-'ил)бензола в нейтральных растворителях, интенсивная флуоресценция в парах, низкие температуры испарения, а также большая фотоустойчивость позволяют считать, что это вещество и родственные ему могут быть активными средами в газовой фазе.

Литература

[1] *Борисевич, Н. А.:* Возбужденные состояния сложных молекул в газовой фазе. Изд. «Наука и техника», Минск (1967).
[2] *Никитина, А. Н., М. Д. Галанин, Г. С. Тер-Саркисян, Б. М. Михайлов:* Опт. и спектр. **6,** 354 (1959).
[3] *Борисевич, Н. А., В. В. Грузинский:* Сб. ст. «Квантовая электроника и лазерная спектроскопия. Минск, 1971, стр. 89.
[4] *Грузинский, В. В., Н. М. Палтарак, П. И. Петрович:* ЖПС, **19,** 352, (1973).
[5] *Набойкин, Ю. В., Л. А. Огурцова, А. П. Подгорный, Ф. С. Покровская, В. И. Григорьева, Б. М. Красовицкий, Л. М. Куцына, В. Г. Тищенко:* Опт. и спектр. **28,** 974 (1970).
[6] *Борисевич, Н. А., И. И. Калоша, В. А. Толкачев:* ЖПС, **19,** 1108 (1973).
[7] *Борисевич, Н. А., И. И. Калоша, В. А. Тугбаев:* ЖПС, **21,** вып. 1 (1974).
[8] *Грузинский, В. В., Л. А. Баркова:* ЖПС, **19,** 254 (1973).
[9] *Грузинский, В. В., Л. А. Баркова, Н. М. Палтарак:* ЖПС, **20,** 619 (1974).
[10] *Борисевич, Н. А., В. В. Грузинский:* Изв. АН СССР, сер. физ., **24,** 545 (1960); ДАН СССР, **175,** 852 (1967).
[11] *Reiser, A. L., J. Leyshon, D. Saunders, M. V. Mijovic, R. Bright, J. Boquie:* J. Am. Chem. Soc. **94,** 2414 (1972).
[12] *Борисевич, Н. А., В. В. Грузинский:* ДАН БССР, **7,** 309 (1963).
[13] *Singh, R. S., S. W. Singh:* Ind. J. Pure Appl. Phys. **5,** 342 (1967).
[14] *Непорент, Б. С.:* ЖЭТФ, **21,** 172 (1951).
[15] *Dobratz, C. J.:* Ind. Eng. Chem. **33,** 759 (1941).
[16] *Шишловский, А. А.:* ДАН СССР, **15,** 29 (1937); ЖЭТФ, **7,** 1252 (1973).
[17] *Грузинский, В. В.:* Изв. АН СССР, сер. физ. **27,** 58 (1963).
[18] *Ware, W. R., P. T. Cunningham:* J. Chem. Phys. **44,** 4364 (1966).
[19] *Борисевич, Н. А., В. В. Грузинский, Л. М. Куцына, Н. М. Палтарак:* ЖПС, **12,** 328 (1970).
[20] *Борисевич, Н. А., И. И. Калоша, В. А. Толкачев:* ДАН СССР, **217,** 74 (1974).
[21] *Steyer, B., F. P. Schäfer:* Opt. Comm. **10,** 219 (1974).
[22] *Непорент, Б. С., Н. А. Борисевич, В. Л. Клочков, О. А. Мотовилов:* Изв. АН СССР, сер. физ. **18,** 674 (1954).
[23] *Непорент, Б. С., В. П. Клочков, О. А. Мотовилов:* ЖФХ, **29,** 305, (1956).

LUMINESCENCE AND STIMULATED RADIATION OF VAPOURS OF PHENYL OXAZOLE AND BENZOXAZOLE

N. A. Borisevich, L. A. Barkova and V. V. Gruzinsky

The spectral and luminescence properties of the molecules with extended system of conjugated bonds: 2,5-diphenyloxazole, 1, 4-bis[2-(5-phehyloxazolyl)]benzene, 1, 4-dibenzoxazolylbenzene are studied in the gas phase. The thermal and optical methods of changing the stored vibrational energy content are found to be equivalent and the vibrational heat capacities are estimated. The luminescence and radiation characteristics of these molecules are compared.

DEFECTS AND AMORPHIZATION IN ION-IMPLANTED SILICON

By

J. GYULAI, P. RÉVÉSZ, L. ZSOLDOS*, G. VÉRTESI* and J. GYIMESI**
Central Research Institute for Physics, Budapest

(Received June 1, 1974)

Defect formation in boron and phosphorus implanted silicon was investigated by infrared spectroscopy, X-ray topography and mechanical surface analyzer. Anneal characteristics are given; an increase in volume after implantation was detected.

Ion-implantation is a very efficient technique for doping materials, first of all semiconductors, but suffers from a side-effect, namely defect formation. Numerous methods were elaborated to study these defects with the aim to eliminate their undesired effect. As today infrared spectroscopy, nuclear backscattering, electron and X-ray diffractography are the widely used methods [1—3]. In the present paper we are going to present results summarizing our work on this matter.

1. *Infrared spectroscopy*

Both transmission and reflection methods were applied to study the damage structure of implanted silicon. The absorption band at 1.8 μm is connected with the presence of divacancies, so-called V—V centers [4]. The thickness of the amorphous layer was determined from the interference structure of the reflection spectrum [5].

A Unicam SP-270 spectrophotometer was used for these experiments. For reflection measurements, a simple mirror system was built. In order to enhance absorption, both surfaces of the sample were implanted with equal dose and energy.

Divacancy absorption. On Fig. 1 the transmission spectrum of an implanted silicon crystal is to be seen, compared with that of a non-implanted wafer. The boron dose was 10^{15} cm^{-2}, the energy 80 keV on each surface. The absorption band at 1.8 μm is very well expressed. In the figure the transmission is to be seen. In the calculations, the difference in αd values (α being the absorption coefficient in cm^{-1}, d the layer thickness) between the implanted and non-implanted case was attributed to the presence of divacancies. In order to restore crystal perfectness, an annealing cycle must be used. The changes in difference of αd for an isochronal anneal* process

* Institute for Experimental Physics, Roland Eötvös University, Budapest.
** Tungsram Works, Budapest.

* "Isochronal" denotes a series of annealing processes in an inert atmosphere with 50 °C steps and 30 minutes duration each.

are shown on Fig. 2. Implantation was made using 80 keV boron ions with 10^{15} and 4×10^{15} cm^{-2} dose. Most of the lattice defects anneal at 500 °C. It is to be noted that the factor four in dose does not mean an increase with the same ratio for the concentration of divacancies. With this relatively high dose, we are getting closer to the limit where the defects are forming clusters or complexes. This process sat-

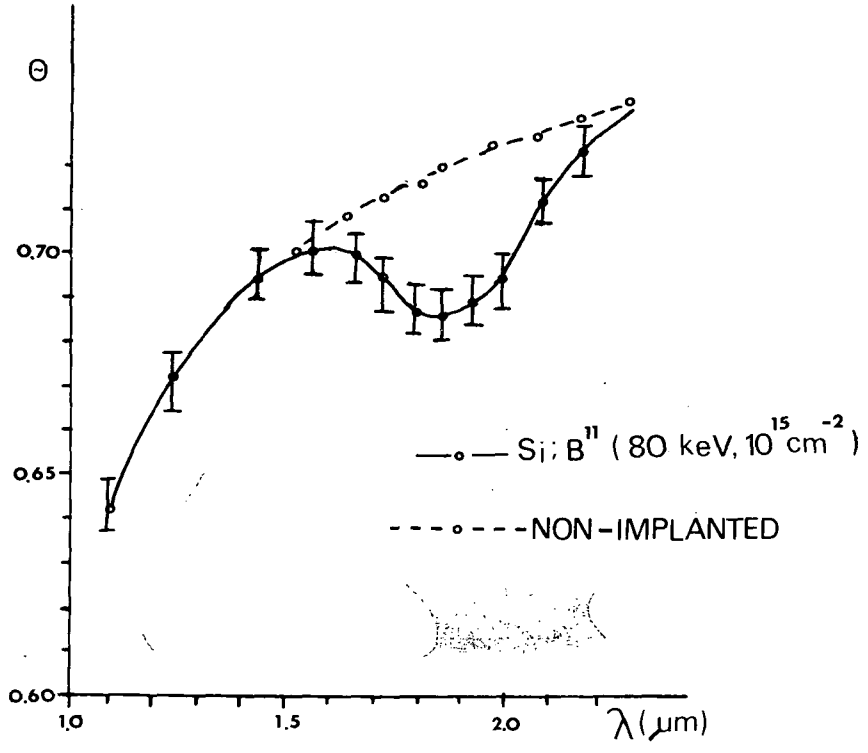

Fig. 1. Optical transmission spectra for boron implanted and non-implanted silicon

urates when the surface is fully amorphous. As Fig. 3 shows, for phosphorus implantation the effective decrease of the N^{vv} divacancy concentration is clear above doses of $2—3\times10^{14}$ cm^{-2}, *i.e.* the concept "divacancy" looses its meaning above this limit. For 80 keV boron implant, this limit is higher in dose; as boron is a light atom the limit does not fall into the range of our measurements.

In cases, when the amorphous phase has been reached, the infrared spectroscopy offers another possibility, which may give an account on the thickness of this layer.

Interference structure of infrared reflection. For amorphous layers, the dielectric constant differs from that of undamaged silicon. In other words, a sandwich of two layers with different optical properties is present. For the thicknesses $d\cong\lambda/4\bar{n}$ of the layer ($\bar{n}$ is the refraction index of the amorphous layer), the reflection spectrum has interference structure [5]. In Fig. 4, the spectra both for 80 keV phosphorus and

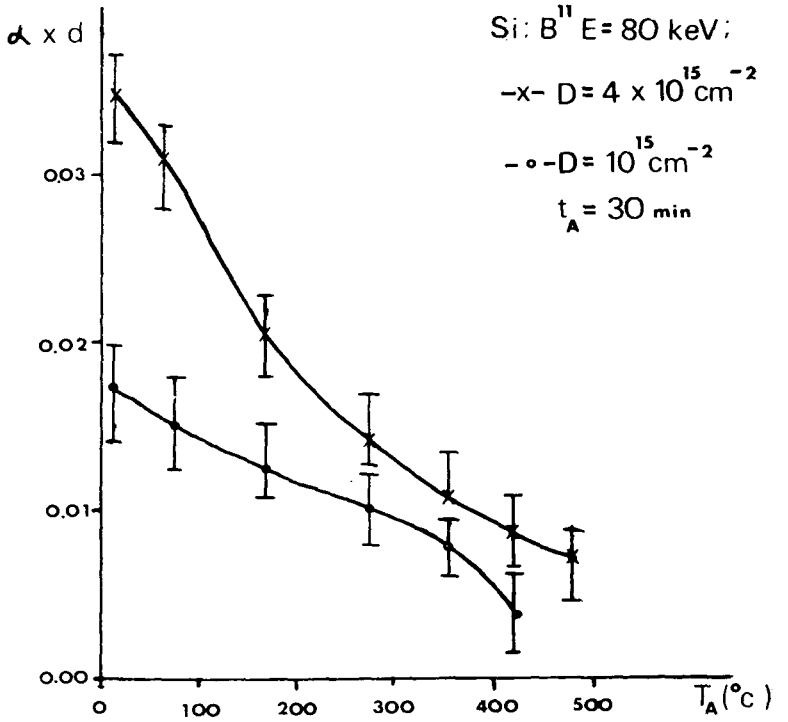

Fig. 2. Anneal characteristics of N^{vv} centers through the values of absorption peaks at 1.8 μm. On the horizontal scale, T_A, the temperature of isochronal anneal sequences is given

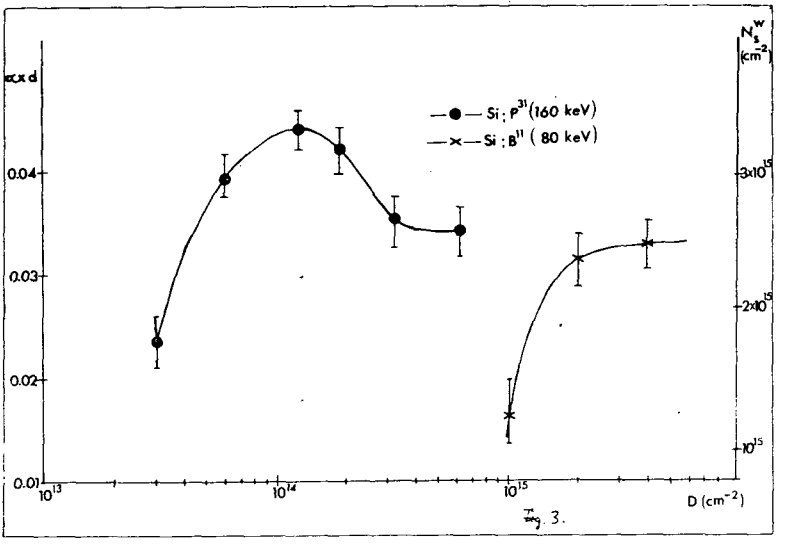

Fig. 3. Dose dependence of N^{vv} and αd for phosphorus and boron implants

boron implants and doses of 1.25×10^{16} and 3.1×10^{16} cm^{-2}, respectively, are shown. It is obvious that the interference structure for phosphorus is more pronounced, as the layer is fully amorphous from optical point of view, while for boron, this is not the case. Another characteristic difference is the distance of the minima, showing that the phosphorus layer is shallower.

In Table I, the examined implants and the corresponding calculated thicknesses of the amorphous layers are listed.

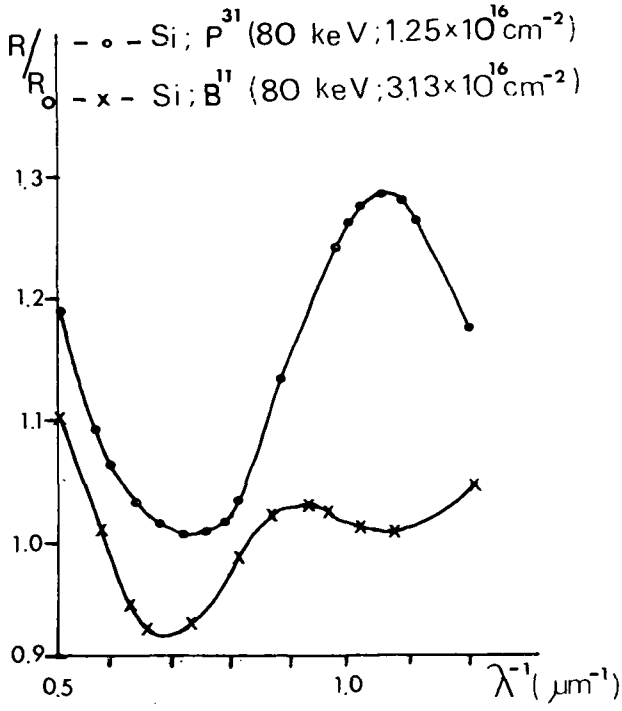

Fig. 4. Interference in reflection spectra, R/R_0, for phosphorus and boron implants

Table I

	Si:P^{31}	Si:B^{11}		
	$E = 80$ keV	$E = 40$ keV	$E = 60$ keV	$E = 80$ keV
1.25×10^{16}	$d = 0.2280\,\mu$m			
2.5×10^{16}	$d = 0.2325\,\mu$m	$d = 0.1850\,\mu$m	$d = 0.2850\,\mu$m	$d = 0.4050\,\mu$m
3.13×10^{16}	$d = 0.2100\,\mu$m			
4.37×10^{16}	$d = 0.2230\,\mu$m	$d = 0.1847\,\mu$m		
6.25×10^{16}	$d = 0.2630\,\mu$m	$d = 0.1855\,\mu$m		

The infrared spectroscopy as a method for measuring layer thicknesses has some specific properties. It gives some kind of average as if a rectangular distribution were present. In case of boron, the thickness of the disordered layer determined by optical method is

$$d_{opt} = R_p + \Delta R_p,$$

where R_p is the projected range and ΔR_p the standard deviation. For phosphorus, the experiments gave a somewhat different result

$$d_{opt} = R_p + 4\Delta R_p.$$

This can be explained qualitatively as follows. The interference structure is connected with the existence of two layers with different optical refraction. Only the amorphization of the silicon will cause sufficient changes in the refraction index, therefore, the measured values may be clarified by calculating the surface concentration (in cm^{-2} units) of atoms penetrating through the effective layer thickness d_{opt}. This concentration appears just below the amorphous limit. For phosphorus, 2×10^{13} cm^{-2} atoms penetrate deeper than $d_{opt}=0.21$ μm. This value is somewhat lower than the amorphous limit which is around 10^{14} cm^{-2}. The same can be said for boron. The more exact solution of the problem is a future task.

2. *X-ray topography*

Changes in lattice constant due to implantation were investigated with X-ray topography. The so-called Berg—Barrett type reflection was used. In this case a monochromatic X-ray produces the diffraction, the information on inhomogeneities or lattice defects can be calculated therefrom [3]. This can be performed with high accuracy by photographing the pattern. According to Bragg's formula, the reflection angle from portions with different lattice constant is somewhat different. Therefore, using a divergent beam, a shift between images of non-irradiated and irradiated portions is found, the shift being proportional to the change in lattice constant.

Photographs were made using the Cu $K_{\alpha 1}$ radiation, with reflection from the (333) plane, parallel with the surface. Photometry was used to determine the shift. The changes in reflection angle, $\Delta\vartheta$, can be determined from the known geometry of the system and the relative change in lattice constant $\Delta a/a_0=(a-a_0)/a_0$, depends on the angles as follows:

$$\frac{\Delta a}{a_0} = -\operatorname{ctg}\vartheta\cdot\Delta\vartheta,$$

where ϑ is the reflection angle for the undamaged surface.

A conventional diode structure was used for this measurement. The thick oxide (SiO_2) was used as a mask and $^{11}B^+$ ions (energy 80 keV, dose 6×10^{15} cm^{-2}) were implanted through the square windows covered by 1200 Å thermal oxide. Measurements were made on as-implanted samples, and after 30 minutes anneal at 600 and 800 °C respectively.

Table II

	$\Delta a/a_0$
as-implanted	$1.6\times10^{-3}\pm10\%$
$T_A = 600$ °C	$0.9\times10^{-3}\pm10\%$
$T_A = 800$ °C	0.6×10^{-3}

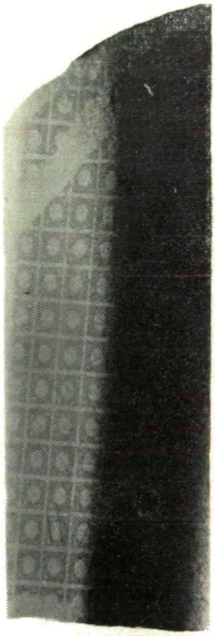

Fig. 5. A (333) X-ray topogram for a boron-implanted diode structure. Implanted are the square portions

In Fig. 5, the reflection topogram of the as-implanted crystal is to be seen. The dark portion on the right is the diffraction maximum from the deep undamaged part of the crystal with dislocation lines visible at the edge. The contrast on the left is due to the implanted squares ($6\times$ magnification).

The calculated changes in lattice constant are given in Table II.

During annealing, the original lattice structure is restored by an epitaxial regrowth.

3. *Mechanical measurement of volume changes*

In order to clarify changes in crystal structure, a series of measurements were made using a mechanical probe to detect volume changes of implanted crystals. In order to get more pronounced effect, we omitted the 1200 Å thick silicon dioxide, *i.e.* all ions were implanted into the silicon. The volume changes were measured by a Talystep equipment (Rank Precision Industries). This equipment used a diamond stylus travelling along the surface, sensing steps on it (Fig. 6). The step height for an as-implanted crystal (boron ions, 80 keV, 6×10^{15} cm^{-2}) was 30 Å. Comparing this value with $\Delta a/a_0$ in the previous section, it is clear that the changes in lattice constant in the deeper portion of the implant layer do not explain this relatively big value. This indicates that the amorphous layer lying above the partly disordered layer is responsible for most of the volume changes. In X-ray measurements, this amorphous part does not play a role in "changes" of the lattice constant.

The correlation between defect production and changes in volume is of great interest. As a first result, in Fig. 7 we present step height values for 80 keV boron, silicon and arsenic implant, showing a decrease in step height with increasing mass. The dose was 3×10^{16} cm^{-2} for all samples. This result correlates with results measured by a cantilever technique [6]. A more complex study of the question is going on.

* * *

It is a distinguished honour to one of the authors (J. G.) to express sincere gratitude to the memory of his first master, Professor A. BUDÓ.

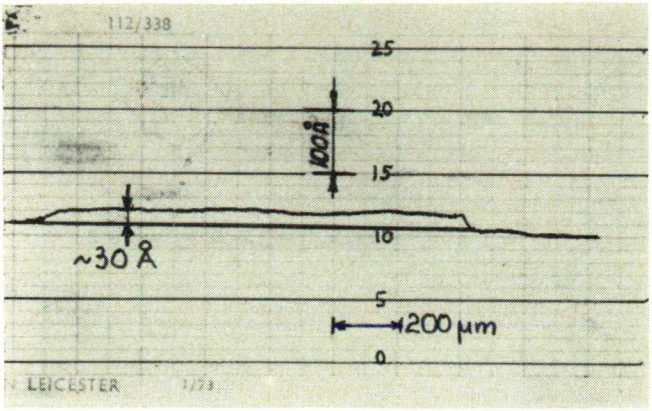

Fig. 6. Step height of an 80 keV, 6×10^{15} cm^{-2} dose boron implant measured with a Talystep. On the vertical scale one small division is 20 Å, horizontal magnification is given in the figure

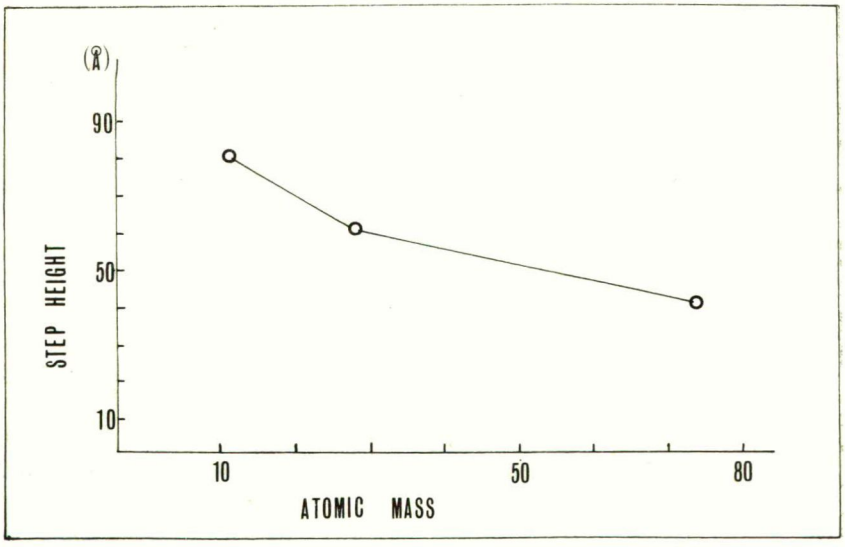

Fig. 7. Step height, *i.e.* volume increase for 3×10^{16} cm^{-2}, 80 keV implants into silicon

References

[1] *Стрельцов, Л. Н.:* Физ. Тех. Полупр. **4**, 715 (1970).
[2] *Eisen, F. H.:* Application to Radiation Damage in Channeling, Ed. by D. V. Morgan (John Wiley, London, 1973), p. 415.
[3] *Lang, A. R.:* Recent Applications of X-Ray Topography, in Modern Diffraction and Imaging Techniques in Material Science, Ed. by S. Amelinckx (North Holland Publishing Company, 1970).
[4] *Stein, H. J.:* Appl. Phys. Letters **14**, 328 (1969).
[5] *Гусев, В. М., Л. Н. Стрельцов:* Физ. Тех. Полупр. **5**, 832 (1971).
[6] *EerNisse, E. P.:* Appl. Phys. Letters **18**, 581 (1971).

ДЕФЕКТЫ И АМОРФИЗАЦИЯ В ИОННО ЛЕГИРОВАННОМ КРЕМНИИ

Й. Дьюлаи, П. Ревес, Л. Жолдош, Г. Вертеши, Й. Дьимеши

Исследовано образование дефектов в слоях кремния, легированных ионами бора и фосфора, методами ИК-спектроскопии, рентгено топографии а также механическим анализатором поверхности кристалла. Получены характеристики отжига дефектов и обнаружено увеличение объёма после ионного легирования.

ON CONCENTRATIONAL DEPOLARIZATION OF PHOTOLUMINESCE IN SOLUTIONS AT DIFFERENT WAVELENGTHS OF EXCITING LIGHT

By

C. BOJARSKI, J. DUDKIEWICZ and A. BUJKO

Institute of Physics, Technical University, Gdańsk, (Poland)

(Received June 1, 1974)

Measurements of the concentrational dependence of photoluminescence emission anisotropy (EA) in glycerol—methanol solutions of acriflavine (system I) and glycerol—water solutions of rhodamin 6 G (system II), at excitation by ν_{0-0} as well as $\nu > \nu_{0-0}$ frequencies, have been carried out.

At excitation by ν_{0-0} frequencies in the range of high concentrations, repolarization effect and good agreement of experimental results with theory has been found.

However, at excitation by $\nu > \nu_{0-0}$ frequencies, the relative values of EA, $\left(\frac{r}{r_0}\right)_\nu$, appeared to be remarkably lower than the values of EA, $\left(\frac{r}{r_0}\right)_{\nu_{0-0}}$ at the excitation by ν_{0-0} frequency, particularly in the range of high concentrations. In this case repolarization effect for system II was not observed.

Introduction

Concentrational depolarization of photoluminescence (CDPL) in isotropic solutions has been a subject of continous and intensive theoretical and experimental investigations [1—8]. Recently [9, 10] some investigations of CDPL in a wide range of concentration have been carried out. In the range of highest concentrations, a repolarization effect has been found in accordance with the prediction of the CDPL theory taking into account excitation energy remigration and concentrational quenching by dimers [6, 11].

This result was obtained at the excitation of luminescence by light of ν_{0-0} frequency, corresponding to $0-0$ transition, not disturbing the thermal equilibrium of active molecules in the medium.

At the excitation with $\nu > \nu_{0-0}$ frequency, however, there is a possible energy transfer before thermal relaxation in excited state occurs, if the interaction between D^* and D molecules is sufficiently strong [5, 12—18].

It can be expected that energy transfer of this kind will occur particularly in the range of high concentrations of active molecules in solutions.

In this work we present the results of investigations concerning the CDPL phenomenon in the range of high concentrations at ν_{0-0} and $\nu > \nu_{0-0}$ frequencies of exciting light.

Experimental Part

The object of the investigations were glycerol—alcohol solutions of acriflavine ($C_{14}H_{14}N_3Cl$; m.w.=259,75; system I) and glycerol—water solutions of rhodamine 6G ($C_{26}H_{27}O_3N_2Cl$; m.w.=450,98; system II). In the case of system I the solvent was glycerol containing 5% (w/w) methanol and in the case of system II glycerol containing 10% (w/w) water with an addition of $3.4 \cdot 10^{-4}$ M/l HCl. All the dyestuffs were purified in an ordinary way by recrystallization and the purity degree was checked spectroscopically. Glycerol ("Strem", Poland) and methanol (p.a. "Oświęcim", Poland) were applied without any further purification. For measuring the emission anisotropy EA, the quantum yield η/η_0 as well as fluorescence spectra, the methods and measuring apparatus described in [10] were applied.

In the case of EA measurements luminescence was excited by a high pressure mercury lamp DRSz-250, applying filters listed in Table I, which also gives those used in the observation.

Table I

Filters applied at the measurements of emission anisotropy

	Excitation	Observation
Acriflavine in glycerol—methanol solutions	SiF 436 Hg	OG-5 ($\lambda > 530$ nm)
	IF 475	OG-5
Rhodamine 6G in glycerol—water solutions	SiF 436 Hg	OG-3 ($\lambda > 570$ nm)
	IF 550	IF 575

For quantum yield measurements luminescence was excited by the light of an incandescent lamp. Instead of filters, monochromators were used for the excitation as well as for the observation.

In working out the results of the measurements, in the case of EA, corrections for secondary fluorescence and, in the case of η/η_0, for secondary fluorescence and anisotropy of the spatial distribution of fluorescence, were taken into account in the way described in [19—21].

The absorption spectra were measured with a VSU 2—P spectrophotometer.

Results and discussion

In Fig. 1 absorption and fluorescence spectra of the solutions are presented. In the case of acriflavine solutions the absorption and fluorescence spectra turned out to be practically independent of the concentration, contrary to the rhodamine 6G solutions which show remarkable changes in the absorption spectra.

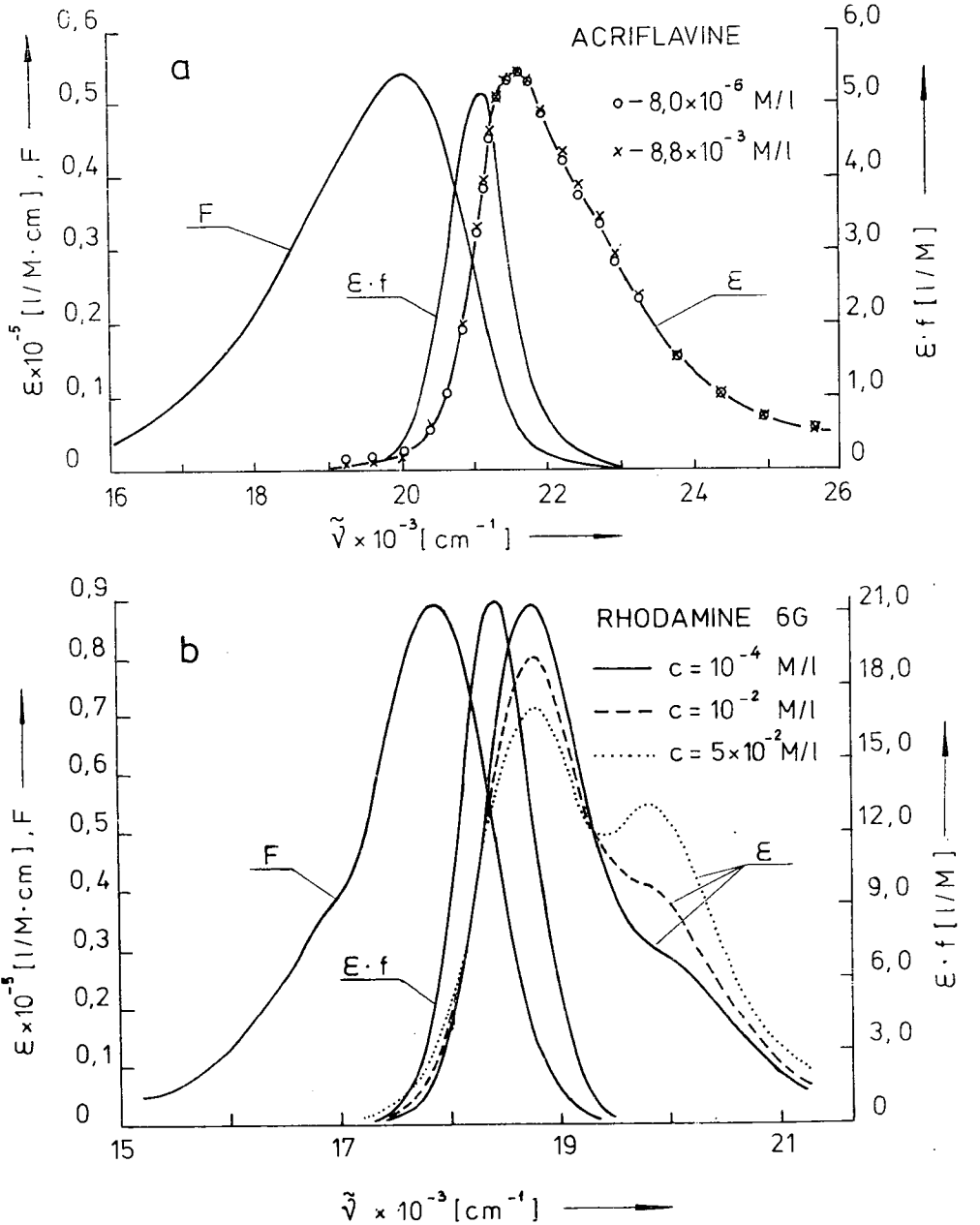

Fig. 1. Electron absorption spectra (ε), fluorescence quantum spectra (F) of glycerol—methanol solutions of acriflavine (*a*) and glycerol—water solutions of rhodamin 6G (*b*). Fluorescence spectra corrected for reabsorption and spectral sensitivity of the photomultiplier

In the case of rhodamin 6G solutions two isosbestic points at frequencies 18 200 cm^{-1} and 19 333 cm^{-1} are visible (Fig. 1*b*). On the base of our assumption, only two kinds of molecules, monomers and dimers appear in rhodamin 6G solutions in the concentration range investigated. Though the absorption spectra of acriflavine solutions do not exhibit practically any concentrational changes (comp. Fig. 1*a*) still the existence of monomers and dimers in them has been accepted. This assumption is necessary to explain the repolarization effect and the decrease of quantum yield observed in the range of high concentrations (comp. Fig. 2*a*). This assumption is justified because it has been pointed out before that proflavine as well as acriflavine form non-fluorescent dimers in solutions [22—24]. Let us add that the absence of concentrational dependence of absorption spectra, regarded by some authors [25, 26] as a criterion of the lack of any associates in solution, is not in general valid [27].

True enough the molecular exciton. theory [28, 29] predicts a split of the excited levels of interacting molecules in the dimer which leads to the appearing of

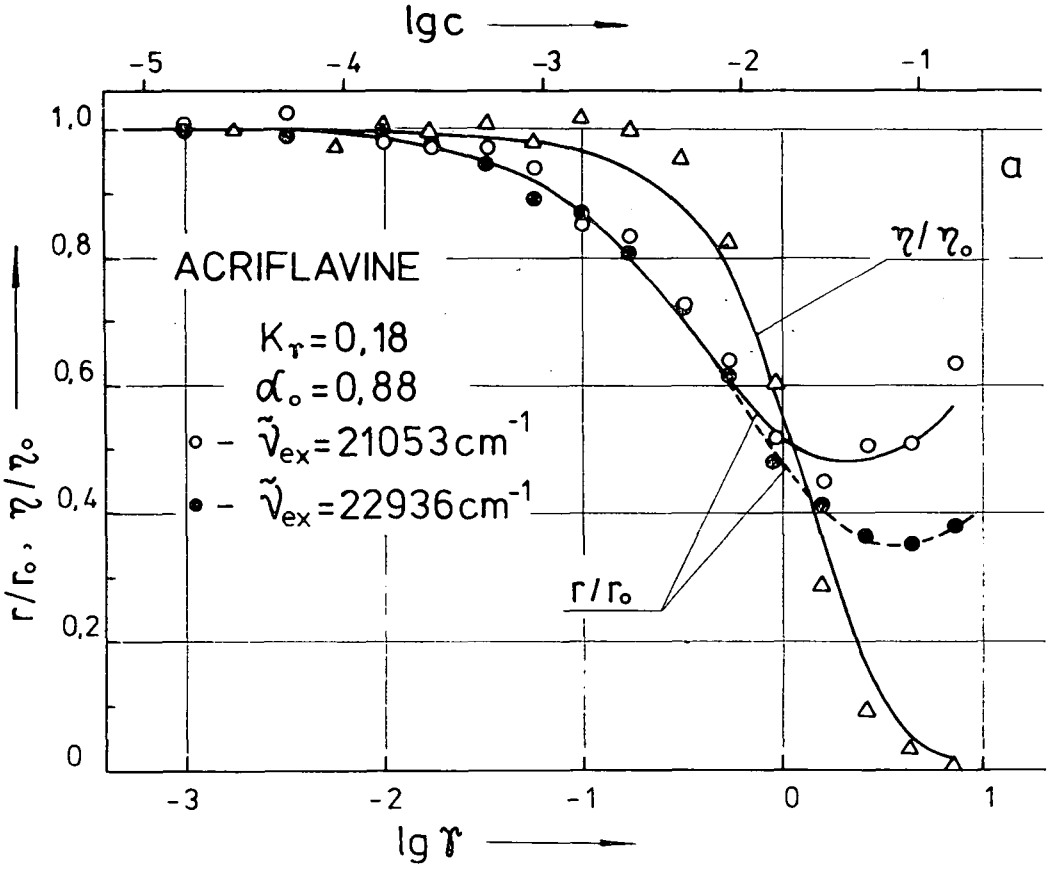

Fig. 2a

two bands in the absorption spectrum of the dimer. Still, depending on the distance and mutual position of monomer units in the dimer, the absorption spectra of the monomers ε' and dimers ε'' can practically overlap. In this case the absorption spectra of the solution do not change with concentration. In Fig. 2*a*, *b* the concentrational dependences of photoluminescence emission anisotropy at excitation frequencies $\nu \cong \nu_{0-0}$ (empty circles) and $\nu > \nu_{0-0}$ (full circles) are presented. At excitation frequencies $\nu \cong \nu_{0-0}$, when the thermal equilibrium between D^* molecules and the medium is not disturbed, the depolarization in both systems investigated is smaller than that at the excitation frequencies $\nu > \nu_{0-0}$. The difference $\left(\frac{r}{r_0}\right)_{\nu_{0-0}} - \left(\frac{r}{r_0}\right)_{\nu}$ of

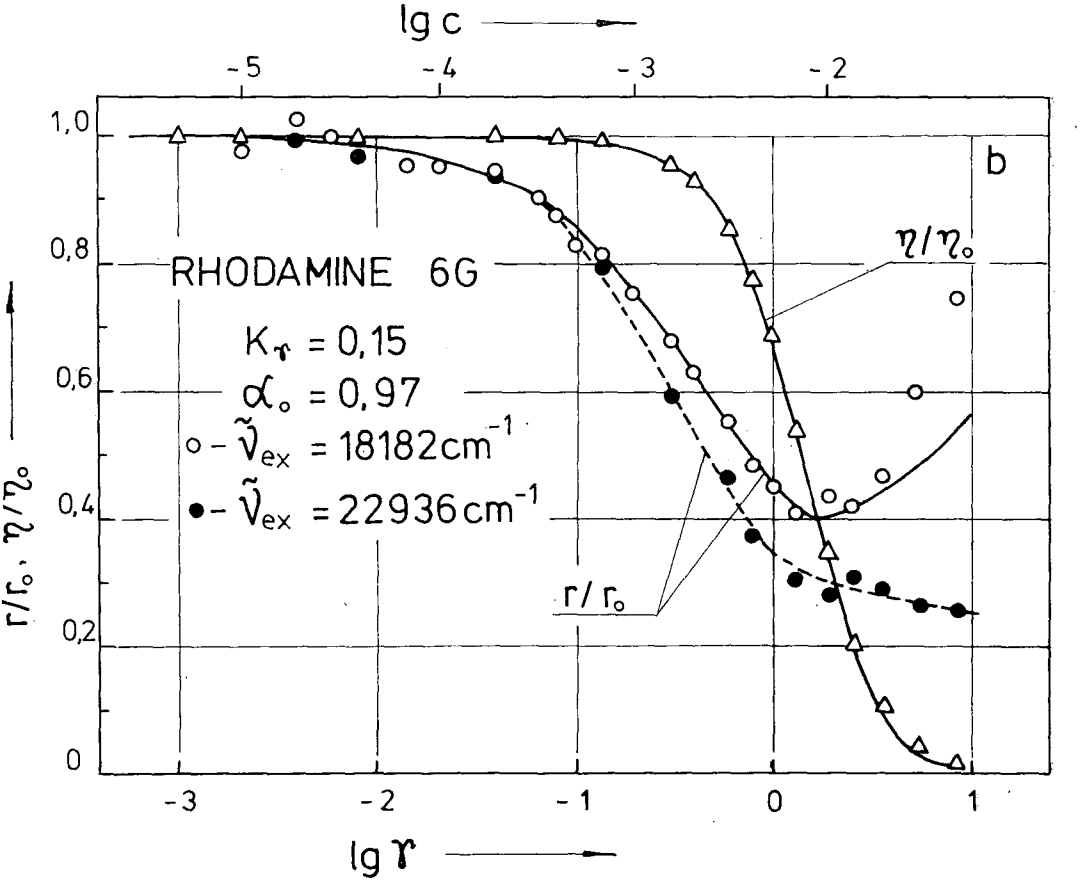

Fig. 2a, b. Concentration dependence of emission anisotropy $\frac{r}{r_0}$ and quantum yield η/η_0 of fluorescence of glycerol—methanol solutions of acriflavine (*a*) and glycerol—water solutions of rhodamin 6G (*b*). Solid lines: theoretical curves of $\frac{r}{r_0}$ and η/η_0, determined by Eqs. (1) and (2); ○, ● and Δ: experimental points

the EA values at the excitation frequencies ν_{0-0} and ν, increases with the dye concentration of the solution. At excitation frequencies ν_{0-0} a repolarization effect connected with a strong concentrational quenching is visible.

This is proved by the course of the quantum yields curves as a function of dye molecule concentration (comp. Fig. 2*a*,*b*).

Concentrational dependences of emission anisotropy $\frac{r}{r_0}$ and quantum yield $\frac{\eta}{\eta_0}$ at the excitation frequency ν_{0-0} can be described by formula (6) in [30], *i.e.*

$$\frac{r}{r_0} = (1-\Phi)\left[1+\frac{1}{2}\frac{\Phi^2}{1-\frac{3}{4}\Phi^2}\right], \tag{1}$$

$$\frac{\eta}{\eta_0} = \frac{1-f}{1-\Phi}, \tag{2}$$

where

$$\Phi = \alpha_0 \alpha f, \tag{3}$$

$$\alpha = \frac{\gamma_D}{\gamma_D+\gamma_{D_{II}}}, \tag{4}$$

$$f = \sqrt{\pi}\,\gamma \exp(\gamma^2)[1-\operatorname{erf}(\gamma)], \tag{5}$$

$$\gamma = \gamma_D+\gamma_{D_{II}} = \frac{\sqrt{\pi}}{2}\left(\frac{c'}{c_0'}+\frac{c''}{c_0''}\right). \tag{6}$$

Here c' and c'' denote monomer and dimer concentrations, c_0' and c_0''-critical concentrations for excitation energy transfer to monomers D and dimers D_{II}, α_0 is the probability of the non-occurence of excitation energy degradation during its transfer between monomers.

In Fig. 2*a*,*b* the solid lines $\frac{r}{r_0}$ and $\frac{\eta}{\eta_0}$ present the theoretical curves determined by expressions (1) and (2), plotted for the parameter values listed in Table II. Beside critical concentrations c_0' and c_0'', the corresponding critical distances R_0' and R_0'' are also given in the table [comp. Eq. (9)].

The values of the parameter $K_\gamma = \gamma_{D_{II}}/\gamma_D^2$ and the critical concentration c_0 can be found from the relations[1]

[1] Relations (6) and (7) in this and in earlier papers [6, 9, 10, 24, 30] had a somewhat different form, namely instead of factor π they contained the factor $\pi\eta_0$. The presence of η_0 beside π was a result of excluding the factor $\eta_0^{1/2}$ from the expressions of type (8) for c_0' and c_0''. Then $\eta_0=1$ should have been put in expr. (8). In the papers quoted above, in spite of the explicite η_0 appearing in the expressions for γ and K_γ, $\eta_0 \neq 1$ was accepted by mistake in, expr. (8). As a result this led to the conclusion that $\gamma \sim \eta_0$ and $K_\gamma \sim \eta_0^{-1}$, whereas from relation (6), (7) and (8) it is clear that $\gamma \sim \eta_0^{1/2}$ and $K\gamma \sim \eta_0^{1/2}$. Let us add that all the conclusions and diagrams quoted in the above papers remain unchanged, only the formerly accepted value of η_0 should be replaced by η_0^2.

$$K_\gamma = \frac{2Kc_0'^2}{\sqrt{\pi}\, c_0''}, \tag{7}$$

$$c_0' = 5.18 \cdot 10^{-10} \frac{n^2 \bar{\nu}'^2}{(\bar{\varepsilon}' \eta_0)^{1/2}} \ [\mathrm{M/l}], \tag{8}$$

where $K = c''/c'^2$ is the dimerization constant, n the refractive index of the medium, $\bar{\nu}'$ the mean value of the wave number in the overlapping region of absorption spetrum ε' of the monomer and the fluorescence spectrum F, $\bar{\varepsilon}'$ is the mean value of the molar decimal extinction coefficient in the overlapping region of ε' and F spectra, at which

$$\varepsilon' = \int_0^\infty \varepsilon'(\nu) F(\nu) d\nu \ [\mathrm{l/Mcm}], \quad \int F(\nu) d\nu = 1.$$

K_γ and c_0'' can be determined directly on the basis of relations (7) and (8) in the case when the absorption spectra of the investigated systems exhibit sufficiently big concentrational changes. Then the absorption spectrum of dimers ε'' as well as the dimerization constant K can be found by means of the method worked out by FÖRSTER [31] and LEVSHIN [32].

Table II

Experimental data for glycerol—alcohol (GA) solutions of acriflavine and glycerol—water solutions (GW) *of rhodamine* 6G

System	1	2	3	4	5	6	7	8	9	10
	η	I	n	$\sqrt{\overline{r^2}}$ [a]	$\bar{\varepsilon}'$	$\bar{\varepsilon}''$	$\tilde{\nu}_{0-0}$	$\bar{\nu}'$	$\bar{\nu}''$	$\underline{\eta_0}$
	P	K	–	Å	10^4 l/Mcm		$\mathrm{cm^{-1}}$	$\mathrm{cm^{-1}}$	$\mathrm{cm^{-1}}$	
Acriflavine in GA solutions	3,9	293	1,460	1,45	0,556	0,556	20 934	21 200	21 200	0,417
Rhodamin 6G in GW solutions	1,7	293	1,456	1,02	1,68	0,332	18 360	18 389	17 953	0,435

System	11	12	13	14	15	16	17	18	19
	c_0'	c_0''	R_0'	R_0''	K	K_γ	α_0	r_0 [b]	P_0
	10^{-3} M/l		Å		l/M	–	–	–	%
Acriflavine in GA solutions	10,1	10,1	33,6	33,6	12,0	0,18	0,88	0,3374 [c] 0,3044 [e]	43,3 39,6
Rhodamine 6G in GW solutions	4,34	2,94	45,0	51,2	20,7	0,15	0,97	0,360 [d] 0,271 [e]	45,8 35,8

[a] mean displacement of luminescent molecule in Brownian diffusive movement during its mean lifetime in excited state.

[b] r_0: emission anisotropy corresponding to the ground polarization degree P_0.

[c] $\tilde{\nu}_{ex} = 21053\ \mathrm{cm^{-1}}$, [d] $\tilde{\nu}_{ex} = 18182\ \mathrm{cm^{-1}}$, [e] $\tilde{\nu}_{ex} = 22936\ \mathrm{cm^{-1}}$.

Still, in the case of GA solutions of acriflavine, a method of this kind could not be applied. Values K_γ and α_0 for each of the systems investigated have been found by choosing from the family of theoretical curves r/r_0 and η/η_0 those which give the best agreement with experimental results.[2] The choice of K_γ and α_0 is not arbitrary, because the fitting of experimental results to theoretical curves is possible only for a definite pair of parameter values K_γ and α_0, as proved in [10, 33]. It can be seen from Fig. 2*a,b* that at excitation frequencies $\nu \cong \nu_{0-0}$ the agreement of experimental results with the CDPL theory is quite satisfactory, still, at excitation frequencies $\nu > \nu_{0-0}$ the experimental points remarkably deviate from the theoretical curves. It should be emphasized that in the case of the investigated systems the course of concentrational changes of the relative quantum yield does not depend on the frequency of exciting light ($\nu > \nu_{0-0}$). Investigations concerning CDPL of glycerol—methanol solutions of tripaflavine and rhodamine B with excitation by light of different frequencies ν have recently been carried out by BAUER and CHEREK [18]. These authors have stated a remarkable decrease of the value of $\left(\frac{r}{r_0}\right)_\nu$ at excitation frequency $\nu > \nu_{0-0}$ in comparison with values $\left(\frac{r}{r_0}\right)_{\nu_{0-0}}$ at the excitation frequency ν_{0-0}. They have observed a noticable effect $\left[\left(\frac{r}{r_0}\right)_{\nu_{0-0}} - \left(\frac{r}{r_0}\right)_\nu \sim 0.1\right]$ already in the range of moderate concentrations ($10^{-3} \div 5 \cdot 10^{-3}$ M). In the case of the systems investigated, only rhodamine 6G shows a comparable effect in this range of concentration (comp. Fig. 2*b*). The greatest effect could be expected in the case of highest concentrations when the value of rate constant k_{D^*D} for nonradiative excitation energy transfer from D^* to D, is comparable with the rate constant for vibrational relaxation[3]. Experiment has fully confirmed this point of view (comp. Fig. 2). BAUER and CHEREK have pointed out that the course of concentrational changes of EA at the excitation frequencies $\nu > \nu_{0-0}$ can be described in the range of low concentrations by the CDPL theory developed recently by JABŁOŃSKI [7]. The agreement of theory with experiment has been obtained there by accepting a bigger value for k_{D^*D}, which is equivalent to accepting a bigger value for the critical distance R_0 (smaller value of critical concentration c_0). However in the cases where repolarization effect appears, this kind of modifying the CDPL theory is not sufficient for a correct description of experimental results r/r_0 at excitation frequencies $\nu > \nu_{0-0}$, because this kind of modification merely leads to a shift of the experimental points along the γ axis (comp. Fig. 2). On account of this explanation, the increasing effect of CDPL at excitation frequencies $\nu > \nu_{0-0}$, only by an increase of k_{D^*D} does not seem to be sufficient.

It could be supposed that an increase of the k_{D^*D} value would also influence the

[2] To optimalize the choice of K_γ and α_0 a special method described in Ref. [34] was applied.

[3] In the case when energy transfer is conditioned by dipole—dipole interaction, the rate constant for this process is [35]

$$k_{D^*D} = \frac{1}{\tau_D}\left(\frac{R_0}{R}\right)^6, \tag{9}$$

where τ_D is the mean lifetime of the donor molecule in excited state when $c \to 0$, R the distance between D^* and D molecules, R_0 critical distance.

effectiveness of nonradiative energy transfer from monomers D to dimers D_{II}. It turns out, however, that the courses of concentrational changes of η/η_0 at the excitation frequencies ν_{0-0} and $\nu > \nu_{0-0}$ are the same. Maybe the observed effect of the influence of the frequency of exciting light on the course of concentrational dependence of $\frac{r}{r_0}$ is connected with the decrease of the probability of the remigration of excitation energy to molecules D_0, primary absorbers of exciting light.

* * *

The authors express their gratitude to A. SODOLSKA and A. HAWARRA for their technical help. This work was supported by the Polish Academy of Sciences within the project 3.2.08.

References

[1] *Schmillen, A., R. Legler:* Landolt—Börnstein, Zahlenwerte und Funktionen aus Naturwissenschaften und Technik, Neue Serie, Gruppe II, Bd. 3, Lumineszenz organischer Substanzen, Springer-Verlag, Berlin, (1967).
[2] *Sarshevskij, A. M., A. N. Sevtschenko:* Anisotropija poglostschenija i ispuskanija sveta molekulami, Minsk (1971).
[3] *Ore, A., E. L. Eriksen:* Phys. Norveg. **5**, 57 (1971).
[4] *Craver, F. W., R. S. Knox:* Molec. Phys. **22**, 358 (1971).
[5] *Dale, R. E., R. K. Bauer:* Acta Phys. Polon. **A40**, 853 (1971).
[6] *Bojarski, C.:* J. Luminescence **5**, 413 (1972).
[7] *Jabłoński, A.:* Acta Phys. Polon. **A41**, 85 (1972).
[8] *Kawski, A., J. Kamiński:* Izv. Ak. Nauk USSR **37**, 761 (1973).
[9] *Bojarski, C., J. Dudkiewicz:* Z. Naturforsch. **26a**, 1028 (1971).
[10] *Bojarski, C., J. Dudkiewicz:* Z. Naturforsch. **27a**, 1751 (1972).
[11] *Bojarski, C.:* Z. Naturforsch. **26a**, 1856 (1971).
[12] *Förster, Th.:* Z. Electrochem. **53**, 93 (1949).
[13] *Guéron, M., J. Eisinger, R. G. Schulman:* J. Chem. Phys. **47**, 4077 (1967).
[14] *Hizhnyakov, V. V.:* phys. stat. sol. (b) **51**, K117 (1972).
[15] *Jabłoński, A.:* Bull. Acad. Polon. Sci., Ser. Sci. Math. Astronom. Phys. **20**, 243 (1972).
[16] *Bauer, R. K.:* Acta Phys. Polon. **35**, 975 (1969).
[17] *Bauer, R. K., L. Szalay, E. Tombácz:* Biophys. J. **12**, 731 (1972).
[18] *Bauer, R. K., H. Cherek:* Bull. Acad. Polon. Sci., Ser. Sci. Math. Astronom. Phys. **20**, 961 (1972).
[19] *Budó, A., I. Ketskeméty:* Acta Phys. Hung. **7**, 207 (1957).
[20] *Budó, A., I. Ketskeméty:* Acta Phys. Hung., **14**, 167 (1962).
[21] *Dudkiewicz, J.:* Z. Nauk. Polit. Gdańsk (IX), **191**, 55 (1972).
[22] *Hangen, R. C., N. H. Melhuish:* Trans. Faraday Soc. **60**, 386 (1964).
[23] *Strauss, G., S. B. Broyde, T. Kuruscev:* J. Phys. Chem. **75**, 2727 (1971).
[24] *Bojarski, C., G. Obermüller, J. Kuśba, J. Dudkiewicz:* Z. Nauk. Polit. Gdańsk **191**, 11 (1972).
[25] *Galanin, M. D.:* Trudy Fiz. Inst. Akad. Nauk USSR **12**, 3 (1960).
[26] *Vavilov, S. I.:* J. of Phys. USSR **7**, 141 (1943).
[27] *Levshin, L. V., E. Ju. Behli, T. D. Slavnova:* Opt. Spektr. **36**, 503 (1974).
[28] *Davydov, A. S.:* Sh. Exp. Teor. Fis. **18**, 210 (1948).
[29] *Kasha, M., H. R. Rawls, M. Ashrat El-Bayoumi:* Pure Appl. Chem. **11**, 371 (1965).
[30] *Bojarski, C., J. Domsta:* Acta Phys. Hung. **30**, 145 (1971).
[31] *Förster, Th., E. Konig:* Z. Elektrochem. **61**, 344 (1957).
[32] *Levshin, V. L., J. G. Baranova:* Opt. i. Spektroskop. **6**, 55 (1959).
[33] *Bojarski, C., A. Bujko. J. Dudkiewicz, J. Kuśba, G. Obermüller:* Acta Phys. Polon. **A45**, 71 (1974).
[34] *Dudkiewicz, J., G. Obermüller:* Ogólnopolska Konferencja Luminescencyjna, Toruń, 1974 (in print).
[35] *Förster, Th.:* Ann. Physik (Leipzig) **2**, 55 (1948).

О КОНЦЕНТРАЦИОННОЙ ДЕПОЛЯРИЗАЦИИ ФОТОЛЮМИНЕСЦЕНЦИИ В РАСТВОРАХ ПРИ РАЗНЫХ ДЛИНАХ ВОЛНЫ ВОЗБУЖДАЮЩЕГО СВЕТА

У. Боярски, Й. Дудкиевич, А. Буйко

Произведены измерения концентрационной зависимости анизотропии эмиссии (АЭ) фотолюминесценции глицериново—спиртовых растворов акрифлавина (система I), а также глицериново—водных растворов родамина 6Ж (система II) при возбуждении частотами ν_{0-0} и частотами $\nu > \nu_{0-0}$. При возбуждении частотами ν_{0-0} в области высоких концентраций обнаружен эффект реполяризации. Констатировано хорошее согласие экспериментальных результатов с теорией. При возбуждении же частотами $\nu > \nu_{0-0}$ относительные значения АЭ, $\left(\frac{r}{r_0}\right)_\nu$, оказались значительно низшими, чем значения АЭ, $\left(\frac{r}{r_0}\right)_{\nu_{0-0}}$, при возбуждении частотами ν_{0-0}, особенно в области высоких концентраций. В этом случае эффект реполяризации для системы II не наблюдается.

n-ELECTRON ($n=2, 4, 6, 8$) SINGLETS AS S^2 EIGENFUNCTIONS

By

F. BERENCZ

Institute of Theoretical Physics, Attila József University, Szeged

(Received June 1, 1974)

n-electron ($n=2, 4, 6, 8$) singlets as S^2 eigenfunctions were constructed by the method of spin operators.

Introduction

Only for certain rather special forms of the potential function is the wave equation completely soluble in closed terms; in general, different approximate methods must be applied. The most important one of these methods is the general method of configuration interaction. In the investigation of molecules by configuration interaction one is usually faced with the problem of setting up the states of definite multiplicity for the various configurations. If the states of the various configurations are described by Slater determinants, the linear combination of Slater determinants can be regarded as the best zero-order eigenfunction. Then, the energy, to first order, is given by the roots of the usual secular equation. The secular determinant can be broken down into a product of determinants of lower order by means of the operators S^2 and S_z. A simple and direct method to construct the suitable eigenfunctions for an n-electron system, fulfilling the operator equation of both operators S^2 and S_z simultaneously, was suggested in former papers [1—3]. This paper presents a brief discussion of the proposed operator technique developed for the problem of n-electron ($n=2, 4, 6, 8$) singlets.

The spin operator

It is well known that the number of independent spin states is in fact [4]

$$N(s) = \binom{n}{\frac{1}{2}n-s} - \binom{n}{\frac{1}{2}n-s-1}.$$

This result may be justified by using the so-called branching diagram, a pictorial description of adding the spin angular momenta of electrons one by one (Fig. 1).

As can be seen, the branching diagram not only shows how many states of a given multiplicity there are for the n-electrons, but application of the methods

of vector addition to the angular momentum immediately shows how the states are actually constructed.

The method suggested for the construction of the S^2 eigenfunction is nothing else than the abstract formulation of the method of branching diagrams. If one unites the part systems $X_1, X_2, X_3, \ldots, X_{2n-1}, X_{2n}$, containing x_1 electrons with

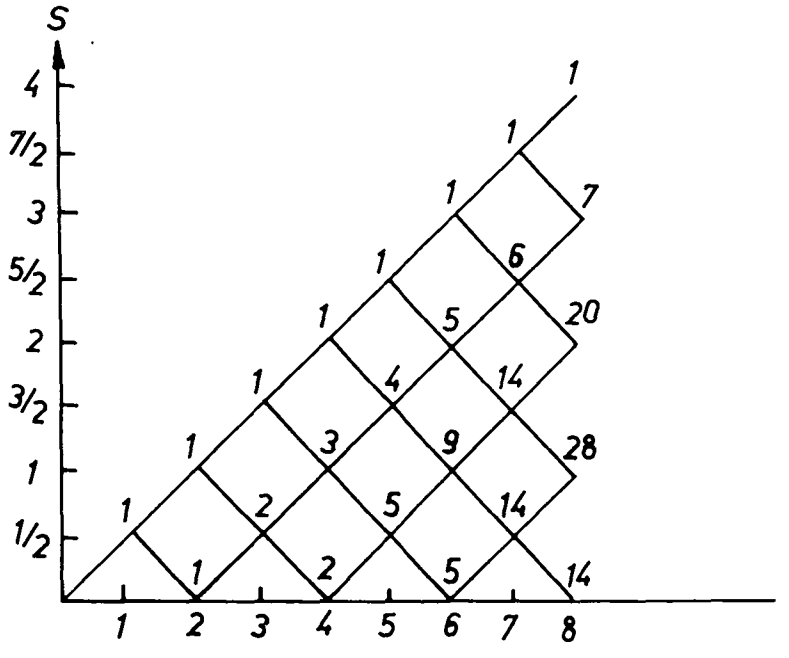

Fig. 1

parallel spin α, x_2 electrons with parallel spin β, x_3 electrons with parallel spin α, ..., x_{2n-1} electrons with parallel spin α and x_{2n} electron with parallel spin β, to a system $X_1X_2X_3 \ldots X_{2n-1}X_{2n}$ with the resulting spin $\frac{x_1}{2} - \frac{x_2}{2} + \frac{x_3}{2} - \ldots + \frac{x_{2n-1}}{2} - \frac{x_{2n}}{2}$, then the spin operator which, when operating on the eigenfunctions of the total S_z operator related to maximal projections of total spin, creates each given-function of the total S^2 corresponding to its different eigenvalues, has according to [2], (3. 10) the following form:

$$O_{X_1X_2X_3 \ldots X_{2n-1}X_{2n}} = \left(\frac{x_1 - x_2 + x_3 - \ldots + x_{2n-1} - x_{2n} + 1}{x_1 - x_2 + x_3 - \ldots + x_{2n-1} + 1}\right)^{1/2} \times$$

$$\times \left(\frac{x_1 - x_2 + x_3 - \ldots x_{2n-3} - x_{2n-2} + 1}{x_1 - x_2 + x_3 - \ldots x_{2n-3} + 1}\right)^{1/2} \times \ldots \times \left(\frac{x_1 - x_2 + 1}{x_1 + 1}\right)^{1/2} \times$$

$$\times \sum_{k=0}^{x_{2n}} (-1)^k \frac{(x_1 - x_2 + x_3 - \ldots + x_{2n-1} - k)!}{(x_1 - x_2 + x_3 - \ldots + x_{2n-1})!\, k!} (S^-_{X_1 X_2 X_3 \ldots X_{2n-1}} S^+_{X_{2n}})^k \times$$

$$\times \sum_{j=0}^{x_{2n-2}} (-1)^j \frac{(x_1 - x_2 + x_3 - \ldots + x_{2n-3} - j)!}{(x_1 - x_2 + x_3 - \ldots + x_{2n-3})!\, j!} (S^-_{X_1 X_2 X_3 \ldots X_{2n-3}} S^+_{X_{2n-2}})^j \times$$

$$\times \ldots \times \sum_{i=0}^{x_2} \frac{(x_1 - i)!}{x_1!\, i!} (S^-_{X_1} S^+_{X_2})^i.$$

The n-electron singlets

Let us denote the Slater determinants describeing the states of n-electron systems as follows:

$n = 2$

$A_1 = |\alpha\beta|, \quad \bar{A}_1 = |\beta\alpha|;$

$n = 4$

$B_1 = |\alpha\alpha\beta\beta|, \quad B_2 = |\alpha\beta\beta\alpha|, \quad B_3 = |\alpha\beta\alpha\beta|; \quad \bar{B}_i = B_i(\alpha \leftrightarrow \beta); \quad B_i^* = B_i + \bar{B}_i;$

$n = 6$

$C_1 = |\alpha\alpha\alpha\beta\beta\beta|, \quad C_2 = |\alpha\alpha\beta\beta\beta\alpha|, \quad C_3 = |\alpha\alpha\beta\beta\alpha\beta|, \quad C_4 = |\alpha\alpha\beta\alpha\beta\beta|,$

$C_5 = |\alpha\beta\beta\beta\alpha\alpha|, \quad C_6 = |\alpha\beta\beta\alpha\alpha\beta|, \quad C_7 = |\alpha\beta\beta\alpha\beta\alpha|, \quad C_8 = |\alpha\beta\alpha\alpha\beta\beta|,$

$C_9 = |\alpha\beta\alpha\beta\beta\alpha|, \quad C_{10} = |\alpha\beta\alpha\beta\alpha\beta|, \quad \bar{C}_i = C_i(\alpha \leftrightarrow \beta), \quad C_i^* = C_i + \bar{C}_i;$

$n = 8$

$D_1 = |\alpha\alpha\alpha\alpha\beta\beta\beta\beta|, \quad D_2 = |\alpha\alpha\alpha\beta\alpha\beta\beta\beta|, \quad D_3 = |\alpha\alpha\alpha\beta\beta\beta\beta\alpha|, \quad D_4 = |\alpha\alpha\alpha\beta\beta\alpha\beta\beta|,$

$D_5 = |\alpha\alpha\alpha\beta\beta\beta\alpha\beta|, \quad D_6 = |\alpha\alpha\beta\alpha\alpha\beta\beta\beta|, \quad D_7 = |\alpha\alpha\beta\alpha\beta\alpha\beta\beta|, \quad D_8 = |\alpha\alpha\beta\alpha\beta\beta\alpha\beta|,$

$D_9 = |\alpha\alpha\beta\alpha\beta\beta\beta\alpha|, \quad D_{10} = |\alpha\alpha\beta\beta\alpha\alpha\beta\beta|, \quad D_{11} = |\alpha\alpha\beta\beta\alpha\beta\alpha\beta|, \quad D_{12} = |\alpha\alpha\beta\beta\alpha\beta\beta\alpha|,$

$D_{13} = |\alpha\alpha\beta\beta\beta\alpha\alpha\beta|, \quad D_{14} = |\alpha\alpha\beta\beta\beta\alpha\beta\alpha|, \quad D_{15} = |\alpha\alpha\beta\beta\beta\beta\alpha\alpha|, \quad D_{16} = |\alpha\beta\beta\beta\beta\alpha\alpha\alpha|,$

$D_{17} = |\alpha\beta\beta\beta\alpha\beta\alpha\alpha|, \quad D_{18} = |\alpha\beta\beta\beta\alpha\alpha\beta\alpha|, \quad D_{19} = |\alpha\beta\beta\beta\alpha\alpha\alpha\beta|, \quad D_{20} = |\alpha\beta\beta\alpha\alpha\alpha\beta\beta|,$

$D_{21} = |\alpha\beta\beta\alpha\alpha\beta\alpha\beta|, \quad D_{22} = |\alpha\beta\beta\alpha\alpha\beta\beta\alpha|, \quad D_{23} = |\alpha\beta\beta\alpha\beta\alpha\alpha\beta|, \quad D_{24} = |\alpha\beta\beta\alpha\beta\alpha\beta\alpha|,$

$D_{25} = |\alpha\beta\beta\alpha\beta\beta\alpha\alpha|, \quad D_{26} = |\alpha\beta\alpha\alpha\alpha\beta\beta\beta|, \quad D_{27} = |\alpha\beta\alpha\alpha\beta\alpha\beta\beta|, \quad D_{28} = |\alpha\beta\alpha\alpha\beta\beta\alpha\beta|,$

$D_{29} = |\alpha\beta\alpha\alpha\beta\beta\beta\alpha|, \quad D_{30} = |\alpha\beta\alpha\beta\alpha\alpha\beta\beta|, \quad D_{31} = |\alpha\beta\alpha\beta\alpha\beta\alpha\beta|, \quad D_{32} = |\alpha\beta\alpha\beta\alpha\beta\beta\alpha|,$

$D_{33} = |\alpha\beta\alpha\beta\beta\alpha\alpha\beta|, \quad D_{34} = |\alpha\beta\alpha\beta\beta\alpha\beta\alpha|, \quad D_{35} = |\alpha\beta\alpha\beta\beta\beta\alpha\alpha|, \quad \bar{D}_i = D_i(\alpha \leftrightarrow \beta),$

$D_i^* = D_i + \bar{D}_i.$

The relating eigenfunctions are as follows:

$$n = 2$$

$$\Phi_1^2 = O_{X_1 X_2} A_1 = \frac{1}{\sqrt{2}}(A_1 - \bar{A}_1);$$

$$n = 4$$

$$\Phi_1^4 = O_{X_1 X_2} B_1 = \frac{1}{\sqrt{3}}\left[B_1^* - \frac{1}{2}(B_2^* + B_3^*)\right],$$

$$\Phi_2^4 = O_{X_1 \dots X_4} B_3 = \frac{1}{2}(B_3^* - B_2^*);$$

$$n = 6$$

$$\Phi_1^6 = O_{X_1 X_2} C_1 = \frac{1}{6}[3(C_1 - \bar{C}_1) + \bar{C}_2 + \bar{C}_3 + \bar{C}_4 + C_5 + C_6 + C_7 + \bar{C}_8 + \bar{C}_9 + \bar{C}_{10} -$$

$$- (C_2 + C_3 + C_4 + \bar{C}_5 + \bar{C}_6 + \bar{C}_7 + C_8 + C_9 + C_{10})],$$

$$\Phi_2^6 = O_{X_1 \dots X_4} C_4 = \frac{1}{2\sqrt{6}}[2(\bar{C}_2 + C_3) - 2(C_2 + \bar{C}_3) + (\bar{C}_6 + C_7 + C_9 + \bar{C}_{10}) -$$

$$- (C_6 + \bar{C}_7 + \bar{C}_9 + C_{10})],$$

$$\Phi_3^6 = O_{X_1 \dots X_4} C_5 = \frac{1}{6\sqrt{2}}\ [4(C_4 - \bar{C}_4) + 2(\bar{C}_2 + \bar{C}_3 + C_5 + \bar{C}_8) - 2(C_2 + C_3 + \bar{C}_5 + C_8) +$$

$$+ (\bar{C}_6 + \bar{C}_7 + C_9 + C_{10}) - (C_6 + C_7 + \bar{C}_9 + \bar{C}_{10})],$$

$$\Phi_4^6 = O_{X_1 \dots X_4} C_6 = \frac{1}{2\sqrt{6}}[2(C_5 + C_8) - 2(\bar{C}_5 + \bar{C}_8) + (\bar{C}_6 + \bar{C}_7 + \bar{C}_9 + \bar{C}_{10}) -$$

$$- (C_6 + C_7 + C_9 + C_{10})],$$

$$\Phi_5^6 = O_{X_1 \dots X_6} C_{10} = \frac{1}{2\sqrt{2}}[\bar{C}_6 + C_7 + \bar{C}_9 + C_{10} - (C_6 + \bar{C}_7 + C_9 + \bar{C}_{10})];$$

$$n = 8$$

$$\Phi_1^8 = O_{X_1 X_2} D_1 = \frac{\sqrt{5}}{60}[D_1^* + 2(D_{10}^* + D_{11}^* + D_{12}^* + D_{13}^* + D_{14}^* + D_{15}^* + D_{20}^* + D_{21}^* +$$

$$+ D_{22}^* + D_{23}^* + D_{24}^* + D_{25}^* + D_{30}^* + D_{31}^* + D_{32}^* + D_{33}^* + D_{34}^* + D_{35}^*) -$$

$$- 3(D_2^* + D_3^* + D_4^* + D_5^* + D_6^* + D_7^* + D_8^* + D_9^* + D_{16}^* + D_{17}^* + D_{18}^* +$$

$$+ D_{19}^* + D_{26}^* + D_{27}^* + D_{28}^* + D_{29}^*)],$$

$$\Phi_2^8 = O_{X_1 \dots X_4} D_5 = \frac{\sqrt{2}}{48} [12D_5^* + 9(\bar{D}_1 + \bar{D}_2 + \bar{D}_4) + 6(\bar{D}_6 + \bar{D}_7 + \bar{D}_{10} + D_{16} + D_{17} + \\ + D_{25} + \bar{D}_{26} + \bar{D}_{27} + \bar{D}_{30}) + 4(D_9^* + D_{12}^* + D_{14}^* + D_{19}^* + D_{21} + D_{23}^* + \\ + \bar{D}_{24} + D_{29}^* + D_{32}^* + D_{34}^*) - 12D_3^* - 4(D_8 + D_{11} + D_{13} + \bar{D}_{18} + \bar{D}_{22} + \\ + \bar{D}_{24} + D_{28} + D_{31} + D_{33}) - (\bar{D}_8 + \bar{D}_{11} + \bar{D}_{13} + D_{18} + D_{22} + D_{24} + \\ + \bar{D}_{28} + \bar{D}_{31} + \bar{D}_{33})],$$

$$\Phi_3^8 = O_{X_1 \dots X_4} D_4 = \frac{\sqrt{6}}{144} [6D_4^* + 18D_4 + 8(D_{15}^* + D_{20}^* + D_{35}^*) + 4(D_8^* + D_9^* + D_{11}^* + \\ + D_{12}^* + D_{18}^* + D_{19}^* + D_{23}^* + D_{24}^* + D_{28}^* + D_{29}^* + D_{31}^* + D_{32}^*) + 2(\bar{D}_8 + \\ + \bar{D}_9 + \bar{D}_{11} + \bar{D}_{12} + D_{18} + D_{19} + D_{23} + D_{24} + \bar{D}_{28} + \bar{D}_{29} + \bar{D}_{31} + \bar{D}_{32}) - \\ - 18(\bar{D}_1 + \bar{D}_{12}) - 8(D_7^* + D_{10}^* + D_{17}^* + D_{25}^* + D_{27}^* + D_{30}^*) - 6(\bar{D}_7 + \\ + \bar{D}_{10} + D_{17} + D_{25} + \bar{D}_{27} + \bar{D}_{30}) - 3(D_3^* + D_5^*) - 9(D_3 + D_5) - \\ - 6(\bar{D}_6 + D_{16} + \bar{D}_{27}) - (D_{13}^* + D_{14}^* + D_{21}^* + D_{22}^* + D_{33}^* + D_{34}^*) - \\ - 3(D_{13} + D_{14} + \bar{D}_{21} + \bar{D}_{22} + D_{33} + D_{34})],$$

$$\Phi_4^8 = O_{X_1 \dots X_4} D_2 = \frac{\sqrt{3}}{36} [9D_2^* + 2(D_{13}^* + D_{14}^* + D_{15}^* + D_{20}^* + D_{21}^* + D_{22}^* + D_{33}^* + D_{34}^* + \\ + D_{35}^*) + (D_7^* + D_8^* + D_9^* + D_{17}^* + D_{18}^* + D_{19}^* + D_{27}^* + D_{28}^* + D_{29}^*) - \\ - 3(D_3^* + D_4^* + D_5^* + D_6^* + D_{16}^* + D_{26}^*) - 2(D_{10}^* + D_{11}^* + D_{12}^* + D_{23}^* + \\ + D_{24}^* + D_{25}^* + D_{30}^* + D_{31}^* + D_{32}^*)],$$

$$\Phi_5^8 = O_{X_1 \dots X_4} D_{10} = \frac{1}{12} [16(\bar{D}_{11} + \bar{D}_{12}) + (\bar{D}_{13} + \bar{D}_{14} + \bar{D}_{20} + D_{25} + \bar{D}_{30} + D_{35}) + \\ + 8(\bar{D}_2 + \bar{D}_4) + 6(\bar{D}_3 + \bar{D}_5 + \bar{D}_8 + \bar{D}_9 + D_{18} + D_{19} + \bar{D}_{28} + \bar{D}_{29}) + \\ + 4(D_{10}^* + D_{15}^*) - 2D_{15} + D_{21}^* + D_{22}^* + D_{23}^* + D_{24}^* + D_{31}^* + D_{32}^* + D_{33}^* + \\ + D_{34}^* - 2(\bar{D}_1 + D_{11} + D_{12} + D_{13} + D_{14} + D_{16} + D_{17} + D_{20} + \bar{D}_{25} + \\ + \bar{D}_{26} + \bar{D}_{27} + D_{30} + \bar{D}_{35})],$$

$$\Phi_6^8 = O_{X_1 \dots X_6} D_{11} = \frac{\sqrt{3}}{24} [8(D_{14} + D_{19} + \bar{D}_{28} + \bar{D}_{29}) + 4(D_{11} + D_{13} + \bar{D}_{14} + D_{17}) + \\ + 3(\bar{D}_3 + \bar{D}_9 + \bar{D}_{27}) + 2(D_{22}^* + D_{23}^* + D_{32}^* + D_{33}^*) + \bar{D}_{11} + \bar{D}_{12} - \\ - 6(\bar{D}_1 + \bar{D}_2 + \bar{D}_6) - 4(D_{12} + \bar{D}_{13}) - 3(\bar{D}_5 + \bar{D}_8) - 2(D_{21}^* + D_{24}^* + \\ + D_{31}^* + D_{34}^*)],$$

$$\Phi_7^8 = O_{X_1 \dots X_4} D_6 = \frac{\sqrt{6}}{432}[72D_6^* + 24(D_{13} + D_{14} + D_{15}^* + \bar{D}_{25}) + 12(\bar{D}_{13} + \bar{D}_{14} + D_{17}^* +$$
$$+ D_{18}^* + D_{19}^* + D_{23}^* + D_{24}^* + D_{25} + D_{27}^* + D_{28} + D_{29} + D_{30}^* + D_{31} + D_{32}) +$$
$$+ 9(\bar{D}_{31} + \bar{D}_{32}) + 6(\bar{D}_4 + \bar{D}_{28} + \bar{D}_{29}) - 36(D_{16}^* + D_{26}) - 28\bar{D}_{26} -$$
$$- 24(D_7 + D_8^* + D_9^* + D_{10} + D_{11} + D_{12}) - 21(\bar{D}_{11} + \bar{D}_{12}) -$$
$$- 18(\bar{D}_7 + \bar{D}_{10} - 15(\bar{D}_{21} + \bar{D}_{22}) - 12(D_{20}^* + D_{21} + D_{22} + D_{33}^* +$$
$$+ D_{34}^* + D_{35}) - 4\bar{D}_2],$$

$$\Phi_8^8 = O_{X_1 \dots X_6} D_8 = \frac{\sqrt{6}}{36}[32\bar{D}_8 + 14(D_{19} + \bar{D}_{29}) + 12\bar{D}_{13} + 4D_8 + 2(D_{12}^* + D_{14}^* + \bar{D}_{19} +$$
$$+ D_{29}) + D_{22}^* + D_{24}^* + \bar{D}_{31}^* + D_{33}^* - 36\bar{D}_1 - 14(\bar{D}_{18} + \bar{D}_{28}) - 12(\bar{D}_2 +$$
$$+ \bar{D}_4 + \bar{D}_5 + D_{16} + D_{17} + D_{26} + \bar{D}_{27}) - 4D_9^* - 2(D_{12} + D_{13} + D_{15} +$$
$$+ \bar{D}_{18} + D_{28}) - (\bar{D}_{11} + \bar{D}_{13} + D_{21}^* + D_{23}^* + D_{32}^* + D_{34}^*)],$$

$$\Phi_9^8 = O_{X_1 \dots X_6} D_7 = \frac{\sqrt{3}}{36}[8D_7^* - 2\bar{D}_7 + 4(D_{15}^* + \bar{D}_{18} + \bar{D}_{19} + D_{28} + D_{29}) + 2(D_{11}^* + D_{12}^* +$$
$$+ D_{18} + D_{19} + D_{20} + D_{25}^* + \bar{D}_{28} + \bar{D}_{29} + D_{30} + \bar{D}_{35}) + \bar{D}_3 + \bar{D}_5 + D_{21} +$$
$$+ D_{22} + \bar{D}_{30} + \bar{D}_{33} + \bar{D}_{34} - 5\bar{D}_{10} - 3(\bar{D}_6 + \bar{D}_8 + \bar{D}_9 - 4(D_8 + D_9 +$$
$$+ D_{10} + D_{13} + D_{14} + D_{17}^* + D_{20} + D_{27}^* + \bar{D}_{35}) - 2(\bar{D}_1 + \bar{D}_2 + \bar{D}_4 + \bar{D}_{13} +$$
$$+ \bar{D}_{14} + \bar{D}_{20} + D_{23}^* + D_{24}^* + D_{31}^* + D_{32}^* + D_{35}) - \bar{D}_{26}],$$

$$\Phi_{10}^8 = O_{X_1 \dots X_4} D_{26} = \frac{\sqrt{2}}{12}[3D_{26}^* + D_{17}^* + D_{18}^* + D_{19}^* + D_{23}^* + D_{24}^* + D_{25}^* + D_{33}^* + D_{34}^* + D_{35}^* -$$
$$- 3D_{16}^* - (D_{20}^* + D_{21}^* + D_{22}^* + D_{27}^* + D_{28}^* + D_{29}^* + D_{30}^* + D_{31}^* + D_{32}^*)],$$

$$\Phi_{11}^8 = O_{X_1 \dots X_6} D_{28} = \frac{\sqrt{3}}{12}[4(\bar{D}_3 + \bar{D}_9) + 2(D_{19}^* + D_{22} + D_{28} + \bar{D}_{29} + D_{32}) + (\bar{D}_{11} + \bar{D}_{22} +$$
$$+ \bar{D}_{24} + \bar{D}_{32} + \bar{D}_{34} - 14\bar{D}_1 - 6(\bar{D}_2 + \bar{D}_4 + \bar{D}_6) - 4(\bar{D}_5 + \bar{D}_8 + \bar{D}_{26} + \bar{D}_{27}) -$$
$$- 2(\bar{D}_7 + D_{16} + D_{18}^* + \bar{D}_{28} + D_{29}) - (\bar{D}_{13} + D_{21}^* + D_{23}^* + D_{31}^* + D_{33}^*)],$$

$$\Phi_{12}^8 = O_{X_1 \dots X_6} D_{27} = \frac{1}{2}[4(\bar{D}_{26} + D_{27}^*) + 2(D_{18} + D_{19} + \bar{D}_{20} + \bar{D}_{25} + \bar{D}_{30} + \bar{D}_{35}) + D_{21} +$$
$$+ D_{22} + D_{23} + D_{24} + D_{31} + D_{32} + D_{33} + D_{34} - 4(D_{16} + D_{17}^*) -$$
$$- 2(D_{20} + D_{25} + \bar{D}_{28} + \bar{D}_{29} + D_{30} + D_{35}) - (\bar{D}_{21} + \bar{D}_{22} + \bar{D}_{23} + \bar{D}_{24} +$$
$$+ \bar{D}_{31} + \bar{D}_{32} + \bar{D}_{33} + \bar{D}_{34})],$$

$$\Phi^8_{13} = O_{X_1 \dots X_6} D_{30} = \frac{\sqrt{3}}{24} [4(D_{30} + D^*_{35}) + 2(D^*_{21} + D^*_{22} + D^*_{23} + D^*_{24}) + \bar{D}_{30} -$$

$$- 4(D^*_{20} + \bar{D}_{25}) - 2(D^*_{31} + D^*_{32} + D^*_{33} + D^*_{34}) - D_{25}],$$

$$\Phi^8_{14} = O_{X_1 \dots X_8} D_{31} = \frac{1}{4} [D^*_{22} + D^*_{23} + D_{31} - 2\bar{D}_5 - (\bar{D}_{11} + D_{18} + D^*_{21} + D^*_{24} + \bar{D}_{28} +$$

$$+ D^*_{32} + D^*_{33} + \bar{D}_{34})].$$

References

[1] *Berencz, F., R. Pauncz:* Proc. Phys. Soc. **71**, 145 (1958).
[2] *Berencz, F.:* Proc. Phys. Soc. **71**, 152 (1958).
[3] *Berencz, F.:* MTA III. Oszt. Közl. (Proceeding of Class III of the Hungarian Academy of Sciences) **8**, 437 (1958).
[4] *Corson, E. M.:* Perturbation Methods in the Quantum Mechanics of n-electron Systems, Blackie, London and Glasgow, 1951.

n-ЕЛЕКТРОН (n=2, 4, 6‘ 8) СИНГЛЕТЫ КАК СОБСТВЕННЫЕ ФУНКЦИИ S^2

Ф. Беренц

n-електрон (n=2, 4, 6, 8) синглеты, как собственные функции S^2 были получены методом спиновых операторов.

VALIDITY OF URBACH'S RULE FOR THE ABSORPTION EDGE OF V_2O_5

By

NGUYEN THE QUANG and I. HEVESI

Institute of Experimental Physics, Attila József University, Szeged

(Received June 1, 1974)

The transmission of V_2O_5 single crystals was measured and the absorption was calculated in a wavelenght range corresponding to the long wave tail of the absorption edge, at temperatures between 90 and 670 °K. The results were analysed in terms of Urbach's rule and the respective parameters were estimated. It could be stated that Urbach's rule is reasonably well fulfilled for temperatures higher than 390 °K. The estimated values of the parameters are in good accordance with the band gaps and absorption constants calculated from the short wavelenght part of the absorption edge.

1. *Introduction*

The character of the absorption edge of V_2O_5 single crystals has been the object of several investigations [1—7]. According to the results of these analyses, it seems plausible that the absorption edge is connected with direct forbidden transitions from the valence band to the conduction band. On the base of this supposition, the band gap E_g was calculated with the formula $K^{2/3} \sim (\hbar\omega - E_g)$, where K is the absorption constant and $\hbar\omega$ the photon energy. These results were confirmed by the values obtained from diffuse reflexion of V_2O_5 powder [3].

It has to be remarked, however, that contrary to the transitions in single crystals, investigations on the reflexion spectra of V_2O_5 powders of different particle size seem to support the supposition of direct allowed transitions [4].

Further information concerning the character of interactions of light with the crystals studied and the type of transitions can be obtained from the long wave tail of the absorption edge. At lower photon energies, the shape of the absorption edge is different from that corresponding to the potence law quoted above. In the investigations of [1] and [2] it was found that the long wave tail of V_2O_5 single crystals shows an exponential dependence on the photon energy and on the inverse of the absolute temperature, respectively, and obeys Urbach's rule expressed by the relation

$$K = K_0 e^{-\sigma \frac{E_0 - \hbar\omega}{k\Theta}}; \tag{1}$$

σ, E_0 and K_0 are constant or weakly temperature dependent; σ is a parameter of

order unity, the dependence of wich on temperature can be expressed by the formula

$$\sigma = \sigma_0 \frac{2k\Theta}{\hbar\omega_p} \tanh \frac{\hbar\omega_p}{2k\Theta}, \tag{2}$$

where σ_0 is a constant and $\hbar\omega_p$ is the phonon energy.

Urbach's rule was found to hold for several insulators and semiconductors; however, no satisfactory and generally valid theoretical explanation of the rule could be given up to now. Therefore it appears justified to collect further experimental material on a broader basis, besides trying to find adequate theoretical models.

The aim of the present paper is to account on measurements concerning the validity of Urbach's rule in a wider temperature range and to estimate the values of the parameters in Eq. (1).

2. *Experimental method*

For determining the absorption contants in the wavelength range corresponding to the long wave tail of the absorption edge, V_2O_5 single crystal plates of different thicknesses were used. In this spectral range and with the thicknesses employed, interference could not be observed and we could calculate with the relation $T=(1-R)^2e^{-Kd}$ where, T is the transmission, R the reflectivity and d the thickness of the plate. The methods of growing the single crystals and preparing the samples, as well as the devices used for transmission measurements are described in a previons paper [8] of one of the authors. The transmission of the crystal plates cut in the (010) plane was measured with two different conditions of polarization ($\mathbf{E}\|c$, and $\mathbf{E}\perp c$ *i.e.* $\mathbf{E}\|a$). The temperature of the crystal was varied from 90 to 670 °K. For producing low temperatures, a cryostat cooled with liquid nitrogen was used. At temperatures exceeding 570 °K, the temperature radiation of the samples was taken into account. Inhomogeneities of the samples were eliminated by taking the average of measurements made on numerous samples. The accuracy of the measurements of transmission and of sample thickness exceeds that permitted by the errors caused by inhomogeneities of the samples.

3. *Results*

Using samples of suitable thickness, it was possible to measure the temperature dependence in the spectral range corresponding to the long wavelength tail of the absorption edge. Figs. 1 and 2 show the wavelength dependence of the transmission at different temperatures Θ for two crystal plates of different thickness under the conditions of polarization mentioned above. The values of K were calculated by comparing the transmissions of similar pairs of plate thicknesses, according to the relation given for the connection between transmission and absorption in Section 2. The curves $T^{\|}(\Theta)$ and $T^{\perp}(\Theta)$, illustrating the temperature dependence of transmission for different wavelengths, were calculated from similar pairs of curves (see Figs. 3

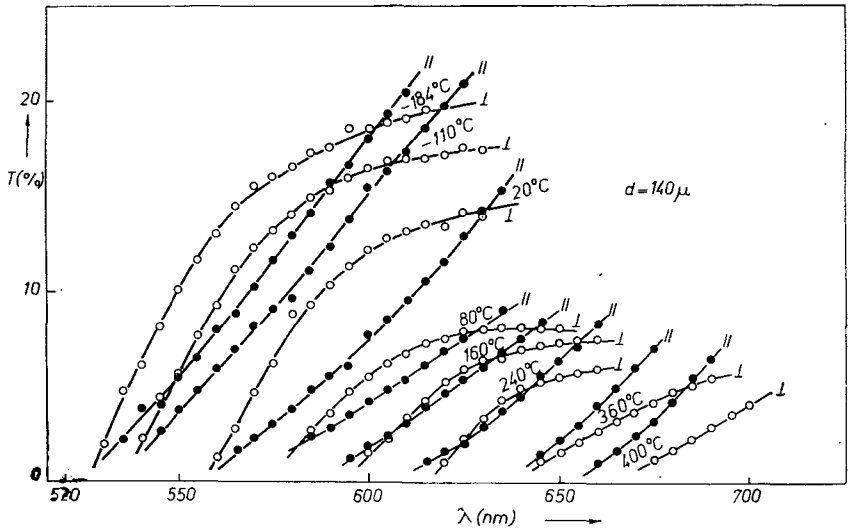

Fig. 1. Dependence on wavelength of the transmission of V_2O_5 single crystals of 140 μ thickness at different temperatures, for ∥ and ⊥ polarization

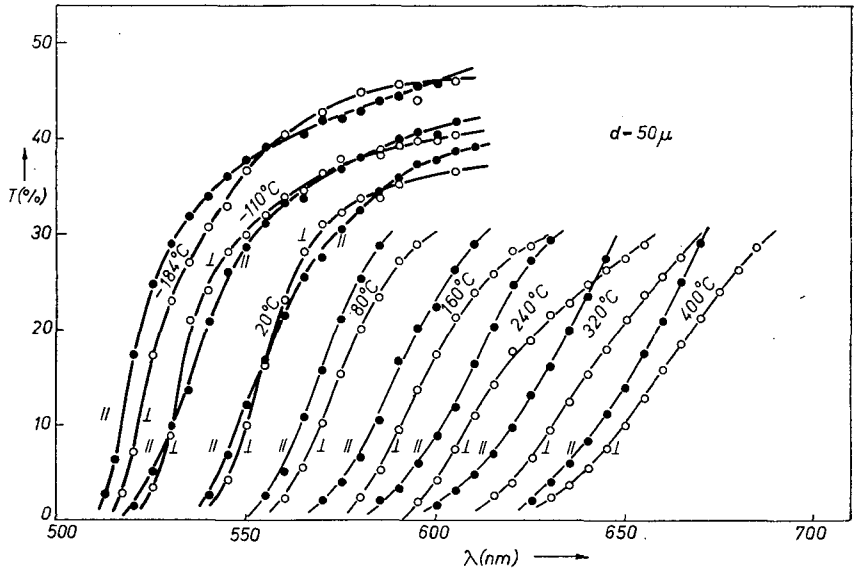

Fig. 2. Dependence on wavelength of the transmission of V_2O_5 single crystals of 50 μ thickness at different temperatures, for ∥ and ⊥ polarization

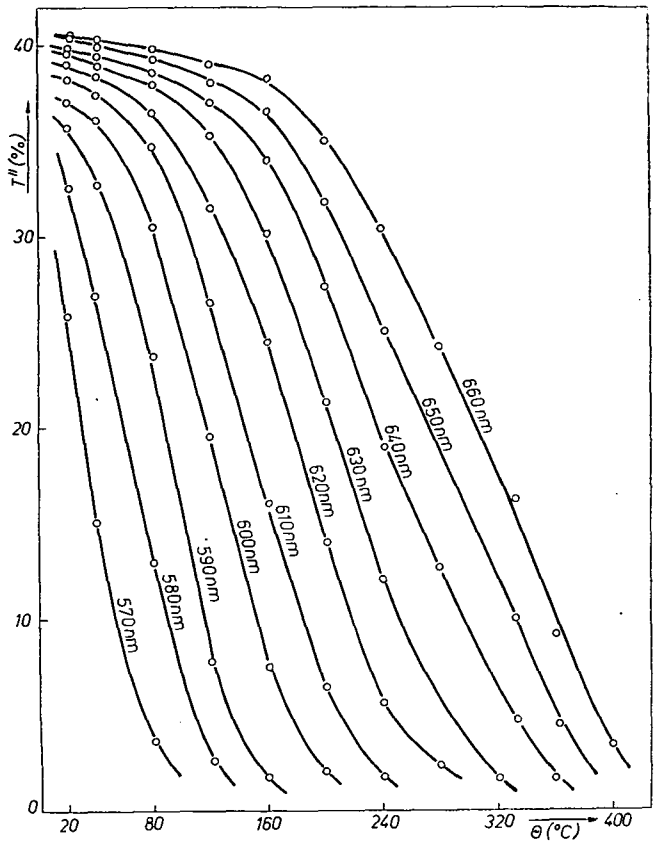

Fig. 3. Dependence on temperature of the transmission at different wavelengths for ∥ polarization

and 4). The values of $T(\Theta)$ were determined from the temperature dependence of the refractive index n (through the relation $T_0=(1-R)^2$), of the sample thicknes d, and of the absorption constant K:

$$\frac{dT}{d\Theta}=\frac{\partial T_0}{\partial\Theta}e^{-Kd}-T\frac{\partial d}{\partial\Theta}K-T\frac{\partial K}{\partial\Theta}d. \tag{3}$$

Supposing that the contribution of the first and second terms of the equation is less important, and the dependence of the absorption coefficient on photon energy and on the inverse of Θ is exponential, a linear dependence of K on $\frac{\Theta^2}{T}\cdot\frac{dT}{d\Theta}$ should result. The validity of this supposition is shown by Figs. 5 and 6, where the linear

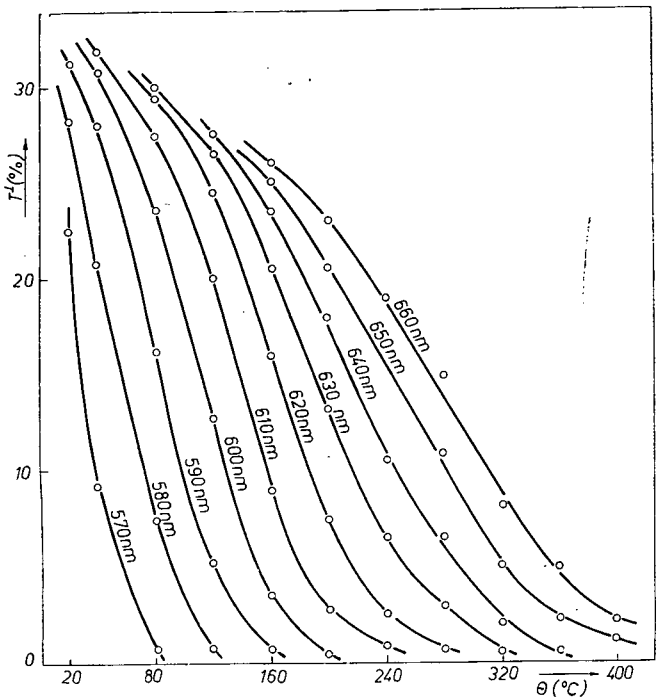

Fig. 4. Dependence on temperature of the transmission at different wavelengths for ⊥ polarization

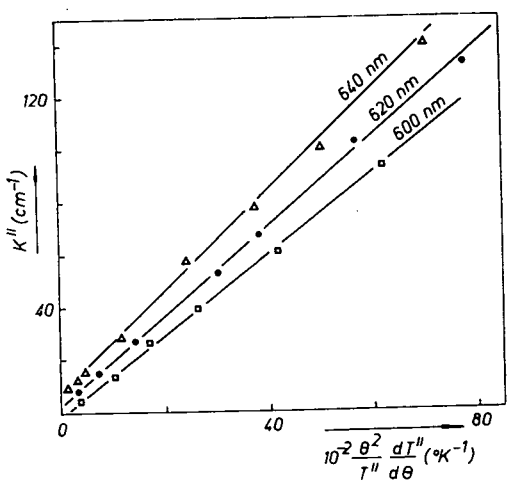

Fig. 5. Dependence of $K^{\parallel}$ on $\frac{\Theta^2}{T^{\parallel}}\frac{dT^{\parallel}}{d\Theta}$ for three different wavelengths

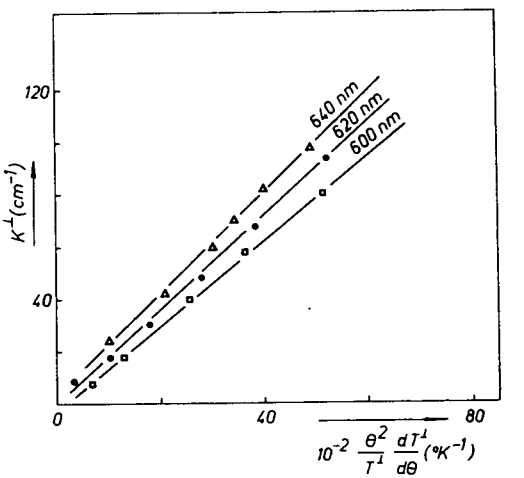

Fig. 6. Dependence of $K^{\perp}$ on $\frac{\Theta^2}{T^{\perp}}\frac{dT^{\perp}}{d\Theta}$ for three different wavelengths

character of the curves and the slopes increasing with wavelength support our supposition.

In Fig. 7, curves of $\ln K$ *vs.* $h\nu$ are shown for several temperatures. In the range of photon energies shown in the figures, the curves are of linear character and their

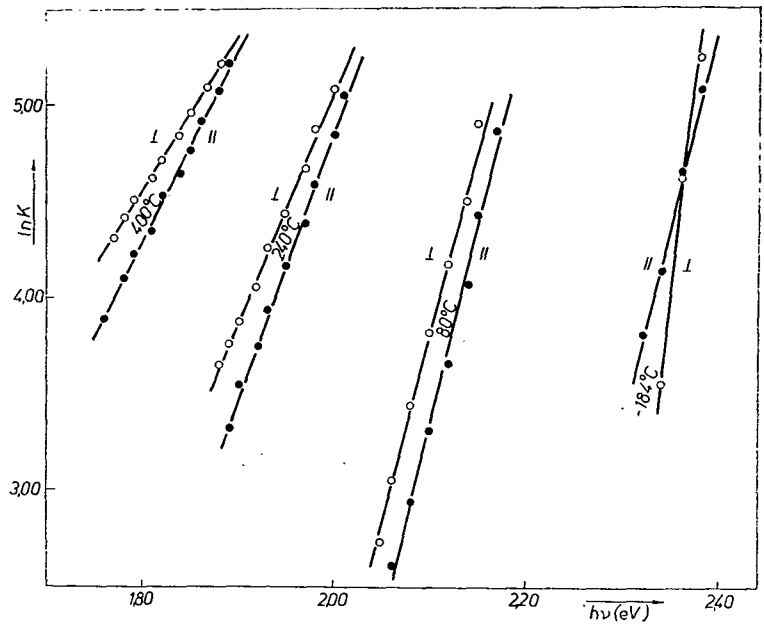

Fig. 7. Dependence of $\ln K$ on photon energy at different temperatures for ∥ and ⊥ polarization

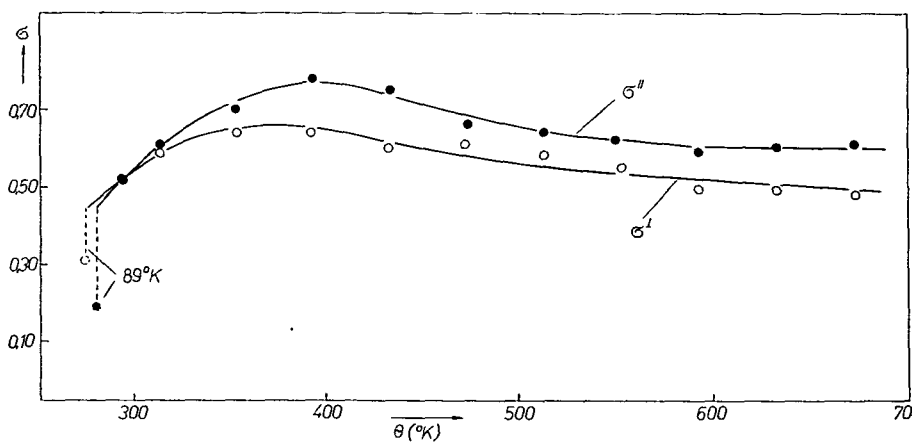

Fig. 8. Temperature dependence of $\sigma^{\parallel}$ and $\sigma^{\perp}$

slopes decrease with increasing temperature. The curves of $\sigma^{\parallel}(\Theta)$ and $\sigma^{\perp}(\Theta)$ calculated from these slopes are presented in Fig. 8. It can be seen that up to about 390 °K, the values of σ change with the temperature; at higher temperatures, both $\sigma^{\parallel}$ and $\sigma^{\perp}$ become constant. For deep temperatures, only the values corresponding to 89 °K, marked in the figure, were calculated. Some calculated values of σ are listed in Table I.

Table I

Values of the Parameters in Urbach's Rule for ∥ and ⊥ Polarization

Θ (°K)	σ		E_0 (eV)		K_0 (cm^{-1})		$\hbar\omega_p$ (meV)	
	∥	⊥	∥	⊥	∥	⊥	∥	⊥
89	0.19	0.31						
313	0.61	0.59						
393	0.78	0.64	2.49	2.54	$1.3 \cdot 10^5$	$2.3 \cdot 10^5$	49	47
513	0.64	0.58						
633	0.60	0.49						

In Figs. 9 and 10 the values of $h\nu$ and Θ pertaining to the same values of the absorption coefficient are shown. Values of E_0 and K_0 estimated from these curves are also given in Table I. The values of $E_0^{\parallel}$ and $E_0^{\perp}$ extrapolated from the straight portions of the curves pertaining to the same absorption coefficient (2.54 ev and

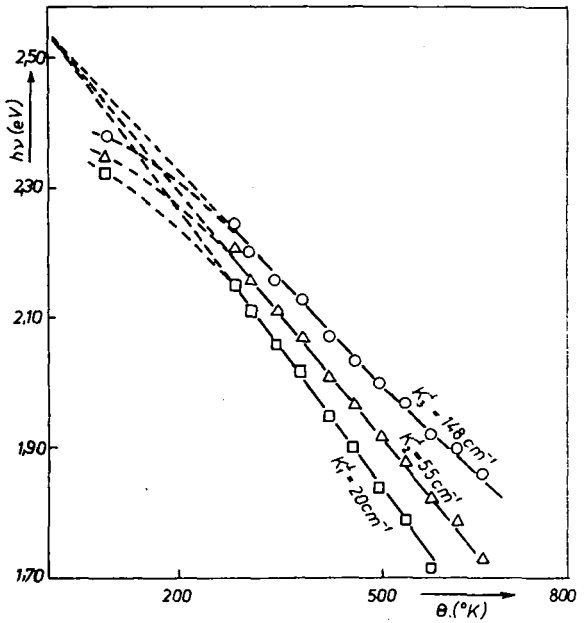

Fig. 9.
Values of $h\nu$ and Θ pertaining to the same values of $K^{\perp}$

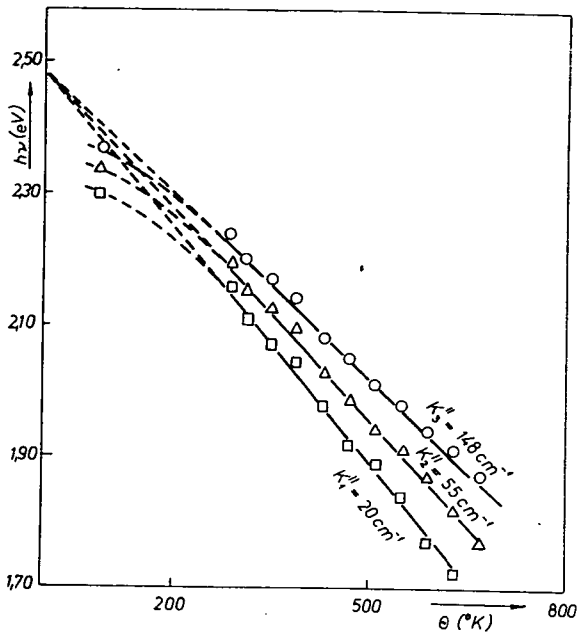

Fig. 10. Values of $h\nu$ and Θ pertaining to the same values of $K^{\parallel}$

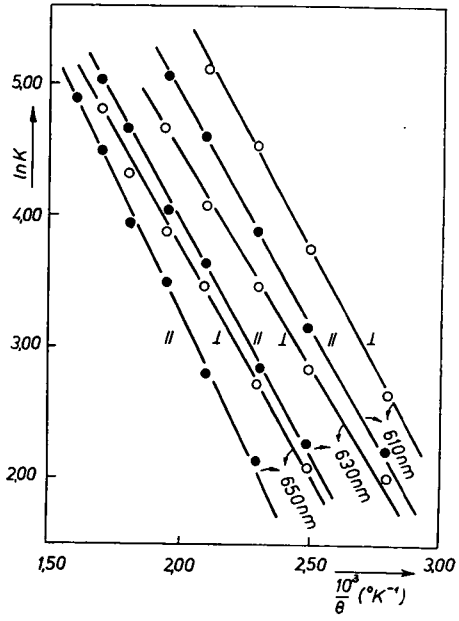

Fig. 11. Dependence of $\ln K$ on $\frac{1}{\Theta}$ at the same wavelengths for ∥ and ⊥ polarization

2.49 eV, respectively, see Table I) are in good agreement with the band gaps at room temperature calculated supposing forbidden direct transitions. The calculated average values of $K_0^{\parallel}$ and $K_0^{\perp}$ ($1.3 \cdot 10^5\,\mathrm{cm}^{-1}$ and $2.3 \cdot 10^5\,\mathrm{cm}^{-1}$, see Table I) are consistent with those pertaining to regions of higher energy of the absorption edge. It can be stated that the estimations of the parameters in Urbach's rule fit well to results of other optical measurements published in literature.

The values of $\ln K$ are plotted *vs.* $1/\Theta$ in Fig. 11. It can be seen that the plots are straight and their slope for the same type of polarization in nearly the same.

* * *

The authors wish to express their thanks to Prof. I. KETSKEMÉTY for his interest in this work.

References

[1] *Kenny, N., C. R. Kannewurf, D. H. Whitmore:* J. Phys. et Chem. Sol. **27**, 1237 (1966).
[2] *Bodó, Z., I. Hevesi:* phys. stat. sol. **20**, K45 (1967).
[3] *Hevesi, I.:* Acta Phys. et Chem. **13**, 39 (1967).
[4] *Karvaly, B., I. Hevesi:* Z. Naturforsch. **26a**, 245 (1971).
[5] *Mokerov, V. G., A. V. Rakov:* Fiz. Tver. Tela **11**, 197 (1969).
[6] *Kutolin, S. A., G. S. Botvinkova, O. M. Kotenko, P. H. Samoilova:* Informatsionno-Spravochnij listok No. 002146 Elektronika (1972).
[7] *Mokerov, V. G.:* Fiz. Tver. Tela **15**, 2393 (1973).
[8] *Hevesi, I.:* Acta Phys. Hung. **23**, 75 (1967).

К ПРОВЕРКЕ ПРАВИЛА УБРАХА У КРАЯ ПОГЛОЩЕНИЯ V_2O_5

Н. Т. Кванг и И. Хевеши

Измерено пропускание и вычислено поглощение монокристалла V_2O_5 в области длин волн, соответствующей длинноволновой стороне края поглощения в интервале температур от 90 °К до 670 °К. Результаты были анализированы на основе правила Убраха, и были оценены соответствующие параметры. Установлено, что при температурах выше 390 °К хорошо выполняется правило Убраха. Оцененные значения параметров находятся в хорошем согласии с полученными данными по измерению ширины зон и коэффициента поглощения в коротковолновой части края поглощения.

О ПРИМЕНИМОСТИ ЭМПИРИЧЕСКИХ ФОРМУЛ ДЛЯ КОНТУРОВ ПОЛОС ПОГЛОЩЕНИЯ И ЛЮМИНЕСЦЕНЦИИ КРАСИТЕЛЕЙ ПРИ РАСЧЁТЕ ИХ ЛАЗЕРНЫХ ПАРАМЕТРОВ

А. Н. РУБИНОВ, И. КЕЧКЕМЕТИ, Л. П. ЕЖОВА, Л. КОЗМА
Институт физики АН БССР, Минск; Институт физики Университета им. Аттилы Йожефа, Сегед

(Поступило в редакцию 1 июля 1974 г.)

Исследована применимость аналитических выражений для спектров поглощения и люминесценции при расчетах лазерных характеристик органических красителей в квазистационарном режиме. Показаны границы применимости этих выражений для определения параметров генерации.

Для расчёта характеристик генерации лазера необходимо знать спектральные контуры полос поглощения и люминесценции его активного вещества. В случае красителей точные аналитические выражения для контуров полос отсутствуют. Поэтому при количественных расчётах параметров генерации в этом случае необходимо пользоваться либо экспериментальными измерениями спектров либо эмпирическими формулами для их описания.

В данной работе рассматривается возможность применения для этой цели эмпирических формул, предложенных в работах [1, 3].

Согласно [2], спектральные зависимости порога генерации и коэффициента усиления ОКГ на красителях определяются выражениями:

$$k_{\text{усил}}(\nu) = n\frac{v^2}{8\pi\tau_0}\cdot\frac{f_q(\nu)}{\nu^2}PS-(1-S)k(\nu)\eta^*(\nu), \tag{1}$$

$$U_{\text{н}}^{\text{пор}}(\nu) = \frac{[k(\nu)+\varrho]\dfrac{1}{\eta_{\max}\tau_0}}{\dfrac{nv^2}{8\pi\tau_0}\cdot\dfrac{f_q(\nu)}{\nu^2}-\dfrac{\varrho+[1-\eta^*(\nu)]\cdot k(\nu)}{P}}, \tag{2}$$

где n — концентрация молекул красителя, v — скорость света в растворе, $\eta_{\max}$ — максимальное значение квантового выхода, τ_0 — время затухания флуоресценции, ϱ — коэффициент потерь резонатора, P и S — постоянные, характеризующие населенность триплетного уровня и интенсивность накачки.

Для расчёта характеристик (1) и (2) необходимо знать функции $k(\nu)$, $f(\nu)$ и $\eta^*(\nu)$. Проведем расчёт в двух вариантах: в первом варианте используем

экспериментальные данные для описания этих функций, во втором — эмпирические формулы из работ [1, 3]:

$$k(\nu) = A \cdot \nu \exp(b_1 \nu) \operatorname{sech}[a_1(\nu_{01} - \nu)], \tag{3}$$

$$f_q(\nu) = B\nu^3 \exp(-b_2 \nu) \operatorname{sech}[a_2(\nu - \nu_{02})], \tag{4}$$

$$\eta^*(\nu) = \frac{c}{1 + D\exp(m\nu)}, \tag{5}$$

где A, B, C — нормирующие множители, a_1, a_2, b_1, b_2, D — эмпирические постоянные.

Заметим, что в обоих вариантах универсальное соотношение Степанова [4] не используется, так как, согласно [5], его применение при количественных вычислениях может приводить к существенным ошибкам.

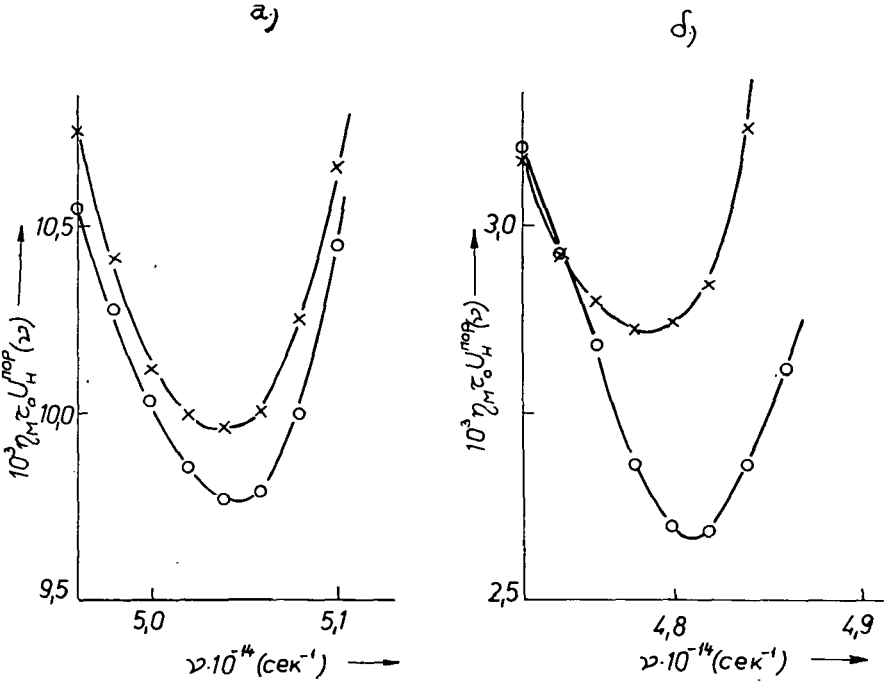

Рис. 1. Зависимость пороговой энергии накачки от частоты. *а)* — родамин 6Ж, *б)* — родамин В в этиловом спирте. ⊙ — по экспериментальным данным, × — по формулам (3)—(5)

Результаты расчётов, полученные в одном и другом случае, приведены на рис. 1, 2.

На рис. 1 даны кривые $U_н^{пор}(\nu)$ для растворов родамина 6Ж и родамина В. Видно, что у родамина 6Ж зависимости, полученные по экспериментальным данным и по формулам (3)—(5), хорошо совпадают. Значения пороговой

плотности накачки в минимумах кривых отличаются всего на 2%. В то же время для родамина В наблюдается заметное расхождение результатов расчёта в рассматриваемых двух случаях: минимальные величины $U_{н}^{пор}(\nu)$ отличаются более, чем на 10% и спектральное положение минимумов не совпадает.

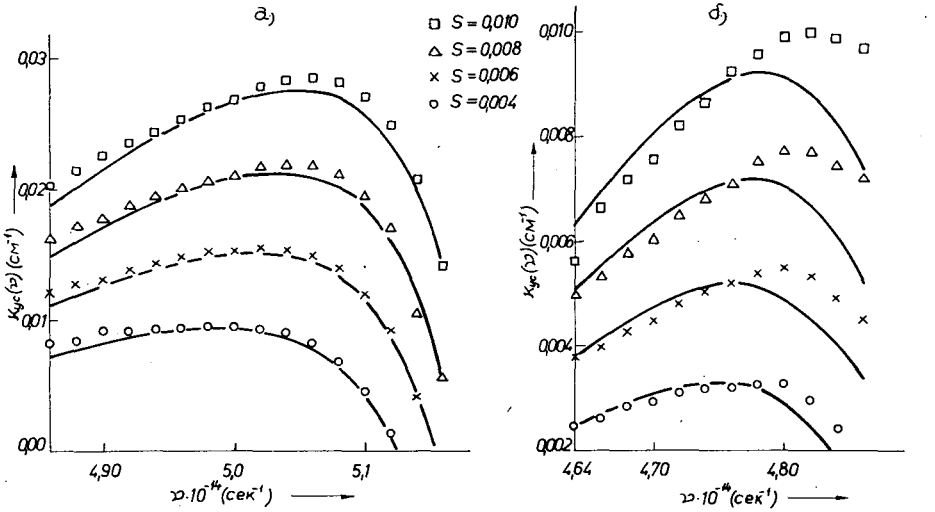

Рис. 2. Кривые усиления красителей (*а*) и (*б*) — те же, что на рис. 1); сплошные кривые по экспериментальным данным, точки — по формулам

На рис. 2 представлены спектры усиления тех же красителей при разных интенсивностях накачки. Из рисунка видно, что для родамина 6Ж коэффициенты усиления, полученные на основе экспериментальных данных и вычисленные по эмпирическим формулам, практически совпадают по всей полосе усиления. Для родамина В совпадение имеется лишь в области малых частот. В коротковолновой области спектра коэффициенты усиления, рассчитанные двумя способами, существенно различаются как по величине, так и по спектральному ходу кривых.

Полученные результаты показывают, что эмпирические формулы (3)—(5) позволяют достаточно хорошо рассчитывать лазерные характеристики красителей с экспоненциальным ходом контура люминесценции в его длинноволновой части. В то же время для красителей, у которых

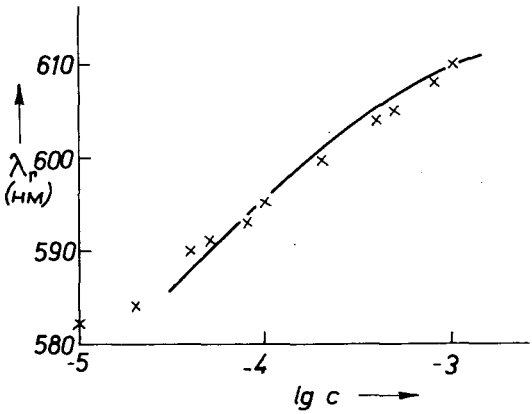

Рис. 3. Зависимость длины волны генерации от концентрации родамина 6Ж. Точки — экспериментальные данные, сплошная кривая — расчёт по формуле (1)

в длинноволновом участке спектра люминесценции наблюдаются побочные максимумы, использование формул (3)—(5) может приводить к ошибкам.

Для иллюстрации применимости формул (3)—(5) к лазеру на растворе родамина 6Ж на рис. 3 представлены зависимости длины волны генерации такого лазера от концентрации красителя, рассчитанные теоретически по формулам (3)—(5) и измеренные экспериментально. Из рисунка видно, что результаты расчёта и эксперимента хорошо совпадают друг с другом.

Литература

[1] *Dombi, J. I. Ketskeméty, L. Kozma:* Acta Phys. et Chem. Szeged **10**, 15 (1964).
[2] *Ketskeméty, I., L. Kozma:* Z. Naturforsch. **27a**, 1685 (1972).
[3] *Хевеши, Й., Л. Козма:* Опт. и спектр. **19**, 434 (1965).
[4] *Степанов, Б. И.:* ДАН СССР **112**, 839 (1957).
[5] *Кечкемети, И., Л. Козма, Й. Хевеши:* Acta Phys. et Chem. Szeged **12**, 83 (1966).

THE APPLICABILITY OF EMPIRICAL FORMULAS OF ABSORPTION AND FLUORESCENCE BANDS OF DYES TO THE CALCULATION OF LASER PARAMETERS

A. N. Rubinov, I. Ketskeméty, L. P. Ezhova, L. Kozma

The paper accounts of the applicability of analytic equations of absorption and emission spectra to the calculation of quasi-stationary dye laser parameters. The limit of applicability of these equations are shown.

TEMPERATURE DEPENDENCE OF THE LUMINESCENCE OF MAGNESIUM METAPHOSPHATE GLASSES ACTIVATED WITH Mn^{2+}

By

L. SZÖLLŐSY, T. SZÖRÉNYI and K. SZANKA

Institute of Experimental Physics, Attila József University, Szeged

(Received June 1, 1974)

The intensity and spectral distribution of the fluorescence of magnesium metaphosphate glasses containing divalent manganese were measured over the temperature range 103 to 603 °K and in a wide range of concentration. With increasing Mn^{2+} concentration the quenching temperature shifts towards lower temperatures. By increasing the temperature at low Mn^{2+} concentrations the red : green ratio decreases and the spectra move to shorter wavelengths. The temperature dependence of the spectral distribution of the glasses with more than 10^{-1} mole Mn^{2+} content shows an anomalous behavior.

The colour of the luminescence emission of Mn^{2+} ions changes from deep red to bright green depending on the host material and the way of preparation. Most authors try to correlate the colour of the luminescence of Mn^{2+} activated glasses with the nature (symmetry) of the environment of the ions, and to use the changes in colour of the emission as an indicator of structural changes in the base glass [1—5].

The structure of binary phosphate glasses was thoroughly investigated by KORDES *et al.* [6, 7]. They found that in metaphosphate glasses with certain alkaline earth metal oxides (MgO, ZnO, BeO) all alkaline earth metal ions are fourfold co-ordinated in the ideal case, and the structure and some other physical properties (dilatation, hardness, u.v. transmission) of these glasses are also similar to those of fused silica. Though WILKE [8], as well as LUNTER *et al.* [4, 5] had studied the concentration dependence of Mn^{2+} luminescence in magnesium and zinc metaphosphate glasses, GORBATCHEVA and KABAKOVA [9] were the first to explain the results with this anomalous glass structure. The observations of GORBATCHEVA and KABAKOVA are well supported by our investigations on the concentration dependence of the luminescence of manganese activated magnesium phosphate glasses, performed in a wider concentration range [10].

Quantitative data concerning the temperature dependence of the emission of glasses containing Mn^{2+} were first given by PARKE [11]. He found that the emission bands were shifted towards longer wavelengths by cooling. The temperature coefficient of fluorescence transition of energy E was given by

$$dE/dT = -5\beta\Delta(dE/d\Delta)$$

where β is the linear coefficient of expansion, Δ the ligand field strength and $dE/d\Delta$ the slope on the energy level diagram. In evaluating these results it has to be taken into account, that his method, generally used in measuring the temperature dependence of the emission intensity, neglects the changes in spectral distribution.

As the temperature dependence of the luminescence of Mn^{2+} activated magnesium, zinc and beryllium metaphosphate glasses has not been investigated before, it seemed justified to extend our investigations on magnesium metaphosphate glasses also in this direction.

Experimental

H_3PO_4 and MgO of analytical purity was used to prepare the samples according to BERAK [12]. The composition of the glass containing no activator was $Mg(PO_3)_2$. 10^{-4} to $5 \cdot 10^{-1}$ mole manganese was introduced in the form of manganous acetate. After drying, the charges were melted in covered biscuit ware crucibles in an electric furnace at 1300 °C. The clear melting was continued for 3 hours. The melt was poured into stainless steel moulds of 16 mm diameter and subjected to 16 hours annealing from 450 °C to room temperature. Samples of 15—20 mm length were cut from the glass bars and polished on both ends with diamond paste using kerosene as lubricant. The glass samples prepared with this "wet" method were almost free from bubbles and under microscope proved to be free from crystallization and phase separation. They were not hygroscopic and showed no changes after several months standing in free air.

The results of chemical analysis showed that the original composition underwent no changes exceeding 5% by losses during the melting process.

The densities of the glasses were measured with pycnometric methods and are listed in Table I.

Table I

Mn content in moles	$5 \cdot 10^{-4}$	10^{-3}	$5 \cdot 10^{-3}$	10^{-2}	$5 \cdot 10^{-2}$	10^{-1}	$5 \cdot 10^{-1}$
Density in g/cm³	2.4176	2.4320	2.4340	2.4363	2.4501	2.4887	2.8237

A home-built spectrophotometer consisting of a xenon lamp XBO 450, quartz prism and glass prism monochromators SPM2, multipliers EMI 9558AQ and Zeiss M10FS25 with Zeiss recorders G1B1 was used. The EMI 9558AQ was held at a constant temperature of −28 °C. A well-defined part of the exciting light was directed through a quantum counter to the Zeiss multiplier and the current of the latter, proportional to the exciting intensity, was recorded. This made possible to refer the emission spectra to the same exciting intensity. Our apparatus was calibrated to obtain correct luminescence quantum spectra.

The temperature dependence of emission was measured with different sample holders according to the temperature range. Between 103 and 303 °K a liquid nitrogen cooled glass dewar with quartz window and glass-to-metal junction was used. The sample was placed in a brass block containing also the heating elements. To

prevent precipitation of moisture, the system was evacuated to 10^{-2} torr. From 303 to 603 °K the brass block containing the samples was placed in an electric furnace. The temperature was held at the desired value by an electronic temperature controller. The error of temperature measurement and control was ± 2 °K maximum.

Results and discussion

On the base of measurements both of the spectral distribution and of the temperature dependence of the intensity of emission the glasses are of two different types depending on the Mn^{2+} content.

Emission spectra measured at 103 °K are shown in Fig. 1. By comparing these with spectra measured at room temperature, it can be stated that the green band

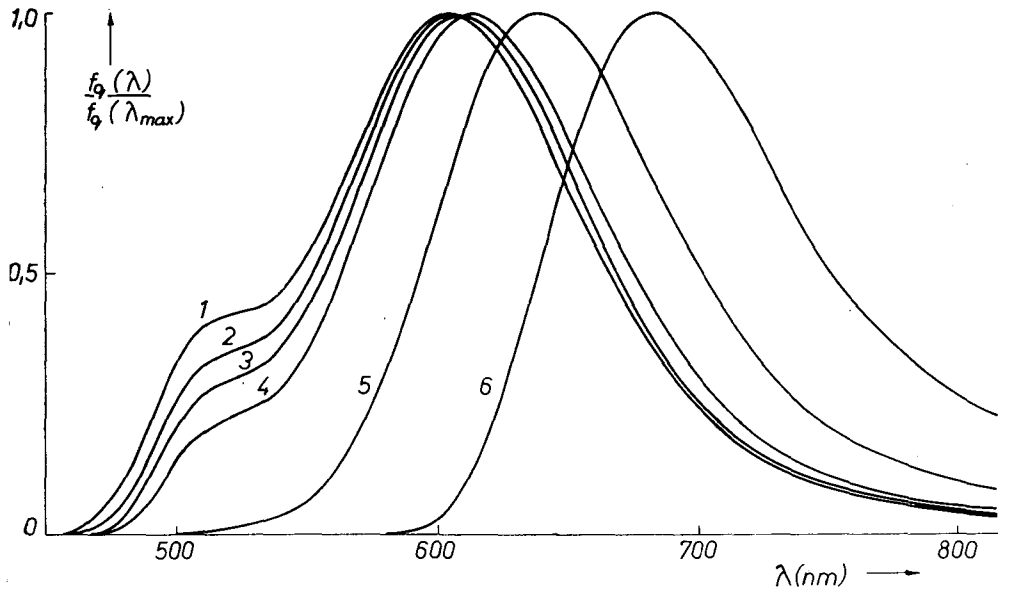

Fig. 1. Low temperature emission spectra of $MgO \cdot P_2O_5$:10^{-3} mole Mn^{2+} (1); $5 \cdot 10^{-3}$ mole Mn^{2+} (2); 10^{-2} mole Mn^{2+} (3); $5 \cdot 10^{-2}$ mole Mn^{2+} (4); 10^{-1} mole Mn^{2+} (5); $5 \cdot 10^{-1}$ mole Mn^{2+} (6) glasses. $\lambda_{exc}=410$ nm

in the emission spectra of glasses containing 10^{-3} to $5 \cdot 10^{-2}$ mole manganese became more pronounced, its position remaining essentially unchanged, while the long-wave band shifted towards the red. The single red band of the glass with the highest ($5 \cdot 10^{-1}$ mole) manganese concentration shifted towards shorter waves. By increasing the temperature from 103 to 603 °K in the concentration range 10^{-3} to $5 \cdot 10^{-2}$ mole Mn^{2+}, the position of the maximum of the red band shifts continuously towards the green. Fig. 2 shows the emission spectra of the sample containing $5 \cdot 10^{-3}$ mole Mn^{2+} measured at different temperatures. The emission maxima of

the glasses with more than 10^{-1} mole Mn^{2+} content showed a long-wave shift from 103 °K to room temperature, while at higher temperatures a short-wave shift was found.

The temperature dependence of the intensity of the fluorescence is presented in Fig. 3 for six different Mn^{2+} concentrations. With increasing Mn^{2+} concentra-

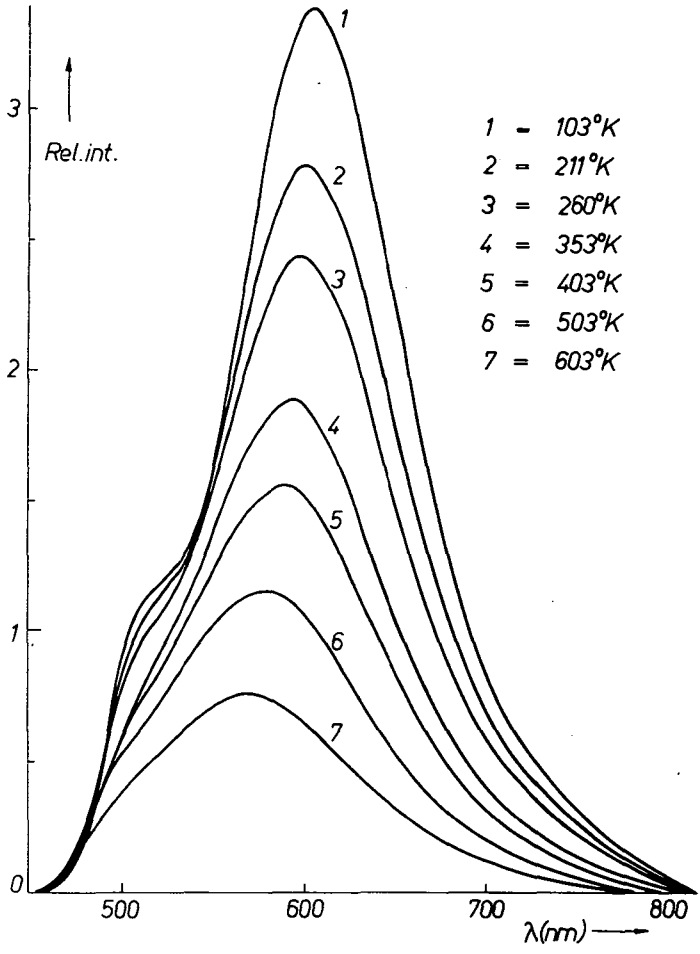

Fig. 2.

tion the quenching temperature (defined as the temperature at which the fluorescence has reached half its maximum intensity) shifts towards lower temperatures. The quenching rate in the concentration range 10^{-3} to $5 \cdot 10^{-2}$ mole Mn^{2+} is essentially lower than in the case of higher concentrations.

The concentration dependence of the luminescence at low activator concentration may be explained by the LINWOOD—WEYL model [2] supposing that the environ-

ment of the manganese ions is partly of tetrahedral and partly of octahedral symmetry. In this case the ions of tetrahedral symmetry would emit the green band and the octahedral ions the red one. Due to the rearrangement caused by the increase in Mn^{2+} concentration only the sites of octahedral symmetry would persist and thus the green band would gradually disappear. This process lasts up to about $5 \cdot 10^{-2}$ mole

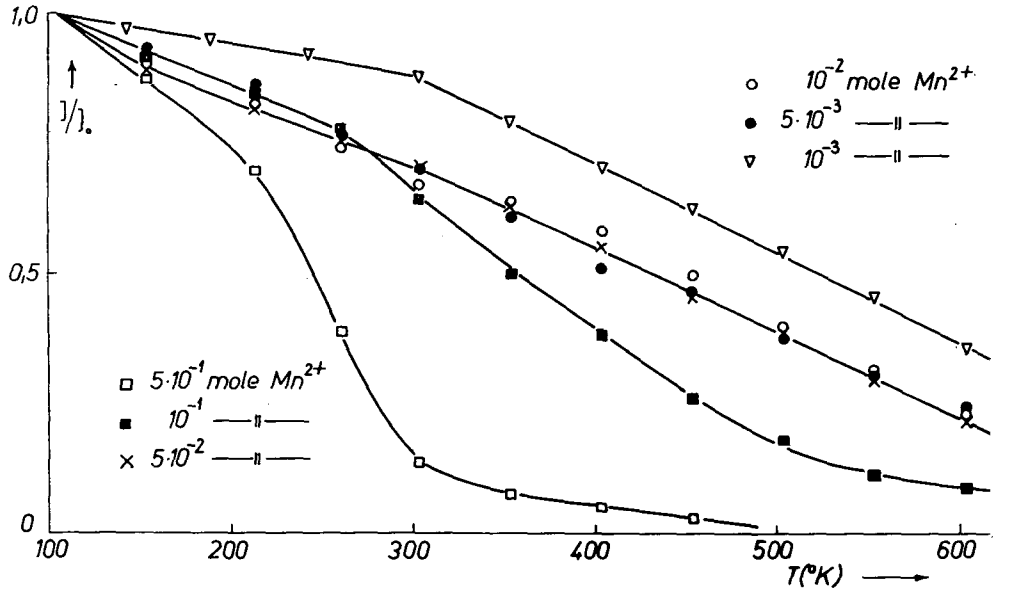

Fig. 3. Concentration dependence of the temperature quenching of $MgO \cdot P_2O_5$ glasses

Mn^{2+} content. At higher concentrations the distance between neighbouring manganese ions would decrease and new luminescence centres (so-called clusters) would form.

Another possible explanation would be, according to KROEGER [13], that several different bands may originate in one centre. The character of the fluorescence emission would depend on the properties of the levels responsible for the bands. Increasing concentration would increase the transition probabilities of the red band(s) and above a certain concentration range—the limits of which cannot be given exactly on the base of the present measurements—this effect would be increased by formation of Mn^{2+} pairs and clusters, resulting in the red shift of the persisting red band.

As to the temperature dependence of the spectral distribution, the change in the red:green ratio occurring at low concentrations may be interpreted by supposed differences in the temperature quenching of both kinds of centres [1]. In the case of higher concentrations the green shift could be explained with the LINWOOD—WEYL model only with the aid of additional suppositions.

Using the other picture [13], the spectral changes observed at low Mn^{2+} concentrations may be explained as follows: The thermal excitation would result in a relative increase in intensity of the green band with increasing temperature. Of course, radiationless de-excitation would compete both with the green and red transi-

tions, its probability increasing with increasing temperature. This picture may be valid up to highest concentrations, namely thermal excitation would enhance transitions of shorter wavelengths also in this case.

The shift observed in glasses of $5 \cdot 10^{-1}$ mole Mn^{2+} content cannot be easily explained by any of the above pictures.

Here we have to do with a luminescent system of a new structure, differing also in other physical properties from the former ones.

The decision of the problem, as to which picture would be more suitable for describing of the observations, may be expected from further measurements of decay time and other parameters.

* * *

The authors wish to express their thanks to Prof. I. KETSKEMÉTY, Director of the Instute of Experimental Physics for his interest during the work.

References

[1] *Weyl, W. A.:* "Coloured Glasses", The Society of Glass Technology, Sheffield, England, 1951.
[2] *Linwood, S. H., W. A. Weyl:* J. Opt. Soc. Am. **32**, 443 (1942).
[3] *Bingham, K. S., S. Parke:* Phys. Chem. Glasses **6**, 224 (1965).
[4] *Лунтер, С. Г., Г. О. Карапетян, Н. М. Бокин, Д. М. Юдин:* ФТТ, **9**, 2875 (1967).
[5] *Лунтер, С. Г., Г. О. Карапетян, Д. М. Юдин:* Изв. Сиб. отд. АН СССР сер. хим. н., **9**, 46 (1967).
[6] *Kordes, E., W. Vogel, R. Feterowsky:* Z. Electrochem. **57**, 282 (1953).
[7] *Kordes, E., J. Navarrete:* Glastechn. Ber. **46**, 113 (1973).
[8] *Wilke, K. Th.:* Z. Phys. Chem. (Leipzig) **219**, 153 (1962).
[9] *Горбачева, Н. А., А. И. Кабакова:* ЖПС **6**, 478 (1967).
[10] *Szöllősy, L., T. Szörényi:* Acta Phys. et Chem. **17**, 135 (1971).
[11] *Parke, S.:* J. Phys. Chem. Solids **32**, 669 (1971).
[12] *Berak, J.:* Roczn. Chem. **32**, 17 (1958).
[13] *Kroeger, F. A., P. Zalm:* J. Electrochem. Soc. **98**, 177 (1951).

ТЕМПЕРАТУРНАЯ ЗАВИСИМОСТЬ ЛЮМИНЕСЦЕНЦИИ МАГНИЙНО-МЕТАФОСФАТНЫХ СТЕКОЛ АКТИВИРОВАННЫХ Mn^{2+}

Л. Селлеши, Т. Сереньи, К. Санка

В работе исследованы в интервале температуры (103—603)°К интенсивность и спектральное распределение флуоресценции магнийно-метафосфатных стекол, содержащих разные количества ионов Mn^{2+}. Температура тушения при увеличении концентрации Mn^{2+} смещается к более низким температурам. При малых концентрациях Mn^{2+} с увеличением температуры уменьшается отношение красная полоса: зеленая полоса, и спектры смещаются к коротким длинам волн. Температурная зависимость спектров показывает аномалию для стекол содержащих Mn^{2+} выше 10^{-1} моль.

О КОГЕРЕНТНОСТИ ПЕРВОГО РОДА ИЗЛУЧЕНИЯ ИМПУЛЬСНОГО ЛАЗЕРА НА КРАСИТЕЛЕ

Т. И. СМОЛЬСКАЯ*, Ф. ПИНТЕР, Л. ВИЗЕ, Л. ГАТИ
Институт экспериментальной физики университета им. А. Йожефа, Сегед

(Поступило в редакцию 1 июля 1974 г.)

Исследовалась интегральная степень когерентности ОКГ на красителе, в зависимости от энергии накачки, энергии излучения лазера, спектральной ширины излучения и расходимости. Оказалось, что среди параметров, измеренных нами, существует однозначная взаимосвязь между интегральной степеью когерентности и расходимостью. Рассчитанная корреляционная функция в зависимости от расходимости хорошо описывает полученные экспериментальные результаты.

Введение

Степень когерентности первого рода излучения лазера на красителе исследовалась нами ранее [1—2]. В этих работах исследовалось изменение степени когерентности по спектру излучения лазера на красителе и зависимость степени когерентности от концентрации красителей. Экспериментальные данные показали необходимость исследования расходимости излучения. Настоящая статья посвящена этим исслед ованиям.

Методы измерения

а) Измерение интегральной степени когерентности. Степень когерентности импульсного лазера на красителе было определено с помощью интерферометра Юнга, без спектрального разделения. Из данных видности $V(\mathbf{r}_1, \mathbf{r}_2)$ абсолютное значение степени когерентности $|g(\mathbf{r}_1, \mathbf{r}_2)|$ было рассчитано на основе работы [3] по формуле:

$$|g(\mathbf{r}_1, \mathbf{r}_2)| = \frac{2\sqrt{I_1 I_2}}{I_1 + I_2} V(\mathbf{r}_1, \mathbf{r}_2), \tag{1}$$

где I_1 и I_2 интенсивности полученные соответственно с мест $\mathbf{r}_1$ и $\mathbf{r}_2$ отдельно на экране. Так как (1) действителен в квазимонохроматическом случае и в наших опытах для излучения лазера $\Delta\lambda/\lambda \sim 0{,}02$ в каждом случае, поэтому условие применимости (1) не меняется [3] если не учитываем спектральное разделение. На основе [3] формула (1) применима для стационарных случаев. Можно показать, что в случае нестационарных процессов $|g(\mathbf{r}_1, \mathbf{r}_2, t - t_1, t - t_2)|$ как функция t, для каждого t, определяется на основе формулы, похожей на

* Физический Институт АН БССР, Минск.

(1). Из сигнала детектора получается среднее значение по времени для $V(t)$, таким образом для $|g(\mathbf{r}_1, \mathbf{r}_2)|$ также получается среднее по времени $\overline{|g(\mathbf{r}_1, \mathbf{r}_2)|}$.

б) Измерение интегральной расходимости. Для измерения расходимости свет лазера падал на обьектив с фокусным расстоянием 1 м, и полученную картину снимали в фокусной плоскости [4]. Из кривой почернения пленки, градуированной с помощью импульса лазера на красителе, определили изменение интенсивности света, потом определили полуширину δ симметричной кривой интенсивности. На основании этих данных расходимость 2ε в мрад была вычислена по формуле $2\varepsilon = \delta/f$. Данные расходимости 2ε, приведенные в таблице 1., корригированы с учётом сферической абберации линзы. Конечно, здесь тоже было измерено среднее по времени для $2\bar{\varepsilon}$.

в) Изменение диаметра пучка лазера на красителе. Для изменения диаметра пучка лазера служила регулирующая круглая диафрагма. Из фотоснимков, сделанных о сечении лазерных пучков, во всех случаях получилось монотонное, однозначное изменение. Это означает, что не существует такого распределения интенсивности, которое величину $\frac{2\sqrt{I_1 I_2}}{I_1 + I_2}$, в выражении (1), сделало бы значительно отличающейся от единицы.

г) Импульсный лазер на красителе и измеряющая система. Система лазера на красителе состояла из следующих элементов: между плоскими зеркалами, коэффициент отражения которых 70% и 99%, находилась кювета с двойной стенкой внутренный и внешний диаметры которой были 10 и 20 мм соответственно. Активным веществом служил родамин 6Ж в этаноле с концентрацией $1 \cdot 10^{-4}$ моль/л. Во внешней оболочке кюветы находился насыщенный водный раствор CH_3COONa для охлаждения и фильтрации длин волн меньших 230 нм. Длина кюветы 100 мм. Питание импульсной лампы типа ИФП-800 было осуществлено конденсаторами 0,28 мкф (9,5—15 кв) и 10 мкф (3,5—6,0 кв). Кювету и импульсные лампы можно было перемешать перпендикулярно к оптической оси лазера. Активное вещество перекачивалось через кювету в течение 1 минуты и до накачки отдыхало в течение 2 минут. Энергия лазера на красителе менялась в области 0,1 мдж—300 мдж. Схема лазера и измеряющей системы показана на рис. 1.

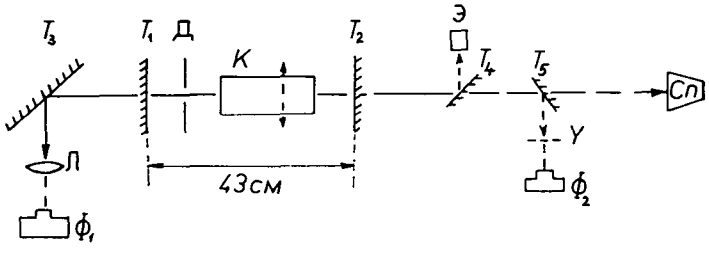

Рис. 1. K — кювета, T_1, T_2 — зеркала лазера, T_3 — отражающое зеркало, T_4, T_5 — полупрозначные зеркала, Φ_1, Φ_2 — фотоаппараты, $Л$ — линза фокусным расстоянием 1 м, $Э$ — калориметр, Y — интерферометр Юнга, $Д$ — диафрагма, $Сп$ — спектрограф

Таблица 1

Диаметр пучка	2,6 мм				3,8 мм				4,0 мм				10,0 мм			
$E_н$ дж	$E_л$ мдж	γ $\times 10^{-12}$ сек$^{-1}$	$\bar{\varepsilon}$ мрад	$\lvert\bar{g}\rvert$ %	$E_л$ мдж	γ $\times 10^{-12}$ сек$^{-1}$	$\bar{\varepsilon}$ мрад	$\lvert\bar{g}\rvert$ %	$E_л$ мдж	γ $\times 10^{-12}$ сек$^{-1}$	$\bar{\varepsilon}$ мрад	$\lvert\bar{g}\rvert$ %	$E_л$ мдж	γ $\times 10^{-12}$ сек$^{-1}$	$\bar{\varepsilon}$ мрад	$\lvert\bar{g}\rvert$ %
61					19	2,33	1,3	51					76	3,42	1,6	64
80	4,0	2,42	0,5	80	40	2,33	1,4	70	5 5 10	— — 2,92	0,1 0,2 0,1	100 100 100	198	2,42	2,0	47
100	4,2 5,4	3,0 2,67	0,6 0,7	79 76	41	2,0	1,6	67	28 29 14	3,08 — 2,5	0,4 0,2 0,2	82 88 100	228	3,92	2,0	48
125	5,4 6,6	2,5 3,25	0,6 0,7	— 86	58 59	2,17 2,58	1,5 1,8	67 67	65 23	3,33 2,58	0,7 0,3	79 100	272	3,0	2,6	42
150	5,6	2,92	0,6	85	62	2,84	1,6	67	79 36	3,16 2,58	0,7 0,4	75 80	300 320	2,92 3,25	2,5 2,5	39 41
180	6,6	3,58	0,7	85	62	2,67	1,8	65	106 43	4,07 3,23	1,0 0,8	73 88				

д) Измерение энергии лазера. Для измерения энергии излучения лазера мы использовали вакуумный микрокалориметр, описанный в работе [5].

е) Градуировка фотопленки. Процедуру для градуировки фотопленки подробно исследовали в работе [6] и в дальнейшем работали на основе этой градуировки.

ж) Определение интегральной степени когерентности по радиальному направлению. Определение интегральной степени когерентности по радиальному направлению было осуществлено при постоянных условиях (базисное расстояние, энергия накачки и концентрация активного вещества были постоянными) так, что кювета с импульсными лампами перемещалась перпендикулярно к оптической оси лазера.

з) Определение ширины полосы излучения лазера на красителе. Для получения спектров излучения лазера на красителе служил трехпризменный спектрограф типа Штейнгейля. Из распределения интенсивности спектров на основе почернения фотопленки определили полуширину спектров (γ).

Результаты измерений

Результаты измерений интегральной степени когерентности, расходимости, полуширины спектра, энергии излучения лазера в случае разных диаметров пучков для красителя родамина 6Ж в этаноле при концентрации $1 \cdot 10^{-4}$ моль/л, в зависимости от энергии накачки даны в таблице 1.

Таблица 2. содержит данные степени когерентности $\overline{\overline{|g(\mathbf{r}_1, \mathbf{r}_2)|}}$ в зависимости от γ для интервала $4{,}2 \cdot 10^{11}$ сек$^{-1}$ и от $\bar{\varepsilon}$ полурасходимости для интервала 0,4 мрад соответственно.

На рис. 2 видно, что при данных диаметрах пучков лазера в пределах погрешности значение $\overline{|g(\mathbf{r}_1, \mathbf{r}_2)|}$ по существу не зависит от энергии накачки и изменение диаметра пучков не вызывает однозначные изменения.

Таблица II.

γ $\times 10^{-12}$ сек$^{-1}$	$\overline{\overline{\lvert g \rvert}}$ %	$\bar{\varepsilon}$ мрад	$\overline{\overline{\lvert g \rvert}}$ %
1,66—2,08	67	0,—0,4	98
2,08—2,5	63	0,4—0,8	81
2,5—2,92	80	0,8—1,2	80
2,92—3,33	68	1,2—1,6	63
3,33—3,75	79	1,6—2,0	66
3,75—4,16	61	2,0—2,4	47,5
		2,4—2,8	41

Соответственно рис. 3, то же самое относится к зависимости $\overline{|g(\mathbf{r}_1, \mathbf{r}_2)|}$ от полуширины спектров γ лазера. Отметим, что в нашем случае полуширина спектров излучения лазера менялась случайно.

На рис. 4 видно значение $\overline{|g(\mathbf{r}_1, \mathbf{r}_2)|}$ в зависимости от энергии излучения лазера. Видно, что значения $\overline{|g(\mathbf{r}_1, \mathbf{r}_2)|}$ в зависимости от $E_{\text{п}}$ монотонно падают.

Было исследовано радиальное изменение интегральной степени когерентности по ранее описанным способам. Результаты показаны на рис. 5. Видно,

что $|\overline{g(\mathbf{r}_1, \mathbf{r}_2)}|$ в зависимости от r/r_0 (где r_0 радиус кюветы, r расстояние места наблюдения от оси кюветы) мало изменяется, и это изменение не превышает ошибку в определении $|\overline{g(\mathbf{r}_1, \mathbf{r}_2)}|$ и таким образом $|\overline{g(\mathbf{r}_1, \mathbf{r}_2)}|$ не зависит от места снятия пробы по диаметру кюветы.

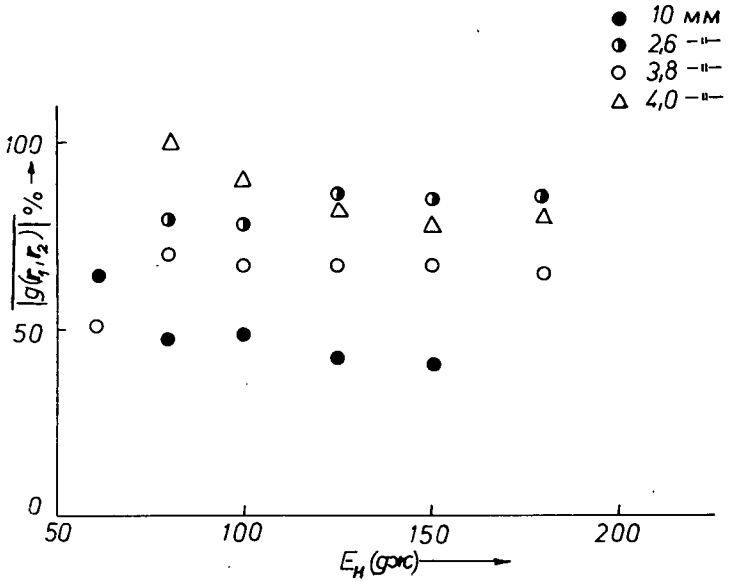

Рис. 2

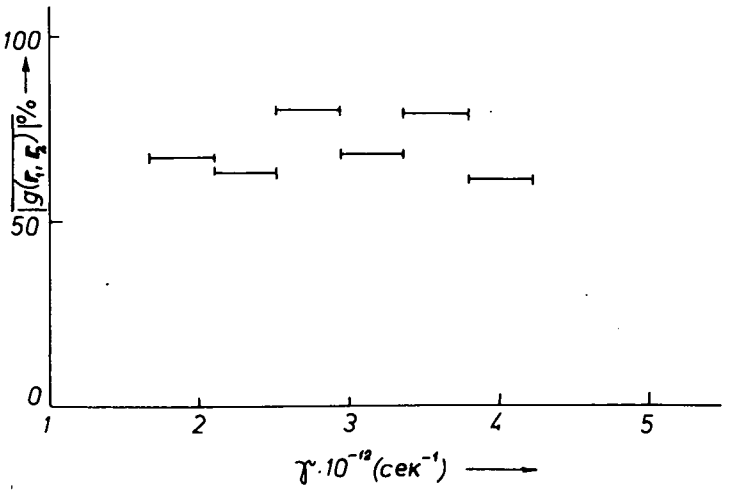

Рис. 3

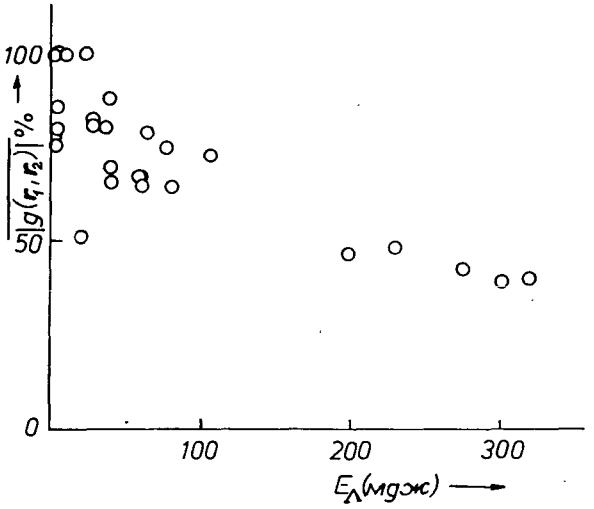

Рис. 4

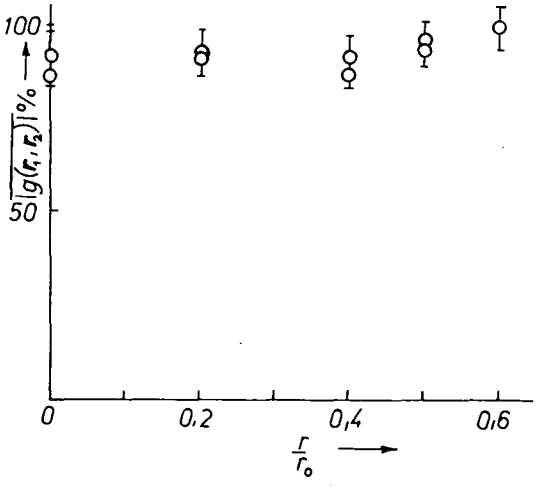

Рис. 5

На рис. 6 показаны значения $\overline{|g(\mathbf{r}_1, \mathbf{r}_2)|}$ в зависимости от полурасходимости $\bar{\varepsilon}$. Хорошо видно, что с увеличением $\bar{\varepsilon}$, $\overline{|g(\mathbf{r}_1, \mathbf{r}_2)|}$ монотонно падает.

На рис. 7 показаны значения расходимости $\bar{\varepsilon}$ в зависимости от энергии излучения лазера. Видно, что расходимость и энергия излучения лазера имеют монотонно увеличивающуюся связь.

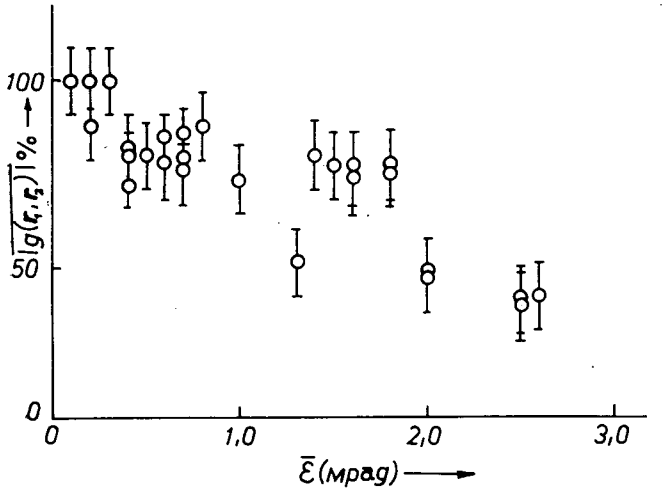
100
50
0
$|\overline{g(r,r)}|$ %
0
1,0
2,0
3,0
$\bar{\varepsilon}$ (мрад)

Рис. 6

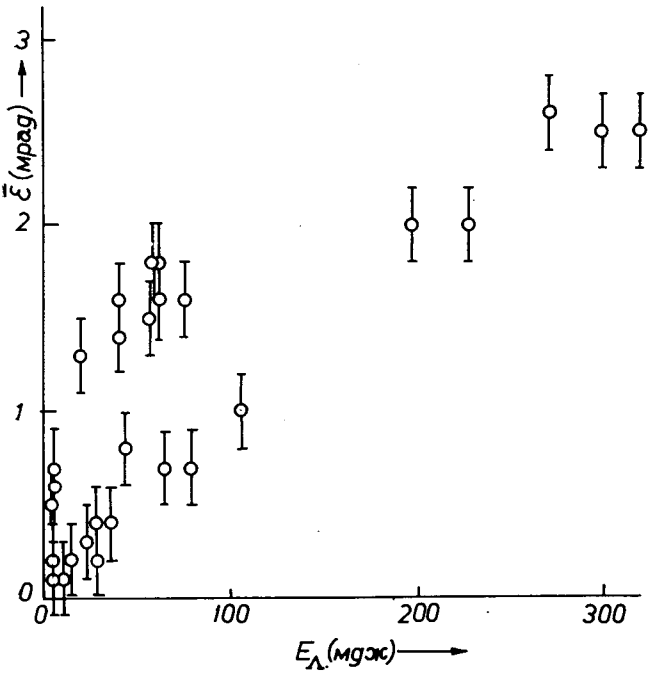
3
2
1
0
$\bar{\varepsilon}$ (мрад)
0
100
200
300
E_Λ (мдж)

Рис. 7

Из наших измерений следует, что из параметров измеренных нами, именно расходимость является тем параметром, который отвечает за однозначное изменение $|\overline{g(\mathbf{r}_1, \mathbf{r}_2)}|$.

Предполагаем, что нам известно расходимость излучения в зависимости от параметров, определяющих работу лазера, и исследуем чисто электромагнитное поле, которое имеет прежнее значение расходимости 2ε, для стационарного поля по Глауберу функция корреляции первого рода [7]:

$$G^{(1)}(\mathbf{r}_1 t_1, \mathbf{r}_2 t_2) = \frac{\hbar}{2(2\pi)^3} \cdot \sum_k \sum_{\lambda=1,2} \hat{e}_{k\mu}^{(\lambda)*} \hat{e}_{k\nu}^{(\lambda)} \langle n_{k,\lambda} \rangle \omega_k \exp\{-i[\mathbf{k}(\mathbf{r}_1 - \mathbf{r}_2) - \omega_k(t_1 - t_2)]\}. \tag{2}$$

Так как измерение было проведено интерферометром Юнга ($t_1 = t_2$), далее $|\mathbf{r}_1 — \mathbf{r}_2| = d$ (расстояние между отверстиями) и в нашем случае волновый вектор $\mathbf{k}$ приблизительно перпендикулярен d, а угол между ними $\frac{\pi}{2} \pm \alpha$ (где $\alpha \ll 1$) для естественного света справедливо:

$$G^{(1)}(d) = \frac{\hbar}{(2\pi)^3} \sum_k \omega_k \langle n_k \rangle e^{-i\frac{\omega_k}{c} d\alpha}. \tag{3}$$

Предполагая, что спектральное распределение излучения лазера с хорошим приближением задается дисперсионной формулой и освещение отвертсвий одинаковое, то есть $W_1 = W_2 = W_0$,

$$\sum_k h\omega_k \langle n_k \rangle \to \int \frac{1}{\pi} \frac{W_0 \gamma}{\gamma^2 + (\omega_0 - \omega)^2} d\omega, \tag{4}$$

тогда корреляционная функция для заданного направления представляется

$$G^{(1)}(d) = W_0 e^{-\gamma\left|\frac{d}{c}\alpha\right|} e^{i\omega_0 \frac{d}{c}\alpha}. \tag{5}$$

Так как нормали плоских волн излучения изменяются между $-\varepsilon$ и $+\varepsilon$, корреляционная функция расходящего пучка:

$$\bar{G} = \frac{1}{2\varepsilon} \int_{-\varepsilon}^{+\varepsilon} W_0 e^{-\gamma\left|\frac{d}{c}\alpha\right|} e^{i\omega_0 \frac{d}{c}\alpha} d\alpha = W_0 \frac{e^{a\varepsilon}(b \sin b\varepsilon + a \cos b\varepsilon) - a}{\varepsilon(a^2 + b^2)}, \tag{6}$$

где $a = -\gamma \frac{d}{c}$; $b = \omega_0 \frac{d}{c}$.

Так как в нашем случае $a \ll b$ и $a\varepsilon \ll 1$,

$$\bar{G}_{12} = W_0 \frac{\sin b\varepsilon}{b\varepsilon}. \tag{7}$$

Для нормированной корреляционной функции (так как $G_{11} = G_{22} = W_0$) получим:

$$|g| = \left|\frac{\sin b\varepsilon}{b\varepsilon}\right|. \tag{8}$$

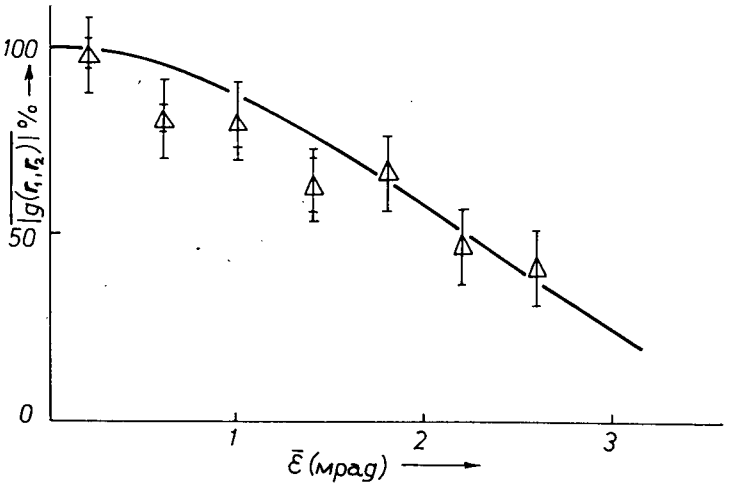

Рис. 8

Сравнение экспериментальных данных с данными (8), показано на рис. 8, где сплошная кривая-теоретическая, а Δ указывает экспериментальные результаты.

Принимая во внимание, что в нашем случае в формуле (8) полуширина спектра излучения не играет роли, понятна независимость $|\overline{g(\mathbf{r}_1, \mathbf{r}_2)}|$ от γ.

* * *

Авторы выражают благодарность профессору И. Кечкемети за постоянное внимание к их работе и полезные советы.

Литература

[1] *Vize, L., F. Pintér, L. Gáti:* Acta Phys. et Chem. Szeged, **18**, 3—4. 107—114 (1972).
[2] *Vize, L., F. Pintér, L. Gáti:* Acta Phys. et Chem. Szeged, **19**, 4, 417—423 (1973).
[3] *Born, M., E. Wolf:* Principles of Optics (Pergamon Press, 1959, p. 503).
[4] *Heard, H. G.:* Laser Parameter Measurements Handbook. (John Wiley and Sons, Inc., New York—London—Sidney, 1968).
[5] *Dombi, J., L. Gáti, I. Ketskeméty, I. Szalma and L. Vize:* Acta Phys et. Chem. Szeged, **16**, 3, (1970).
[6] *Jung, J., L. Vize, F. Pintér, L. Gáti:* Acta Phys. et Chem. (в печати)
[7] Квантовая оптика и квантовая радиофизика, Изд. "Мир", Москва, 1966.

ON FIRST ORDER COHERENCE OF THE RADIATION OF A PULSED DYE LASER

T. I. Szmolszkaja, F. Pintér, L. Vize and L. Gáti

The integral degree of coherence of the radiation of a pulsed dye laser as a function of the pumping energy, the energy of emission, the bandwidth and divergency of the laser beam has been investigated. Among the parameters measured by the authors, unambiguous connection between the integral degree of coherence and the divergency has been found. The correlation function calculated as a function of divergency adequately describes the results of the measurements.

ENERGY TRANSPORT BY GAMMA-RAY EXCITATION IN FLUORESCENT LIQUID SOLUTIONS

By

A. KĄWSKI and T. WAŚNIEWSKI

Luminescence Research Group, Institute of Physics, University of Gdańsk (Poland)
Institute of Physics, Technical High School, Białystok (Poland)

(Received June 1, 1974)

Experimental results on the radioluminescence efficiency η_s of a number of scintillators (solutes) in two different solvents under gamma-ray excitation are presented. These results are compared with the Kallmann—Furst theory and the three Kallmann parameters P, Q, R are determined. Linear dependence of η_s on the ratio of P/R is found for different solutes in a given solvent. The physical significance of the Kallmann parameters is studied.

Introduction

A very large number of organic compounds have been tested hitherto as solutes for scintillator solutions [1, 2]. FURST and KALLMANN [3] have measured the light intensites of the solutions as a function of the solute concentrations. The light emission of the solutions in the case of gamma-ray excitation was referred to the emission of an anthracene crystal of the same mass and in the same geometrical setting. Such relative fluorescence intensity values at the optimum concentration were described by KALLMANN and FURST as the relative physical efficiencies. Since the gamma-ray results for all the investigated solutions are referred to the same mass, which means approximately the same amount of absorbed gamma-ray energy, the number of electrons per gramme (of the solvent excited in unit time) is essentially the same for all the organic solutions. The experimental results of the relative yield are in good agreement with the theory given by KALLMANN and FURST [3, 4]. In the theoretical expression three parameters appear. These can be determined from the experimental data (see below).

In this paper we present further experimental data about the physical efficiences for some compounds in two different solvents, and in particular, the physical significance of the Kallmann parameters is studied.

Experimental

The light intensities of all investigated solutions were measured as a function of the solute concentrations, using an EMI 9514S photomultiplier. With this photomultiplier, the spectrum from 350 nm to 550 nm can be adequately covered. The relative radioluminescence efficiency was determined with an arrangement USB—2

described previously [5, 6]. The solutions were bombarded with gamma-radiation (^{60}Co). The gamma-ray results for all the solutions are referred to the same mass and to the emission yield of an anthracene crystal, similarly as in the investigations of FURST and KALLMANN [3].

Results and discussion

The results for 2-phenylindole in toluene and xylene are reproduced in Fig. 1, where the points give the experimental values and the full lines are curves calculated to fit the experimental points closely by means of the three Kallmann parameters occurring in Kallmann and Furst's theory. The theoretical expression found by

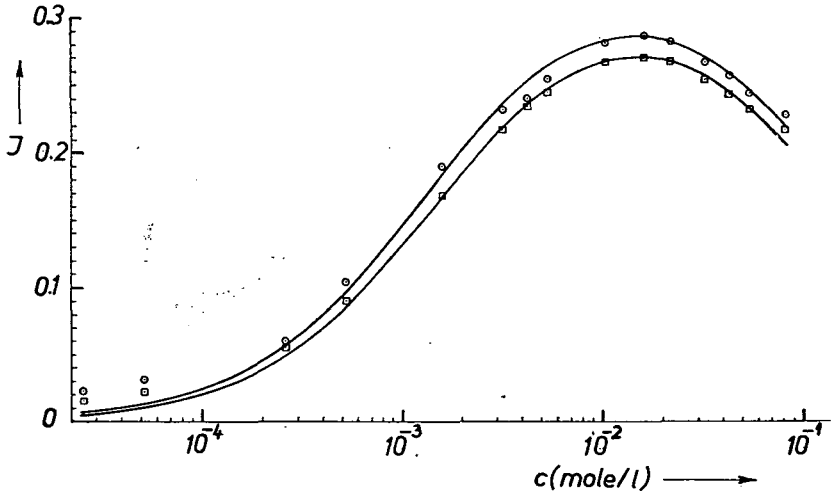

Fig. 1. Variation of emitted light intensity for various concentrations of 2-phenylindole in toluene (circles) and xylene (squares) for gamma-ray excitation. Full curves, theoretical curves calculated by means of equation (1)

KALLMANN and FURST [4, 7] for the variation of intensity I with concentration c is

$$I = \frac{P \cdot c}{(Q+c)(R+c)}, \tag{1}$$

where P, Q and R are the Kallmann parameters.

The Kallmann—Furst theory assumes that there is an energy transfer from the excited solvent molecules to the solute, where the energy is trapped. The parameter Q is associated with the energy transfer. It is shown in [8] that $Q\eta_{sv} = 1/\alpha \cdot \tau_{nt}$, where α is a measure of the cross section for transfer from the directly excited solvent to the solute, τ_{nt} the lifetime for nontransferring processes in the solvent alone and

η_{sv} is the solvent efficiency. A high value of Q indicates poor transfer. The parameters P and R are

$$P = \frac{n_e \delta}{\beta \tau_e} \tag{2}$$

and

$$R = \frac{1}{\beta}\left(\frac{1}{\tau_e} + \frac{1}{\tau_i}\right), \tag{3}$$

respectively, where n_e denotes the number of electrons of the solvent excited per unit time, capable of transferring their energy to the solute, δ is a constant which transforms the number of emited quanta into meter units, β a parameter (probability for unit time) connected with the process of self-quenching at higher concentrations, $\frac{1}{\tau_e}$ the probability (for unit time) of light emission of the solute, and $\frac{1}{\tau_i}$ the probability (for unit time) of internal quenching in the solute.

From (2) and (3) we get

$$\frac{P}{R} = \frac{n_e \delta}{1 + \frac{\tau_e}{\tau_i}}. \tag{4}$$

According to (4), the value P/R depends only on the number of excited solvent electrons n_e and the ratio of $\frac{\tau_e}{\tau_i}$.

Table I

Solution parameters. Solvent: toluene

No	Solute	η_s	c_{opt} (mole/l)	P	Q	R	P/R	$\frac{\tau_e}{\tau_i}$
2	Acenaphthene	0.044	0.039	0.0465	0.00143	0.980	0.0474	15.6
3	Eugenole	0.054	0.00653	0.0053	0.000431	0.0855	0.0620	11.68
4	Methyleugenole	0.052	0.00438	0.00567	0.000275	0.0983	0.0577	12.65
5	Isoeugenole	0.061	0.0164	0.0183	0.000626	0.2720	0.0671	10.75
6	Methylisoeugenole	0.075	0.0356	0.05245	0.00202	0.626	0.0838	8.37
7	N-phenyl-2-naphtylamine	0.093	0.0137	0.0185	0.00100	0.172	0.1076	6.32
8	2-phenylindole	0.288	0.0155	0.0510	0.00130	0.148	0.3446	1.28

Table I and II give the Kallmann parameters, the values of P/R and the physical efficiencies η_s for different solutes in toluene and xylene. We observed that the values of η_s corresponding to the optimum concentrations, of the different solutes are proportional to P/R for a given solvent (Figs. 2 and 3). It follows from Figs. 2 and 3 that

$$\eta_s = \alpha \frac{P}{R}, \tag{5}$$

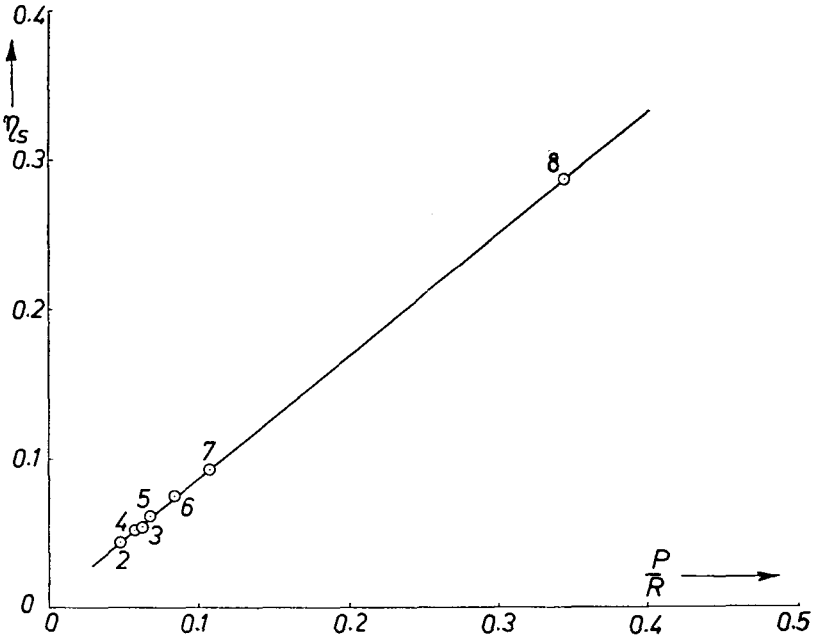

Fig. 2. Relation between η_s and P/R for different solutes (for the solutes see Table I) in toluene

where $a=1.27$ for toluene and 1.23 for xylene. From the definition of quantum yield and equations (5) and (4), we have $\alpha \approx \frac{1}{n_e \delta}$. Therefore, for a given mass of solvent the number of effective excited electrons available for energy transfer is constant ($a=$const.) and information concerning the dependence of $\frac{\tau_e}{\tau_i}$ on the solvent can be obtained by comparing the P/R values of a given solute in different solvents. For toluene and xylene, $n_e\delta=0.787$ and $n_e\delta=0.813$, respectively.

Table II.

Solution parameters. Solvent: xylene

No	Solute	η_s	c_{opt} (mole/l)	P	Q	R	P/R	$\frac{\tau_e}{\tau_i}$
1	2,6-Dimethylnaphtalene	0.044	0.013	0.0081	0.00095	0.158	0.0513	14.85
2	Acenaphthene	0.048	0.039	0.0530	0.00156	1.020	0.0520	14.65
3	Eugenole	0.052	0.00653	0.0051	0.000584	0.0835	0.0611	12.30
4	Methyleugenole	0.054	0.00438	0.00556	0.000265	0.0928	0.060	12.50
5	Isoeugenole	0.060	0.0164	0.0189	0.000593	0.287	0.0658	11.33
6	Methylisoeugenole	0.069	0.0356	0.04438	0.00225	0.569	0.0780	9.42
7	N-phenyl-2-naphthylamine	0.097	0.0137	0.0180	0.00100	0.1585	0.1136	6.15
8	2-phenylindole	0.274	0.0155	0.0460	0.00148	0.1380	0.3333	1.44

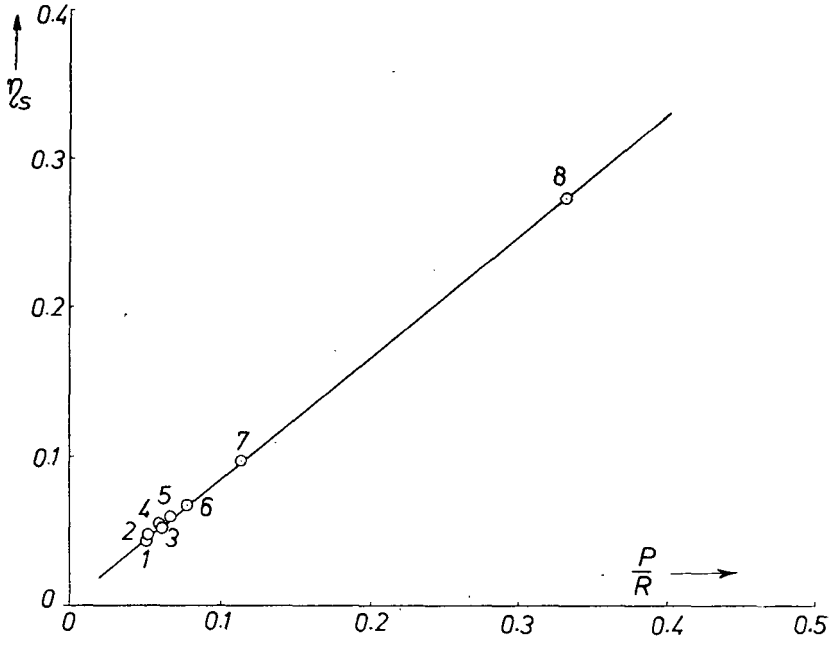

Fig. 3. Relation between η_s and P/R for different solutes (for the solutes see Table II) in xylene

In Table I and II, also the values of $\frac{\tau_e}{\tau_i}$ for different solutes in toluene and xylene are given.

If the decay time τ is known $\left(\frac{1}{\tau}=\frac{1}{\tau_e}+\frac{1}{\tau_i}\right)$, the time constants τ_e and τ_i can be individually evaluated from the following equations

$$\tau_e = \tau \frac{n_e \delta}{P/R} \tag{6}$$

and

$$\tau_i = \tau \frac{n_e \delta}{n_e \delta - P/R}. \tag{7}$$

For example, the measured value of the decay time τ for acenaphthene in xylene is $\tau = 10.6$ nsec, and from this $\tau_e = 166$ nsec and $\tau_i = 11.3$ nsec. It can be seen that if the solution is not of the highest efficiency (for acenaphthene in xylene $\eta_s = 0.048$), the lifetime τ is only approximately given by τ_i. However, for 2-phenylindole, the time constants τ_e and τ_i are comparable (see Tables I and II).

References

[1] *Birks, J. B.:* Scintillation Counting, Pergamon Press, Oxford, 1964.
[2] *Schmillen, A., R. Legler:* Landolt—Boernstein, Zahlenwerte und Funktionen aus Naturwissenschaften und Technik, Neue Serie, Gruppe II, Bd. 3: Lumineszenz organischer Substanzen, Springer-Verlag, Berlin, 1967.
[3] *Furst, M., H. Kallmann:* Phys. Rev. **85**, 816 (1952).
[4] *Kallmann, H., M. Furst:* Phys. Rev. **79**, 857 (1950).
[5] *Kawski, A., T. Waśniewski:* Bull. Acad. Polon. Sci., Ser. sci. math. astr. et phys. **21**, 189 (1973).
[6] *Mańk, A., J. Malesa:* Nukleonika **5**, 143 (1960).
[7] *Kallmann, H., M. Furst:* Phys. Rev. **81**, 853 (1951).
[8] *Furst, M., E. Levin, H. Kallmann:* International Symposium on Luminescence, München 1965, Verlag K. Thiemig KG München, 1966.

ПЕРЕНОС ЭНЕРГИИ В ФЛУОРЕСЦИРУЮЩИХ ЖИДКИХ РАСТВОРАХ, ВОЗБУЖДЁННЫХ ГАММА-ЛУЧАМИ

А. Кавски и Т. Васьневски

Приведены экспериментальные результаты эффективности радиолюминесценции для ряда сцинтилляторов (растворенных молекул) в двух различных растворителях при возбуждении гамма-лучами. Эти результаты сравнили с теорией Калмана — Фурста и определили три параметра по Калману P, Q и R. Авторы нашли линейную зависимость эффективности от отношения P/R для различных сцинтилляторов в том же самом растворителе. Проведено обсупсдение физического смысла параметров по Калману.

NEW APPROXIMATE HARTREE—FOCK MODEL

By

R. GÁSPÁR

Institute of Theoretical Physics, Kossuth Lajos University, Debrecen
and
Group for Quantum Theory, Institute of Physics, Technical University, Budapest

(Received June 1, 1974)

A new approximate Hartree—Fock theory is put forward. The main point of the theory is the replacement of the exact exchange term with an approximate one. This approximate exchange potential is spin-dependent but it is the same for all of the electronic shells in the system.

The theory has been applied to the atom argon and the agreement of the exact and approximate Hartree—Fock theories is very good.

Introduction

An approximate exchange potential has been suggested by SLATER [1] to simplify the Hartree—Fock theory by replacing the exchange term by a simpler one. This term is proportional to the one-third power of the local electronic density. After this replacement, approximate Fock-equations have been derived and solved by the self-consistent field method. Later the author of this paper has given a modified version of the above theory in which the exchange potential is two thirds of that mentioned above [2]. SLATER [3] has shown that the exchange term may be considerably improved by introducing a factor α which replaces unity in the Slater type exchange term and which is dependent on the atomic number if determined by adjusting the total energy of the theory to the total energy of the Hartree—Fock theory [4]. It was shown later [5] that a natural intrinsic explanation may be given to this atomic number dependent α.

In this paper we are introducing and discussing an average exchange term, which has been mentioned in [5]. This exchange term is introduced in a self-consistent manner and it may be extended to atoms, molecules and solids as well. It is applied to an atomic system, and the agreement with the exact Hartree—Fock theory is excellent.

The Approximate Hartree—Fock model

In an atomic system the electron density is

$$\varrho = \varrho^{\downarrow} + \varrho^{\uparrow} \tag{1}$$

where

$$\varrho^{\uparrow} = \sum_{j^{\uparrow}} n_j u_j^* u_j \quad \text{and} \quad \varrho^{\downarrow} = \sum_{j^{\downarrow}} n_j u_j^* u_j \tag{2}$$

denote the density of the electrons with spins up and down resp., $u_j - s$ are spin-orbitals and $n_j - s$ are occupation numbers of these spin-orbitals.

The total energy is given in the form

$$E = \sum_i n_i \int u_i^*(1) f_1 u_i(1)\, dv_1 + \frac{1}{2}\int \varrho(1)\varrho(2) g_{12}\, dv_1\, dv_2 + \\ + \frac{1}{2}\int [\varrho_\uparrow U_\uparrow(1) + \varrho_\downarrow(1) U(1)] dv_1 \tag{3}$$

where f_1 is the sum of one-electron operators and $g_{12} = e^2/r_{12}$ the two particle interaction. In the last term, which is the exchange term, $\frac{1}{2} U$ is the exchange energy density of the swarm of electrons with a given spin.

By a variational method we get from Eq. (3) the approximate Fock equations

$$m[-\nabla_1^2 + V_C(1) + V_{X\uparrow}(1)] u_{i\uparrow}(1) = \varepsilon_{ix\uparrow} u_{i\uparrow}(1) \tag{4}$$

and a corresponding equation for the electrons with spin down. In Eq. (4)

$$V_C(1) = \int \varrho(2) g_{12}\, dv_2 + \sum_i \frac{z_i}{r_i} \tag{5}$$

is the Coulomb potential of the electrons and the nuclei and V_X is the exchange potential of the electrons and is connected to the energy density U by the equation

$$V_{X\uparrow}(1) = \frac{1}{2}\left\{U_{X\uparrow}(1) = \varrho_\uparrow(1) \frac{\delta U_{X\uparrow}(1)}{\delta \varrho_\uparrow(1)}\right\}. \tag{6}$$

The derivative in the last term is the functional derivative of $U_\uparrow$ according to $\varrho_\uparrow$. By integrating Eq. (6) we get the relation

$$U_{X\uparrow}(1) = \frac{2}{\varrho_\uparrow(1)} \int_0^{\varrho_\uparrow} V_{X\uparrow}(\varrho'_\uparrow)\, d\varrho'_\uparrow \tag{7}$$

where $V'_{X\uparrow}$ is the same functional of $\varrho'_\uparrow$ as $V_{X\uparrow}$ is that of $\varrho_\uparrow$. Eq. (7) gives us the possibility of finding an exchange energy density after the proper definition of an exchange potential.

The new exchange potential

When the exchange potential is evaluated, it turns out that each electron is surrounded by a hole i.e. a small region, where the other electrons with the same spin projection avoid being present with great probability [6]. The number of electrons missing from this region is one and the potential of this missing electron is the so called exchange potential. This potential is localized to a great extent and so may be a functional of the total charge ϱ in that point of reference and the density of the electron in question v.

In a region where the potential field is slowly changing the electrons of density ϱ exert an exchange potential

$$V_{X\uparrow}(1) = -8F(\eta)\left[\frac{3}{4\pi}\varrho_{\uparrow}(1)\right]^{1/3}, \tag{8}$$

where

$$F(\eta) = \frac{1}{2} + \frac{1-\eta^2}{4\eta}\ln\left|\frac{1+\eta}{1-\eta}\right|. \tag{9}$$

The Fermi energy of the system of electrons is

$$E_{F\uparrow} = k_{F\uparrow}^2 = (6\pi^2\varrho^{\uparrow})^{2/3} \tag{10}$$

where $k_{E\uparrow}$ is the Fermi momentum. The relative momentum of the electron in question is

$$\eta = k|k_F \tag{11}$$

If we average the exchange potential in (8) in the momentum space over a thin shell near the Fermi-momentum and that region of momentum space contains v electrons, we get the exchange potential

$$V_{X\,\mathrm{SHELL}\uparrow}(1) = -6\left[\frac{3}{4\pi}\varrho_{\uparrow}\right]^{1/3}\frac{\varrho^{\uparrow}}{v_{\uparrow}}\left\{1 - \frac{1}{2}\eta^3 - \frac{1}{2}\eta + \frac{1}{4}[1-\eta^2]^2\ln\left|\frac{1+\eta}{1-\eta}\right|\right\} \tag{12}$$

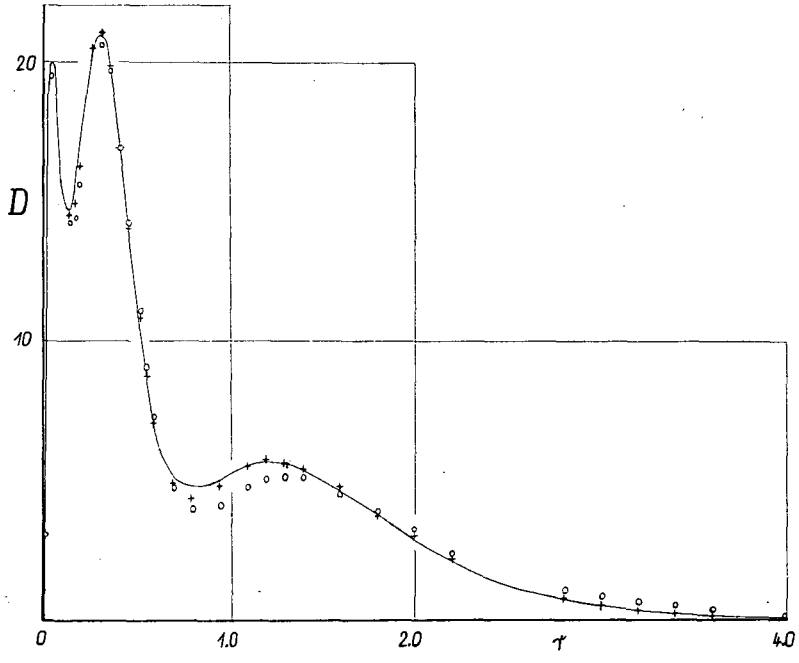

Fig. 1. The total density of the argon atom as calculated by the new method ———, the method of Hartree ∘ ∘ ∘ ∘ and the method of Hartree—Fock + + + +

which is different for each shell, and where

$$\eta = \left(1 - \frac{\nu_\uparrow}{\varrho^\uparrow}\right)^{1/3}. \tag{13}$$

This exchange potential depends from the position of the electron in a complicated way. A drawback of this potential is that it is not the same for all electrons and so the resulting self-consistent orbitals are not orthogonal and they need to be orthogonalized separately. This may be avoided by a further averaging which gives

$$\bar{V}_{X\uparrow} = \frac{\sum_i N_{i\uparrow} V_{X\,\mathrm{SHELL}\uparrow i}}{\sum_i N_{i\uparrow}}. \tag{14}$$

This potential field is still quite general and can be determined in a self-consistent way. There is no parameter in this theory which has to be adjusted to another theory or to be determined semiempirically.

Results and discussion

For testing the above theory, we have calculated the electronic structure of the argon atom. The electronic configuration of the argon atom is $(1s)^2(2s)^2(2p)^6$. The approximate Fock equations have been solved and the total particle density has been calculated. In Fig. 1 we have displayed this curve with the Hartree and the Hartree—Fock curves. The agreement of the exact Hartree—Fock theory and the approximate one is surprisingly good. Other applications of the theory are in preparation.

References

[1] *Slater, J. C.:* Phys. Rev. **81**, 385 (1951).
[2] *Gáspár, R.:* Acta Phys. Hung. **3**, 263 (1954); see *e.g. Kohn, W., L. I. Sham:* Phys. Rev. **140A**, 1133 (1965).
[3] See *e.g. Slater, J. C., K. H. Johnson:* Phys. Rev. **5**, 844 (1972).
[4] *Schwarz, K.:* Phys. Rev. **35**, 2466 (1972).
[5] *Gáspár, R.:* Acta Phys. Hung. **35**, 213 (1974).
[6] See *e.g. P. Gombás:* Die Statistische Theorie des Atoms und ihre Anwendungen, Springer Verlag. Wien, 1949.

НОВАЯ ПРИБЛИЖЁННАЯ МОДЕЛЬ ТЕОРИИ ХАРТРИ—ФОКА

Р. Гашпар

Описано новое приближение теории Хартри—Фока. Главной особенностью теории является замена точного обменного члена на приближённый. Приближённый потенциал зависит от спина, но одинаков для всех электронных оболочек систем.

Теория применена к атому аргона. Результаты точной и приближённой теории Хартри—Фока находятся в хорошем согласии.

ELECTRIC FIELD EFFECT ON THERMALLY STIMULATED CONDUCTIVITY IN TRIAGONAL SELENIUM

By

J. KISPÉTER

Institute of Experimental Physics, József Attila University, Szeged

and

P. SVISZT

Research Institute for Technical Physics of the Hungarian Academy of Sciences, Budapest

(Received June 15, 1974)

The experimental conditions related to the appearance of the fluctuant TSC curve observed earlier in polycrystalline trigonal selenium were investigated. It was found that there exsists a threshold field strength above which the fluctuations of the TSC curve appear at about 120 Vcm^{-1}. This value corresponds to the non-linear part of the current-voltage characteristic of the sample. For the fluctuant TSC to appear, the threshold voltage has to be applied during the recording of the TSC curves, independently from the voltage applied during the illumination and decay periods. No significant changes in the shape of the fluctuant TSC were observed for different heating rates.

Several mechanisms are suggested by which the electric field can, in principle, cause the fluctuant character of a TSC curve.

Introduction

Several papers have been published in recent years on the study of thermally stimulated conductivity (TSC) of traps in selenium. From the TSC curves two [1] or three [2—4] trapping levels were derived and the depth and concentration of the traps were determined. The effect of the duration of illumination on the shape of the TSC curves in amorphous selenium was also investigated [5].

The shape of TSC curves measured in polycrystalline samples of trigonal selenium depends on the applied voltage, and, at a certain voltage, a fluctuant TSC curve appears [6]. In this paper further information concerning the influence of the electric fied on the TSC measured in the same samples is presented.

Experimental

The material used was selenium of 99.996% purity. Rectangular samples of 12 mm×5 mm×0.8 mm were prepared from amorphous selenium by compressing and sintering, crystallized by heat treatment (at 200 °C for 30 minutes), machine polished using an Al_2O_3 grit (<0.1 micron grain size), and etched with sodium sulphite solution. Evaporated gold was used for current contacts to the sample.

Electrical and structural data, obtained at room temperature are found in Table I. Calculating the least Se—Se distances from the X-ray diffraction patterns by the computer method described in [7], good agreement was found with data for selenium single crystals published in the literature [8]. The polycrystalline structure

Table I

ELECTRIC DATA			
Electric conductivity	Thermo-electric power	Hole concentration	Mobility of holes
$4.5 \cdot 10^{-5} \Omega^{-1} cm^{-1}$	870 μV/K	$0.8 \cdot 10^{16} cm^{-3}$	$3.44 \cdot 10^{-2} cm^2/Vs$

X-RAY DIFFRACTION DATA	
Degree of crystallization:	100%
Size of the crystallites:	540 Å

LEAST Se—Se DISTANCES IN THE LATTICE			
In the sample studied:	2.379 Å	3.431 Å	3.720 Å
In Se single crystals [8]:	2.373 Å	3.436 Å	3.716 Å

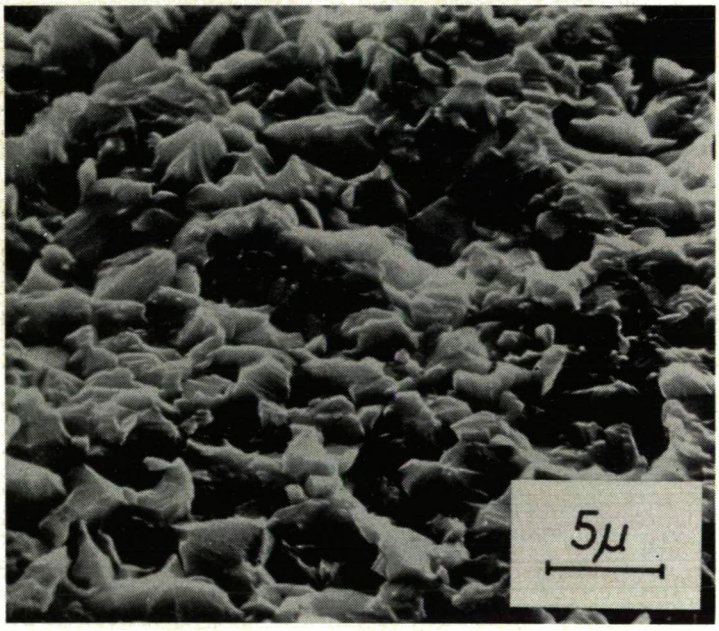

Fig. 1. Scanning electron micrograph of a sample etched with Na_2S solution

and the arrangement of the crystallites can be seen in Fig. 1, which shows a scanning electron micrograph of a sample examined here. Well differentiated crystallites and concretions of the latter are visible. The formation of the concretions may be connected with residual impurities in the sample.

The TSC curves were measured and recorded in the usual way. The samples were illuminated up to saturation by a stabilized 100 W tungsten lamp at 100 °K. The heating rate was 0.1 °K sec^{-1}.

Results and discussion

Current-voltage characteristics of the samples were measured to obtain information on the character of the gold contacts.

Mesurements in the dark at room temperature showed the characteristic to be

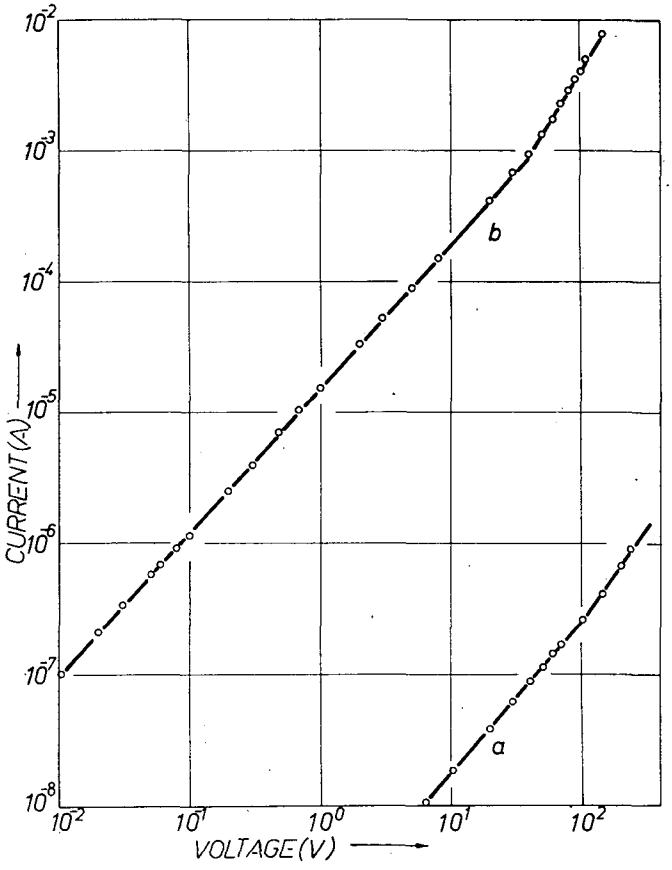

Fig. 2. Current-voltage characteristics obtained at 100 °K; *a*: in a previously not illuminated sample, *b*: after illumination of 5 min, followed by a decay period of further 5 min

linear in the range from $1 \cdot 10^{-4}$ Vcm^{-1} to $5 \cdot 10^{3}$ Vcm^{-1}. The results of I—V measurements made at 100 °K are shown in Fig. 2. Curve *a* shows the I—V characteristic measured in a previously not illuminated sample, curve *b* that after illumination of 5 min., followed by a decay period of further 5 min. It can be seen that curve *a* is linear up to 100 V (*i.e.* 120 Vcm^{-1}) while curve *b* only to 40 V (*i.e.* 50 Vcm^{-1}).

Fig. 3 shows the effects of the electric field on the TSC process. In TSC measurements, generally three periods can be distinguished: those of illumination, decay and heating, respectively. We used two characteristic voltages in our measurements: 10 and 150 V in different combinations during the above periods. Our results were as follows:

1. Applying 10 V during the whole measurement, the result shown in Fig. 3,*a* was obtained. It is to be noted that, on illumination, the conductivity increases by a factor of about 10^4 compared with the dark conductivity, and about 80% of the increased conductivity persists for a long time after the illumination has ceased. In this case the TSC curve has a maximum at 146 °K.

2. Illuminating at 150 V (see Fig. 3,*b*), the intensity of the photocurrent increases in comparison with the former case, and saturation is reached in a shorter time. The decay, measured again at 10 V, is somewhat stronger than in the former case, therefore the TSC curve starts from a lower current intensity. The maximum of the curve is now at 166 °K, *i.e.* it has shifted to higher temperatures.

3. If the decay is measured at the same voltage of 150 V as the illumination was made (Fig. 3, *c*), then the decay is very rapid and very strong; the photocurrent decreases by a factor of about 2 orders of magnitude. The intensity of the TSC curve, measured with 10 V applied voltage also in this case shows a further decrease compared with curves *a* and *b* of Fig. 3 and a simultaneous shift of the maximum to 212 °K.

4. Applying 150 V during the whole measurement of the TSC curve, fluctuations in the TSC curve appeared (Fig. 3,*d*).

5. Similarly, a fluctuant TSC curve (Fig. 3,*e*) was obtained by heating the sample with 150 V applied voltage, while the voltage during the illumination and decay was 10 V. It should be mentioned that in this case 150 V was applied already after 4 min. decay time, with the result that the intensity of the current suddenly increased, then, after reaching a maximum, it decreased nearly to the value of the dark current. This value was lower than that obtained in the former case (Fig. 3,*d*), therefore the fluctuation of the TSC began at a higher temperature.

On the basis of the measurements described, it can be seen that, for the fluctuation of the TSC curve to appear, the voltage of 150 V has to be applied during the recording of the TSC curves, independently from the voltage applied during the illumination and decay periods.

The development of the pattern of fluctuations in the TSC curve as a function of the applied voltage can be seen from Fig. 4. In this case the same voltage was applied during the whole TSC measurement. It can be observed that the threshold voltage for the fluctuations of the current is about 100 V, which value coincides with the break-point on the curve *a* of Fig. 2. With increasing voltage, the fluctuations appear at higher temperatures and a very marked increase in the amplitudes of the curves is to be seen.

No significant changes in the shape of the fluctuant TSC were observed for

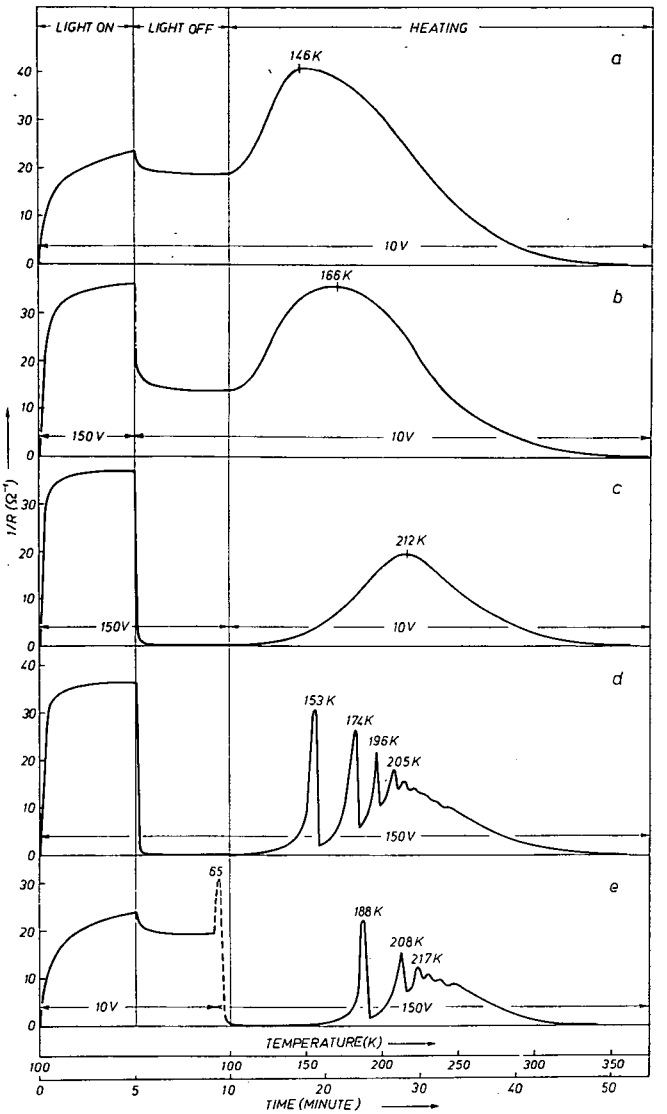

Fig. 3. Effect of the electric field on the TSC curves

different heating rates, but by increasing the heating rate, the maxima shifted to higher temperatures, as usual in the TSC curves.

There are several processes by which the electric field can, in principle, cause the fluctuant character of a TSC curve.

a) Quenching of the conductivity by the field [9] explained by the barrier model for conduction in selenium, as developed by STUKE [10].

b) Negative resistance produced by impurity centres under double injection. This concept was used to explain the spontaneous fluctuations under dc applied voltage in gold-doped Ge at 77 °K [11].

c) Changes in the capture cross section, barrier height, and frequency factor of Coulomb-attractive trapping centres, due to a deformation of the potential around the centre (field-enhanced ionization) [12].

The present results do not enable us to decide between the possible processes given above. Still it seems worth while to point out some observations which may

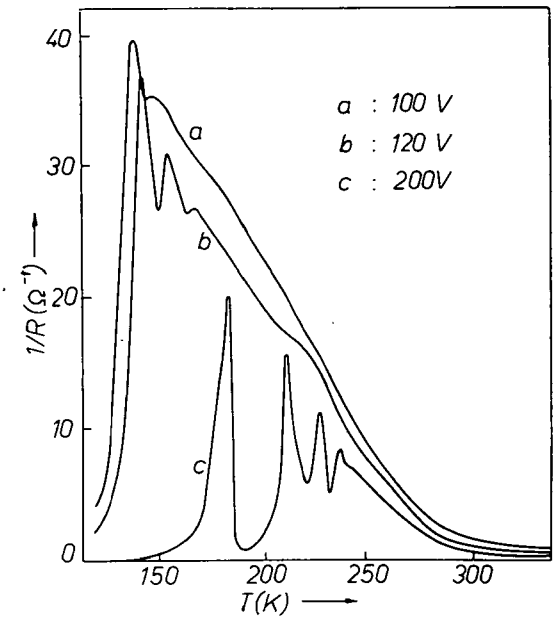

Fig. 4. Development of the pattern of the fluctuant TSC as a function of the voltage applied

help in understanding the described phenomenon. First of all, the fluctuations on the TSC curve appear if the applied voltage is in the non-linear part of the current-voltage characteristic. Further, from the voltage dependence of the development of the fluctuations (Fig. 4), it seems that the phenomenon is associated with negative resistance. Finally, the areas under the TSC curves of Figs. 3*c* and 3*d* are equal, which shows that the number of thermally freed charge carriers after decay to the same photocurrent intensity is independent from the voltage applied during the heating of the sample.

It is possible that more than one of the above processes take place simultaneously. Further experiments are needed to state which processes are really involved and to what extent each of them is effective.

* * *

The authors would like to thank Dr. I. KETSKEMÉTY, Director, Institute of Experimental Physics, József Attila University (Szeged), and Dr. G. SZIGETI, Director, Research Institute for Technical Physics of the Hungarian Academy of Sciences for their interest and encouragement.

References

[1] *Henisch, H. K., M. H. Engineer:* Phys. Letters **26A**, 188 (1968).
[2] *Kolomiets, B. T., K. Hodosevich:* Fiz. Tver. Tela **6**, 3196 (1964).
[3] *Bakirov, M. Ya., N. Z. Dzhalilov:* Fiz. Tver. Tela **9**, 1244 (1967).
[4] *Vishchakas, Yu. K., G. S. Kabalyauskene, M. P. Mikalkyavichyus, V. S. Rinkyavichyus:* Liet. fiz. rink. XII. 799 (1972).
[5] *Cherkasov, Yu. A., I. Yu. Yurkan:* Fiz. i Tekh. Polupr. **2**, 1006 (1968).
[6] *Kispéter, J.:* Z. Naturforsch. **24a**, 1317 (1969).
[7] *Kispéter, J., B. Ribár, R. Herak:* Acta Phys. et Chem. Szeged **19**, 35 (1973).
[8] *Unger, P., P. Cherin:* Selenium Tellurium, Proc. Ins. Symp. 1967, Pergamon Press, p. 223 (1969).
[9] *Shiosaki, T., S. Fukuda, A. Kawabata:* Jap. J. Appl. Phys. **12**, 252 (1973).
[10] *Stuke, J.:* phys. stat. sol. **6**, 441 (1964).
[11] *Lampert, M. A., P. Mark:* Current injection in solids, Academic Press, New York and London, p. 311 (1970).
[12] *Dussel, G. A., K. W. Böer:* phys. stat. sol. **39**, 375 (1970).

ВЛИЯНИЕ ЭЛЕКТРИЧЕСКОГО ПОЛЯ НА ТЕРМОСТИМУЛИРОВАННУЮ ПРОВОДИМОСТЬ ТРИГОНАЛЬНОГО СЕЛЕНА

Й. Кишпетер и П. Швист

Исследованы экспериментальные условия появления ранее наблюдаемых флюктуаций на кривой термостимулированной проводимости (ТСП) в поликристаллическом тригональном селене. Найдено, что критическое значение поля для появления флюктуаций тока около 120 $Vсм^{-1}$. Это значение находится в нелинейной части вольтамперной характеристики кристалла. Для появления флюктуаций на кривой ТСП критическое поле должно подаваться на кристалл во время снятия кривой ТСП, независимо от значения поля во время освещения образца и следующего периода затухания фототока. Применение различных скоростей нагрева не привело к заметным изменениям формы и числа флюктуаций кривой ТСП. Предложены механизмы, через которые электрическое поле может, в принципе, вызвать флюктуационный характер кривой ТСП.

PREPARATION AND INVESTIGATION OF THICK Si(Li) *p-i-n* GAMMA DETECTORS*

By

Á. SÜLI, L. MICHAILOVITS

Institute of Experimental Physics, Attila József University, Szeged

and

F. LISZT

Roland Eötvös Institute of Geophysics, Budapest

(Received June 1, 1974)

Si detectors of about 3.2 cm^3 volume and 10 mm compensated layer thickness were prepared by Li ion-drift process. The pulse amplitude spectrum of the detectors was measured in the temperature range −50 to +5 °C by irradiating the detectors with 323, 662, 1170 and 1330 keV energy of Cr^{51}, Cs^{137} and Co^{60} γ radiating sources. Peaks characteristic for the energy of γ radiation did not appear in the spectra, as the γ radiation of the energy range investigated is absorbed by several subsequent Compton interactions in the Si. The position of the decay sections of the spectra obtained is characteristic for the energy of radiation. The absolute counting yield of the detectors for Co^{60} γ radiation was found to be 4.8 and 4.5%, respectively. Storing the detectors at room temperature under reverse bias for several months, practically no changes in the parameters of the detectors could be found. The shape of the pulses produced by irradiation of the detectors in the temperature range −65 to −30 °C was also investigated.

Introduction

Si detectors prepared with the Li ion-drift method are extensively used for investigation of nuclear radiations, especially for measuring the energy spectra of α and β radiation. For investigating γ radiation, mainly Ge(Li) detectors are used, as the absorption coefficient of Ge for γ radiation is comparatively high, and so the detecting yield of the Ge detectors of big volume is high. These detectors are operated at liquid nitrogen temperature; at such low temperatures the reverse current of the detectors is very low, therefore the noise of the detectors is small, too, which permits very good energy resolution. In practice, however, a serious disadvantage of Ge(Li) detectors is the circumstance that they cannot be operated and stored above this temperature, as repeated heating to room temperature, even for short periods, results in deterioration of the detectors. (The recently developed intrinsic Ge detectors are free from this disadvantage, but also they can be used only at very low temperatures).

On the other hand, Si(Li) detectors with thick compensated layer (5 to 10 mm) can be stored at room temperature for unrestricted time, without observable deteriora-

* This work was supported by the Roland Eötvös Institute of Geophysics.

tion of their parameters [1—4]. The absorption coefficient for γ radiation of Si is comparatively low because its low atomic number; so the yield of a Si detector is less that of a Ge detector of the same volume. The absorption coefficient rapidly decreases with increasing energy of the γ radiation and therefore Si detectors detecting radiation of higher energies (above 300 keV) must have a great volume. With the method applied, we tried to prepare Si detectors which can be used for detection of radiation of higher γ energies with acceptable yield at temperatures not much lower than room temperature. The requirement of great volume was fulfilled by preparing detectors of 3.2 cm^3 in volume with 10 mm compensated layer thickness. Detectors of great volume show, on the other hand, a high reverse current consisting of two components:

i) the thermal generation current proportional to the thickness of the compensated layer and;

ii) the leakage current proportional to the area of the detector.

Both components show a strong increase with increasing temperature of the detector. Owing to the high reverse current of the detectors of great volume, the energy resolution is limited by the detector noise [5]. In the investigated case of energies >300 keV the radiation is absorbed in the Si by Compton interactions, therefore there are no photopeaks in the signal spectrum of the detectors (so we cannot speak of energy resolution in the usual sense), and the functioning of the detectors, especially the maximum operating temperature, is limited by the detector noise. In preparing detectors, we aimed at reaching low leakage currents, without using, however, a guard ring [6] which would drastically reduce the leakage current. We did not extend the investigation to energy resolution in the region of lower γ energies, where photopeaks should appear, as for obtaining notable energy resolution, the detectors should have been cooled to lower temperatures than used in our experiments.

Preparation of the detectors

The Si(Li) detectors were prepared from a *p*-type Si single crystal of 1000—1100 Ω cm resistivity, 7000—9000 cm^{-2} dislocation density, and 1100—1300 μsec lifetime of the minority carriers. The diameter of the cylindrical ingot was about 22 mm, the orientation of its length axis was (111). As last step in the mechanical processing of the four cylindrical samples cut from the ingot, their surfaces were mirror-polished with diamond paste of 5 μ grain size on teflon foil. After carefully degreasing and washing the samples, the preparation of the detectors was continued with the steps described below.

The final diameter of all detectors was about 20 mm, the thickness of detector No. 1, 2 and 3 was 10 mm, that of detector No. 4 was 5 mm. Beside these detectors, rectangular samples of 4 mm×15 mm×1 mm size were cut from the ingot. On these samples all steps of the detector preparation were performed together with the cylindrical samples, or at least under the same conditions, to study processes making necessary the damaging of the samples during the investigation.

In preparing the detectors, the methods described in [1] were used with small modifications.

1. *Preparation of the n^+ contact by phosphorus diffusion.* One of the contacts was prepared with phosphorus diffusion. The samples were etched in CP4A at

20 °C for 3 minutes. The etching was finished by continuous dilution and washing with de-ionized water (of 2 MΩ resistivity) with special care for not exposing the samples to contact with air before totally removing the etchant. Then the samples were dried in a stream of pure nitrogen gas. Subsequent etchings, except the stabilizing etching, were performed with the above method. Phosphorus diffusion was made in a quartz furnace of two temperature zones with the carrier gas method, using P_2O_5 vapour at 1025 °C temperature for 2 hours [7, 8]. In the lower temperature zone of the furnace, the P_2O_5 of analytical purity was sublimated and carried to the 1025 °C temperature zone by an Ar stream of 99.99% purity. The conditions and the quantity of P_2O_5 were adjusted in a way to keep the phosphorus concentration constant in the neighbourhood of the samples during the period of diffusion. The rate of heating the samples to 1025 °C and cooling down to room temperature was 5 °C min^{-1}. According to [7, 8], diffusion at 1025 °C for 2 hours results in a diffusion depth of 2 μ, the concentration of the phosporus atoms in the surface layer being 10^{21} cm^{-3}. After removing with HF the phosphate glass covering the samples, the phosphorus concentration was determined by measuring the surface conductivity with a four probe method, and the diffusion depth by staining [9] after lapping the samples, diffused together with the detectors, at an angle of 5°. The values determined in this way were in good accordance with those found in the quoted literature.

After masking one of the base surfaces of the sample with picein, the phosphorus diffusion layer was removed from the free surfaces by two subsequent etchings of 3 minutes, then the masking picein was carefully removed by dissolving in trichlorethylene and carbon tetrachloride.

2. *Preparation of p^+ contacts by aluminium alloying.* The samples were deoxidized with HF, washed and dried, then 200 μg cm^{-2} Al of 99.99% purity was evaporated in 2×10^{-6} torr vacuum onto the base surface opposite to the n^+ contact. During the evaporation, the samples were covered with a mica plate provided with a circular aperture, permitting Al evaporation only to the surface wanted. Before evaporation, the Al was carefully degreased and etched. The evaporated Al layer on the samples was alloyed with the Si by heat treatment of 10 minutes in a furnace of 675 °C in dry inert atmosphere. The rate of heating and cooling the samples was 5 °C min^{-1} in this case again.

3. *Evaporation and diffusion of lithium.* After repeated deoxidation with HF, lithium essentially exceeding the quantity necessary for compensation was evaporated onto the phosphorus diffused base plane in 2×10^{-6} torr vacuum. During the evaporation, the samples were covered by a mica mask with a circular aperture, as described above. The heating of the samples was started in the vacuum before beginning the evaporation, then after the evaporation of Li, the samples were held at 320 °C in the vacuum for 12 minutes before cooling. The Li diffusion took place during the heat treatment. Excess Li was removed from the samples by washing in ethanol, then, after masking the contacts with picein, the free surfaces were etched. After removing the picein the samples were boiled in carbon tetrachloride for 5 minutes, then stabilized in air for 24 hours. After stabilization, the reverse current of each detector at 120 V bias, measured at 20 °C was less than 10 μA cm^{-2}.

Rectangular samples of 1 mm thickness evaporated and diffused together with the detectors were lapped at an angle of 5° and the depth of Li diffusion was determined with the staining method [9, 10]. A diffusion depth of 0.11—0.14 mm was

obtained in accordance with [11]. The Li concentration of the surface layer was estimated to about 8×10^{17} cm^{-3}.

4. *Lithium ion-drift.* The compensation by Li of the detectors No. 1, 2 and 3 with 200 V reverse bias at 115 °C temperature lasted nearly 3 months. In the first hours of the drift, lower voltage was applied, which gradually increased to 200 V. The detector No. 4 was drifted in a similar way, but the drifting period was about 4 times shorter. Cooling of the detectors during the drifting process was performed by filtered and purified air stream. The drifting apparatus was secured against thermal runaway. For time to time the drifting process was interrupted, the detectors cooled to room temperature, and the drifted depth checked by capacity measurement.

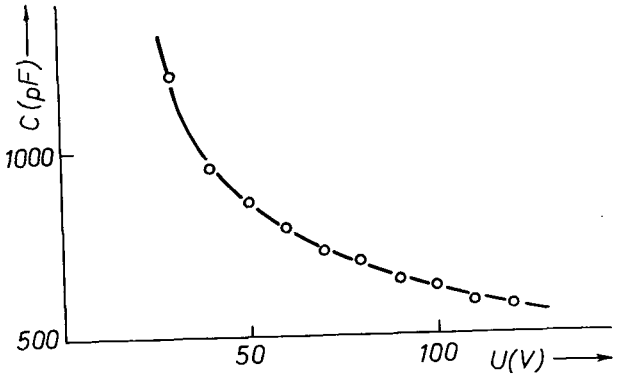

Fig. 1. Capacity *vs.* reverse bias characteristic of the detector No. 2 before the drift process

The increase in thickness of the compensated layer with increasing drifting time was in good accordance with the values determined from the nomograms published in [1]. The compensation process performed at 115 °C was followed by a flattening drift at 80 °C with 200 V reverse bias for one week; the aim of the latter was smoothing of the drift profile.

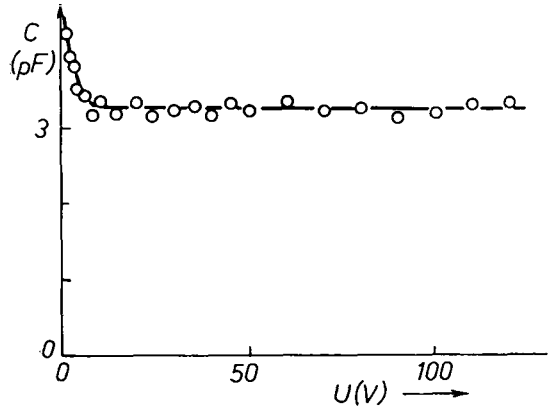

Fig. 2. Capacity *vs.* reverse bias characteristic of the detector No. 2 after the drift process

In Figs. 1 and 2 the capacity *vs.* reverse bias characteristics of the detector No. 2 are shown before and after the Li ion-drift, respectively. While the capacity before drift is very high and strongly voltage dependent, the capacity after drift is small and practically independent of voltage above 10 V; the measured capacity was equal to the geometrical capacity (~3.2 pF) of the detector to a good approximation;

this shows that the detector was compensated in its full thickness of 10 mm. The C—U curves of detector No. 1 and 3 were practically the same as those shown in Figs. 1 and 2.

5. *Stabilization of the detector.* After the drift the detectors were subjected to the stabilizing etching described in [5] before measuring the C—U curve shown in Fig. 2. This process resulted in a stable surface; minimizing of the leakage current of the detectors and of their capacity by gas cycling was superfluous; the process proved to be well reproducible; repeated stabilizing etching always restored the original I—U characteristics. It is worth mentioning that the leakage current minimized with the above method did not show observable increase even after repeatedly cooling down the detectors to −50 °C and warming up again to room temperature.

We tried also to wash the ready detectors with hot de-ionized water and to boil them in de-ionized water according to [5, 12]. The original reverse current of 10 μA cm^{-2} of the 1 mm thick detectors compensated in their whole thickness measured at 120 V at 20 °C temperature decreased to 1 μA cm^{-2} 24 hours after boiling in de-ionized water for about 15 minutse. The reverse current of thicker detectors (5—10 mm) increased, however, by this treatment and the original value before treatment could only be restored by the stabilizing etching mentioned above.

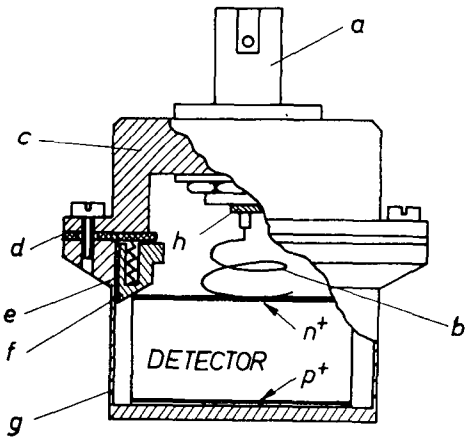

Fig. 3. Diagram of the detector capsule: *a)* output connection of the detector; *b)* spring and electric contact; *c)* upper part of the Al capsule; *d)* silicon rubber seal; *e)* spring of the distance ring; *f)* teflon distance ring; *g)* 0.5 mm thick side-wall of the Al capsule; n^+ and p^+ denote the contacts of the detector

6. *Encapsulation of the detectors.* The ready detectors were placed in an airtight Al capsule in pure nitrogen atmosphere (Fig. 3). The thickness of the side wall of the capsule was 0.2 mm. This thin wall did not practically absorb the radiation investigated.

Testing of the detectors

The current *vs.* reverse bias characteristics of the detectors No. 2 and 4 measured at 25 °C are presented in Fig. 4. The very rapid increase of the current in the range 0 to 10 V is noticable. (A curve of similar character can be seen *e.g.* in [13].) At voltages exceeding 40 V the increase of both curves was nearly linear. Fig. 4 shows our general experience that in the case of detectors of identical diameter but of different thickness, prepared from the same ingot, it was always the current of the thicker detectors which was higher and these higher currents generally increased more steeply at higher voltages. This phenomenon can be accounted for only partly by the higher generation current of thicker detectors.

While the breakdown of the detectors before compensation at room temperature generally began at 180—250 V reverse bias, depending on the detector, in the case of detectors with 10 mm depletion layer no sign of breakdown was observed up to 1100 V bias tested. It can be supposed that the breakdown occurs at considerable higher voltages.

In Fig. 5 the current *vs.* reverse bias characteristic of detector No. 1 is shown at different temperatures. It can be seen from the figure that the current of the detector

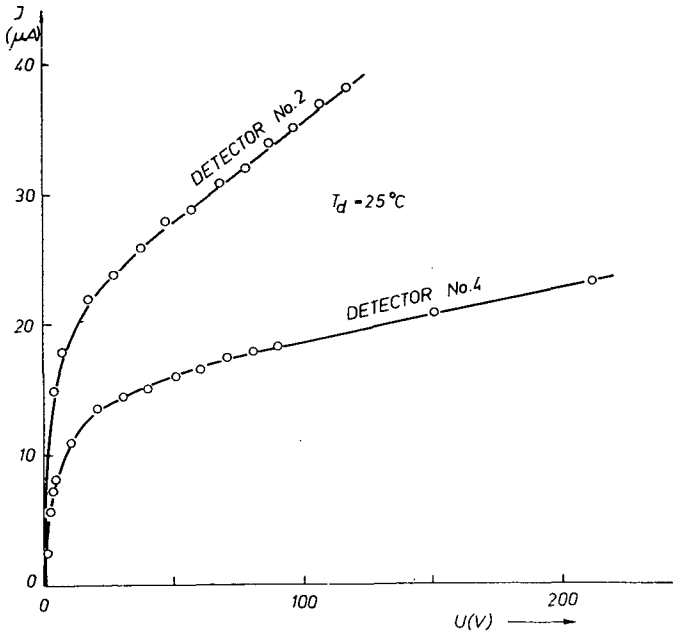

Fig. 4. Reverse current *vs.* voltage characteristics of detectors No. 2 and 4

strongly decreases with decreasing temperature, but at the same time below −10 °C the I—U curves become considerably steeper. The I—U curves of the detector No. 2 were in good accordance with those shown in Fig. 5, while the curves of detector No. 3 were somewhat different.

In order to study the shape of the pulses produced by γ photon absorption, the encapsulated detector was put in a thermostat which could be regulated between −10 to −70 °C. A lead plate of 20 mm thickness was placed immediately beside the detector, with the γ source of 1 μC activity behind it. The γ photons penetrated into the detector through a hole of 0.5 mm diameter in the lead plate and through the wall of the capsule, parallel to the plane of the detector contacts. A coaxial cable of low capacity served to connect the detector with the charge sensitive preamplifier which did not contain integrating and differentiating elements. The output of the latter was connected with the input of a high frequency oscilloscope. The pulses were observed and/or photographed on the screen of the oscilloscope. The

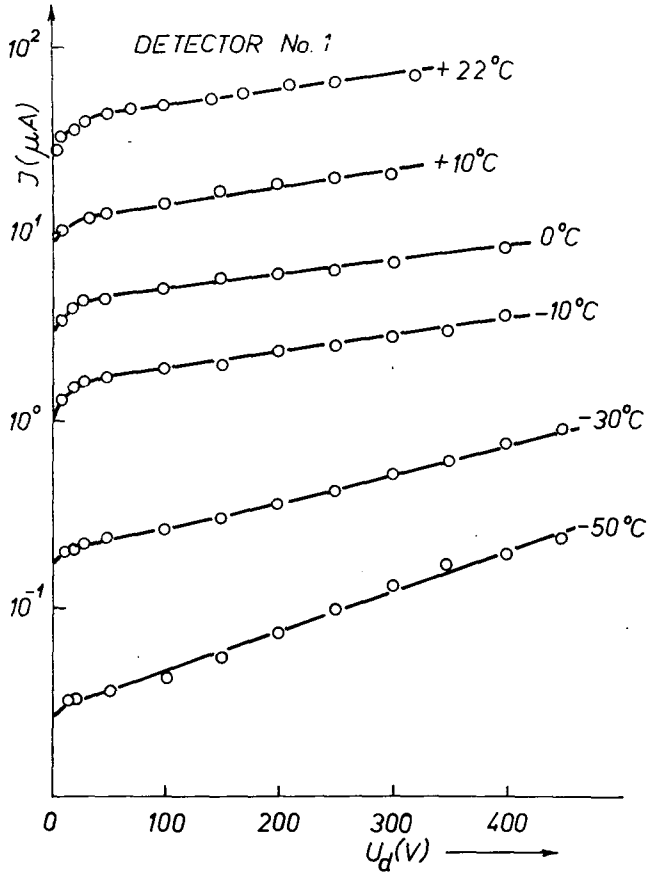

Fig. 5. Current *vs.* reverse bias characteristics of the detector No. 1 at different temperatures

value of the load resistor of the detector was 50 MΩ. The 100 V reverse bias of the detector was supplied by an anode battery. The pulses obtained with the detector No. 2 by the γ radiation of 662 keV energy of a Cs^{137} source at -65 °C detector temperature are shown in Fig. 6*a*, those obtained with the γ radiation of 1170 and 1330 keV energy of a Co^{60} source in Fig. 6*b*. The smallest scale divisions in both figures mean 100 μsec and 10 mV on the horizontal and vertical axis, respectively. The number of the pulses in Fig. 6*a* is higher than in Fig. 6*b*, due to the fact that the absorption coefficient of Si for γ radiation of lower energies is higher than for radiation of higher energies. (Both sources were of nearly the same activity and the experimental conditions were identical in both measurements.) In Fig. 6b there are also higher pulse amplitudes than in Fig. 6*a* this can be attributed to the higher energy of the radiation.

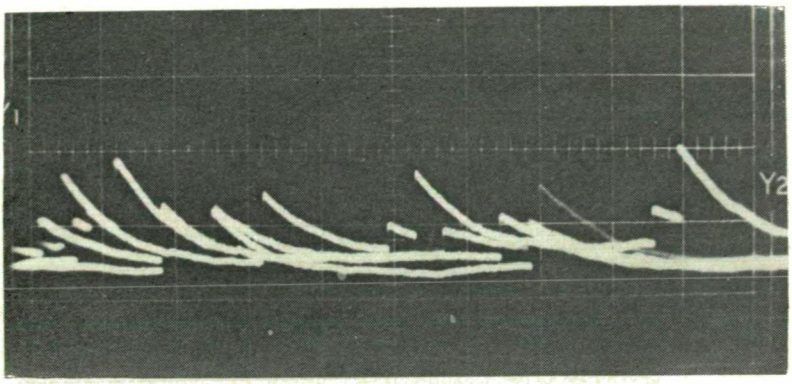

Fig. 6a. The pulses of the detector No. 2 due to gamma radiation of a Cs^{137} source, obtained at -65 °C detector temperature

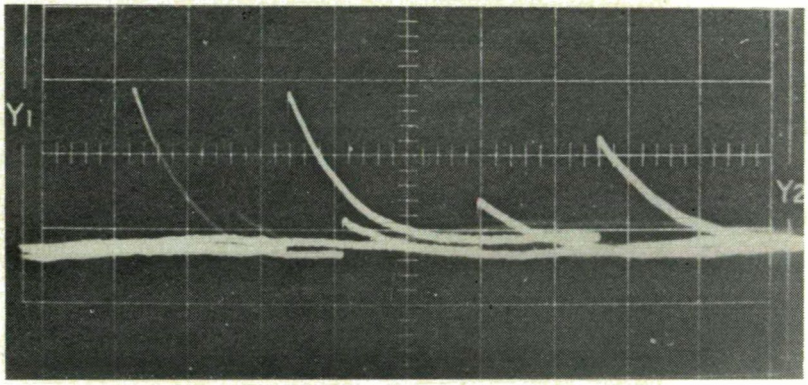

Fig. 6b. The pulses of the detector No. 2 due to gamma radiation of a Co^{60} source, obtained at -65 °C detector temperature

By studying the pulses of detectors with higher time resolution, it was possible to determine the carrier collection time of the detectors, which resulted to be about 0.5 μsec at 100 V detector voltage near -60 °C detector temperature; this is near to the value calculated from the carrier mobility, the thickness of the detector, and from the field strength in the detector.

In Figs. *7a*, *7b* and *7c* the pulses of the detector No. 2 due to γ radiation of a Cs^{137} source, obtained at detector temperatures of -65, -50 and -30 °C, respectively, can be seen. This bias of the detector was 100 V, the value of the load resistor 50 MΩ, the smallest scale division on the horizontal axis 100 μsec, on the vertical axis 4 mV in all three cases. The figures show a strong increase of the detector noise with increasing temperature.

Performing the same investigations with the detectors No. 1 and 3, it was found that the rise and decay times of pulses of detector No. 1 due to γ radiation, as well

as the mean value of the amplitude maxima determined from numerous measurements were practically the same as obtained with detector No. 2 under identical conditions. In the case of detector No. 3 the main pulse amplitude proved to be about 20% less, while the rise time of the pulses was about 15% higher. This deviation of the parameters of detector No. 3 was attributed to the lower lifetime and mobility of the carriers.

The pulse amplitude spectra of the detectors were also measured with γ radiation of Cr^{51}, Cs^{137} and Co^{60} at different detector temperatures, detector voltages and load resistors. The block diagram of the measuring apparatus* is shown in Fig. 8. The detectors were connected with the preamplifier Tannelec type TC-135 by a cable of low capacity. The load resistor was varied between 1 and 47 MΩ. The signals obtained from the preamplifier were further amplified to the level necessary for the analyser by a main amplifier Canberra type 1417 B provided with an active filter (integrator and differentiator). The pulses were analysed with an amplitude analyser of 1024 channels, type ND-2200 of Nuclear Data. The information stored in the analyser was recorded on a tape, the spectra were plotted and the measurements evaluated. The correct functioning of the measuring system was checked by a pulse generator BNC type GL-3 connected immediately with the preamplifier.

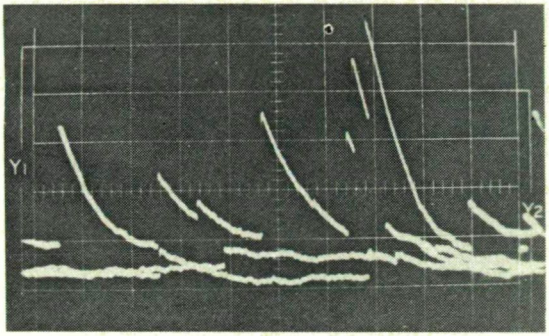

Fig. 7a. The pulses of the detector No. 2 irradiated by gamma radiation of a Cs^{137} source at −65 °C temperature

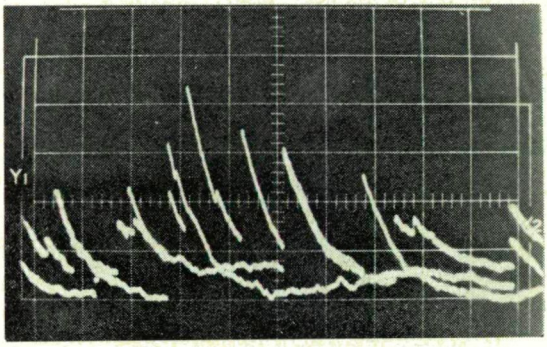

Fig. 7b. The pulses of the detector No. 2 irradiated by gamma radiation of a Cs^{137} source at −50 °C temperature

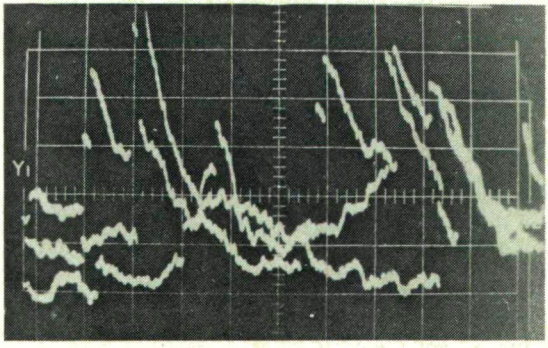

Fig. 7c. The pulses of the detector No. 2 irradiated by gamma radiation of a Cs^{137} source at −30 °C temperature

* These measurements were made in the Hungarian Bureau of Measurements

The method of measurement was as follows:

i) the noise spectrum of the detector during a period t_m was recorded;

ii) the pulse spectrum of the detector was recorded with γ irradiation for the time t_m again;

iii) the noise counts were subtracted from the counts due to irradiation of the respective channels, and the spectra were plotted from these differences.

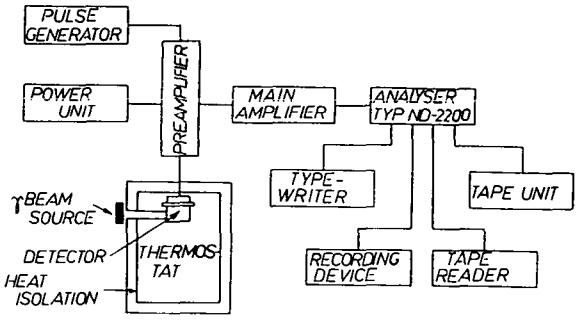

Fig. 8. Block diagram of the measuring apparatus.

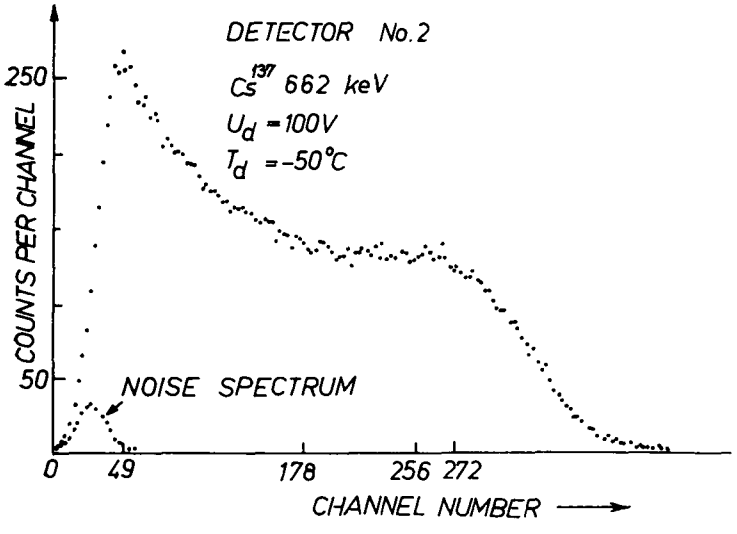

Fig. 9.

Fig. 9 shows the pulse amplitude spectrum of detector No. 2 produced by 662 keV γ irradiation of a Cs^{137} source. The temperature of the detector was $T_d = -50\,°C$, the bias $U_d = 100$ V, the value of the load resistor $R_L = 10$ MΩ, the time constant of the integrator and differentiator in the main amplifier (denoted in the following shortly as time constant) $\tau = 1$ μsec, and the period of measurement

$t_m = 100$ sec. The numbers of the channels are indicated on the horizontal axis, the counts per channel on the vertical axis of the figure. The sharp peak characteristic for the energy of the radiation does not appear in the pulse spectrum, because the radiation of energy >100 keV is absorbed mainly by Compton interaction with

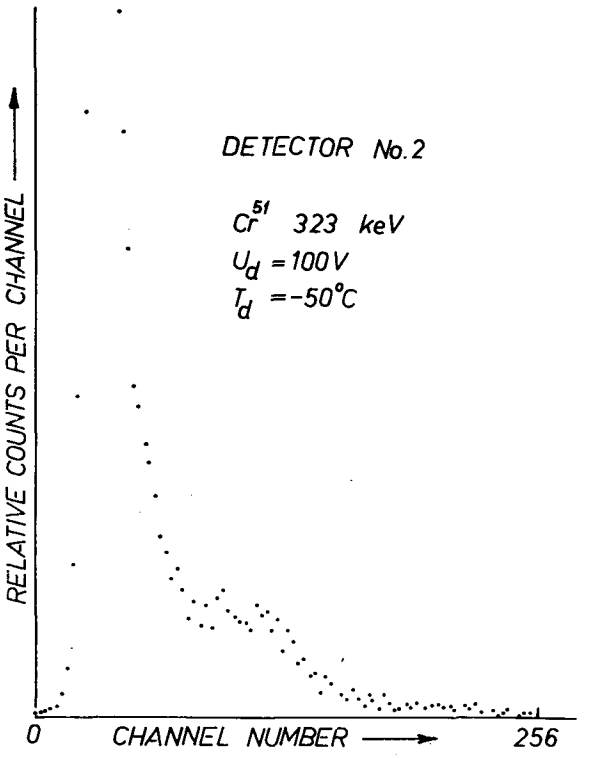

Fig. 10.

Si [14]. In the spectrum shown in Fig. 9, four regions may be distinguished on the basis of the counts per channel with increasing channel number (or pulse amplitude):

In region I (channel numbers from 0—49) a sharp increase is seen;

In region II (channel numbers from 49—178) a rapid decrease, gradually slowing down;

In region III (channel numbers from 178—272) the counts are nearly constant;

In region IV (channel numbers higher than 272) the counts decrease again, approaching 0 at the end of the region.

In Fig. 10 the pulse amplitude spectrum of detector No. 2 irradiated by 323 keV γ rays of a Cr^{51} source is presented. The experimental conditions in the case of Figs. 9 and 10 were identical. The main difference between the curves of both figures is to be found in the fact that regions II, III and IV of Fig. 10 are shorter and the counts

reach the 0 level at a lower channel numbers, which is clearly due to the lower energy of the radiation.

Figs. 11, 12 and 13 show the counts per channel *vs.* channel number curves of the detector No. 1 irradiated under identical conditions by a Co^{60}, Cs^{137} and Cr^{51}

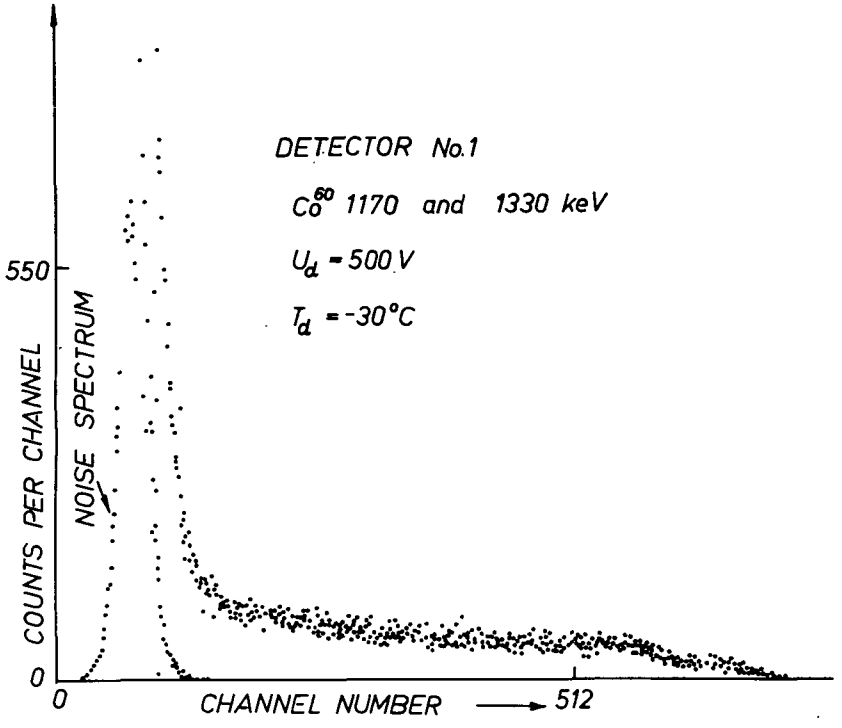

Fig. 11.

source, respectively. The parameters $T_d = -30$ °C, $U_d = 500$ V, $R_L = 10$ MΩ, $\tau = 1$ μsec, $t_m = 200$ sec were used in all three cases. The noise spectrum, or its part corresponding to higher channel numbers is also plotted in all these figures. The detector noise, compared with that for -50 °C, markedly increased (see Figs. 9 and 10). The spectral range IV, characteristic for the energy of radiation is influenced in a less degree in Figs. 11 and 12, while in Fig. 13 this influence is significant. From this it can be concluded that the detectors can be used at the higher temperatures, the higher the energy of the γ radiation.

Similarly as it was observed for the spectra shown in Figs. 9 and 10, the decay section IV of the pulse amplitude spectra gradually shifts towards higher channel numbers (pulse amplitudes) with increasing energy of the γ radiation; therefore the energy can be estimated from the position of the decay region of the spectra. The

decay is decidedly more sharp in Fig. 12 than in Fig. 11; this can be attributed to the circumstance that the radiation of Cs^{137} is monochromatic, while that of Co^{60} is not.

The pulse amplitude spectra of detector No. 2 irradiated with a Co^{60} source at $+5\,°C$ and $-50\,°C$ detector temperature, respectively, are presented in Figs. 14

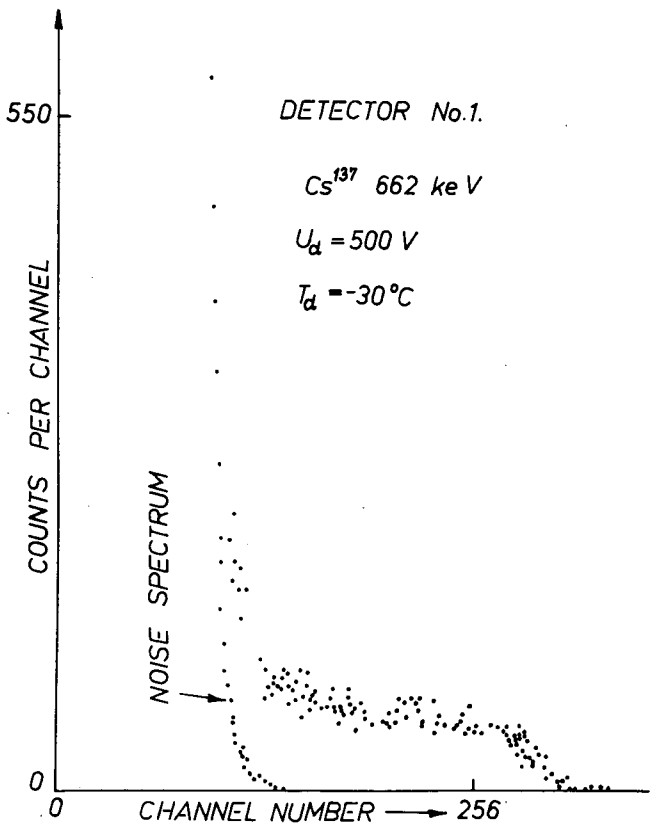

Fig. 12.

and 15. Apart from the detector temperature, the conditions of measurement were the same in both cases. The results shown in Fig. 14 point to the fact that, for counting γ photons of higher energies, the detectors can be used even at $+5\,°C$ temperature.

The absolute counting yield η of the detectors

$$\left(\eta = \frac{\text{total counts}}{\text{number of the incident photons}}\right)$$

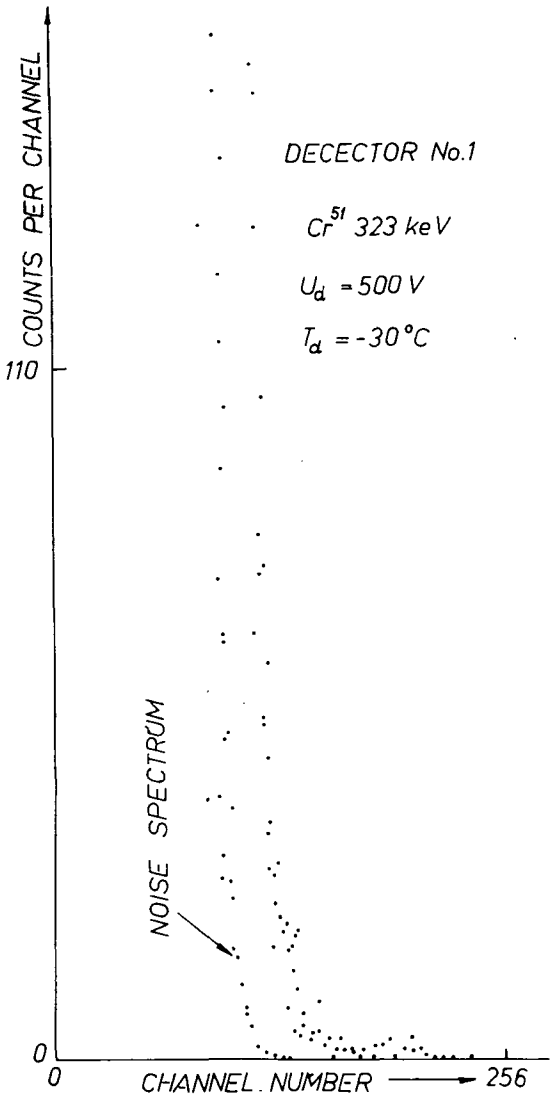

Fig. 13.

was determined at $-30\,°C$ and with a time constant of 1 μsec using a Co^{60} source of 17.21 μC activity placed at a distance of 25 cm from the detector. Knowing the geometry of the detector, as well as the distance and the activity of the γ source, the number of the γ photons incident on the detector was determined supposing the formation of two photons per radioactive decay. The differences of the counts obtained during the period of measurement and the noise counts determined for

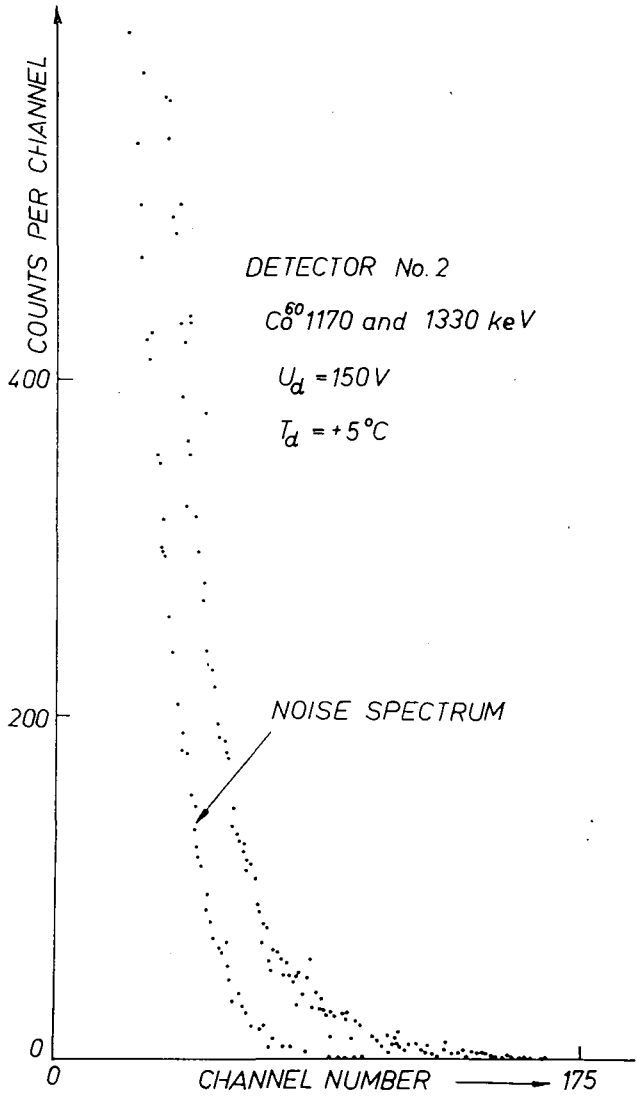

Fig. 14.

the same time were used as total counts. η was found to be 4.8 and 4.5%, respectively, for the detectors No. 1 and 2. The absolute counting yield showed practically no changes on varying the detector bias between 150 and 500 V and the values of load resistor between 1 and 47 MΩ.

In order to determine the optimum time constant of the integrator and differentiator in the main amplifier in connection with the detector used, the detector

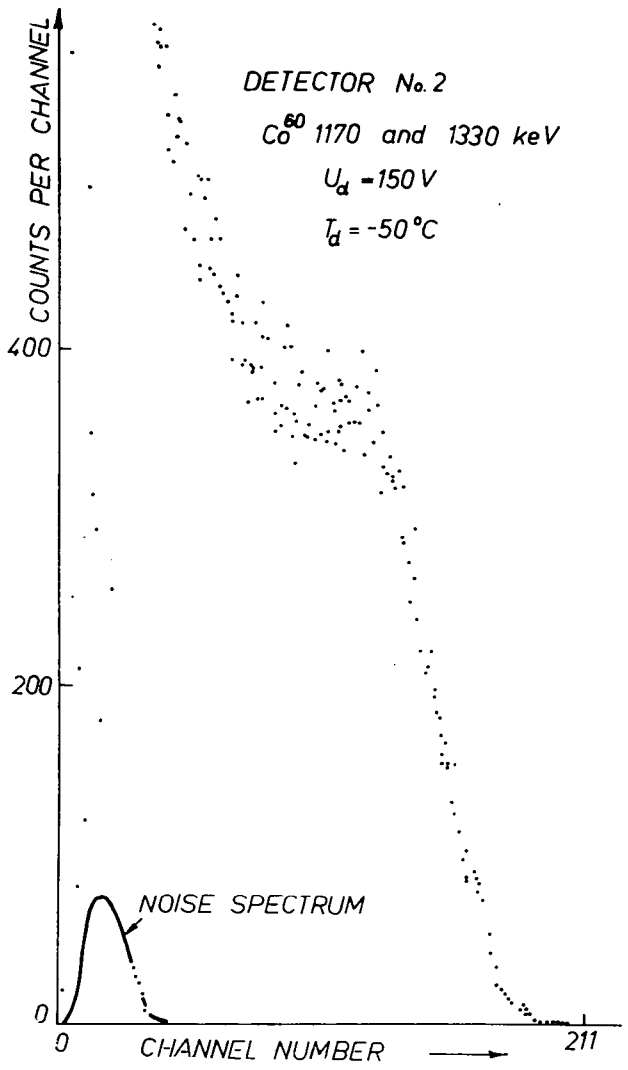

Fig. 15.

No. 2 was irradiated by a Co^{60} γ source and the time constant was set to 0.25, 0.5, 1, 2 and 4 μsec; the number of the total counts in 200 sec at 150 V detector bias was determined with each time constant (Fig. 16). The optimum time constant at −30 °C temperature resulted to be 0.5 μsec. As the optimum time constant depends also on the detector temperature through the carrier mobility, and the counts varied only slightly with the time constant, the time constant $\tau = 1$ μsec was used for all spectral measurements described in this paper.

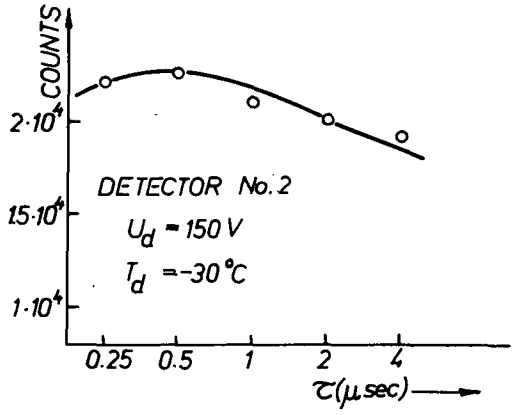

Fig. 16. Total counts *vs.* time constant caractehristic of the detector No. 2

Discussion

Irradiating the detectors by γ rays between 323 and 1330 keV energy, no sharp peak characteristic for the energy of radiation appeared in the spectra. This can be attributed to the fact that radiation of the energy range investigated is absorbed by several subsequent Compton interactions in the Si. The first Compton interaction generates a hot electron and a γ photon of less energy than the incident one. The hot electron is slowed down in the detector by generating hole-electron pairs; the secondary photon either interacts repeatedly with the crystal, or leaves the detector without further interaction. The signal of maximum amplitude is produced if the γ photon loses its total energy in the detector by repeated Compton interactions or photoeffects. Beside the effects mentioned, also the detector noise plays a role in determining the shape of the pulse amplitude spectrum. Therefore the region IV pertaining to higher channel numbers is characteristic for the energy of the γ radiation. Due to this circumstance, the detectors studied are less suitable for measuring the energy of γ radiation, while they can be used for counting the γ photons of higher energies, especially at lower detector temperatures.

The absolute counting yield of the detectors for γ radiation of a Co^{60} source was higher than 4%; it is clear that this value increases rapidly with decreasing energy of the radiation, owing to the increase of the absorption coefficient of Si for γ radiation.

The parameters of the detectors can be significantly improved by reducing the leakage current, using a guard ring or other suitable methods.

References

[1] *Blankenship, J. L., C. J. Borkowski:* IRE Trans. nucl. Sci. NS-**9**, 181 (1962).
[2] *Elliott, J. H.:* Nuclear Instruments and Methods **12**, 60 (1961).
[3] *Ristinen, R. A., D. A. Lind, J. L. Homan:* Nuclear Instruments and Methods **56**, 55 (1967).
[4] *Mann, H. M., F. J. Janarek:* Nuclear Instruments and Methods **17**, 71 (1962).
[5] *Llacer, J.:* IEEE Trans. nucl. Sci. NS—**13**, 93 (1966).
[6] *Wang, L., M. R. Zatzick, F. P. Ziemba:* IEEE Trans. nucl. Sci. NS-**11**, 314 (1964).
[7] *Tannenbaum, E.:* Solid-State Electronics **2**, 123 (1961).
[8] *Trumbore, F. A.:* Bell System Techn. J. **39**, 205 (1960).
[9] *Fuller, C. S., J. A. Ditzenberger:* J. Appl. Phys. **27** (5), 544 (1956).
[10] *Ammerlaan, C. A. J., K. Mulder:* Nuclear Instruments and Methods **21**, 97 (1963).
[11] *Kuhn, A.:* Halbleiter und Kristallzähler, Leipzig 1969, Akademische Verlagsgesellschaft Geest & Portig K.-G. p. 175—177.
[12] *Przyborski, W., J. Chwaszczewska, W. Czarnacki:* Nukleonika 12 Nr. **11**, 993 (1967).
[13] *Miller, G. L., B. D. Pate, S. Wagner:* IEEE Trans. nucl. Sci. NS-**10**, 220 (1963).
[14] *Grodstein, G. W.:* N. B. S. Circular **583**, (1957).

ИЗГОТОВЛЕНИЕ И ИССЛЕДОВАНИЕ ТОЛСТЫХ Si(Li) *p-i-n* ГАММА-ДЕТЕКТОРОВ

А. Шьюли, Л. Михайлович, Ф. Лист

Изготовлены Si детекторы с обьёмом 3,2 см^3 и 100 мм толстым компенсированным слоем при помощи диффузии Li в электрическом поле. Спектр амплитуды импульса детектора измерен в интервале температур от -50 °C до $+5$ °C при облучении детекторов радиоактивными источниками Cr^{51}, Cs^{137} и Co^{60} с энергией 323, 662, 1170 и 1330 кэв. Характерные пики для энергии гамма-излучения в спектре не наблюдались, т. к. энергия излучения исследованного диапазона поглощалась в Si, вследствие нескольких комптоновских взаймодействий Положение затухающих участков полученных спектров характерно для энергии излучения. Абсолютная эффективность счёта детекторов, относящаяся к гамма-излучению Co^{60}, оказалась 4,8 и 4,5% соответственно. При хранении детекторов при комнатной температуре под маленьким обратным смещением в течение нескольких месяцев, параметры детекторов практически не изменялись. Также исследовалась форма возникшего импульса при воздействии на детекторы гамма-излучения в интервале температур от -65 до -30 °C.

INVESTIGATION OF THE POSSIBILITY OF POLYMERIZATION FOR THE BeH_2 MOLECULE

The Ground State of the BeH_2, Be_2H_4 and Be_3H_6 Systems by the FSGO Method

By

I. TAMÁSSY-LENTEI and J. SZANISZLÓ

Institute of Theoretical Physics, Kossuth Lajos University, Debrecen

(Received July 1, 1974)

Calculations were carried out for the ground state energy and equilibrium geometry of the BeH_2, Be_2H_4 and Be_3H_6 molecules by the FSGO method. According to the investigations, the BeH_2 molecule tends to have a polymerized form. The calculated dimerization and trimerization energy values are in good agreement with other calculated values available.

Introduction

Nowadays the subject of quantum-mechanical and quantum-chemical studies shifts more and more towards the larger systems, the molecules. When a certain system is repeated several times, in principle many times, as a result of the increasing process or additional reaction, *e.g.* a chain-type compound will be formed. The polymerization process has been observed in many cases; an interesting possibility is that the polymer formation of beryllium-hidride, $(BeH_2)_n$, is an existing polymer structure. The BeH_2 molecule is a very simple one, but experimental data on its properties are actually not available. Since the experimental determination of the polymerization energy of the discrete BeH_2 is not easy, therefore theoretical investigations have an increased importance.

The energy, the electronic and geometrical structure and other properties of a quantum-mechanical system may be determined by the solution of the Schrödinger equation. For small molecules there are many well treatable approximation methods producing precise results, but for larger systems we must content ourselves with the use of relatively simple methods. One of these is the FSGO (Floating Spherical Gaussian Orbital) method. The main advantage of its application is that it is an *ab initio* method, without any empirical parameters, and it is very easy to determine the integrals necessary for the calculations; and on the other hand the computer demand of the method is not too large. It was BOYS [1] who first proposed Gaussian-type one-electron orbitals centered on the nuclei. Then, to achieve better results,

PREUSS [2] and others suggested to use floating-type (off-centre) spherical Gaussians having the form:

$$\psi_i = (2/\pi\varrho_i^2)^{3/4} \exp[-(\mathbf{r}-\mathbf{R}_i)^2/\varrho_i^2] \tag{1}$$

as orbitals.

To determine the approximative wave-function of a system applying the variational method in the customary way, in (1) the orbital radii ϱ_i, but also the position vectors $\mathbf{R}_i$ have to be treated as variational parameters. In the FSGO method the wave-function of a $2n$-electron system for a singlet ground state is considered as a single Slater determinant composed from n different double occupied one-electron spherical Gaussians.

Lately FROST [3] started an extensive computation series with this model to determine the total energy, equilibrium geometrical structure and other physical properties of some systems. Previously, the method proved to be well applicable among others for the description of interaction potentials of atoms and ions [4], for the calculation of proton affinities [5], for the determination of dissociation energies [6].

In the present paper we intend to apply the FSGO method for the investigation of the polymerization of the BeH_2 molecule. Regarding the computational details, we refer *e.g.* to [5]. The calculations were carried out on the ODRA 1204 computer of the University Computer Center.

The BeH_2 *system*

The BeH_2 is a very symmetrical molecule. Therefore it is natural to center one of the orbitals on the Be nucleus (inner shell orbital) with orbital radius ϱ_{in} and the other two on the BeH line, equidistant from the Be (bonding orbitals) with orbital radii ϱ_B. The result of the variational calculation is, that the BeH_2 is a linear molecule. So the X-axis was chosen as molecular axis, taking the Be atom as origin, and the co-ordinates of the bonding orbitals were denoted with $\pm X_B$. The results of the calculation (total energy E; equilibrium internuclear distance R) are summarized in Table I. (Atomic units are employed throughout.) Accordingly, the BeH_2 is a stable system in the ground state, though this is not known from experiments.

Table I

	BeH_2
ϱ_{in}	0.510
ϱ_B	2.108
X_B	2.107
R	2.669
E(FSGO)	−13.214*

* See Ref. [3(b)]

The Be_2H_4 *system*

The Be_2H_4 molecule was considered as a planar system, in the $X-Y$ plane. The two Be atoms were placed on the X-axis, being at the same time the molecular axis, and symmetrically to the origin, with co-ordinates X_{Be}. Two H atoms were localized symmetrically to the X-axis, two others to the Y-axis with co-ordinates X_{H_i}, Y_{H_i} ($i=1, 2, 3, 4$), (see Fig. 1). Two inner orbitals were localized on the X-axis, near the Be atoms, at the points P_1, P_2, with co-ordinates X_1, X_2 and orbital radii

ϱ_1, ϱ_2. The four further bonding orbitals were placed close to the H atoms, in the points P_i, with co-ordinates X_i, Y_i; and orbital radii ϱ_i ($i=3, 4, 5, 6$); obviously two of them were always laid symmetrically to a co-ordinate-axis, namely, the bond bridge was assumed to be of rhomboid form. According to the calculations the

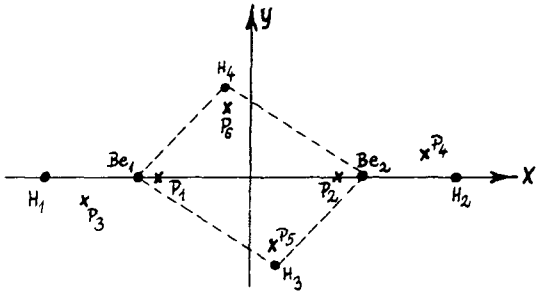

Fig. 1

two inner orbitals are centred practically on the Be atoms, two H atoms and two bonding orbitals are centred on the X-axis, and the other two on the Y-axis. The results for both cases are presented in Table II (in atomic units). Consequently, the experimentally unknown Be_2H_4 is more stable, than the configuration belonging to the separated BeH_2 molecules.

Taking into account the geometry of the Be_2H_4 molecule, first the following molecular structure was supposed for the Be_3H_6: The three Be atoms and two of

Table II

	Be_2H_4	
$\varrho_1 = \varrho_2$	0.51069	0.51068
$\varrho_3 = \varrho_4$	2.1052	2.1069
$\varrho_5 = \varrho_6$	2.0345	2.0309
$X_{Be_1} = -X_{Be_2}$	−1.9096	−1.9018
$X_{H_1} = -X_{H_2}$	−4.5831	−4.5774
$Y_{H_1} = -Y_{H_2}$	−0.0001375	0 (fixed)
$X_{H_3} = -X_{H_4}$	0.0001175	0 (fixed)
$Y_{H_3} = -Y_{H_4}$	−2.1719	−2.1708
$X_1 = -X_2$	−1.9083	$X_{Be_1} = -X_{Be_2}$ (fixed)
$X_3 = -X_4$	−4.0325	−4.0275
$Y_3 = -Y_4$	$-10^{-5} \sim 0$	0 (fixed)
$X_5 = -X_6$	$10^{-5} \sim 0$	0 (fixed)
$Y_5 = -Y_6$	−1.6481	−1.6453
E(FSGO)	−26.4742	−26.4740
$R(\overline{Be_1 Be_2})$	3.8192	3.8036
$R(\overline{H_1 Be_1})$	2.6735	2.6755
$R(\overline{H_3 H_4})$	4.3438	4.3416
$R(\overline{Be_1 H_3})$	2.8920	2.8861
$H_3 Be_1 H_4 \sphericalangle$	98.35°	97.56°

The Be_3H_6 system

the H atoms (H_1, H_2) were placed on the X-axis, which was chosen as the molecular axis (see Fig. 2*a*). Two other H atoms (H_3, H_4) and two of the Be atoms (Be_1, Be_2) were supposed to form a rhombus. The line connecting the H_3 and H_4 was considered

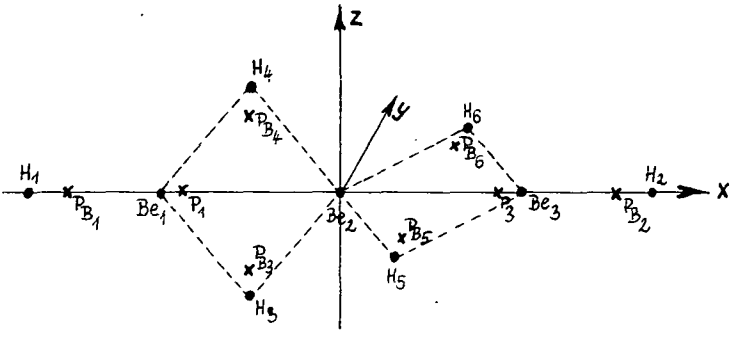

Fig. 2a

as parallel to the Z-axis. The plane of the other rhombus determined by the Be_2, Be_3, further by the H_5, H_6 was presumed to be orthogonal to the former one, so it is lying in the $Y-Z$ co-ordinate-plane. (We shall call this form a linear form.) One inner orbital was placed on the Be_2 atom, at the origin. The other orbitals were

Table IIIa

	Be_3H_6	
$\varrho_1 = \varrho_2 = \varrho_3$	0.51095	0.51091
$\varrho_{B_1} = \varrho_{B_2}$	2.1072	2.1072
$\varrho_{B_3} = \varrho_{B_4} = \varrho_{B_5} = \varrho_{B_6}$	2.0329	2.0296
$X_{Be_1} = -X_{Be_3}$	−3.8122	−3.793
$X_{H_1} = -X_{H_2}$	−6.4905	−6.4711
$X_{H_3} = X_{H_4} = -X_{H_5} = -X_{H_6}$	−1.9106	−1.90
$Z_{H_3} = -Z_{H_4} = Y_{H_5} = -Y_{H_6}$	−2.1753	−2.1754
$X_{P_1} = -X_{P_3}$	−3.811	$X_{Be_1} = -X_{Be_3}$ (fixed)
$X_{B_1} = -X_{B_2}$	−5.9427	−5.924
$X_{B_3} = X_{B_4} = -X_{B_5} = -X_{B_6}$	−1.9071	−1.8971
$Z_{B_3} = -Z_{B_4} = Y_{B_5} = -Y_{B_6}$	−1.6609	−1.6593
E(FSGO)	−39.7398	−39.7397
$R(\overline{Be_1\,Be_2})$	3.8122	3.493
$R(\overline{H_1\,Be_1})$	2.6783	2.678
$R(\overline{H_3H_4})$	4.3506	4.3508
$R(\overline{Be_1\,H_3})$	2.8892	2.885
$H_3Be_1H_4\sphericalangle$	97.68°	97.86°

centred near the Be_1 and Be_3, at the points P_1, P_3 on the X-axis with co-ordinates X_1, X_3. According to the calculations, it was nearly unimportant, whether the P_1 resp. P_3 were kept fixed on the place of the Be_1 resp. Be_3 or not. Six bonding orbitals were centred on the connecting lines of the Be_1—H_1, Be_3—H_2, H_3—H_4 and H_5—H_6, near the H atoms, symmetrically. For both cases (inner shell orbitals centred on the Be atoms, or not) the results are collected in Table IIIa (in atomic units). The notations are used in quite similar sense as before.

Another possibility is to consider the Be_3H_6 as a system having cyclic planar molecular structure (see Fig. 2b). For reasons of symmetry the Be_1, Be_2, Be_3; the H_1, H_2, H_3 and the H_4, H_5, H_6 atoms were placed on the same circles. Further the centres of the orbitals P_1, P_2, P_3, the P_{B_1}, P_{B_2}, P_{B_3} and the P_{B_4}, P_{B_5}, P_{B_6}, were each also similary situated on circles. The variational procedure was carried out in such a way that the points P_1, P_2, P_3 coincided with the three Be atoms, or their co-ordinates were considered as variational parameters. The equivalent bond lengths and angles were assumed to be equal. The results obtained for both cases are collected in Table III*b* (in atomic units). As it can be seen, although the cyclic structure for the Be_3H_6 is a stable one, but the linear form is energetically more favourable, so it is the more stable conformation.

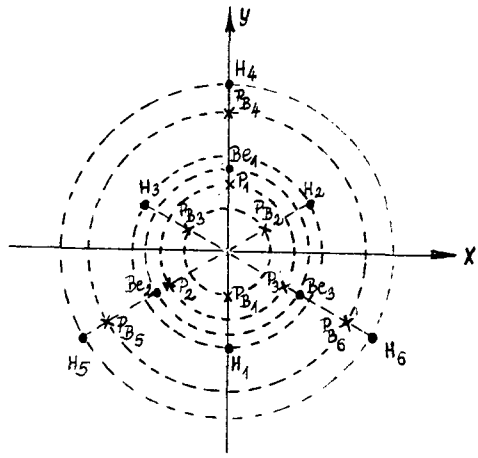

Fig. 2b

Table IIIb

	Be_3H_6 (cyclic)	
$\varrho_1 = \varrho_2 = \varrho_3$	0.51089	0.5109
$\varrho_{B_1} = \varrho_{B_2} = \varrho_{B_3}$	2.0036	1.9969
$\varrho_{B_4} = \varrho_{B_5} = \varrho_{B_6}$	2.0959	2.0990
Y_{Be_1}	2.7437	2.767
Y_{H_1}	−2.8293	−2.771
Y_{H_4}	5.4261	5.455
Y_{P_1}	2.7421	Y_{Be_1} (fixed)
Y_{B_1}	−2.4221	−2.393
Y_{B_4}	4.8854	4.911
E(FSGO)	−39.6964	−39.6952

Discussion

In the last decade there are numerous theoretical calculations concerning the BeH_2 systems dealt with here. Now the configuration interaction study of HOSTENY and HAGSTROM [7] can be regarded as the most accurate treatment with an optimized 80-term wave-function. One can find further detailed references concerning the BeH_2 in [7]. According to this very precise investigation, but also those of other authors, the BeH_2 is a stable molecule. (This follows from the FSGO model

too, using the energetical data of the Be and H_2 [5].) All the same, the system is unobservable because of unfavourable experimental conditions of measurement. Beside this it seems that the BeH_2 has the property of polymerization. The experimental values of the polymerization energy of the BeH_2 are uncertain, but the theoretical values can be estimated. It is rather easy to get the dimerization and trimerization energies as simple energy differences. Our calculated values are given in Table IV

Table IV

	FSGO	Theor.*
E_{dim}(dimerization energy) $= 2E(BeH_2) - E(Be_2H_4)$	0.046	0.0445 resp. 0.05 ± 0.01**
E_{trim}(trimerization energy) $= E(Be_2H_4) + E(BeH_2) - E(Be_3H_6)$	0.051 (for chain structure)	0.0553 resp. 0.063 ± 0.015**

* Values from [8]
** Estimated value in [8]

(in atomic units). There are no experimental data available for comparison. The only theoretical study on this subject known by the authors is the recent computation of AHLRICHS [8]. This *ab initio* investigation, starting from an SCF calculation, includes the electron correlation energy of the valence shell electrons too. Our calculated values are in good agreement with the results mentioned above (see [8]). Accordingly, the very simple FSGO model seems to be appropriate to predict the existence of the tendency for polymerization in the investigated system.

It is possible to calculate the energy of the $(BeH_2)_n$ linear polymer system for $n \leqq 4$, and the polymerization energy of polymers higher than the trimer, too. However, the computer requirements are significantly larger. It is probable that the polymerization energy generally has a value near 0.05 of order per molecule.

References

[1] *Boys, S. F.:* Proc. Roy. Soc. London, **A200**, 542 (1950).
[2] *Preuss, H.:* Z. Naturforsch. **11a**, 823 (1956).
[3] (a) *Frost, A. A.:* J. Chem. Phys. **47**, 3707, 3714 (1967).
(b) *Frost, A. A.:* J. Phys. Chem. **72**, 1289 (1968); for further references see *e.g.* Ref. [5].
[4] *Tamássy-Lentei, I., J. Szaniszló:* Acta Phys. Chim. Debr. XVIII/IV, 61 (1972—73).
[5] *Tamássy-Lentei, I., J. Szaniszló:* Acta Phys. Hung. **35**, 201 (1974).
[6] *Tamássy-Lentei, I., J. Szaniszló:* Acta Phys. Chim. Debr. (to be pusblihed).
[7] *Hosteny, R. P., S. A. Hagstrom:* J. Chem. Phys. **58**, 4396 (1973).
[8] *Ahlrichs, R.:* Theor. Chim. Acta **17**, 348 (1970).

ИССЛЕДОВАНИЕ СТЕПЕНИ ПОЛИМЕРИЗАЦИИ МОЛЕКУЛЫ BeH_2

Основное состояние систем BeH_2, Be_2H_4 и Be_3H_6 по методу FSGO

И. Тамашши-Лентеи, Й. Санисло

Проводились рассчёти по энергиям основных состояний и равновесных геометрий молекул BeH_2, Be_2H_4 и Be_3H_6 методом ФШГО. На основе этих исследований молекула BeH_2 показывает тенденцию полимеризоваться. Получённые значения энергий димеризации и тримеризации хорошо согласуются с известными рассчётными результатами.

MIGRATION OF THE ELECTRON EXCITATION ENERGY IN SYSTEMS OF ORDERED STRUCTURE

I. Absorption properties

By

E. BOR and J. HEVESI

Institute of Biophysics, József Attila University, Szeged

(Received June 1, 1974)

An aqueous detergent (sodium-lauryl-sulphate) solution containing three luminescent dyes in equimolar concentration was applied as *in vitro* photosynthetic model system. Experiments were made for studying the changes in the absorption properties of dyes due to the increase in dye and detergent concentration. It was found that with increasing dye-concentration different kinds of complexes of the dyes and of dyes and detergent come into being, which will be solubilized by increasing detergent concentration. The solubilization contributes to the increase in effectivity of the energy migration in these mixed solutions. This can be demonstrated by the fluorescence properties of the investigated system.

Introduction

It is well known that photosynthesis begins with a photochemical process subsequent to the absorption of light energy. The absorbed energy is transferred from the absorbing pigment molecules to those actually taking part in the photosynthesis, to the so-called reaction centrum.

Investigations of the energy migration in *in vivo* systems are very difficult owing to the fact that these systems are very sensitive to light, to heat, to experimental conditions and, in most cases, the composition of the pigment present in the system is not known. These difficulties can be partly eliminated by performing the investigations in model systems which approximate the structure of the photosynthesizing system.

Models used for this purpose are often solutions containing micelles [1]. The lamellar structure of the detergent (sodium lauryl sulphate) system applied imitates, at least to some extent, the structure of the chloroplasts in the photosynthesizing *in vivo* systems.

The migration of electron excitation energy from thionin (Th) to methylene blue (MB) in systems containing these dyes in an aqueous solution of sodium lauryl sulphate (SLS) was studied by SINGHAL *et al.* [2], HEVESI and co-workers [3], [4] and RÓZSA [5]. The model applied by BÁLINT *et al.* [6] and LEHOCZKI *et al.* [7] consisted of aqueous solution of SLS, containing rhodamine 6G (Rh6G) and thionin. The results of these experiments showed that the efficiency of the energy

transfer from Rh6G to Th or from Th to MB is the highest at the critical micelle concentration of the detergent (c.m.c.) and at room temperature. It was also shown [8] that the effectivity of the energy migration is very closely connected with the number of the micelles present in the system, and therefore with the structure of the dye-detergent solutions.

To extend these earlier investigations performed in aqueous SLS solutions containing rhodamine 6G and thionin or Th and methylene blue, respectively, a system consisting of the above three luminescent dyes in detergent solutions was investigated. This system represents a better approach to the *in vivo* system, where usually more than two kinds of pigment are present in the chloroplast.

The aim of the present paper is to study the influence of the change in concentration of the dye and the detergent on the effectivity of the transfer of excitation energy. These changes can be demonstrated by the changes in luminescence intensity of the dyes applied. Therefore, the properties of the absorption and fluorescence in three-component micellar systems were measured.

Composition of the systems. Experimental methods

Sodium lauryl sulphate was used as detergent, rhodamine 6G, thionin and methylene blue were applied as luminescent dyes. Mixed solutions containing equimolar quantities of these dyes were studied, the concentration of the dyes was varied from $2 \cdot 10^{-6}$ M to $1 \cdot 10^{-4}$ M. The detergent concentration changed from 0 to $8 \cdot 10^{-3}$ M. For preparing the solutions, first the required volumes of stock solutions of the dyes were pipetted into the flask, than the detergent was added to the solution, and finally the mixture made up to the mark with water distilled in a three-stages quartz distillation apparatus. Each set of the measurements was completed within 48 hours after the preparation of the solutions. The experiments were repeated several times, and the mean values of the results were used for drawing the conclusions.

The absorption spectra of the systems were recorded on an Optica Milano Type CF—4DR spectrophotometer, the recording unit was a compensograph Type Specdomax C. The fluorescence spectra were measured on a spectrophotometer DFS—12 (Leningrad). The light source was a low-pressure mercury lamp HBO 500. The sample was contained in a 1 cm cell. The wavelength of exciting light was 436 nm and 494 nm, respectively. The fluorescence spectra were corrected for reabsorption [9] and for spectral response of the photomultiplier. The experimental temperatures were kept constant within ± 1 °C in an adequate sample holder with the aid of an U—10 type Höppler ultrathermostat.

Results and discussion

The absorption and luminescence properties of mixed solutions containing three luminescent dyes and detergent were investigated. The measured characteristics seemed to be influenced both by detergent and dye concentration. The absorption spectra of the systems are not additive; the absorption spectra of mixed solutions cannot be built up from the absorption spectra of the one-component systems. This indicates

the presence of chemical interactions among the investigated dyes and between the dyes and the detergent used. This is supported by the deformation of the absorption spectra of mixed solutions containing detergent, compared with the absorption spectra of the corresponding aqueous solutions.

Figs. 1 and 2 show the absorption spectra of the solutions of $2 \cdot 10^{-6}$ and $5 \cdot 10^{-5}$ M dye concentration at different SLS concentrations. The figures show, that the addition of a small amount of detergent to the solutions shifts the maxima

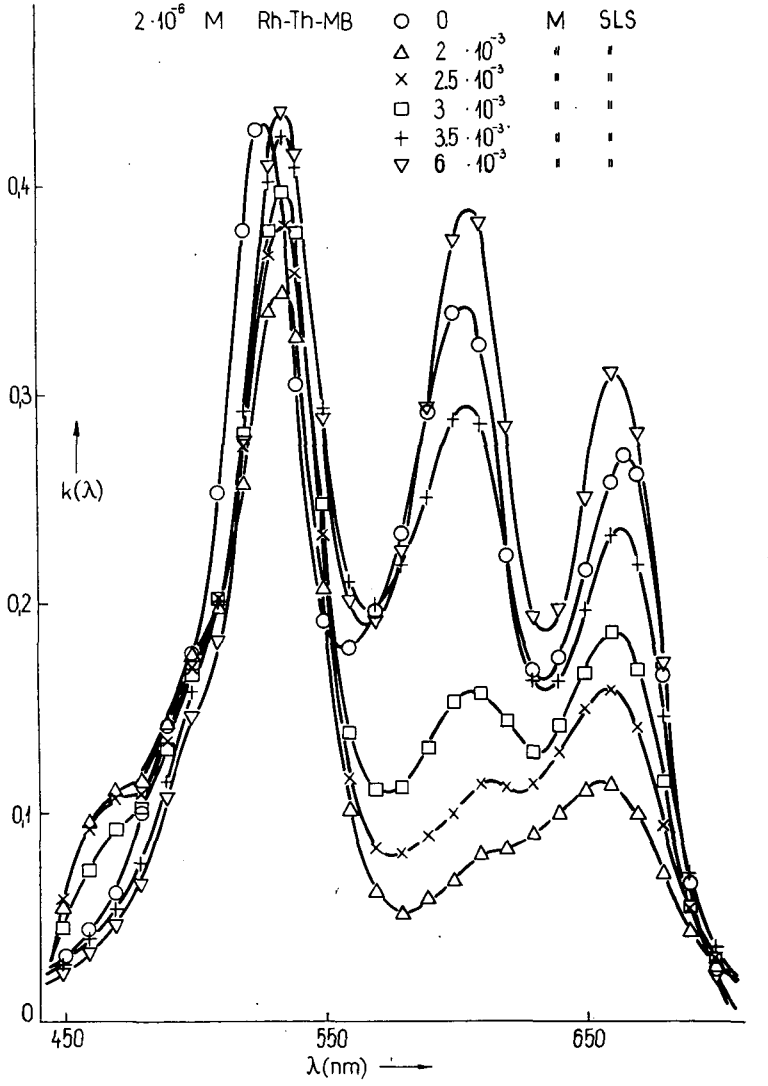

Fig. 1

of the absorption spectra toward longer wavelengths, but further increases in detergent concentration have no essential effect on the position of the maxima. The extent of these shifts in mixed solutions is in good accordance with the results measured in one-component systems [2, 5—7, 10, 11]. An exception is the behaviour of the α-band of MB, which is at 665 nm in aqueous solutions. Adding detergent to the aqueous mixed solution this peak shifts toward shorter wavelengths and the extent of the shift depends on the detergent concentration. This phenomenon can be explained by the circumstance that the α-band of MB is partly overlapped by the

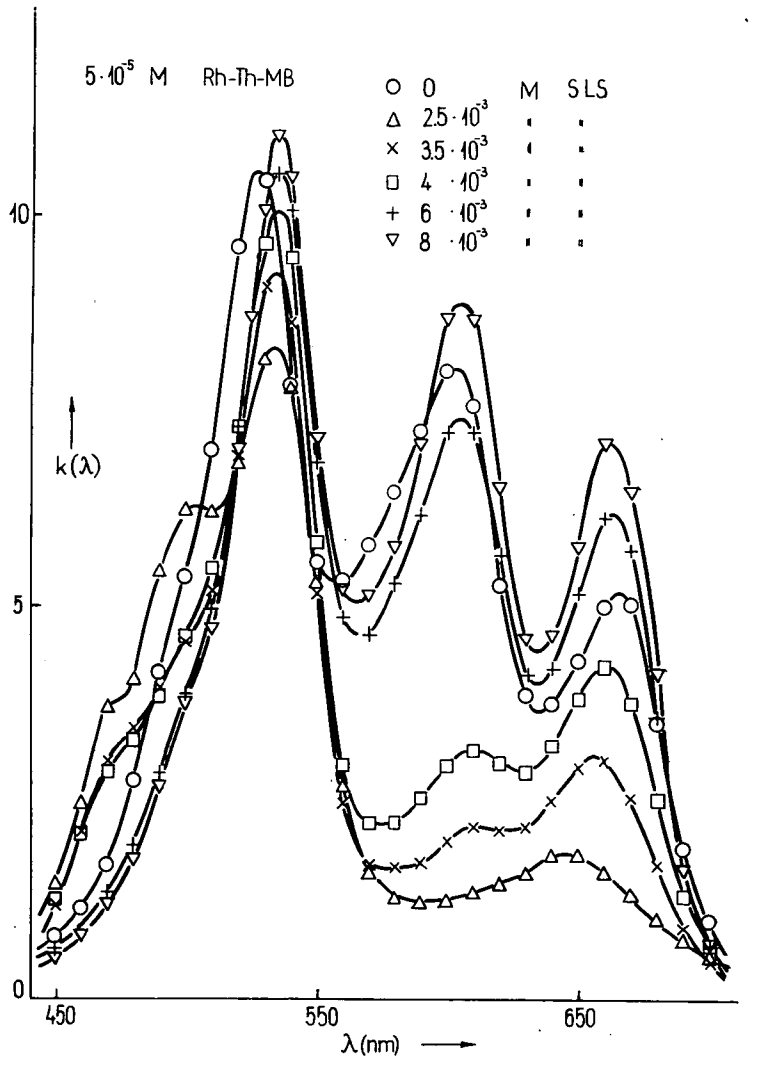

Fig. 2

δ-band (640 nm) of Th. This conception is supported by the fact that in mixed solutions at low detergent concentrations (below the c.m.c.) the maximum of the α-band of MB is higher than that of Th, contrary to the respective values measured in aqueous solutions. Comparing the Figs. 1 and 2, it can be seen that, with increasing dye concentration, different types of associates can be formed.

Adding detergent to the solutions, the values of the α-maximum of Rh6G (528—534 nm) first decrease, then gradually increase reaching the value measured

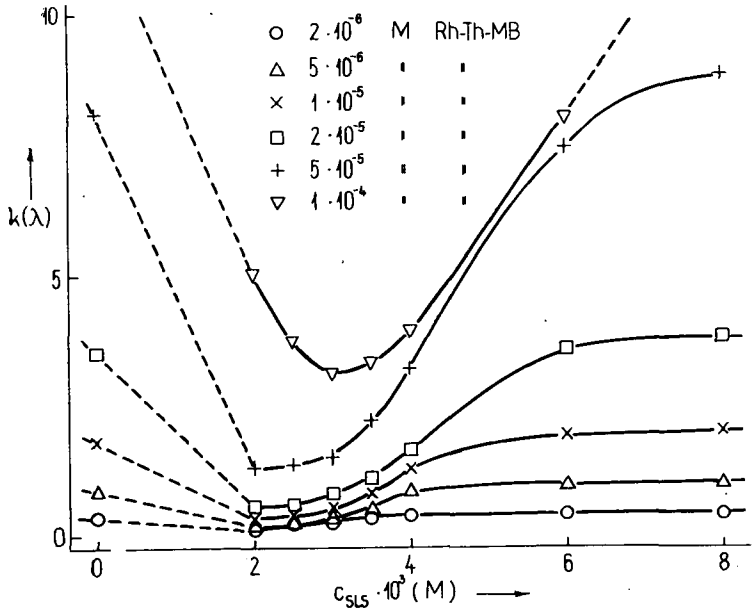

Fig. 3

in aqueous solutions. The minimum of the absorption coefficients is at the same SLS concentration ($2 \cdot 10^{-3}$ M) for each dye concentration.

Figs. 3 and 4 show the change in the maximum of the α-band (600—605 nm) and γ-band (465 nm) of Th, respectively, as a function of SLS concentration at different dye concentrations. It can be seen that, adding some detergent to the system, the absorption coefficients of the α-band maxima of Th decrease; further increase in the SLS concentration raises the values of the maximum over those measured in aqueous solutions.

With increasing dye concentration, the increase in $k(\lambda)$ values begins at higher and higher SLS concentrations. This means that at a given SLS concentration, with increasing dye concentration, more and more dye-aggregates or dye-detergent complexes are formed. This statement is supported by the changes in the γ-band maxima of Th observed at different concentrations of dyes and detergent. The appearance of the γ-band of Th is attributed to the water-insoluble dye-detergent salts developed

in the system at low detergent concentrations. These salts become water-soluble at higher detergent concentrations, therefore the values of the maxima of this band decrease with increasing detergent concentration.

Comparing the minima of the curves of Fig. 3 and the maxima of the curves of Fig. 4, it can be seen that the increase in intensity of the γ-band takes place at

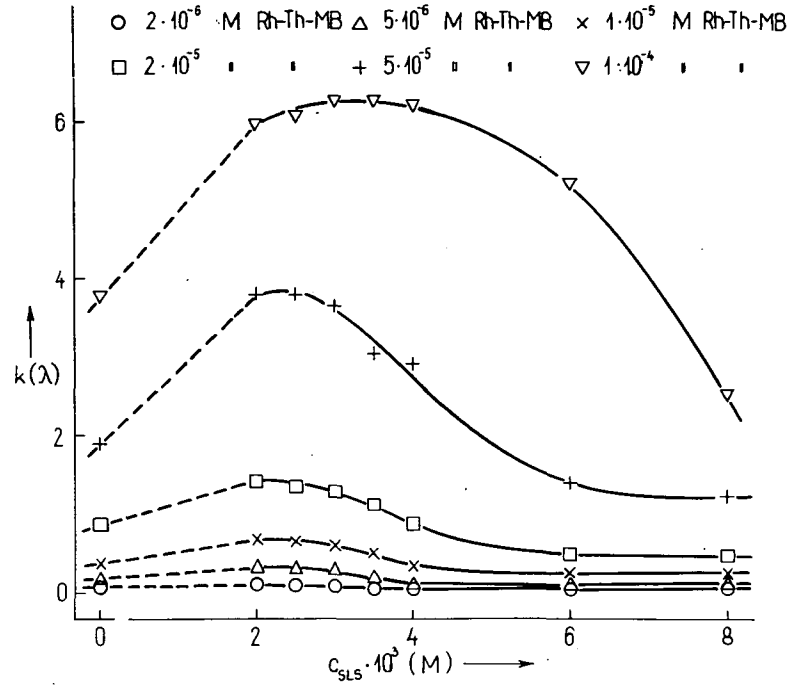

Fig. 4

the expense of the intensity of the α-band, which proves that the Th monomers form complexes with detergent molecules.

Similar changes were found by investigating the changes in α-band maxima (665 nm) of MB and the 500 nm maxima of MB—SLS complexes as a function of detergent concentration at different dye concentrations. The results of these experiments are presented in Figs. 5 and 6. It can be seen that at a given dye concentration the intensity of the maxima at 500 nm is the highest at the same detergent concentration where the α-band intensities of MB are the lowest. Therefore, it can be stated that at high dye concentrations, MB forms dye-detergent complexes which dissolve with further increasing detergent concentration, and the intensity of the α-band of MB increases again. At $6 \cdot 10^{-3}$ and $8 \cdot 10^{-3}$ M SLS concentrations the intensity of the α-band characterstic for MB monomers exceeds the value measured in aqueous solutions. This can be explained by the circumstance that in aqueous

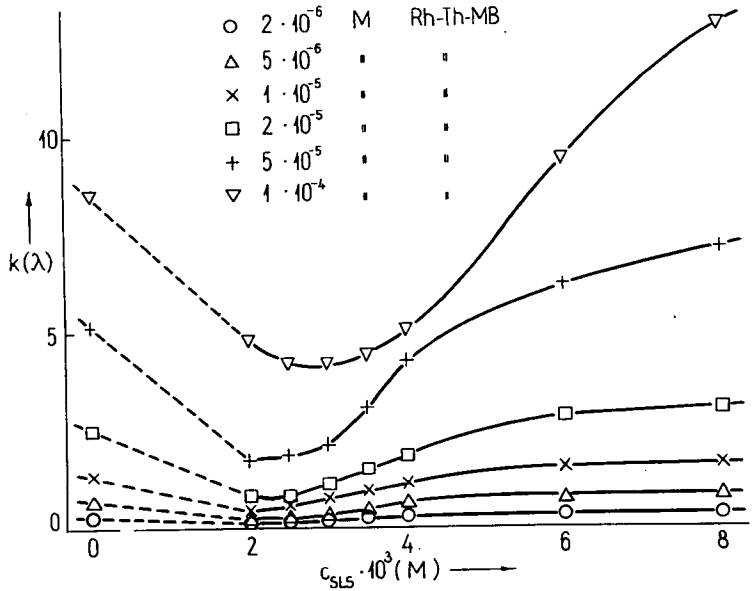
o 2 · 10⁻⁶ M Rh-Th-MB
Δ 5 · 10⁻⁶
× 1 · 10⁻⁵
□ 2 · 10⁻⁵
+ 5 · 10⁻⁵
▽ 1 · 10⁻⁴
k(λ)
10
5
0
0
2
4
6
8
c_SLS · 10³ (M)

Fig. 5

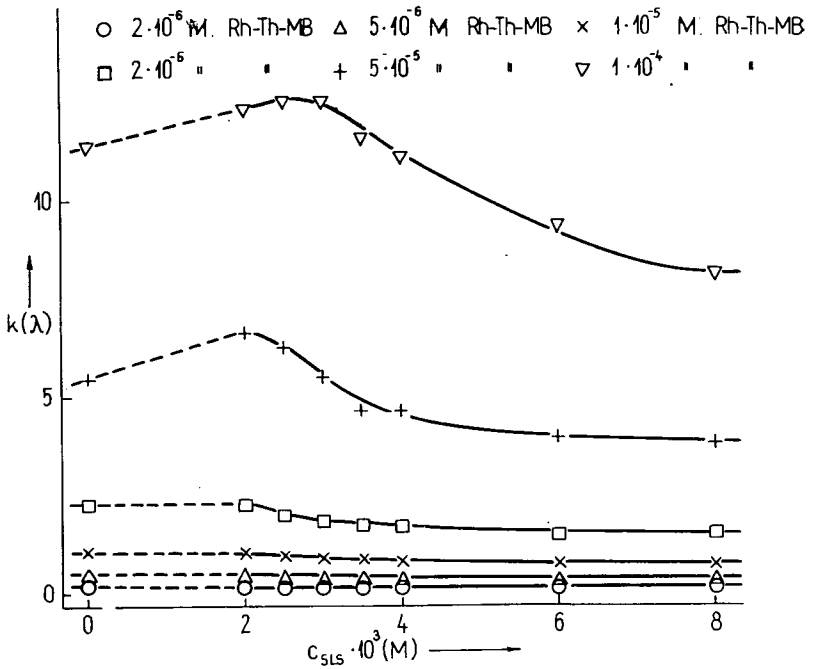
o 2·10⁻⁶ M. Rh-Th-MB
Δ 5·10⁻⁶ M Rh-Th-MB
× 1·10⁻⁵ M. Rh-Th-MB
□ 2·10⁻⁶
+ 5·10⁻⁵
▽ 1·10⁻⁴
k(λ)
10
5
0
0
2
4
6
8
c_SLS · 10³ (M)

Fig. 6

solutions over 10^{-5} M dye concentration, non-absorbing dye aggregates are present, which become soluble at higher detergent concentrations.

The presence or absence of the β-band maximum of Th (565 nm), characteristic for thionin dimers, could not be determined in mixed solutions because of the significant overlap of the absorption spectra of Rh6G and Th.

References

[1] *Teale, F. W. J.:* Nature **181**, 416 (1958).
[2] *Singhal, G. S., E. Rabinowitch, J. Hevesi, V. Srinivasan:* Photochem. Photobiol. **11**, 531 (1970).
[3] *Hevesi, J., E. Lehoczki, E. Bálint:* Zs. Prikl. Spektr. **13**, 458 (1970).
[4] *Hevesi, J., E. Bálint, E. Lehoczki:* Acta Phys. Polon. **A38**, 185 (1970).
[5] *Rózsa, Zs.:* Doctoral Thesis, Szeged, 1973.
[6] *Bálint, E., E. Lehoczki, J. Hevesi:* Acta Phys. et Chem. Szeged **17**, 15 (1971).
[7] *Lehoczki, E., E. Bálint, J. Hevesi:* Zs. Prikl. Spektr. **16**, 97 (1972).
[8] *Hevesi, J., E. Bálint, E. Lehoczki:* Acta Phys. Polon. **A38**, 829 (1970).
[9] *Förster, Th.:* Fluoreszenz Organischer Verbindungen (Vandenhoeck and Ruprecht, Göttingen, 1951).
[10] *Hevesi, J., Zs. Rózsa:* Acta Phys. et Chem. Szeged **17**, 127 (1971).
[11] *Lehoczki, E.:* Doctoral Thesis, Szeged (1971).

МИГРАЦИЯ ЭНЕРГИИ ВОЗБУЖДЕНИЯ ЭЛЕКТРОНОВ В СИСТЕМАХ ПРАВИЛЬНОЙ СТРУКТУРЫ

I. Абсорбционные свойства

Э. Бор, Я. Хевеши

Водный раствор детергента (натрий-лаурилсульфат), содержащий три люминесцирующего красителя с эквимолярной концентрацией, использовался в качестве in vitro модельной системы фотосинтеза. Эксперименты проводились с целью изучения изменений абсорбционных свойств красителей при изменении концентрации красителей и детергента. Найдено, что при повышении концентрации красителя образовались разные комплексы красителей и красителя с детергентом, которые при повышении концентрации детергента растворялись. Растворение повышает эффективность миграции энергии в таких смешанных растворах, о чём свидельствуют флуоресцентные свойства исследованных систем.

BOOK REVIEW

ANHARMONIC LATTICES, STRUCTURAL TRANSITIONS AND MELTING

edited by

T. RISTE

The book contains the papers presented at the conference on "Anharmonic Lattices, Structural Transitions and Melting" held in Geilo, Norway, 24th April—1st May, 1973.

The volume of 451 pages, edited by T. RISTE, Chairman of the Institute for Atomic Energy in Kjeller (Norway), contains 26 papers by leading scientists throughout the world in this field. The lectures are divided almost equally between review papers summarizing the most advanced current work using a variety of experimental techniques and up-to-date theory, and research reports dealing with subjects closely connected with the topics under review.

We find in the book, among others, important review contributions on Phase Transitions, Anharmonic Solids and Liquids by G. NIKLASSON and A. SJÖLANDER; Nonlinear Fluctuations and the Central Mode by J. FEDER; Rewiev of Methods for Obtaining a Central Mode by F. SCHWABL; Phonon Transport Theory and the Central Mode by R. KLEIN; The Jahn—Teller Effects as a Mechanism for Structural Phase Transitions, and Soft Modes at First and Second Order Phase Transitions, both by H. THONNES. The papers on Computer Simulation of a Discontinuous Phase Transition in the Two-Dimensional, One-Spin-Flip Ising Model by T. SCHNEIDER and E. STOLL, and on Melting: Theories and Recent Computer Simulations by R. M. COTERILL, E. J. JENSEN and W. D. KRISTENSEN are of interest from the point of view of the methods applied. The emphasis of the programme moves gradually from second order to first order transitions, covering such topics as order-disorder structural transitions in simple molecular crystals and tricritical phenomena. The last part is devoted to melting, including discussions on the dynamics of solids and liquids near their melting points.

The edited volume is of interest mainly to physicists and material scientists specializing in phase transition phenomena. The book of fine presentation belongs to a series comprising contemporary scientific issues published by Nordhoff International Publishing, Leiden (Holland).

L. VIZE

(Institute of Experimental Physics, Attila József University, Szeged)

A kiadásért felel: Dr. Leindler László
1974
A kézirat nyomdába érkezett: 1974. okt. 4. Megjelenése: 1975. január
Példányszám: 550 Ábrák száma: 110 Terjedelem: 16,1 (A/5) iv
Készült monó szedéssel, íves magasnyomással, az MSZ 5601—54 és az MSZ 5602—50 A szabványok szerint
74-4491 — Szegedi Nyomda